Diss. ETH No. 18082

A Combined Coding Scheme for Visual Stimuli

A dissertation submitted to
ETH ZURICH

for the degree of
DOCTOR OF SCIENCES

presented by
Stephan Roth
Diploma in Zoology, University of Zurich (UZH)
born May, 8th, 1970
citizen of Altishofen (LU), Switzerland

accepted on the recommendation of

Prof. Dr. Rodney J. Douglas, examiner
PD Dr. Daniel C. Kiper, co-examiner
Prof. PD Dr. Thomas Haslwanter, co-examiner

2008

Acknowledgments

My first thanks go to PD Dr. Daniel Kiper, who supervised this work and who raised my passion for neuroscience. I would like to thank him for his continuous support, the valuable discussions and his ability to create a creative and friendly scientific atmosphere, which made it a pleasure to work in his group.

Further I would like to thank Prof. Paul Verschure for his valuable discussions on parts of the work, and for introducing me to appreciated members of his research group.

I'm particularly grateful to Dr. Reto Wyss, Dr. Philipp Knüsel and Dr. Alexis Guanella, who introduced me into computational modeling of brain functions, and provided parts of the simulation framework, and who provided valuable comments on my work. I'm very pleased as well to work with the members of Daniel Kiper's group: Martin Wiesmann, Lisa Holper, Henning Proske, Elias Rentzeperis, Paul Rogister and Konstanze Hofstetter who gave well appreciated feedback on the occasion of my given talks. In addition special thanks go to Elisha Ruesch who provided the reconstruction data for the *Nereda* framework examples presented in chapter 9, and to German Köstinger who kindly provided screenshots of *Nereda*-triangulated axonal trees rendered in *Blender*.

I would like to thank Prof. Rodney Douglas and Prof. Kevan Martin for the very stimulating and unique research environment they created with the Institute of Neuroinformatics (INI). In addition I thank PD Dr. Thomas Haslwanter for accepting my invitation to be part of the Ph.D. defense committee.

Outside of the lab, I thank my beloved girlfriend Mireille for her patience, support and the wonderful time we spend together! Finally, I'm deeply grateful to my parents Erwin and Marlis, who fueled my interests in nature, its functions and mechanisms already in childhood, and supported me all the time since then. Additional thanks go to all friends of the family, like Alois Arnold, for their interest in my work, and to all my friends who gave me the necessary distraction with mountain-bike or pub tours, which challenged my brain and body in many different ways.

This research was supported by the ETHZ Grant 0-20214-04.

CONTENTS

Abstract (English)

Animals or humans identify and categorize features or objects under large variation and viewing conditions, and excel in localization tasks. Since Hubel & Wiesel the focus of a large body of research studies investigated the underlying neuronal mechanisms. Most of the data emphasizes the rate based coding properties of single neurons. But this view may be largely biased by the available physiological techniques. Even nowadays it's still difficult to record the activity of a larger population of neurons with single cell and sub-millisecond resolution. However with the advances of electrophysiological methods and the support of computational modeling approaches, in the recent years more and more evidence accumulated that the coding of stimuli maybe based on population activities and at least partially on precise spike timings, rather than on averaged activities of single neurons. With the new insight researchers revisited the question how brain anatomy is related to its function, and start to partially move away from the purely feed-forward view, where in the case of visual stimuli, a scene is decomposed into small features which are combined along the visual hierarchy to form a coherent percept of an object in higher visual areas.

Recently Reto Wyss et al. proposed a coding scheme which emphasizes the recurrent inner-areal connectivity found in visual areas of many mammalian species. The modeling study reveals that the long range horizontal projections denote a coding substrate for a temporal population code, which revealed to be robust against stimulus distortions and noise, and which proved to scale to a large number of stimulus classes. The scheme represents a non-hierarchical approach to explain the fast and reliable stimulus classification properties of humans or primates. The model further demonstrates that based on symmetrical connectivity patterns a temporal code is generated which is inherently invariant to stimulus rotations and translations.

The symmetric lateral connections of the model, which produce the desired fast, robust invariant properties, are at the same time its weakness, however. Any distractor stimulus closely positioned to a target object will perturb the produced temporal code and will lead to a performance break-down in classification tasks. In addition the model is not able to produce position information or to code orientation properties of the target stimulus. This brings up the question whether additional fundamental anatomical patterns, found along the visual hierarchy, play a role to solve these problems.

We first address the question whether modulation of dendritic information processing can control the contextual influence of lateral connections, in a way to avoid the code perturbations found in the original TPC model. Using a neurophysiologically constraint model, we show that a temporal population code can be generated which is highly robust to closely positioned distractors, and which includes the potential to code the stimulus position. The model relies on the notion that feed-forward connections with distance related transmission delays can serve as a coding substrate, and that cholinergic

input is able to affect the contextual influence of horizontal connections in the early visual areas. A principle which was recently demonstrated in cat experiments, which revealed that acetylcholine (*ACh*), the neurotransmitter of cholinergic projections originating from the basal forebrain, reduce the efficacy of horizontal connections by virtue of muscarinic receptors, and boost the feed-forward information flow by virtue of nicotinic receptors. We demonstrate that the new coding model not only is robust to distractors but also augments the coding capacities of a purely lateral-information-flow based principle.

In a second part we investigate whether the newly introduced model can solve a widely used psychophysical localization task, i.e. the *Vernier* acuity task. We show that the previously presented coding principles augmented with feature selective properties of cells in the early visual cortex, i.e. populations of neurons which cover the whole orientation space, are capable to solve the *Vernier* task with hyperacuity. Hence, the model is not only capable to generalize over stimulus distortions, as shown by Reto Wyss, but also produces highly specific responses, required to separate *Vernier* stimuli.

In the third part of the thesis we focus on the properties of the new model with respect to learning of new stimuli. The results represent the first steps towards a categorization and identification network, which comprises the capability to exploit not only the rate but also the temporal aspects of stimulus dependent codes produced by the network presented in the first and second part of the thesis. We demonstrate that the modulatory stimulation, i.e. cholinergic input, can control the learning properties of *NMDA*-synapses, since the signal decides whether the synapse performs in *LTP* or *LTD* mode. Hence the cholinergic signal hypothetically could constitute a supervisor learning signal which shapes the responses of visual areas by virtue of their plastic properties. We show that a simple implementation of this principle is able to separate bar stimuli with small separation angles again, and is able to solve the *Vernier* task with hyperacuity.

Taken together our results indicate that the fundamental connectivity patterns found in the mammalian visual cortex, i.e. extensive horizontal inner-areal connections, fast feed-forward inter areal projections and modulatory cholinergic input from the basal forebrain, form a flexible combined coding machinery, which allows dynamic control over the coding principles. Invariant code properties are best generated and explored by virtue of neuronal activities produced by symmetric horizontal connectivity patterns, and readout by very fast feed-forward connections. The coding of position or orientation properties and information about stimulus features in cluttered scenes is augmented by the coding capabilities of feed-forward projections and the attentional-like modulatory influence of cholinergic input. Hypothetically, both coding principles can co-exist, whereas the cholinergic input in principle has the capacity to define the mixture during the information processing by modulating its effects on the muscarinic and nicotinic receptors.

In an additional part of the thesis we present a framework to facilitate analysis of neuronal anatomical data. As we state in the thesis, the quality of computational models of neuronal networks is strongly dependent on how precise these designs reflect the biological properties of the circuitry. Many models can lead to the same outcome, i.e. reproduce some features of biological networks, however only the biophysically restricted ones will have a good predictive power. For cortical models it is essential to reflect the principal connectivity patterns of the target area. This requires precise quantitative data of neuronal anatomy. With *Neurolucida*™ a 3D-neuron-reconstruction software package is available which supports the anatomist in gathering information about the spatial structure of axons and dendrites. The process is very time-consuming and requires a lot of experience. In addition the reconstruction data is saved in a proprietary format, which makes it hard to export it to data processing tools like *Matlab* to obtain quantitative results.

With the framework presented in this thesis, with the name *Nereda*, we introduce an open source solution that provides flexible access to the collected data for quantitative analyze. Existing algorithms as well as new approaches can easily be implemented in the solution. Additionally it supports scientists in the reconstruction process by providing validation tools to detect implausible structures. The framework architecture guarantees future expandability and robustness with a strong emphasize on code reusability and collaboration. Beside of the data analysis part *Nereda* provides visualization capabilities to present reconstructed neurons in various use cases, i.e. schematic ad-hoc representations as well as high quality 3D-rendered presentations based on *STL* data format. In this thesis mainly the framework architecture is illustrated. Based on actual data descriptive examples are provided, which show the functioning and properties of the software. A collection of code examples shows how to use and extend the framework along the provided guidelines.

Altogether *Nereda* facilitates reconstruction data analysis and provides an open platform for future requirements. This in turn allows building of improved cortical network models with plausible biological constraints with presumably good predictive power.

Abstract (Deutsch)

Sensorische Wahrnehmung und die Verarbeitung dieser Informationen sind essentielle Grundlagen für die bemerkenswerte Fähigkeit der Säugetiere komplexe visuelle Aufgaben mit hoher Präzision zu lösen. Tiere und Menschen identifizieren und klassifizieren Objekte auch unter stark variierenden Sehbedingungen, und bestechen durch ihre herausragenden Leistungen in Lokalisierungsexperimenten, mit Wahrnehmungsschwellen unterhalb der fovealen Rezeptordistanz. Seit der Beschreibung der Antwortcharakteristiken von Neuronen der frühen visuellen Gehirnareale durch Hubel & Wiesel, befasste sich eine grosse Zahl von Studien mit der Informations-verarbeitung entlang der kortikalen Sehbahn. Die meisten Berichte heben die Wichtigkeit der frequenzbasierten Kodierung auf der Ebene von individuellen Zellen hervor. Diese Interpretation der Daten dürfte allerdings durch die damals und heute verfügbaren physiologischen Methoden beeinflusst sein. Erst seit reltaiv kurzer Zeit, ist es möglich, wenn auch immer noch mit grossen methodischen Schwierigkeiten behaftet, die Aktivität von grösseren Hirnzellpopulationen mit genügend hoher räumlicher und temporaler Auflösung, sprich bis auf die Ebene von indiviuellen Neuronen und mit Submillisekunden-Auflösung, zu messen. Erwähnenswert sind hier vor allem die Fortschritte in den elektrophysiologischen Recording-Techniken und die neu entwickelten Imaging-Verfahren. Sie erlauben immer genauere Einblicke in das in-vivo Verhalten von grösseren Zellverbänden während der Präsentation von externen Stimuli, und bilden damit die Basis für neue Modelle der Informationsverbarbeitung in biologischen Netzwerken. In neuerer Zeit erhärteten sich die Hinweise, dass Stimulusinformation nicht ausschliesslich in der gemittelten Aktivität von individuellen Neuronen kodiert ist (frequenzbasiert), sondern dass sie teilweise auf der Ebene grösserer Zellpopulationen und durch präzises Spike-timing repräsentiert ist. Diese Sicht wird auch von computerbasierten neuronalen Netzwerkmodellen unterstützt. Die neuen Einblicke führten zu einer Reinterpretation der Funktion der anatomischen Strukturen in den untersuchten Arealen. Während der traditionelle Ansatz die Wichtigkeit des feed-forward Informationflusses hervorhebt, gehen neuere Theorien dazu über, den reziproken Verknüpfungsmustern innerhalb der Areale, und den feed-back Projektionen von höheren zu niedrigeren Gehirnarealen grössere Bedeutung beizumessen.

Kürzlich haben Reto Wyss et al. ein Modell vorgeschlagen, welches eben diese Kodierungseigenschaften von reziprok verknüpften Zellpopulationen zeigt. Das computerbasierte Modell zeigt, dass die weitreichenden ekzitatorischen lateralen Verknüpfungen, wie sie unter anderem in visuellen Hirnarealen gefunden werden, ein Kodierungssubstrat für einen temporalen Populationscode darstellen. Der Code erwies sich als schnell und robust und skalierte bis zu mehreren hundert Stimulusklassen. Das Kodierungsprinzip repräsentiert einen nicht-hierarchischen Ansatz, die schnellen und zuverlässigen Stimulus-Klassifizierungseigenschaften von Menschen und Primaten zu erklären.

Die symmetrischen weitreichenden Verknüpfungen, welche den temporalen Code erzeugen, sind jedoch gleichzeitig auch die Schwäche des Modells. Ein Distraktor der nahe bei dem zu klassifizierenden Stimulus (Target) präsentiert wird, produziert substantielle Störungen im produzierten Code und damit zu schwerwiegenden Leistungseinbussen in Klassifizierungsexperimenten. Zudem ist das Modell aufgrund seines nicht topologischen Prinzips nicht fähig die Stimulusposition oder -orientierung zu kodieren. Das führt zur Frage, ob die zusätzlichen, fundamentalen anatomischen Strukturen, wie beispielsweise schnelle feed-forward Verknüpfungen oder Feedback-Informationsströme, die entlang der Sehbahn gefunden werden, eine wichtige Rolle bei der Lösung der angesprochenen Probleme spielen.

In dieser Doktorarbeit befassen wir uns zuerst mit der Frage, ob die Modulation von dendritischer Informationsprozessierung die Beeinträchtigung der Klassifizierungsleistung durch nah platzierte Distraktoren verhindern kann. In der Tat zeigen wir, dass mit einem neurophysiologisch plausiblen Modell ein Code erzeugt wird, der robust gegenüber kontextuellen Einflüssen von nah platzierten Distraktoren ist, welcher auch das Potential für die Kodierung von Stimulusposition und –orientierung hat. Das Modell nutzt die Vorstellung, dass auch feed-forward Verknüpfungen mit distanzabhängigen Signaltransduktionsverzögerungen als Kodierungssubstrat dienen können, und dass zusätzlich vorhandener modulatorischer Input in der Lage ist den kontextuellen Einfluss von Distraktoren einzschränken. Die Betonung von feed-froward Informationen gegenüber lateral verteilten Signalen, wurde kürzlich auch in physiologischen Experimenten in Katzen nachgewiesen. Acetylcholin (*ACh*), der Neurostransmitter cholinerger Projektionen mit Ursprung im basalen Vorhirn, reduziert die Wirksamkeit von horizontalen Verknüpfungen durch Aktivierung von muskarinen Rezeptoren, und erhöht gleichzeitig die Effizienz von feed-forward Projektionen durch nikotine Rezeptoren. Wir zeigen in diesem ersten Teil der Arbeit, dass das neue Kodierungsmodell nicht nur robust gegenüber Distraktoren ist, sondern auch die Präzision der rein lateral basierten Kodierung erweitert.

Im zweiten Teil untersuchen wir, ob das vorgeschlagene Modell den *Vernier Acuity Task,* einen psychophysikalisch sehr gut untersuchten Lokalisierungstest lösen kann. Wir zeigen, dass unser Modell, erweitert durch orientierungsselektive neuronale Einheiten, wie sie ähnlich auch im primären visuellen Kortex vorhanden sind, in der Lage ist den *Vernier* Task mit *hyperacuity* zu lösen. Der Begriff *hyperacuity* bezeichnet dabei die Tatsache, dass die gemessene Wahrnemungsschwelle unterhalb der minimalen Rezeptordistanz liegt – welche beim Menschen in der Fovea ca. 30 sec arc entspricht. Das Modell ist also nicht nur in der Lage über Stimulusverzerrungen zu generalisieren und robust gegenüber kontextuellen Störungen, sondern liefert auch hochspezifische Antworten wie sie zur Separierung von *Vernier* Stimuli benötigt werden.

Im dritten Teil der Doktorarbeit fokussieren wir auf die Eigenschaften des Modells in Bezug auf das Erlernen und Wiedererkennen von Stimuli. Die Resultate

repräsentieren die ersten Schritte hin zu einem Kategorisierungs- und Identizifizerungsnetzwerk, welches die Fähigkeit hat, nicht nur gemittelte Aktivitäten sondern auch temporale Aspekte von Codes, wie sie von unserem Modell erzeugt werden, auszunutzen. Wir demonstrieren, dass der zuvor verwendete modulatorische cholinerge Input in Lernexperimenten in der Lage ist, die Eigenschaften von Modell-Synapsen, welche die Merkmale von biologischen *NMDA*-Rezeptoren widerspiegeln, in sinnvoller Weise zu kontrollieren. Die Modulation bestimmt debei, ob die Synapse im *LTD*-mode (long term depression) oder im *LTP*-mode (long term potentiation) arbeitet, sprich ob die Effizienz der Synapse steigt oder sinkt. Das cholinerge Signal stellt hypothetisch ein Supervisor-Lernsignal dar, welches im Laufe der Lernphase die Antworten von visuellen Arealen durch die plastischen Eigenschaften ihrer Synapsen beeinflusst. Wir zeigen, dass eine einfache Implementation dieses Prinzips in der Lage ist linienbasierte Stimuli zu klassifizieren und dass das Modell wiederum mit *hyperacuity* im *Vernier* Task arbeitet.

Zusammenfassend zeigen unsere Resultate, dass die grundlegenden Verknüpfungsmuster, die im Säugetiercortex gefunden werden, sprich die zahlreich vorkommenden, reziproken, lateralen Verknüpfungen innerhalb von Gehirnarealen, sowie die schnellen feed-forward Verknüpfungen zwischen den Arealen, und die modulatorischen, cholinergen Projektionen vom basalen Vorhirn, eine flexible Kodierungsmaschinerie bilden, welche eine dynamische Kontrolle über die Antworteigenschaften von Zellpopulationen erlaubt. Rotations- oder Translations-invariante Codes werden am besten durch das lateral basierte Kodierungsframework erzeugt, dann durch sehr schnelle feed-forward Verbindungen ausgelesen und an nachfolgende Porzessierungsstationen verteilt. Robustheit gegenüber Distraktoren und Informationen über Stimulusorientierung und -position wird aber am besten mittels mittelschneller feed-forward Projektionen und unter Zuhilfenahme von modulatorischen Mechanismen erreicht. Diese Mechanismen ähneln Aufmerksamkeitsmodellen, wie sie mehrfach in Säugetieren gemessen und postultiert wurden. Hypothetisch können beide Kodierungsprinzipien koexistieren, wobei das cholinerge Signal das Potential hat, über die Aktivierung der muskarinen und nikotinen Rezeptoren, die aktuelle Mischung zu bestimmen.

In einem zusätzlichen Kapitel präsentieren wir ein Software-Framework, um die Analyse von anatomischen, neuronalen Rekonstruktionsdaten zu erleichtern. Wie in dieser Doktorarbeit dargelegt, ist die Qualität eines computerbasierten neuronalen Netzwerkmodells essentiell davon abhängig wie genau die relevanten Aspekte des biologischen Vorbilds wiedergegeben werden. Viele Modelle können gleiche, oder ähnlichen Resultate liefern, aber nur die biophysikalisch Korrekten werden eine grosse Aussagekraft aufweisen. Für kortikale Modelle ist es entscheidend, die grundlegenden Verknüpfungsmuster des Zielareals wiederzuspiegeln. Das allerdings braucht präzise, quantitative Daten über die neuronale Anatomie. Mit *Neurolucida*™ steht eine 3D-Rekonstruktionssoftware für Neuronen zur Verfügung, welche den Forscher beim Sammeln von Axon- und Dendritenstrukturdaten unterstützt. Der Prozess ist langwierig

und benötig viel Erfahrung. In Bezug auf die quantitatve Analyse kommt erschwerend hinzu, dass die Daten in einem propriertären Format abgelegt werden, was die Verwendung in flexiblen Datenanalyse-Werkzeugen wie *Matlab*™ erschwert.

Mit dem in dieser Arbeit präsentierten Software Framework, mit Namen *Nereda*, soll dieser Umstand verbessert werden. Das Framework erlaubt flexiblen Zugriff auf die gesammelten Strukturdaten, um sie quantitativ zu analysieren. Bestehende Algorithmen und neue Ansätze können gleichermassen leicht in das Framework implementiert werden. Integrierte Validationswerkzeuge unterstützen den Wissenschaftler im Aufspüren von unplausiblen Strukturen. Die Framework-Architektur garantiert zudem auch zukünftig Erweiterbarkeit und Robustheit. Neben dem quantitativen Analyseteil bietet *Nereda* auch Visualisierungsmodule, um rekonstruierte Neuronen in verschiedenen Anwendungs-szenarien darzustellen. Die Möglichkeiten reichen von ad-hoc Darstellungen die als Diskussionsgrundlage dienen können, bis hin zu qualitativ hochwertig gerenderten 3D-Ansichten, basierend auf dem *STL*-Format (Surface Triangulation Language). In dieser Doktorarbeit wird vor allem auf die Software-Architektur eingegangen. Anhand von anschaulichen Beispielen basierend auf aktuellen Daten, wird dem Leser ein Einblick in die Möglichkeiten und die Arbeitsweise der Software gegeben. Eine Serie von Programmbeispielen erläutert wie das Framework gebraucht und gemäss den definierten Richtlinien erweitert werden kann.

Zusammengefasst soll *Nereda* die Analyse von Rekonstruktionsdaten erleichtern und eine offene und robuste Plattform für zukünftige Anforderungen bieten. Die gewonnenen Daten können wiederum in verbesserte neuronale Modelle einfliessen, um ihre biologische Aussagekraft zu vergrössern.

LIST OF FIGURES

Chapter 1

Introduction

Sensory perception and subsequent processing of information are the basis for the remarkable ability of animals to react fast and accurately to external stimuli. In primates, vision is a fundamental source of information about the external environment. Accurate responses require classification or identification of features or objects in the visual scene under large variations in viewing conditions. The neuronal mechanisms and cortical structures responsible for these amazing performances are still debated.

Classical approaches explain the properties of the visual system by means of hierarchical and purely feed-forward information processing, where single units, i.e. neurons, represent sharply tuned feature detectors (Hubel and Wiesel, 1959). In recent years however this local processing view by single units was challenged. More and more evidence accumulated that the underlying processing of information in the brain uses population activity and the temporal structure of responses to encode external stimuli (Konig et al., 1995; Dan et al., 1998). Examples of single neurons which temporally encode significant amounts of information about stationary stimuli were found in the primate visual pathway and also in the auditory cortex of cats encoding sound localization. Consideration of the temporal code allowed an increase in the coding accuracy, compared to a purely rate based approach. Measurement of reaction times in human psychophysical tasks suggest, that neurons can only use one or two spikes per neuron to compute a subsequent output signal (Kirchner and Thorpe, 2006). Temporal encoding in such short time windows would be very restricted in situations where the code is based on single neuron activity. With a whole population of neurons encoding stimulus information the number of spike patterns expressible in a very short time window is no longer restricted by the properties of a single cell, e.g. refractory period. Temporal encoding across ensembles of neurons has been demonstrated in the frontal cortical areas of the primate brain. The spike patterns were found to be very precise in the order of a few milliseconds, and seemed to correlate with behavioral situations (Abeles et al., 1993). Recent findings of information encoding in the olfactory bulb of moth further support the idea of temporal population encoding (Knusel et al., 2007).

Recently it was shown that networks that incorporate dense intra-areal lateral excitatory connections, a connectivity pattern which is vastly found between pyramidal neurons in the visual cortex of primates and cats, transform spatial stimulus features into a specific temporal population activity (Wyss and Verschure, 2003). The so called temporal population code (*TPC*) supports rapid invariant classification, has a high capacity and is robust to noise (Wyss and Verschure, 2003). The recent neurophysiological findings and the fact that a model based on recurrent excitatory

connectivity can produce a code representing class relationship of presented stimuli poses the question whether this stereotyped connection pattern found in many mammal species represents the anatomical substrate for a temporal population encoding.

1.1 Goals of the thesis

The main goal of this thesis is to explore the limits of the *TPC* and present possible extensions to overcome its limitations. To investigate the topic we use a specific psychophysical task which was studied in great detail during the last decades, i.e. the *Vernier line discrimination task*. We also present data and comment other object recognition and classification tasks, e.g. object classification in cluttered scenes, or dot pattern classification. Many studies showed that the *Vernier* line discrimination seems to be restricted by neuronal properties of the early visual cortex, which in part isolates the system and makes it accessible for biologically plausible modeling. The model should further be distractor-robust to open it for real world application. Besides testing the optimal performance of the system, the model should reflect the learning dynamics found in *Vernier* tasks under various conditions. Finally, the model should be able to separate dot patterns as used in many psychophysical tasks into different classes, and should again show similar learning dynamics as human observers.

This leads to the following questions:

- How can a laterally coupled model with biophysically constrained properties become distractor robust?
- Can the new model encode dot pattern stimuli as used in psychophysical and physiological experiments (Knowlton and Squire, 1993; Reber et al., 1998b)?
- Can temporal population codes produced by a model including the major connectivity and tuning properties of the primary visual cortex achieve similar performance benchmarks in a *Vernier line discrimination task* as human observers? How can the *TPC* model be extended to achieve the goal?
- Is an extended model which includes synaptic plasticity able to reflect learning dynamics and performance found in the *Vernier* task?
- What can be learnt from the limitations of the *TPC* and extension in this thesis? Can we attribute functions to the fundamental connectivity patterns in the cortex?

In a separate chapter we additionally present a framework to gather information about anatomical properties of neurons, which can be implemented in biophysical

constraint neural networks as used in this thesis. In the course of the thesis it became clear that it is quite hard to get precise neural anatomical data. Quantitative data analysis of reconstructed neurons is circumstantial. This is mainly due to the fact, that current neural reconstruction tools, e.g. *Neurolucida*™ do not provide convenient export formats to transfer anatomical data into flexible data processing environments like Matlab. Precise anatomical data are however crucial for biologically meaningful simulations like the ones performed in this thesis. Hence a further goal of the thesis was to develop a framework which overcomes this limitation by providing a convenient, robust and extendable architecture to handle reconstruction data. The framework should allow collaboration between researchers with a focus on flexibility, code reusability and stability to speed up the analysis of reconstruction data. This as a consequence should lead to biologically relevant, high quality computational simulations.

1.2 Methods

To reach the goals of this thesis a neurocomputation approach which allows for simulation of a large amount of spiking neurons was chosen. The single units were modeled in a biologically plausible way as conductance based leaky-integrate-and-fire neurons, whereas the connections between the neurons reflected the broad connection patterns found in the visual areas of primate brains. Following this modeling approach allowed for rapid investigation and evaluation of various ideas, about how object recognition based on temporal population encoding could be implemented in the brain.

The simulations were performed in the *wSim* environment on Linux. Code of model neurons, connections and synapses was written in *C++*, data analysis was performed in *Matlab*™.

1.3 Motivation

This work aims for a better understanding of the neural mechanisms underlying object recognition, i.e. identification and categorization. In particular an encoding strategy biological neural networks could follow, i.e. temporal population coding, is investigated to see whether the strategy can reflect the performance properties and learning dynamics of the human visual system in selected psychophysical tasks – *Vernier acuity, dot pattern classification and object classification in cluttered scenes*. While traditional neurocomputation approaches build on the idea of hierarchical feed-forward networks, temporal population coding offers an alternative non–hierarchical and biologically plausible way to explain the performance benchmarks of natural visual systems.

The motivation to explore the *TPC* in combination with the mentioned psychophysical tasks is twofold. First of all, a deeper understanding of the network

dynamics emerging in neural networks with biologically plausible parameter sets can contribute to one of the main goals in neuroscience, namely to conceive the function of brain structures by their anatomy and their physiological properties. Second, results in this field of neurocomputation research may influence engineering approaches in machine vision, which try to mimic the robust, accurate and fast behavior of primate vision systems.

Why adopting a neurocomputation modeling approach when dealing with temporal population encoding? Directly understanding the encoding strategies of the brain needs access to data in living tissue. In the past decades a series of techniques were developed which allow recording of neuronal activity with single cell and sub-millisecond resolution. But none of these methods exhibits high temporal- (millisecond scale) and high spatial resolution (single cell) when a large amount of neurons have to be recorded simultaneously. *Classical neuro-electrophysiology* which uses electrodes to collect activity data has millisecond resolution. But it is very difficult to obtain single unit activity of a large number of neurons at the same time. In addition, due to tissue movement and immune reactions against the electrode surface, the same units can only be measured during a restricted time period.

Functional Magnet Resonance Imaging (fMRI) which non-invasively captures *BOLD* signal (hemodynamic response) differences in the brain allows observation of intact neural networks down to millimeter scale. Although its non-invasiveness is a huge advantage and opened up a large field in medical diagnostics, the spatial resolution is still low if it is compared to the package density of neural tissue. But the major limitation of the method lies in its lack of temporal resolution. Time-resolved single-trial event-related *fMRI* allows changes in neural activity to be detected at a temporal resolution on the order of one second. However, most neural processes occur on a time scale of milliseconds, rather than seconds. The limited resolution is the result of a combination of physical restrictions of the scanners and the time-course of the hemodynamic response in the brain, which peaks about five seconds after stimulus presentation.

In recent years several flavors of *optical imaging* were developed which partially overcome the temporal- or spatial resolution limitations of the other methods. Electrical activity of neurons is related to local metabolic activity and blood flow. In optical imaging the change of light scattering on the brain surface caused by ion and water movement is detected by highly sensitive cameras which are positioned on the opened skull above the area of interest. The higher the activity the darker the recorded region appears. The method allows repeated data collection under controlled conditions, but usually delivers noisy results within trials, which restricts the spatial resolution of the approach. Probably the most promising optical imaging variant is the *two-photon excitation microscopy* aka *calcium imaging*. In this approach a laser beam scans the calcium state of each cell (which is activity related). This fluorescence imaging technique allows the observation of living tissue up to a depth of one millimeter, with millisecond

and single cell resolution. Although very promising, this new technique is still under construction, and only a few studies showing its potential are available up to now (Ohki et al., 2006).

In the mean time modeling offers an alternative and complementary way to study activity dynamics on a network scale, with both single cell resolution and a temporal resolution down to the sub-millisecond scale. With these properties and the available biologically plausible neuron models, the properties of temporal population encoding in tasks similar to human psychophysics can be explored. In this way modeling may propose and evaluate new strategies how object recognition could be implemented in the brain. The predictive power of the approach may be evaluated by the new imaging techniques which are under development now.

1.4 Structure

The Thesis is organized in 10 chapters. *Chapter 2* gives an introduction into coding of information by spiking neurons. In the chapters 3 and 4 performance benchmarks of the human visual system and an overview about the neural correlates of object recognition in primate brains are reported. *Chapter 5* describes previous modeling approaches in object recognition and localization acuity. We try to convince the reader that temporal coding in ensembles of neurons is an important scheme in object recognition and categorization of mammalian brains, and that the extensive lateral connectivity is a possible neural substrate for the transformation of information into the temporal domain.

Chapters 6-8 are directly related to the goals of this thesis. They show the performed modeling experiments and the results together with the conclusions.

Chapter 6 describes a limitation of the *TPC* model presented by Wyss et al. (Wyss et al., 2003a; Wyss and Verschure, 2003). If several stimuli are presented simultaneously, due to the lateral interactions, the produced code is no longer able to represent each of the objects accurately. We use properties of cells measured in the primary visual cortex of marmoset monkeys (Roberts et al., 2005) together with position specific readout of the *TPC* by virtue of fast feed-forward connections to overcome the segmentation problem. Roberts et al. have shown that Acetylcholine is able to dynamically control spatial integration properties of cells by virtue of changing the attenuation characteristics of dendritic structures. This feature is assumed to play a role in the control of spatial attention. We show that a transient increase of attenuation after stimulus onset, possibly mediated by acetylcholine, produces a highly distractor robust system, which provides better performance than a laterally uncoupled- or a completely coupled systems.

One of the main goals of this thesis is to evaluate whether the *TPC* can explain performance benchmarks of humans in psychophysical tasks. One of the best examined

tests in psychophysics is the *Vernier* acuity task, where observers have to judge the displacement of two vertical line segments. In *chapter 7* we use the enhanced model in such a *Vernier* task and evaluate its characteristics. We show that the model exhibits discrimination thresholds below receptor distance, and further reflects similar threshold dependencies on various stimulus parameters like line length and line separation, as gained in humans (Westheimer and McKee, 1977a). In line with earlier results (Wilson, 1986) we show in addition that the performance depends on the correct weighting of responses originating from cell populations with different preferred orientation tunings and receptive field sizes.

The weighting is gained by a perceptron which uses the response rates of the orientation tuned filters to calculate an optimal weight map. In *chapter 8* we extend the idea to a biologically more plausible approach, and use calcium-controlled synapses to model synaptic plasticity in a *Vernier* supervised learning task. The used synapses mimic various plasticity characteristics of biological synapses, e.g. weight change in pairing experiments or postsynaptic spike frequency dependency or spike-timing dependent plasticity (*STDP*) (Shouval et al., 2002b). We show that the model reaches hyperacuity without the mechanisms proposed in earlier models, and demonstrate that its learning behavior resembles the dynamics of human subjects.

In *chapter 9* conclusions over the whole thesis are being drawn. The contributions of the experiments are summarized, and again evaluated against biology. Finally the possible future steps are sketched.

As we state continuously in this thesis, the quality of simulations is strongly dependent on how well it fulfills the biophysical constraints of the target brain area. For cortical simulations one of the main parameter to consider is the neural anatomy and the connectivity of the cells. In the *appendix* we present a framework to analyze and visualize such neuronal anatomical data. The software is designed to gather reconstruction data from *Neurolucida*™ and to provide an extendable and robust architecture to analysis and visualize the information.

Chapter 2

Coding of information with spiking neurons

2.1 Coding schemes

Action-potentials are the fundamental symbols for the encoding of the external world in animal brains. One of the fundamental issues in neuroscience is to understand how the sequence of these symbols relates to the information content. To answer this question is far from trivial. The human brain contains about 10^{10} neurons which are heavily interconnected. Even in a 100 ms time window, which seems to be a reasonable time window for visual perception (Kirchner and Thorpe, 2006), a binary neural alphabet has 2^{100} symbols. If ensemble encoding is allowed the number of possible symbols becomes astronomic. Neurons which have to decode the spike train based information of previous stages may recognize specific properties of these symbol strings and may reduce the complexity and noisiness by averaging parts of it. The minimum set of symbols capable of representing the biological relevant information defines the encoding scheme used in animal brains. Several schemes were proposed in the past. Rate codes which average over time windows in single or population of neurons, or temporal codes which use precise spike timing and the resulting temporal correlations of individual spikes. The goal of this section to give an overview on the proposed encoding schemes and to provide evidence that temporal coding is important in information processing of animal brains.

In the past decades it has been thought that the information is mostly encoded in the mean firing rate of individual neurons. But this view was presumably biased by the available electrophysiological tools and the experiments protocols. It is much easier to examine the mean firing rate of individual neurons, than to collect spiking data of whole neuronal populations or even networks with high temporal resolution. The rate encoding idea already early became strong support by the findings of Hubel & Wiesel, who characterized the precise tuning properties of cortical neurons by their firing rate (Hubel and Wiesel, 1959). The majority of the subsequent electrophysiological studies followed this scheme.

At least two definitions of mean firing rate of single neurons were developed. One defines the rate of neurons as the temporal average within a given time window, e.g. 100 ms or 500 ms. The other uses the peri-stimulus-time histogram (*PSTH*), also known as spike density, to average the activity over several stimulus presentations and within small time windows, e.g. around one or a few milliseconds.

The former was successfully applied in experiments on sensory or motor systems, which show that the average neuronal activity within a period of 500 ms correlates with

the applied force to a muscle spindle (Adrian, 1926; Adrian and Zotterman, 1926) or to a touch sensor in leech (Kandel et al.).

On a single neuron level the latter needs several stimulus repetitions to reveal clear results, which is obviously not feasible in natural situations. However, it can be assumed that the brain contains a large amount of neurons with similar properties, e.g. ensembles of neurons in the columns in the striate cortex of monkeys. The *PSTH* rate definition can therefore be extended to neuronal populations to define the activity as a population-rate, i.e. the number of spikes in a small time window elicited by an ensemble of similar neurons. The population-rate is able to reduce noise on a single trial basis by averaging over the whole population, and may reflect changes in the stimulus conditions nearly instantaneously.

Whether averaging of many spikes within large time is used in brains is after decades of electrophysiological measurements and information theoretical considerations still under debate. It is clear however that averaging the activity of neurons in accordingly large time windows loses all the temporal information that is in the spike. Furthermore it completely neglects the precise spike timing of populations of neurons which could represent an additional coding domain. The concept of mean firing rate was therefore repeatedly criticized in the past (Bialek et al., 1991); (Shadlen and Newsome, 1994); (Hopfield, 1995); (Softky, 1995); (Oram et al., 1999). But one of the main arguments against temporal averaging of information over large time windows emerges from measurements of reaction times in psychophysical experiments. Humans detect highly trained categories, e.g. animals or faces, within 120ms (Fabre-Thorpe et al., 1998; Kirchner and Thorpe, 2006). Thorpe already in earlier experiments brought up the idea that processing that underlies rapid object recognition may be based on only a few spikes per neuron. He gives the following arguments: Highly object selective responses of neurons in the temporal lobe start around 100-140 ms after stimulus onset. Given the number of processing stages from the retina to the temporal lobe, about 10 synaptic layers must be crossed within 100ms. Hence, in a first feed-forward information sweep through the cortex the processing has to take place in a time window as little as 10 ms. Taking into account the typical firing of cortical neurons (0-100 Hz) this means that in each layer only 1-2 spikes/neuron are produced before the subsequent layer starts with its response. Thorpe argues that stimulus information is encoded in relative arrival times of spikes (Thorpe, 1990). The importance of information in very early small time bins was supported by physiological measurements in temporal lobe visual cortical areas of rhesus macaques (Tovee et al., 1993). The experimental findings reveal that in the 0-400 ms period after onset of the neural response the first 20-50 ms can carry as much as 84.4% of the maximum information (Tovee et al., 1993; Kjaer et al., 1994; Van Rullen et al., 1998). Additional data emphasizing the speed of processing comes from a human *EEG* study where pictures in an animal/no-animal categorization task were flashed for only 20 ms. Observers exhibited an accuracy of over 90% and the reaction times peaked at 400 ms. Differential event-related-responses (ERPs) appeared 170 ms after stimulus onset.

Reaction times for the recognition task were even faster and subjects were more accurate, i.e. reaction time peaked at 337 ms and accuracy was over 98% (Delorme et al., 2004). Recent results again from *EEG* studies argue that the early *ERP* differences do not reflect object or category recognition per se, rather they are meant to be the trace of attribute postsensory decision processes (Johnson and Olshausen, 2005). Nevertheless, as shown by its high accuracy, the visual system was able to extract sufficient information from an image flashed for only 20 ms. Findings in flight control of the fly which are able to change direction within 30-40 ms in response to an external stimulus is another example which challenges the concept of averaging neuronal activities over large time windows (Borst and Haag, 2002).

With the advance of electrophysiological methodology it became possible to test population encoding theories, which argue that the brain uses ensembles of neurons as an encoding substrate. Recent findings show that even simple behaviors of vertebrates are concerted by a large number of neurons, e.g. visuomotor response guided by populations of neurons in the superior colliculus (Lee et al., 1988; Crish et al., 2006) or the direction of arm movements predicted by cell populations in the motor cortex of monkeys (Georgopoulos et al., 1986b).

The population-rate which assumes a large amount of neurons with similar intrinsic properties and equal input output connections was criticized as well, since it demands neuronal substrates which probably only reflect a minor fraction of the projection patterns present in brains. Hence it can be assumed that a certain amount of heterogeneity is omnipresent and that the connectivity does not follow a simple feed-forward input-output pattern. The *population vector* coding which is an extension of the basic population-rate idea partially solves this problem. It defines the rate as weighted population average and in that way allows heterogeneity in a suitable defined population of neurons. The scheme was successfully applied to recordings of monkey motor cortex, to understand the coding of arm movements in neuronal ensembles (Georgopoulos et al., 1986a).

An alternative group of encoding schemes assumes that information is not encoded in rates but in precise spike timing of single neurons or populations (Tiesinga et al., 2008). Temporal schemes use the precise spike timing and the temporal correlation of spikes to encode information. Like the rate code schemes they were proposed on a single neuron level or in ensembles of cells.

The separation between temporal and rate encoding is not always clear, especially if the rates are based on small time bins. On one hand a precise spike-timing per se does not guarantee that the information is encoded in the temporal domain. On the other hand a rate code is most likely consistent with a *time-to-first spike* temporal scheme, since neurons with higher rates will presumably elicit the first spike earlier than those with low rates. The rate and temporal idea are conceptually different however. In temporal

encoding schemes neurons transform stimulus information into the temporal domain, which might not be temporal in nature, i.e. the spikes in time do not have to reflect stimulus modulations over time. In order to exclude that the timing of events is induced by stimulus modulations only, a rigorous definition only accepts the term *temporal coding* if the temporal structure of the spike code is more precise than the temporal structure of the stimulus (Theunissen and Miller, 1995). However most of the literature does not adopt this rigorous definition, and accepts a code to be temporal if the precise spike timing contains more information than a rate based code.

The importance of exact phase relationships in neuronal activity or precise spatio-temporal spike patterns in general was extensively investigated in several experimental (Eckhorn et al., 1988; Engel et al., 1991; Engel et al., 1992b; Engel et al., 1992a; Abeles et al., 1993; Schillen and Konig, 1994; Singer, 1994; Lestienne, 1996; Maass, 1998) and model studies (Abeles et al., 1993; Schillen and Konig, 1994; Wyss et al., 2001; Wang et al., 2003; Wyss et al., 2003a; Wyss and Verschure, 2003). A widely established model uses precise interaural time differences (ITDs) of spike latencies for sound localization (Carr and Konishi 1990; Skottun, 1998; McAlpine and Grothe, 2003).

Several areas in the visual pathway of monkeys and cats revealed to produce temporal encoding schemes as well. The precise spike timing correlation patterns between pairs of *LGN*-neurons contain considerably more information than the spike count. On average an increase of 20% for strongly correlated pairs was found (Dan et al., 1998). The authors conclude that the precise temporal correlation could be used as an additional information channel between the thalamus and the primary visual cortex. Later Buonomano proposed that cortical organotypic slices produce reliable action potential times up to 300 ms after a single stimulus (Buonomano, 2003). The authors assumed that the timed late responses are the result of the propagation of activity throughout the network, i.e. a population of neurons was able to produce precise spike timing.

Previous work in cat area 17 suggested that synchronization of neuronal activity relates spatially distributed features belonging to one object. But a closer look to new cell recordings revealed systematic deviations of the zero phase lag on a millisecond scale (Konig et al., 1995). The data shows that the phase lags are feature specific which supports the idea of coarse encoding of stimuli with populations of optimally and sub-optimally tuned neurons. Another electrophysiological study in area 17 which shows a rapid onset and offset of *LFP* (local field potential) synchrony among interacting populations of neurons comes to a similar result (Gray et al., 1992). The additional information content contributed by temporal information seems to be stimulus dependent however. In extracellular recordings of cat *V1* only transient stimuli, i.e. drifting edges, were able to code contrast temporally in spike time and Fourier space, while non-transient, i.e. drifting sine waves, were not. It is argued that an abrupt change in the adapted state which could signal a behaviorally relevant stimulus change triggers temporal structuring of spike trains (Mechler et al., 1998). A study in the areas *V1* and *V2*

of anesthetized monkeys additionally shows that the spike timing precision varies with stimulus modality (Victor, 2000), with the contrast modality producing the highest timing precision in both areas. The additional modalities, i.e. size, orientation, spatial frequency and texture type, revealed an area-specific temporal precision.

Systematic analysis of cell responses to *Walsh-patterns* in area *IT* of alert monkeys further revealed that the temporal structure of the spike train contained supplementary information which could not be explained by the spike count (Richmond et al., 1987). An additional study compared the cell responses of several areas in the visual pathway of awake monkeys in one experiment, i.e. retinal ganglion-, *LGN*-, *V1*- and area *IT*-cells (McClurkin et al., 1991). During presentation of stimuli based on *Walsh*-functions all four stages simultaneously carry multiple stimulus-related temporal code segments in a multiplexed manner. The complexity of the temporal messages increases along the visual pathway, and the temporal codes of the different stages seem to overlap in time. This supports the notion of parallel processing with feedback and lateral interactions to refine computations based in the first sweep of information that is transferred across the visual hierarchy. Temporal coding of information was also found outside of mammals. The weakly electric fish elicits synchronization/desynchronization of the electroreceptor population depending on the social context, without changing the mean firing rate (Benda et al., 2006). The projection neurons in the antennal lobe of the locust, a functional analog of mitral-tufted cells in the vertebrate olfactory bulb, seem to encode odors in spatially and temporally distributed ensembles of coherently firing neurons (Laurent et al., 1996).

Overall, experimental evidence accumulates that neurons consider the fine temporal structure of spike trains to augment their encoding power. Especially in conjunction with population encoding temporal schemes suggest an interesting way how neuronal networks convey and process information about the external world in an accurate, fast and robust manner. However, the simultaneous recording of a large population of neurons with millisecond time resolution is difficult and often still out of reach with current methods. Hence a lot of the temporal considerations on the population level are model based. Abstract model approaches use the time-to-first spike in neuronal populations (Hopfield, 1995; Sejnowski, 1995; Jensen and Lisman, 1996), or the phase of single spikes compared to a global oscillation as the base for coding stimulus information. The model approach used in this thesis, i.e. the Temporal Population Code (*TPC*), uses in contrast full spike train sequences to encode stimulus information on a time scale comparable to biology (Wyss and Verschure, 2003). It exhibits biologically plausible connection patterns of recurrently connected neurons, and reveals to maintain the encoding robustness even under noisy conditions. It is therefore a strong candidate.

2.2 Noise in spiking neuron networks

It seems that neurons in principle can react in a very reliable manner. Spatially uniform random flicker elicits a reproducible spike train in retinal ganglion cells (Berry et

al., 1997). The same is true for neurons in the extrastriate cortex of behaving monkey, which respond to temporally structured stimuli with markedly reproducible temporal modulation (Bair and Koch, 1996). However in the absence of temporally structured stimuli single cell recordings of cortical neurons are generally characterized by a large amount of irregularities. The question whether the virtually random spikes that appear in these neuronal recordings are really noise or just an efficient way of coding information on a network level cannot easily be answered. Recent findings propose that the activity of populations of cortical neurons represent probability distributions which are combined by *Bayes'* rule (Ma et al., 2006). The authors argue that the Poisson-like variability in the responses reduces a broad class of Bayesian inference to simple linear combinations of population activity. But in general trial-to-trial variation which cannot be attributed to any external stimulation is considered as noise, i.e. spikes which do not carry information about the presented stimulus.

The origin of noise is poorly understood. Beside variation in the external stimulation, some is attributed to cell inherent properties, e.g. stochasticity of ion channels (Schneidman et al., 1998) or thermal noise in the system, which can lead to spontaneous firing. These effects are often called intrinsic noise. On the other hand there is also external noise, i.e. noise due signal transmission and network effects. Only about 10-30% of presynpaptic spikes do elicit a postsynaptic response (Markram and Tsodyks, 1996). Due to the limited understanding of the origin of spike irregularities, noise in modeling is commonly added externally on a single-neuron level and in the form of additional Poisson distributed spikes.

2.3 Quantifying the information

Estimating the information in a spike train or more commonly how reliably a system transmits information are topics covered by information theory. Many current methods and knowledge about how information can be transmitted over a noisy channel, are based on seminal publications of C. E. Shannon (Shannon, 1997). To give a complete overview on this topic is far beyond the focus of this section. A detailed introduction into exploration of neural codes and the quantization of information is available in *Spikes* by Rieke et al (Rieke et al., 1999). In the current section only an introduction in the notions used in this thesis is given. More detailed information about how the concepts were applied to the data is available in the respective result section.

Analogue to Shannon's view the neural system can be seen as a communication system which transmits source messages (X) about the stimulus over noisy channels to a receiver that converts it back into destination a message (Y). We observe the output Y and are trying to gain information about the input X, whereas X is the sensory signal and Y is a set of spike time arrivals, or a single value covering the spike times, e.g. the temporal correlation between two spike trains.

In practice the process of spike train analysis can be separated into several steps (Awiszus, 1997). First the recorded data has to be processed by extracting single unit action potential occurrences in time. This is usually done with elaborate spike sorting algorithms. Due to full control over all parameters, i.e. single cell and high temporal resolution, this step can usually be omitted if one deals with responses produced by model networks. Depending on the assumed encoding scheme the spike times are then binned in the second step. For temporal encoding this is usually a small time bin around one millisecond. For spike trains of single neurons, due to the refractoriness of the cell, this leads to a binary representation of the spike trains, i.e. strings consisting of *1s* for spikes and *0s* for no-spikes. In a third step information content is quantified. A characteristic measure of the maximally available information or the variability in such strings is the entropy. It was first applied and estimated in neuronal data by McKay and McCulloch (MacKay and McCulloch, 1952). The entropy per spike is dependent on the selected time bin size and on the mean spike count in the strings, being small for low timing precision and for high mean spike count (Rieke et al., 1999). The entropy of a whole spike train corresponds to the $\log_2 K$, where K represents the number of all distinguishable spike trains given the time bin size. In an ideal code all the individual spike trains would correspond to individual stimulus classes. Hence the entropy sets a physical limit a neuron can convey with a spike train. Related to the entropy is the term *mutual information.* Intuitively it describes how much our uncertainty about the input X is decreased when we know the output Y. Presumably, only a limited set of signals X is consistent with an observation Y. This reduction in entropy is the information gained by observing Y. The average information gain by observing Y is defined as the *mutual information,* which by definition cannot be bigger than the entropy.

In the simulations of this thesis the upper concepts were not applied directly to spike trains but to input/output alphabets based on stimulus classes and network response classes. However, the response classes were calculated based on temporal correlations of spike trains produced by populations of model neurons.

2.4 Summary

With the advances in recoding techniques and data analysis tools the collection and interpretation of population data has come into reach, and allowed new insights into the manner how neuronal networks encode the external world. In the last years more and more information accumulated that temporal encoding may represent a crucial encoding scheme in neural networks. Recording data of neurons in the mammalian visual pathway which was previously assumed to reflect rate based encoding at a closer look exhibits complex and precise spike timing. To understand the underlying encoding schemes is a crucial step to relate the brain anatomy, i.e. neuronal properties and connectivity patterns, to the function, which is one of the main goals of current neuroscience. Modeling studies can help to provide deeper insight into the biophysical-functional relationship, since they

allow control over parameters which are not accessible in vivo. The Temporal Population Code presented in this model, uses the current knowledge about anatomical substrates in the visual pathway and votes for a functional role of the in vivo connectivity patterns in the formation of temporal codes representing the external world.

Chapter 3

Localization acuity & object categorization performance

A high visual acuity is the prerequisite to detect single features in a visual scene, i.e. distinguishing between features which are spatially very close to one another. On the other hand the ability of animals to categorize objects is a crucial skill to survive in a complex environment. It allows them for example to distinguish between predator and prey, or puts them into the position to select the most appropriate behavior in new situations which are related to ones experienced in the past.

3.1 Measurement of the primate visual function in psychophysics

Visual perception occurs inside brains, and cannot easily be measured directly. The performance of the human visual system is therefore usually measured via psychophysical tools. Most psychophysical studies are designed to determine a perceptual threshold, which is defined as the minimum value of a certain stimulus parameter, i.e. the independent variable, required to elicit a desired response. Random variations in the physical stimulus or in physiological and psychological states of the brain introduce noise into the system. That's why the psychophysical method has to be chosen carefully, and stimulus presentations usually have to be repeated several hundreds of times to exhibit a meaningful average performance. A common protocol is the two-alternative-forced-choice (*2-afc*). In a *2-afc* task observers are forced to choose one of two time intervals, or one of two positions in which the target stimulus appeared, or *left vs. right* in a *Vernier line discrimination task* (Westheimer and McKee, 1977b; Poggio et al., 1992; Fahle et al., 1995b). The approach has several advantages, first it allows for control of subject biases, i.e. guessing rate is trial number dependent, and second the examiner can provide the subject feedback about the correctness of the response on trial-by-trial bases. To accurately measure the relationship between external world and internal perceptual response, one has to use stimuli with physically well-defined properties. Usually one property of the stimulus is varied, e.g. distortion level in a categorization task or displacement magnitude in a line discrimination task. The test subjects signal their perception verbally, by button-presses, or by eye-saccades. The gathered responses over a limited range of the independent variable are subsequently fitted to a model described by the psychometric function, which is thought to underlie perception. The psychometric function is usually of a sigmoid shape. In the simplest case the threshold is the value of the independent variable at half height between chance level, i.e. 50% in a *2-afc* task, and 100% correct. State-of-the-art methods can deal with small data sets, correct for stimulus independent biases, and use bootstrap algorithms and adjusted goodness-of-fit analysis to

estimate the optimal parameter set (Wichmann and Hill, 2001b, a). In addition they reveal confidence intervals for all relevant variables, i.e. slope and threshold of the psychometric function.

A way to understand the threshold variability observed in psychophysical tasks, and to control subject biases, was introduced by signal detection theory (Norton et al., 2002). Neurons are not completely deterministic. Recordings of neuronal activity are characterized by a high degree of irregularity. Especially responses to static stimuli which do not exhibit any temporal structure, lead to random occurrences of spikes. These trial-to-trial variations in responses are often considered as noise. One way to perform a comparison between the signals in presence or in absence of a target is termed Receiver Operating Characteristics (*ROC*). Responses to target stimuli and to non-target stimuli or noise-only responses represent two distributions along the selected criterion e.g. spike counts or temporal correlations of spike patterns (***Figure 3.1***). The amount of overlap between the two distributions can be interpreted as the difficulty to distinguish two stimulus classes - the bigger the overlap the more difficult the decision. Whether an observer categorizes a presented stimulus as member of the first or the second distribution depends on his individual threshold, which is set to a task dependent optimum. The threshold divides the overlapping distributions into four regions which can be attributed to true positives (*TP* or hits), false positives (*FP* or false alarms), false negatives (FN or misses), and true negatives (*TN* or correct rejection). The false alarms (*FP*) plotted against the hits (*TP*) for each possible threshold represents the receiver operating characteristics curve. The curve defines a tradeoff characteristics, i.e. the proportion of false alarms (*FP*) made while detecting a given fraction of targets (*TP*), and vice versa. It can be shown that the area under the curve is equivalent to the *Man-Whitney U* which tests for the median difference between scores obtained in the two distributions. A perfect classifier would exhibit an area of *one*, and completely random system an area of 0.5 with a curve equivalent to the diagonal. The curve can be represented in a single value (*d'*), which is calculated as the distance of the means of the two distributions divided by their standard deviation. Under the assumption that both distributions are normal and have the same standard deviation, the shape of the *ROC* curve depends only on *d'*.

Signal detection theory also applies to human perceptual responses. Stimulus strength near the threshold, e.g. line segment displacement of only a few arc sec in a *Vernier line discrimination task*, leads to distributions which overlap almost over the whole range of perceptual responses. For bigger line displacements the distributions are shifted to larger distance, i.e. less overlap between the two. As *d'* increases the *ROC* curve becomes increasingly curved. The corresponding area under the *ROC* curve would approach *one*. The actual criterion depends on what is important for the subjects in the actual task. An animal which has to detect predators would set its criterion threshold very low, for detecting all possible enemies, with the tradeoff of frequent false alarms. In a situation where false alarms are punished, as in the line discrimination task, the criterion is shifted to higher values.

In practice in addition to the perceptual threshold often the observer's trial based reaction time is collected as well. This allows observation of the learning dynamics during the experiment, and gives feedback about the processing speed and the possible underlying neuronal systems.

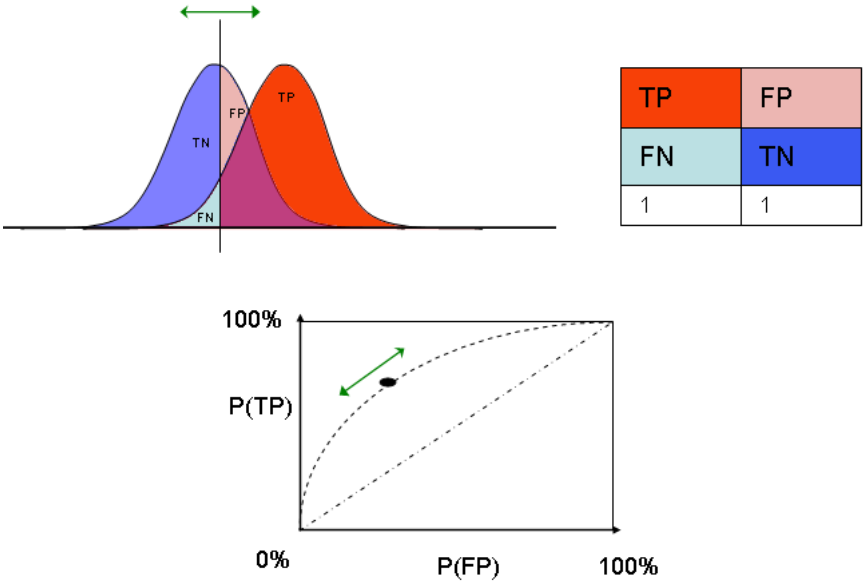

Figure 3.1: Receiver Operating Characteristics (*ROC*): Responses to target stimuli and to non-target stimuli or noise-only responses represent two distributions along the selected criterion e.g. spike counts. The amount of overlap between the two distributions can be interpreted as the difficulty to distinguish two stimulus classes - the bigger the overlap the more difficult the decision. The *ROC*-curve describes the difficulty as the dependency of the hit rate (*TP*) on the false alarm rate (*FP*). Whether an observer categorizes a presented stimulus as member of the first or the second distribution depends on his individual threshold, which is set to a task dependent optimum.

3.2 Performance of the primate visual system

In the past decades many properties of mammalian vision systems were investigated. In this thesis we focus on the encoding and decoding of spatial stimulus features into their neuronal representations. Deeper insights into these coding processes are the base to understand the classification and object recognition performance of biological systems, and finally can help to attribute functions to the observed anatomical structures of the involved visual areas.

Primates with their highly developed visual system exhibit an amazingly high performance in localization acuity or object categorization/detection task. A large amount of studies deals with the performance of human observers in localization acuity tasks like the famous *Vernier* line discrimination. In this psychophysical task the subject has to

detect the displacement of two vertical line segments. The performance of highly trained subjects is surprisingly high and is often smaller than the minimal receptor distance in the retina, i.e. only a few seconds of arc compared to about 30 seconds of arc as the receptor center-to-center distance in the fovea (Foley-Fisher, 1973; Westheimer and McKee, 1977a; Harris and Fahle, 1995, 1996). The performance is thereby depending on the retinal eccentricity, with the smallest thresholds in the foveal region. The learning dynamics depends crucially on the feedback given to the observer. Subjects which get no trial based error signal only marginally increase their performance during many repeated presentations (Herzog and Fahle, 1997, 1999). The fact that an increase in performance is neither transferred between the eyes, nor the retinal position nor between line segment presentation angles (Fahle and Morgan, 1996) lead to the conclusion that early stages in the visual hierarchy, e.g. the striate cortex, with their monocular cells and retinotopy are responsible for the performance changes.

Categorization tasks in which sample stimuli have to be attributed to predefined categories were widely investigated in the past. A huge amount of literature in different research areas is available. Most recent results and a closer review of older studies reveal that humans probably have several, at least four, strategies, and correspondingly several distinct neuronal networks involved in category learning (Ashby and O'Brien, 2005); (Ashby and Maddox, 2005). These categorization types, i.e. *rule-based tasks (explicit reasoning), information-integration tasks (x-ray interpretation), prototype distortion tasks (dot pattern classification), and the so-called weather prediction task*, seem to be so different that they have to be judged independently. Furthermore one has to distinguish between category representation and category formation during learning of new categories. For an excellent review about category types and category learning see (Ashby and Maddox, 2005).

Humans are remarkably fast in categorization and detection tasks. If tested with highly trained categories like detection of animals or faces a human observer can notify the target in as little as 120 ms, by an eye saccade (Kirchner and Thorpe, 2006). In addition it was reported that subjects categorize an object as fast as they detect it (Kalanit and Nancy, 2005). In dot pattern prototype distortion tasks humans draw a decision boundary, i.e. member/not-member of the category, based on the distortion level. Referring to the performance observers asymptotically increase their accuracy to an upper limit, with a parallel decrease of the reaction times.

In spite of the large amount of data and increasing insight a detailed knowledge about neuronal networks which perform with hyperacuity is still lacking. It remains unclear what biophysical changes on a neuronal and network level underlie the performance increase during learning of *Vernier* tasks. This thesis argues towards a system which uses precise spike timing of a recurrently connected neuronal population as a coding substrate, which satisfies the restrictions drawn by psychophysical collected data.

Chapter 4

Biology of object recognition and categorization

4.1 The Visual Pathway

4.1.2 The retina

Much of the primate cortex is devoted to visual processing. In the macaque monkey at least 50% of the neocortex appears to be directly involved in vision, with over twenty distinct areas (***Figure 4.1***). In the past the visual system of mammals was often considered as a hierarchical feed-forward system, containing the eye and the visual brain areas, which enables the individual to gain a coherent perception of its visual environment. The light that enters the eye passes through the cornea and the lens before being focused on the retina, where it elicits a biochemical cascade mediated by photopigment molecules stacked in the outer segments of the photoreceptors in the outer nuclear layer – the rods and cones. The rods are responsible for the scotopic vision (nightvision) and are totally saturated during daylight. Cones, responsible for daylight vision come in three subtypes with distinct spectral absorption functions, which form the bases for chromatic vision (Gegenfurtner and Kiper, 2003; Kiper, 2003). The packing density of the receptors depends on the retinal eccentricity. Close to the fovea, where the optical aberration is the smallest and only small cones are present, the receptor center-to-center distance is approximately 20-40'' (Christine A. Curcio, 1990). More peripheral the packing is lighter, and consequently, the spatial acuity, which is the smallest detail that can be detected, is decreased (Norton et al., 2002).

Already in the retina the incoming information is processed. First in an analog way by horizontal- (outer plexiform layer), bipolar- and amacrine cells (inner plexiform/nuclear layer), which distribute the sensory information along horizontal and vertical pathways, and later by the retinal ganglion cells, the first spiking neurons in the visual pathway. The activity of ganglion is modulated by inputs from a restricted area of the retina forming the receptive field. Most of the receptive fields of the ganglion cells have two prominent features, they are circular and they exhibit center-surround ON- and OFF-regions. ON-center cells are excited when light falls onto the center of their receptive field, light onto the surround inhibits them. OFF-center cells show the opposite behavior. In the foveal region the receptive field center size of primates corresponds to approximately one minute of arc, whereas in the periphery they usually bigger and reach up to ten minutes of arc (Lee et al., 2000). Due to the retinal network interactions and cell intrinsic properties already these early components of the visual pathway exhibit a

complex temporal response behavior to chromatic or achromatic stimuli (Benardete and Kaplan, 1999, 2000). Because of the center-surround opponent organization (ON-/OFF-regions) ganglion cells are mainly sensitive to local contrast differences and only weakly to an overall illumination of a larger fraction of the visual field, which makes them good transponders for local object features. Two subtypes of ganglion cells where identified, i.e. *M*- and *P*-cells, which form the bases for two information streams that seem to be kept separated from the lateral geniculate nucleus (*LGN*) up to higher areas of the vision system.

4.1.3 The lateral geniculate nucleus (*LGN*)

Ninety percent of the retinal axons terminate in the lateral geniculate nucleus. The optic nerve fibers coming from the retinal ganglion cells cross and distribute at the optic chiasm before reaching the left and right fractions of this thalamic structure. The *LGN* exhibits a layered structure, receives topographic input from the retina and sends its projections to the primary visual cortex. The receptive fields of *LGN*-cells inherit the concentric ON- or OFF-center receptive fields from the corresponding retinal ganglion cells. 50% of the *LGN* represent the small foveal region, while the peripheral region is much less well represented. The lateral geniculate nucleus of primates contains six laminae dividing into two ventral magnocellular layers (M channel) and four dorsal parvocellular layers (P channel). An individual layer receives input from one eye only. P layers receive input from P ganglion cells only, and respond to color changes between red/green and blue/yellow regardless of their relative brightness. M layers in contrast contain cells which get input from M ganglion cells only, and respond weakly to color differences when their brightness is matched. In addition *M*-layer cells tend to have lower spatial resolution and higher temporal resolution than *P*-layer cells. As a consequence P cells are critical for vision which requires high spatial and low temporal resolution.

As the converging point of almost all sensory information (not only visual) the function of the *LGN* has long been seen as a primary relay station between the periphery and the primary sensory areas of the cortex. However, more recent research has shown adaptational and modulatory properties of *LGN* cells (Sanchez-Vives et al., 2000). Precisely correlated spikes in *LGN*-cells seem to be able to code visual information (Dan et al., 1998). A further observation speaking against a pure relay function is the fact that the majority of synapses in the *LGN* originate from layer 6 pyramidal neurons in the primary visual cortex, i.e. feedback information. The corticothalamic afferents seem to control the response modes of the *LGN* cells, being either bursting or tonic which has important consequences on the oscillation properties of cortical columns in the subsequent primary visual cortex.

4.1.4 The primary visual cortex

Most of the efferents from the *LGN* terminate in layers 4Cα (M cells) and 4Cβ (P cells) of the primary visual cortex (also named *V1*, area 17 or striate cortex). *V1* contains

a retinotopic view of the visual scene with a disproportionate fraction representing the foveal region (a phenomenon known as cortical magnification). The primary visual cortex of humans is about 2 mm thick and exhibits the stereotypical six layered structure of the neocortex. The layers are numbered from the surface to the depth from 1-6. Layer 1, contains only few assumable inhibitory neurons. Layers 2/3 which do not show a distinct boundary, contain pyramidal neurons which increase their size from the surface to the depth. Beside of connecting the local proximity these neurons run axons to the deep layer 5, without forming synapses in layers 4 or 6 and send projections to other cortical areas. Most of the feed-forward input into layers 2/3 originates from layer 4Cβ and 4B, which gets its input from 4Cα. But the most pronounced connection pattern is formed by the horizontal projections which run within the layers 2/3 and mostly connect to other distant pyramidal neurons. The projections can extend up to several millimeters before they exhibit small axonal arbors visible as patches in stained slices (Kisvarday and Eysel, 1992). The major fraction of the axons seems to connect pyramidal neurons with similar physiological properties like orientation preference or ocular dominance (Gilbert and Wiesel, 1989). In addition most of the connections exhibit an anisotropic distribution, elongated along the preferred orientation (Bosking et al., 1997b; Kisvarday et al., 1997); (Sincich and Blasdel, 2001). Anatomical studies in cat area 17 a homologue to the human *V1* reveal a map of the whole cortical circuit with very few *strong* but many *weak* excitatory projections (Binzegger et al., 2004). Findings in ferret and cat showed that the lateral excitatory connections seem to distribute the information within the layer, while the inhibitory fraction seems to shift the response both in space and time, suggesting that inhibition driven by horizontal connections sculpts the distribution of activity in this cortical network (Hirsch and Gilbert, 1991; McGuire et al., 1991; Tucker and Katz, 2003; Shapley et al., 2007). At least in macaque monkey however the lateral connections seem to be too slow and cover too little visual field to subserve all the functions of the receptive field's suppressive surround of *V1* neurons. Beyond the coverage of the lateral projections feedback connections are the most likely substrate for contextual influences (Zipser et al., 1996; Angelucci and Bullier, 2003). This finding was questioned however by experiments with static texture stimuli in anesthetized monkeys. Inactivation of *V2* neurons, e.g. turning off feedback signals to *V1*, had no effect on the center/surround interactions in *V1*. Rather the main effect of *V2* inactivation was a decrease of the response onset in *V1* (Hupe et al., 2001).

Even though the 2D-projections of axonal arbors of different types of neocortical neurons in this areas appear to be highly dissimilar their one-dimensional metrics are surprisingly equal, and can be predicted by a random branching model (Binzegger et al., 2005).

While a lot is known about the feed-forward connections and their influence on the response of cortical neurons, the exact role of the lateral axonal arrangement is still under debate. Previously thought to be important in feature binding and contour integration by synchronization of neuronal groups (Singer, 1999b; Stettler et al., 2002;

Womelsdorf et al., 2007), evidence accumulates that this architecture allows computation of more complex functions like believe propagation (also known as sum-of-product algorithm to compute marginal probabilities in a factor graph (Wikipedia, 2009)(Wikipedia, 2009)(Wikipedia, 2009) or the transformation of information from the spatial- into the temporal domain.

The processed information leaves the primary visual cortex over distinct pathways. Layers 2/3 and 4B project to extrastriate cortical areas of the visual pathway (e.g. *V2*, *V3*, *V4*, V5, *MT*) whereas cells of the deep layers 5 and 6 project to the superior colliculus, the pulvinar, the pons and back to *LGN* or the claustrum.

Beside of excitatory pyramidal cells the cortex contains mainly two groups of small non-pyramidal cells, the excitatory spiny stellates and the inhibitory smooth stellates. These two types mainly use glutamate or aspartate and γ-aminobutyric acid (*GABA*) respectively as neurotransmitters.

Based on their response to elongated stimuli Hubel & Wiesel categorized the cells in the primary visual cortex into two major groups, the simple and complex cells. Simple cells show distinct ON- and OFF-regions in their receptive field, which are either in an even or odd arrangement. Complex cells on the other hand exhibit overlapping ON- and OFF regions. It seems that the simple cells integrate the information of distinct *LGN*-cells to gain their elongated receptive fields with the distinct ON- and OFF-regions. The complex cells subsequently seem to survey the activity of a group of simple cells, which shows a first convergence of the pathways from the retina over the *LGN* to the primary visual cortex, to develop the capacity for abstraction at higher levels, e.g. according to Hubel & Wiesel separating the visual scene into line segments.

If the physiological properties of the cells are examined a characteristic arrangement of the cell bodies appears. Neurons with similar properties seem to cluster together. In addition cells corresponding to the same point of the visual field form vertical columns which extend vertically over all layers. From a functional point of view the primary visual cortex is organized in overlapping maps covering orientation-, ocular dominance-, spatial frequency- and direction of motion domains. Hubel & Wiesel described the arrangement of the functional maps in their famous ice cube model. Later optical imaging studies confirmed their model and showed sharp borders between regions responsible for different preferred orientation (Ohki et al., 2006). A detailed view revealed a radial arrangement of the preferred orientations forming pinwheel-like structures. The exact relation between the orientation preference map and the retinotopic map is however still debated (Buzas et al., 2003). The ocular dominance map grouping cells which respond predominantly to the right or left eye only overlays the orientation preference map, and cuts it roughly perpendicular between the pinwheel centers. The further modalities, i.e. direction of motion and spatial frequency preference are represented in additional overlaying maps with distinct distribution patterns.

Whether color sensitive cells are grouped as well is controversial. Previously the cytochrome blobs, barrel shaped structures located in layers 2/3 were thought to be the processing centers for color perception in *V1*. However this view has changed with the discovery of sparsely distributed color sensitive cells all over the striate cortex (Kiper, 2003).

It was argued that the functional architecture of *V1* is the result of an evolutionary adaptation, and represents the optimal way to cover the most modalities in the smallest possible volume. However, the existence of species with highly developed visual systems, e.g. gray squirrel or rodents in general, which completely lack orientation preference or ocular dominance maps argues against a functional role of the maps, rather they could be an epiphenomenon of the development in some species (Purves et al., 1992). However whenever functional maps are present a patchy organization of lateral connectivity is there as well. So at least the dense lateral connections with the periodic small axonal arbors seem to have functional implications.

4.1.5 The extrastriate areas and object recognition/categorization

In monkey the term extrastriate cortex describes the sum of all visual areas after the primary visual cortex, i.e. areas *V2-V4*, *IT* (inferotemporal cortex), *MT* (medial temporal cortex). Already in *V1* a functional segregation of two information flows is apparent, which later in the extrastriate areas form two not-mutually separated streams with distinct functional properties, i.e. the dorsal and the ventral visual pathway (Ungerleider and Mishkin, 1982; Gattass et al., 1990; Haxby et al., 1991; Ungerleider and Haxby, 1994).

During object categorization or identification the response of cells in area *IT* seems to be task independent (Suzuki et al., 2006) and the last step which is dominated by the sensory perception of the object. Hence this stage is often considered as the endpoint of the ventral pathway (Gross and Schonen, 1992). It contains mainly neurons which recognize objects or object categories and the spatial relationship among object parts (Yamane et al., 2006), whereas area *MT* (medial temporal cortex) as the endpoint of the dorsal pathway revealed to be responsible mainly for object localization, motion and depth cues. However this functional and anatomical separation is not exclusive. Anatomical and physiological studies in monkey revealed an extensive crosstalk between the two streams. Area *MT* contains cells which are responsive to object categories as well (Kreiman et al., 2000). Nevertheless the vast majority of *MT* cells seem to be influenced much less by the shape or color of objects than area *IT* cells. The same is true for lateral intraparietal cortex (*LIP*, a high-level dorsal area) cells if compared to *IT* neurons (Lehky and Sereno, 2007).

Compared to the primary visual cortex cells in the higher visual areas have much larger receptive fields, e.g. 10 times larger in *V2* than in *V1*, and tend to respond to more complex shapes the higher they are in the visual hierarchy. While in *V2* the retinotopic

organization is preserved in the higher areas this anatomical organization pattern is replaced by a functional map which is no longer related to the position in the visual field. Area *IT* for example exhibits a clustering of cells which respond to similar complex features or objects in a columnar structure elongated vertical to the cortical surface (Tanaka, 2003). These cells show responses invariant to object size, or object position in the visual field and are mostly color sensitive. In addition the shape selectivity of these neurons remains the same even if partially occluded (Orban et al., 1996; Vogels and Orban, 1996).

Electrophysiological measurements in monkey inferotemporal cortex (*IT*) revealed that an accordingly small population of cells, i.e. 100 randomly selected cells, is able to represent the stimulus identity and category in an accurate manner. In a *SVM*-classifier analysis with only 12.5 ms wide time bins they perform with 70% correct 125 ms after stimulus onset (Hung et al., 2005). Beside animals and monkey faces the experimental setup did also include e.g. tools, fruits, and cars. Thus the first sweep of information reaching the inferotemporal cortex seems to contain a significant amount of category information not only for highly specialized categories but also for newly trained ones. A detailed analysis of the time course of information encoded in populations of *IT* neurons revealed that the early parts contain information about the global category, i.e. human faces versus monkey faces, whereas the fine categorization in the later part of the response (Matsumoto et al., 2005). Based on the evolving structure of the encoded information the authors suggest that the hierarchical relationship of the test stimuli is represented temporally by populations of *IT* neurons. This is supported by data which shows that feature configuration of whole objects is reflected in the modulation of spike correlation among populations of *IT* neurons (Hirabayashi and Miyashita, 2005). Spike correlation of cell pairs signaled the presence of face-like feature configurations within 300 ms after stimulus onset. Another study which shows that the response of populations of *IT* neurons is correlated with relative positions of several simultaneously presented objects in a scene (Aggelopoulos and Rolls, 2005), comes to similar results. However to what extent modulation of spike correlation in populations or precise spike timing in common are used to encode visual stimuli in the endpoint of the ventral pathway is still debated. A study which investigates whether macaque *IT* neurons bind stimulus features to a coherent object by spike synchronization reveals that maximally 6% of information is represented by stimulus-dependent spike synchronization (SDS), whereas between 94-99% can be explained by a rate encoding (Aggelopoulos et al., 2005).

In complex scenes, an important feature of *IT* cells is their reduction of the receptive field size to the size of the object fixated by the animal. The underlying mechanisms are unclear but it is argued that it plays a role in the optimal stimulus encoding under natural conditions, where the object of interest is presented simultaneously with clutter (Aggelopoulos et al., 2005; Aggelopoulos and Rolls, 2005).

The human object-selective brain areas were mostly investigated by *fMRI*. They indicate that the lateral and ventral occipito-temporal areas are important in perceiving and recognizing objects and faces (Grill-Spector, 2003). Additional insights were revealed by electrophysiological recordings in epileptic patients by Kreiman et al. (Kreiman et al., 2000). He found neurons that were selectively activated by certain classes of stimuli in the hippocampus, amygdala, and adjacent cortical areas.

With respect to the anatomy a prominent feature which is preserved in *IT* and all the other extrastriate areas is the earlier described extensive inner-areal lateral connectivity. Studies in monkey revealed a stronger anisotropy of the horizontal connections in area *IT* compared to the primary visual cortex, which was argued to be related to the functional properties of this stage in the visual hierarchy (Sincich and Blasdel, 2001; Tanigawa et al., 2005a). Additionally *LFP* signal analysis in area *IT* point to the horizontal connections as a possible anatomical substrate for the similar shape selectivity of these signals on a scale of 5 mm (Kreiman et al., 2006).

Beside to the feed-forward and horizontal information distribution all visual areas seem to be strongly modulated by feedback signals from higher stages the visual hierarchy (Zipser et al., 1996; Stettler et al., 2002; Angelucci and Bullier, 2003; Delorme et al., 2004; Huang et al., 2007). The importance of feedback signals in object recognition or categorization was questioned however when regarded in combination with the processing speed primate brains exhibit. In a forced choice task where two scenes are flashed simultaneously into the right and the left hemifield, human observers can reliably detect and saccade to the side which contains an animal or a face in as little as 120 ms (Kirchner and Thorpe, 2006). Macaques were able to reliably detect the presence of food or animals in pictures that were flashed for 80 ms only (Fabre-Thorpe et al., 1998). This lead to the conclusion that the processing needed for object recognition can only include one or two spikes per cell in each stage, and that massively fast feed-forward connections transport the information to higher visual areas like *IT*. However criticism aroused because of the target stimuli that were used in the experiments. Animals and faces are highly trained categories for which the primate brain could have developed distinct pathways involving specialized brain areas. Indeed *fMRI* studies revealed a specialized face-processing network in human brains, including core regions of the visual hierarchy and limbic and prefrontal areas as well (Ishai, 2007). The main entry point in face detection and recognition tasks seems to be the lateral fusiform gyrus. It has to be kept in mind as well that the onset latencies in the different visual brain areas do not follow a simple serial scheme. Rather they reveal a complex onset pattern, most probably produced by feedback and inner-areal lateral connectivity (Schmolesky et al., 1998a). Against a pure feed-forward speak clearly the presence of the large amount of lateral and feedback connections, which modulate cell activities in presence of stimuli. The functional consequences of the feedback connectivity were explicitly demonstrated in electrophysiological experiments in monkeys. First, at least in *V1* the feedback connectivity is responsible for part of orientation selective surround effects in the

receptive fields (Angelucci and Bullier, 2003). Second, all stages of the visual pathway seem to be strongly modulated by selective attention. Beside of the known bottom-up effects on attention several monkey studies point to a top-down (via feedback connections) information flow (Sarter et al., 2001; Buschman and Miller, 2007; Saalmann et al., 2007). Acetylcholine mediated modulation of the dendritic integration has shown to influence cells in the primary visual cortex as expected in attention driven tasks (Roberts et al., 2005).

In summary the early visual areas, i.e. up to *V4*, of the visual pathway exhibit a clear retinotopy, and contain cells tuned to distinct features of different modalities, i.e. sculpting feature maps in the orientation, ocular dominance or spatial frequency domain. The subsequent stages reveal increasingly complex receptive fields. This is especially true for the ventral pathway converging in the inferotemporal cortex (*IT*), which is attributed to object recognition and categorization. All the visual areas share fundamental anatomical patterns. They show the layered arrangement of cells common for the whole cortex, and exhibit fast feed-forward inter-areal connections. In addition all areas contain an extensive amount of lateral inner-areal projections that can extend several millimeters. They are typically slower than the feed-forward connections. The distribution of the connections seems to be the more anisotropic the higher the area in the hierarchy. The feedback connections which are present between all areas are distributed more uniform and can extend even further than the lateral connections.

In extreme cases the human neural processing machinery is able to encode the presented stimuli and to provoke an appropriate behavioral response in around 100 ms. Any model of coding in the visual hierarchy should take into account these speed restrictions, and should reflect the fundamental anatomical and biophysical properties of the networks. The model presented in this thesis reveals to fulfill these requirements and produces a robust and highly accurate stimulus code that evolves with biologically meaningful speed.

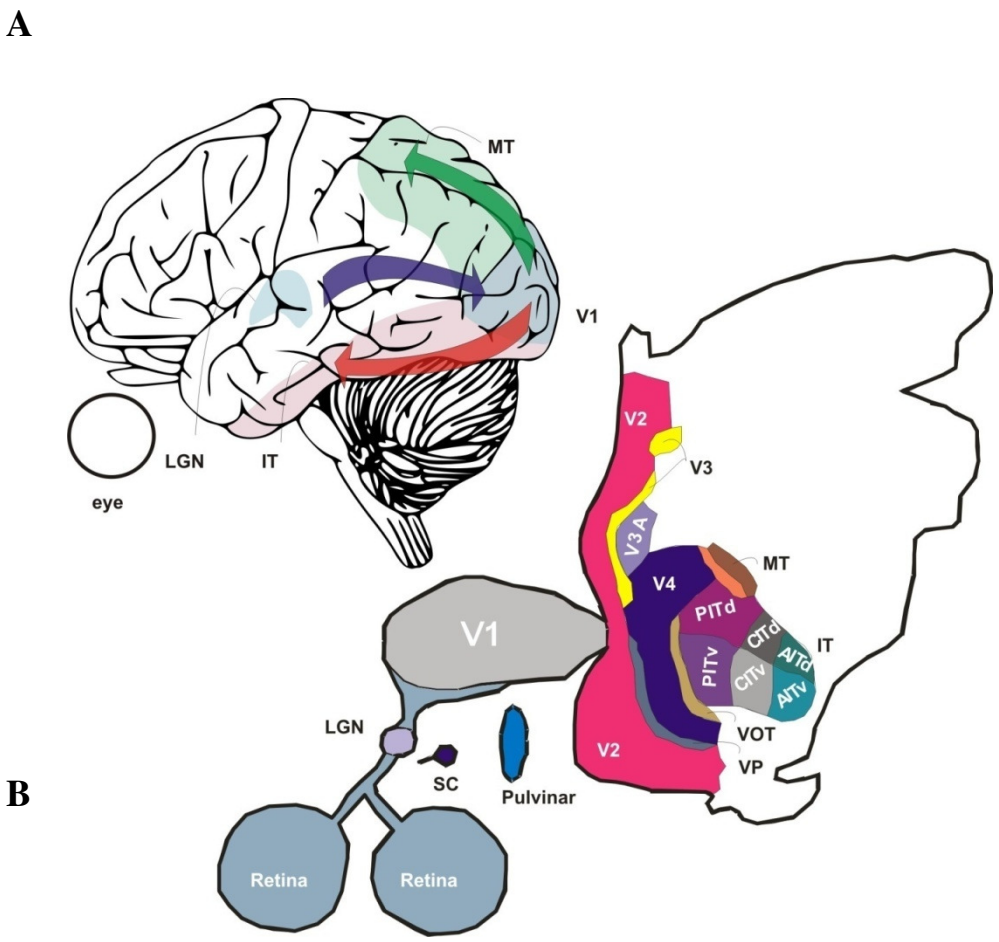

Figure 4.1: Schematic drawings of a human and a monkey brain: (*A*) Human brain with the main processing streams in the visual pathway. The optic nerve transports the visual information from the eye to the lateral geniculate nucleus (*LGN*), from where it is transmitted to the striate cortex (blue arrow). Two fundamental information streams are kept not mutually separated, i.e. the dorsal *where*-pathway projecting to area *MT* (green arrow), and the ventral *what*-pathway, projecting to area *IT*, presumably responsible for object recognition (red arrow). All structures are bilateral, whereas the right visual hemifield is transported to the left hemisphere and vice versa. (*B*) Flattened monkey cortex with visual areas. After the striate cortex (*V1*) a multitude of brain areas, summarized as *extrastriate cortex*, processes the incoming information in the two main information streams, i.e. the dorsal and ventral visual pathway ending at area *MT* and *IT* respectively. Illustrations are adapted from web (*A*) and (Van Essen et al., 1992) (*B*).

4.2 Learning dynamics and plasticity in object categorization

Cortical plasticity describes the organizational changes in the brain that occur as a result of experience. These alterations can profoundly change the pattern of neuronal activation and thus dictate system's category learning dynamics. As a consequence of stimulus exposure during learning, neurons increase their ability to reflect the stimulus categories by their activity. The learning dynamics in a given brain area are thereby crucially dependent on the task. Several categorization task schemes were described in the past (Miller et al., 2003; Ashby and Spiering, 2004; Ashby and Maddox, 2005). The focus of this study is on perceptual learning, perceptual categories, and their representation in the network activity. The two terms, although similar, describe two separate concepts in neural plasticity: perceptual learning is thought to occur any time the same or closely related stimuli are presented within a short time window. It sharpens the response of neurons exclusively based on stimulus features. Perceptual categories on the other hand describe the existence of neuronal response clusters which reflect acquired, task-dependent stimulus groups. Perceptual categories have more or less sharp boundaries even though the members on either side of the category boundary may vary only slightly (Ashby and Spiering, 2004; Ashby and Maddox, 2005; Ashby and O'Brien, 2005).

In recent years a multitude of brain areas were identified which are involved in category learning and category representation. Depending on their properties and their position in the processing hierarchy, they show distinct changes in their pattern of neural activation during task acquisition. The functional relationship between the observed learning dynamics and the underlying anatomical substrates is still poorly understood. The question remains how the existing projection patterns and the plastic properties of the neurons shape and restrict the observed response characteristics. In this section we review the gathered experimental data. We will conclude by emphasizing the importance of the dedicated interplay of information distributed by the horizontal and feed-forward connections, and the cholinergic feedback signals originating from the basal ganglia. The results put strong restrictions on possible explanatory learning models. The temporal population code model presented below satisfies most of these constraints. The model produces his spatiotemporal dynamics by virtue of the horizontal connectivity, and uses the activity as input to biologically plausible plastic synapses (Shouval et al., 2002b), in combination with modulatory cholinergic signals to fully augment its categorization performance.

4.2.1 Brain regions

The early stages (*V1-V4*): In the past it was thought that in contrast to late stages the lowest neocortical areas, e.g. *V1* or the primary auditory cortex, are not target of learning related reorganizations. But years of research have revealed that the very early steps already are subject to remarkable changes following stimulus exposure. These changes, which are often termed *perceptual learning*, can lead to changes in the selectivity in different modalities, e.g. orientation, contrast or direction (Fahle, 1994; Crist et al., 2001). The fact that some psychophysical performance improvements, e.g. in localization acuity, is not transferred between eyes, retinal position or orientation allowed to pinpoint the underlying mechanisms to the very early visual pathway, i.e. the primary visual cortex (Fahle and Morgan, 1996; Fahle, 2004).

Several studies also reveal top-down influences on the primary visual cortex. The neurons took over novel functional properties related to the attributes of the trained objects (Li et al., 2004). In addition neurons in *V1* responded very differently to the same stimulus depending on the involved task, suggesting that feedback information from higher cognitive areas is probably able to profoundly influence plastic changes occurring in the early visual stages. In particular suppression of signals that interfere with performance was reported (Ghose, 2004).

Inferotemporal (*IT*) & prefrontal cortex (*PFC*): Recent electrophysiological experiments in monkeys, allowed untangling some aspects of the neural plasticity in these stages.

Neurons in monkey *IT* cortex are able to acquire object selectivity throughout adulthood. Monkeys with *IT* lesions exhibit impaired object identification when the stimuli are transformed in size or orientation (Weiskrantz and Saunders, 1984), indicating view invariant prototype representations in the inferotemporal cortex (Logothetis et al., 1995). The invariance is not absolute however. Recent results indicate that *ITC* shows stronger selectivity for a trained orientation than for rotated versions of the stimuli (Freedman et al., 2006). Not all of the observed invariance seems to be experience related however. In a recent study Hung et al. show position and size invariant responses of *IT* neuron populations to novel objects not presented during training (Hung et al., 2005). *IT* cells however after learning show increased sensitivity to stimulus features which are relevant for the task (Hasegawa and Miyashita, 2002; Sigala and Logothetis, 2002; Sigala, 2004), which argues for a top-down influence in addition to the bottom-up stimulus driven information processing.

An intuitive view would argue that categorization performance is restricted by *IT* cells which sharpen their tuning properties during training. Recent findings however characterize the tuning of coding relevant *IT* cells after learning still as broad, covering several of the presented training stimuli (Kobatake et al., 1998). After training cells of

area *TE* in *ITC* were not sharply tuned to single training stimuli, but rather broadly covered several training stimuli. The cells responded to features common to several stimuli. The distances among the training stimuli in the response space spanned were thereby significantly greater in the trained monkeys than those in the control monkeys. The broad tuning was confirmed by measurement of *IT* single unit activity in macaques in a task where stimuli had to be grouped into *fish/no-fish* or *tree/no-tree*. The responses to the stimuli were fed into a Kohonen-self-organizing map (*SOM*), and the results suggest that populations of broadly tuned neurons, and not the fine tuned cells, are critical for categorization representation (Thomas et al., 2001). This contrasts the intuitive view that neurons reach a degree of specialization that allows in the extreme case a category representation by a single cell, aka *grandmother cell*. A more detailed analysis of the response properties uncovered that each *IT* cell occupies a tuning function in the multidimensional shape space, and integrates several contour elements of the trained stimuli (Brincat and Connor, 2004). Whenever a stimulus exhibits the features covered by these tuning functions, the cell becomes active.

Anatomical studies revealed that area *IT* exhibits a training related functional clustering of cells (Tanaka, 2003). Cells with similar properties are organized in columns pointing to the brain surface. Several of the columns are interconnected by long-range horizontal connections.

A comparison of *ITC* and the prefrontal cortex (*PFC*) in a single experiment revealed distinct roles of the two interconnected areas in the categorization tasks. *IT* cortex seems be mainly involved in the analysis of the stimulus features whereas prefrontal cortex shows a stronger tendency to encode stimuli by their behavioral meaning (Freedman et al., 2003). In contrast to *ITC* the prefrontal cortex changes the activity to reflect new behaviorally relevant groupings when stimuli are rearranged into new categories (Freedman et al., 2002); (Freedman et al., 2001). This botto*m-up stimulus driven & top-down task specific processing view* during categorization was confirmed by *fMRI* measurements in humans, using fast adaptation techniques (Jiang et al., 2007). Categorization training with fully parameterized stimuli (morphed cars) induced significant release from adaptation for small shape changes in the lateral occipital cortex irrespective of the category membership. In contrast an area in the prefrontal cortex (*PFC*) showed selective activity when the category membership of the stimulus was changed.

Again human *fMRI* measurements showed increased activity in *PFC* during presentation of categorical dot patterns, which contrasts the decrease of the *fMRI* signal in the visual areas for the same patterns (Reber et al., 1998a; Little et al., 2004). This was seen as an implication of the training induced specialization of the circuitry in the visual areas, while the prefrontal cortex increases its activity due to processing related to retrieving information about learned exemplars. Further, human subjects that performed a *yes/no dot-pattern categorization task* revealed mainly three brain regions with category

related activity (Reber et al., 1998a). A *posterior occipital cortical area* exhibited significantly less activity during processing of the category members than during processing of non-categorical patterns. And two higher visual areas, i.e. left and right *anterior frontal cortex* and right inferior lateral *frontal cortex* which showed increased activity during processing of the categorical stimuli. This is questioned however by another human study which shows decreased occipital volumes for categorical stimuli only when the category was learnt incidentally. Intentional learning in addition lead to an increase of volumes in the hippocampus, right prefrontal cortex, left inferior temporal cortex, precuneus, and posterior cingulate (Aizenstein et al., 2000; Reber et al., 2003).

The resulting picture implies that the perceptual learning of stimulus features in early steps is abstracted to more complex and behaviorally relevant categories in later stages. This view was confused by data acquired by Squire however (Knowlton and Squire, 1993; Reber et al., 1998b). He showed that amnesic patients, i.e. without declarative memory capabilities, who cannot learn to identify specific instances of objects, are perfectly able to form a category representation of the presented stimuli. Category learning appeared to be independent of declarative memory and thus unconstrained by limbic and diencephalic structures essential for remembering individual stimulus items (Knowlton and Squire, 1993; Squire and Knowlton, 1995). However recent experiments with normal participants and reinterpretation of the Squire data by Zaki & Nosofsky argue that object recognition and categorization have different memory requirements (Zaki and Nosofsky, 2001a), which were not equated correctly in the experiments of Squire. In this view the observed dissociation between object categorization and recognition is the effect of tasks inequalities, and do not necessarily imply parallel processing systems.

Hippocampus, amygdala and entorhinal cortex: The hippocampus, amygdala and entorhinal cortex receive input from temporal neocortical areas. Mammalian hippocampus cells transfer sensory information into memory. Macaque monkeys in delayed-match-to-sample task showed category related encoding of visual stimuli in hippocampus cells (Hampson et al., 2004). Each of the measured hippocampus neurons thereby used individual features combinations for the encoding, probably depending on their experience history. By extracting unique feature combinations the category cells are able to restrict their encoding to behaviorally relevant aspects of the stimuli, instead of encoding the full feature space. Electrophysiological measurements in human patients, which were part of brain surgery preparations, revealed a remarkable amount of hippocampus, amygdala and entorhinal cells with category-specific firing (Kreiman et al., 2000) as well. In the experiment the authors used visual stimuli from different categories including faces, natural scenes, famous people and animals, and performed *PSTH*- and subsequent *ROC* analysis to quantify the categorization performance. *fMRI* experiments in humans confirmed learning related changes in the hippocampal region during explicit learning of a dot-pattern categorization task (Aizenstein et al., 2000).

Experimental data from humans reveals that a subset of human medial temporal lobe (MTL) neurons selectively fire to complex images such as faces and objects. Furthermore the neurons exhibit an astonishing invariance over various stimulus modalities. They for example selectively become active for stimuli related to famous individuals, e.g. written names, pictures of the person or related objects (Quiroga et al., 2005b). This degree of multimodal invariance in single cells is unexpected, and also contrasts the findings in monkey areas which show unimodal broadly tuned neurons which points to population coding and not single cell representation.

Basal ganglia: The basal ganglia are a group of nuclei interconnected with the cerebral cortex, the thalamus and the brain stem. Five individual nuclei make up the primate basal ganglia, i.e. the striatum (with the putamen, the caudate nucleus and the nucleus accumbens) and the subthalamic nucleus as well as the substantia nigra. The striatum serves as the entry point for basal ganglia input to the neocortex. One feature which makes the striatum a candidate for category learning is the dopamine input it receives from the substantia nigra, which is widely thought to provide a signal in reward-related learning (Montague et al., 1996; Ashby and Spiering, 2004). The dorsal part of the striatum (head of the caudate nucleus) is known to be important in categorization related to task and rule-switching. Moreover lesions of the dopamine projections from the ventral tegmental area into the *PFC* have a paradoxical effect in *WSCT* (Wisconsin Card Sorting Test). *WSCT* is a neuropsychological test where subjects have to categorize a stack of cards based on a previously presented card set. Lesioning the dopamine fibers improves the performance of monkeys in an analogue of the WCST, even though it impairs their spatial working memory (Roberts et al., 1994). It turns out that the lesions lead to an increase of dopamine in the basal ganglia which results in the increased switching capabilities of the animals.

Many basal ganglia studies in rat and monkey report that the tail of the caudate is necessary for visual discrimination learning. Rats with lesions in this region no longer learn to elicit the correct behavioral response signaled by vertical or horizontal lines on platforms in a water maze task (Packard and McGaugh, 1992), i.e. categorizing the two platforms based on texture features is impaired. However they show normal learning rates if the expected behavioral response is signaled by the position of the platforms.

A recent human *fMRI* study which investigated the activity of the striatal regions, i.e. the head of the caudate, body, tail, and putamen revealed distinct activation magnitudes in the three regions during an observational task (Cincotta and Seger, 2007). In observational tasks subjects have to judge whether correct category labels where assigned to presented stimuli. Activity of the left head of the caudate was modulated by the presence of feedback, in a way that the activity with feedback was bigger. In contrast, the other regions, i.e. the body and tail of the caudate and the putamen were active to a similar degree in both conditions. These results support a functional dissociation between the striatal regions, such that the head of caudate is involved in feedback processing, and

further emphasizes the importance of the presumably cholinergic feedback signals in category learning.

Medial temporal area (*MT*) and lateral intraparietal area (*LIP*): The lateral intraparietal (*LIP*) and middle temporal (*MT*) areas are two connected areas of the dorsal visual pathway which are known to be involved in visual motion processing. In a recent study it was shown that area *LIP*, known to be implicated in visuo-spatial attention, motor planning and decision making, reflects the category of motion as a result to learning. The category boundary was readjusted after the monkey was retrained with newly grouped motion directions. In contrast the neuronal response in area *MT* was dominated by the perceptual similarity, and did not show relearning. Hence *LIP* might be important for the transformation of visual direction selectivity to more abstract task-specific representations (Freedman and Assad, 2006), while *MT* reflects the pure stimulus related response with less task-dependent top-down influence.

Basal forebrain: See the section '*Role of acetylcholine in perception and Learning*'

In summary, all visual and behavior related areas in the mammalian brain show learning related changes. The details gathered in the recent years sketch a complex interplay between different brain areas during visual category learning. Information collected and preprocessed in the retina is transmitted over fast feed-forward connections via *LGN* to the early visual areas. The retinotopic organized areas contain cells tuned to certain stimulus features, which are interconnected by an extensive amount of slower horizontal connections. The horizontal projections seem to couple cells with similar tuning properties, e.g. orientation preference. Already these early areas are target to experience related changes during stimulus exposure, i.e. perceptual learning. During category learning cells in the early stages show typically a continuous decrease in volume activation, which can be interpreted as the footprint for an experience related specialization. Perhaps a bit surprising is the fact that several studies couldn't show a significant learning related change of the tuning properties in the early visual pathway cells. Thus, the observed performance changes during category learning seem more a result of the altered pooling of the population activity in these early stages. Beside the feed-forward and horizontal connectivity all visual areas exhibit inter-areal feedback connections. From a tuning perspective they reveal an unspecific connection pattern and can extend even further than the horizontal connections. They seem to be part of a top-down information system which shapes the activity of lower visual areas based on past experiences or expectations. These fundamental projections patterns can be found along the whole visual hierarchy. A system of bottom-up-, inner-areal-, top-down-processing

appears which seems to be the anatomical substrate for the learning related changes in all visual areas, e.g. *V1-V4* or *IT*, even if they differ in their characteristics in the different areas. Neurons in area *IT*, one of the last perceptual stages in the visual hierarchy, are directly target to learning related alterations and show after training broad tuning functions in the stimulus feature space. On the population level they show an increase of categorization performance with training. Neurons with similar tuning features seem to be clustered in vertical columns, comparable to the retinotopic columns in *V1*. The areas after *ITC* like the prefrontal context reveal a strong tendency to group stimuli based on the behavioral category. While *IT* population activity reflects the feature based category *PFC* cell tune their responses to task-dependent stimulus groups, and show increased volume activation for categorical stimuli in *fMRI*. They seem to be strongly influenced by top-down signals, which allow the formation of abstract, not feature based categories. Later stages like the hippocampus follow the tendency to code for behaviorally important aspects of the stimuli. The hippocampus as the gate to memorization reveals to encode only the relevant aspects of the stimuli, and the different cells seem to decorrelate their activity to reach an optimal non-redundant representation of the features space.

Very widespread connectivity is exhibited from the basal ganglia as well, which can be seen as part of the top-down processing pathway. As several studies showed the transmission of information by virtue of the widespread dopaminergic system of the basal ganglia plays a crucial role in category learning. Parts of the basal ganglia are suspect to influence the processing of categories by reward signals. Lesions in the tail of the caudate lead to a loss of visual discriminations skills. Affected animals are no longer able to form stimulus feature based categories, although they do well on other modalities as for example position in space. On the other hand, an increase of dopamine in the basal ganglia which are interconnected with *PFC* leads to improved task-switching performance in rule based tasks in monkey.

As illustrated in one of the next sections, another system comprising widespread connectivity to the whole neocortex, the cholinergic system of the basal forebrain, plays an important role in perception and therefore in category formation, as well. Acetylcholine as the neurotransmitter of the cholinergic system has important effects in attentional tasks, by modulating the contextual influences in information processing.

The model presented in this thesis uses the described feed-forward- horizontal- and top-down interplay to fully exploit the encoding of visual stimuli.

4.3 Synaptic plasticity

Since decades studies try to investigate the neuronal mechanisms underlying category learning and object recognition. Already early on the synapses as the fundamental junction points between neurons were suspected to play a crucial role in the changes that occur during learning of new tasks and memorization, e.g. object category learning. Inspired by Hebb's postulate (Hebb, 1949) a large amount of experimental evidence for synaptic plasticity has accumulated. Hebb proposed that synapses change their weights depending on correlated firing of the pre- and postsynaptic neurons. The coincident firing of both neurons in this scheme leads to an increase of the weight which can last for several hours or even days, i.e. long term potentiation. A decrease of the synaptic efficacy in cases of uncorrelated firing of the two neurons is termed long term depression (*LTD*). During the last years the proposed learning rules became highly diverse. But the learning functions based on Hebb's proposal are still very popular and find their correspondents in many recent electrophysiological experiments (Bi and Poo, 2001). The appeal of Hebbian learning is that it only requires local information to perform the weight changes which is accessible by single synapses.

In the original formulation of Hebb's rule the exact temporal structure of spike trains is not considered. The question remains when two neurons are considered to be active at the same time. This question is addressed by *STDP* learning (spike-time-dependent plasticity). *STDP* proposes that the amplitude or even the sign of the synaptic efficacy change depends on the temporal delay between presynaptic spike arrival at the synapse and the postsynaptic action potential triggering (Markram et al., 1997; Froemke and Dan, 2002; Kepecs et al., 2002; Dan and Poo, 2004, 2006). *STDP* defines a temporal delay based learning window where the sign of the efficacy change switches around 0 ms, i.e. coincident presynaptic spike arrival and postsynaptic firing. Further it assumes that the bigger the temporal delay the smaller the weight amplitude change. Similar learning windows were found experimentally.

In the last years the learning schemes were refined by showing that the weight change is also dependent on the position of the synapse on the dendrite (Johnston et al., 2003; Froemke et al., 2005; Sjostrom and Hausser, 2006), or that under certain conditions a mixture of pre- and postsynaptic *LTP*/*LTD*-changes is induced (Sjostrom et al., 2007). Recent work even emphasizes the importance of astrocytes which actively influence the transfer and storage of synaptic information in the hippocampal area by increasing the probability of transmitter release without affecting the amplitude of synaptic events (Perea and Araque, 2007). Special interest was also devoted on how synapses which keep their plasticity over a lifetime keep their balance between adaptability and stability, i.e. between learning and forgetting (Abbott, 2003; Senn and Fusi, 2005a, b; Fusi and Senn, 2006).

It has also been recognized that calcium ions are important second messengers for the induction of *LTP* and *LTD* (Sjostrom et al., 2001). Particularly well investigated is the

NMDA synapse in the hippocampus where calcium enters through *NMDA* receptors, a glutamate receptor subtype. If an action potential arrives at the synapse glutamate is released into the synaptic cleft and binds to the *NMDA*- and AMPA-receptors on the postsynaptic site. The binding to the AMPA-receptors leads to an opening of associated ion channels, and as a result to depolarization of the postsynaptic membrane. When the depolarization is strong enough the block in channels controlled by *NMDA*-receptors is released and calcium ions can enter the cell. Calcium influx is the first step in a complex biochemical cascade that finally leads to a modulation of the glutamate sensitivity of the postsynaptic membrane, i.e. a change of the synaptic efficacy. Shouval et al. recently presented a model which changes the synaptic weight based on the calcium changes and the membrane potential (Castellani et al., 2001; Shouval et al., 2002b). The model reproduces many of the experimental findings, e.g. spike time dependence comparable to *STDP* learning and goes beyond: The model is able to reproduce the weight changes found in pairing experiments where the postsynaptic cell is clamped to a certain membrane potential and is stimulated via low frequency pulses injected via the presynaptic cell. In addition the weights converge to meaningful values in cases where the presynaptic frequency is varied. Together this data makes the model to a strong candidate to capture temporal aspects of spike trains.

In this thesis we show that the calcium based synaptic model can be used in category learning based on signals produced by the *TPC* models. The synapses capture the precise temporal aspects of the *TPC* model, and converge under the influence of top-down signals to weights which allow postsynaptic cells to distinguish between stimulus categories. The top-down signals model cholinergic input and represent a supervisor signal known to be important for many psychophysical tasks (Fine and Jacobs, 2002), e.g. category learning or localization acuity.

4.4 Role of acetylcholine in perception and learning

The wide innervation of cholinergic projections throughout the cortex (***Figure 4.2***) implies that acetylcholine (*ACh*) plays an essential role in information processing. Although the connectivity as a whole is very widespread retrograde axonal tracers indicated that the projection of individual cells is limited to a small cortical area of 1-1.5 mm in diameter only (Price and Stern, 1983). Several recent results postulate that *ACh* enables feed-forward input to dominate over intracortical, i.e. horizontal and feedback processing (Roberts et al., 2005). A long history of psychopharmacological experiments on the effects of nicotine and muscarinic receptor antagonists (such as scopolamine and atropine) have strongly implicated cholinergic systems in sustained attention (Sarter et al., 2001). In sustained attention performance, the subject knows where to expect what type or modality of signal, and how to respond in accordance with previously acquired response rules. The available evidence from studies on the effects of loss of cortical cholinergic inputs demonstrates that selective lesion of the basal forebrain is sufficient to

produce profound impairments in these tasks (McGaughy et al., 1996). The lesion-induced impairment in performance is thereby restricted to target trials only while correct rejections remain unaffected, reflecting the absence of the normally augmenting effects of cortical acetylcholine. The performance is affected by mechanisms that range from changes in sensory signal processing to the enhanced filtering of distractors and the modification of decisional criteria.

The capacity of the cholinergic system to reduce contextual target-distractor interactions makes it to a good candidate to solve the reported failure of a recently presented model (Wyss et al., 2001), which is based on horizontal connections, to accurately encode target stimuli in presence of distractors. The following section gives an overview about the known mechanisms how *ACh* influences information processing in the neocortex. How the concepts were applied to the model can be found in chapter 6, *Segmentation in a biophysically restricted population code*.

Early studies in cat have shown that cholinergic neurons within the basal forebrain give rise to a projection that terminates throughout the neocortex (Carey and Rieck, 1987). Via the neuromodulator acetylcholine (*ACh*) the projections influence a variety of cortical functions (Zinke et al., 2006). While the reports on the effects are diverse (Sillito and Kemp, 1983), e.g. depolarization, hyperpolarization as well as synaptic facilitation and suppression, the *ACh* effect on propagation of excitation seems to be very clear. Acetylcholine strongly suppresses intracortical connections through presynaptic muscarinic receptors, while at the same time it boosts thalamocortical/feed-forward afferents via nicotinic receptors (Kimura et al., 1999; Kimura, 2000; Roberts et al., 2005; Zinke et al., 2006). Previous findings in anaesthetized cats that acetylcholine can cause an improvement of the signal-to-noise-ratio (*SNR*) in *V1* (Everitt and Robbins, 1997) however could not be reproduced in later studies. But acetylcholine can reduce the variability of spike occurrences within spike trains (Zinke et al., 2006). Whole cell recordings from CA1 pyramidal cells in rat hippocampal slices revealed a postsynaptic effect of *ACh* which modulates somatodendritic processing of EPSPs. The reduction of the EPSP amplitude seems to be mediated by the cholinergic activation of a G protein-activated, inwardly rectifying K^+ (*GIRK*) conductance, which partially shunts excitatory input in postsynaptic compartments (Seeger and Alzheimer, 2001; György, 2005).

Additionally a characteristic electroencephalogram waveform, i.e. the theta rhythms (4-8 Hz), was associated with sleep & wakefulness and memory and learning tasks (Robert, 2005). The theta rhythms are believed to be vital to the induction of long-term potentiation (*LTP*), which represents a potential mechanism of learning and memory. A number of studies closely investigated the origin and effects of the rhythms (Patricio T. Huerta, 1996). They revealed that the rhythms can be induced by acetylcholine (*ACh*) or carbachol (*CCh*), and that they have a direct effect on the synaptic plasticity. While previous studies argued that an initial high frequency pulse determines the sign of synaptic modification, recent results reveal that in presence of theta frequency

oscillations can induce both, *LTP and LTD*. What determines the sign is the timing of stimulation with respect to the phase of oscillation.

In conclusion, *ACh* differentially influences feed-forward and lateral/feedback connections. The neuromodulator among other effects changes the center-surround effects in pyramidal neurons of the early visual pathway by reducing the extent of spatial summation. In addition it seems to play an important role in memory retrieval and learning in later stages of the processing hierarchy, i.e. it is able to switch between *LTP*- and *LTD*-modes of synapses. As chapter 6 reveals the modulation can be used improve the coding robustness of a model which uses the extensive lateral connections found in the neocortex as a coding substrate. In combination with fast feed-forward connections the model augments its full coding power in presence of distractor stimuli via *ACh* mediated modulation of dendritic integration. Chapter 8 finally shows that the same mechanism, i.e. reduction of EPSPs by partial shunting and attenuation along the dendrite, can switch between *LTP* and *LTD* in an *NMDA* synapse model. Hence the cholinergic input could constitute a supervisor learning signal which modulates cortical activity according to expectations or additional knowledge about a task.

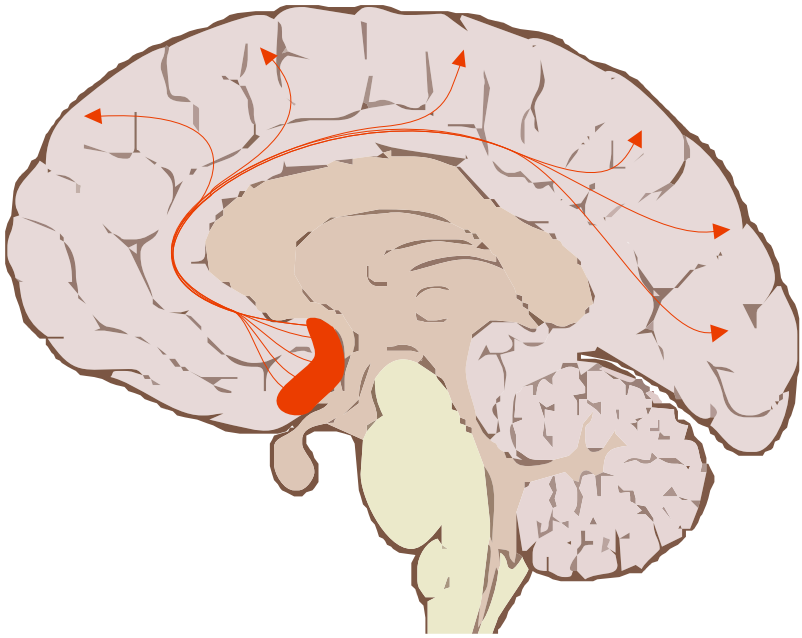

Figure 4.2: Cholinergic system of the brain: Saggital cut through the human brain with the cholinergic innervations of the cortex originating from the *Nucleus basalis* of the basal forebrain.

Chapter 5

Models of object recognition and localization acuity

Object identification and categorization are two fundamental tasks in object recognition. Whereas identification describes the process of recognizing a distinct object, e.g. the own dog, categorization names the task where an observer detects the class an object belongs to, e.g. animals. In the last years, computer vision made substantial progress. As it turned out object identification can be solved relatively easily and reliably in artificial systems, but even the most recent systems exhibit severe difficulties to categorize stimuli in a robust way. For biological systems, however, there are hints from reaction time studies that categorization is simpler or equally difficult as object identification (Kalanit and Nancy, 2005). In addition, at a first glance, identification and categorization seem to be dissociable in human subjects (Knowlton and Squire, 1993). Neuropsychology interpreted these findings as evidence for at least two independent systems working in parallel, in the primate object recognition machinery (Logothetis and Sheinberg, 1996). In contrast, in classical computer vision systems the two aspects of object recognition are usually two stages in a hierarchy, where the systems first separates and identifies the object based on a gathered features list, and subsequently categorizes it based on the identity. Recent biologically inspired object recognition systems however shed new light on the question whether parallel recognition systems have to be assumed in primate brains. They take the view that identification and categorization represent two points in a spectrum of generalization levels, rather than being two distinct tasks, or even parallel systems (Zaki and Nosofsky, 2001b; Serre et al., 2007b). Especially in prototype distortion tasks the distinction between categorization and identification is mostly semantic in these systems. In categorization the system has to generalize over bigger variations to form and detect a category, while in identification it has to exhibit specificity. Many of the recent biologically inspired models go back to the *Neocognitron* (Fukushima, 1980), a hierarchical multilayer network based on spatial feature detectors. This flavor of object recognition models were substantially improved in the last years and exhibit nowadays impressive performance and robustness (Rolls and Stringer, 2006; Stringer et al., 2006; Masquelier et al., 2007; Serre et al., 2007b). However these models completely neglect the temporal aspects of spike trains found in neuronal responses. Recently the temporal structure of neuronal activity has gained increased attention. Information theoretic, activity data analysis, and model studies emphasize the role of temporal coding (McClurkin et al., 1991; Buonomano and Merzenich, 1995; McClurkin et al., 1996; Bair, 1999; Buonomano and Mezernich, 1999; Singer, 1999a; Buonomano, 2000, 2003; Wyss and Verschure, 2003; Knüsel et al., 2004).

A lot of the modeling dealing with localization acuity in primates was based on theoretical mathematical models which are difficult to relate to biological situations (Wilson and Gelb, 1984; Wilson, 1986; Weiss et al., 1993). They propose that correctly weighted responses of features specific neurons in the early visual areas are the substrate to explain hyperacuity in trained subjects. However, they do not consider the temporally structured output of spiking neurons, and do not precisely state how the learning of the optimal weights is performed in strictly biophysically constraint neuronal networks.

Here we will argue that a recently presented model exhibiting a temporal code is extendable to reflect performances comparable to psychophysical results. We will report and justify the assumptions and simplifications in the model, and will take the standpoint that the model due to its close anatomical and biophysical relationship to the cortex reflects fundamental coding aspects of primate object recognition and localization acuity. For comparison reasons a selection of the recent hierarchical and temporal models is reviewed at beginning of the section.

5.1 Localization acuity models

In visual localization acuity tasks an observer judges the displacement of a target stimulus to a reference element (**Figure 5.1**).

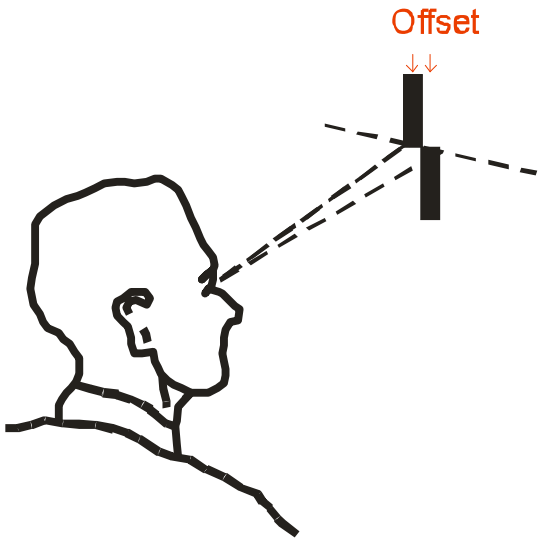

Figure 5.1: Human subject in a *Vernier* localization tasks: The observer has to signal the displacement side (*left/right*) of a line segment, compared to the reference segment. The threshold represents the minimal detectable offset between, measured as the visual angle.

5.1.1 Oriented filter banks

In the mid eighties of the last century H. R. Wilson presented a purely mathematical model of a system based on tuned filter banks that can gain hyperacuity in a *Vernier line discrimination task* (Wilson and Gelb, 1984; Wilson, 1986). The model

consists of a number of spatial filters resembling the receptive field properties of simple cells in the primary visual cortex. The filters comprise elongated excitatory and inhibitory regions which cover the full range of orientations and spatial positions. As the model shows slightly tilted receptive fields produce differential responses for vertical line segments, depending on whether the reference segment is displaced to the right or the left side (**Figure 5.2**). Thus, the slightly tilted ones and not the aligned receptive fields with the strongest responses are important for the differential output and the performance.

The model was able to reproduce performance functions for a range of psychophysical tasks, e.g. *Vernier* acuity, bisection acuity or chevron acuity. However the proposed model is purely based on filter properties of single units, and does not include detailed biophysical properties of neurons or anatomically plausible connectivity patterns.

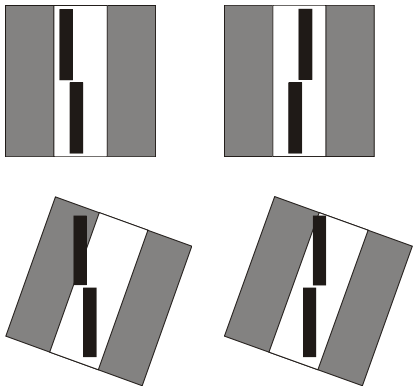

Figure 5.2: Receptive fields of cells in the early visual stages: Excitatory regions (bright) are flanked by inhibitory regions (dark). The excitatory regions exceed the displacement magnitudes of the *Vernier* line segments. Aligned and congruent receptive fields are excited the most (first row), but only tilted- (second row) or slightly displaced (not shown) receptive fields are capable to produce a differential response.

5.1.2 *HyperBF* related networks

Weiss et al. presented a model for perceptual learning with *Vernier* acuity (Weiss et al., 1993) based on concepts of Poggio & Girosi and Herzog & Fahle (Poggio and Girosi, 1990; Herzog and Fahle, 1998). The learning is based on a concept of hyper basis function (*HBF*) neural networks. In *HBF* networks the mapping is approximated by a sum of several functions (*Gaussian* basis functions with different widths), each one with its own prior. The authors use *HyperBF* networks and extensions to it, i.e. instead of radial symmetric functions as in *HyperBF* they also use orientation selective neurons similar to cortical simple cells, to produce hyper acuity in a line discrimination task. The processing in the basic version of the model contains two steps (***Figure 5.3***). In a first step the input is transformed non-linearly into a set of basis functions, e.g. radial basis functions (*RBF*). In the second step the output is computed as a linear combination of these basis functions. In a multilayer network the activity in the hidden layer can represent the basis functions, and the connections between the hidden layer and the output unit build the weighted sum of the intermediate responses.

The authors discuss unsupervised and supervised learning schemes which are applicable to their model. As Fahle et al. showed, *HyperBF* networks can learn to solve spatial discrimination tasks with hyperacuity (Fahle et al., 1995b). Starting from states where no predefined spatial filter tunings are present, the model gradually increases its performance with more stimulus presentations. Weiss et al. show that the same is true for an approach where the basis functions are represented by a predefined set of orientation tuned filters. In addition they state that the model is able to learn with a non-feedback dependent, i.e. unsupervised, learning rule (*EDL* – exposure dependent learning). They assume that *EDL* is involved in the improvement of the performance while human subjects learn *Vernier* tasks.

The model extends the ideas of Wilson and Poggio et al. by using more realistic orientation tunings and learning functions. However it does not state how these principles are implemented with units that produce temporally structured outputs. In addition it is a member of feed-forward (and feedback in the supervised case with a teacher signal) networks. The inner-areal processing exhibited by cortical circuits is neglected.

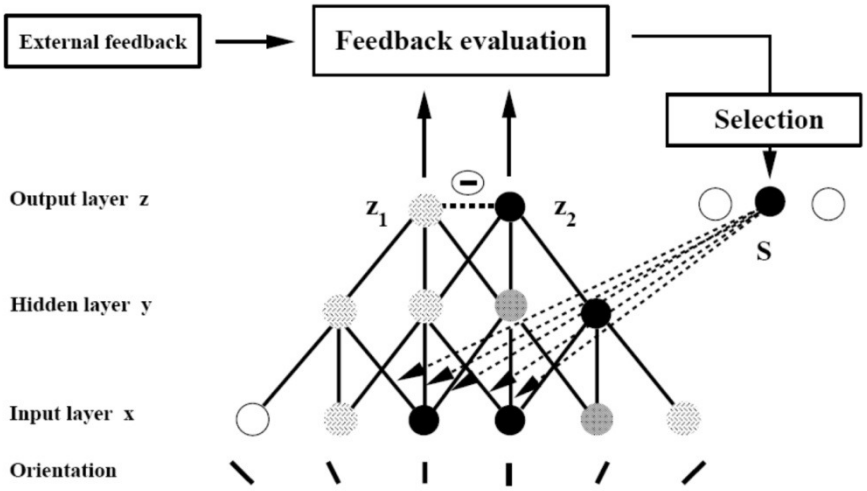

Figure 5.3: The model for perceptual learning in the *Vernier* acuity task, proposed by *M. H. Herzog & M. Fahle*: The model calculates the difference between the desired output and the actual output in combination with an external feedback signal which *scans* the network for the optimal input. Units which lead to an increase to the response difference are inhibited. With learning the network decreases the efficacy of the vertical (receptive fields aligned with the *Vernier* stimulus) units and increases the efficacy of the slightly tilted units, which are responsible for the weak differential response (figure taken from (Herzog and Fahle, 1998))

5.2 Object recognition models

5.2.1 Hierarchical feed-forward models

Fukushima et al. (Neocognitron)

The *Neocognitron*, proposed by Fukushima (Fukushima, 1980, 1987; Fukushima, 2003; Fukushima, 2004, 2007) is a hierarchical multilayered neural network capable of object recognition through learning. The model consists of hierarchically arranged layers of *S*- and *C*-cells (***Figure 5.4***). *S*-cells mimic the simple cells in the primary visual cortex. Their input connections are modified through learning, in a way that after having finished the training phase the *S*-cells are tuned to particular features of the input stimuli. Local features, i.e. edges of particular orientation, are extracted in the lower stages, more global and complex stimulus arrangements in the higher stages. *C*-cells on the other hand resemble the complex cells of the visual cortex. They receive their excitatory input from the *S*-cells, whereas the connections between the two cell-types are fixed, i.e. not changed during learning. Due to the connectivity pattern *C*-cells are less sensitive to feature position shifts, and in this way introduce a certain amount of invariance into the system. Each hierarchical step contains a number of two-dimensional *S*- and *C*-cell planes. Each plane shows similar tuning properties and identical but shifted input connection patterns.

During the process of feature extraction the local features of the lower stages are gradually integrated into more global features in the higher hierarchy steps. Small positional errors of local features are absorbed by the integration in the *C*-cells. Thus *S*-cells of higher stages robustly respond to specific stimulus features even if they are slightly distorted or shifted. *C*-cells in the highest stage work as object detectors, and indicate the result of the pattern recognition. The performance of the model revealed to be sensitive to the initial training patterns, the number of planes, the receptive fields and the selectivity (by varying the units' threshold) (Shi et al., 1999).

Unsupervised and supervised learning principles have been proposed for the Neocognitron. In unsupervised learning the network performs self-organization based on a winner-take-all rule and on a principle which guarantees that the earlier mentioned connection symmetry is preserved during learning. Supervised learning approaches are often implemented via genetic algorithms (*GA*).

The Neocognitron was developed further in recent years. Subsequent derivates for example include feedback connections to recognize objects if they are occluded by distractors, or to introduce an attentional element into the model which allows selection individual patterns in cases where several object are presented simultaneously.

The Neocognitron resembles some aspects of the connection patterns and the anatomy of the mammalian visual cortex. However, it does not include the large amount of horizontal connections found in all stages of the visual pathway. In addition it completely neglects temporal aspects of neuronal responses, i.e. single units in the

Neocognitron represent their activity by a single scalar value and not by a temporally structured response.

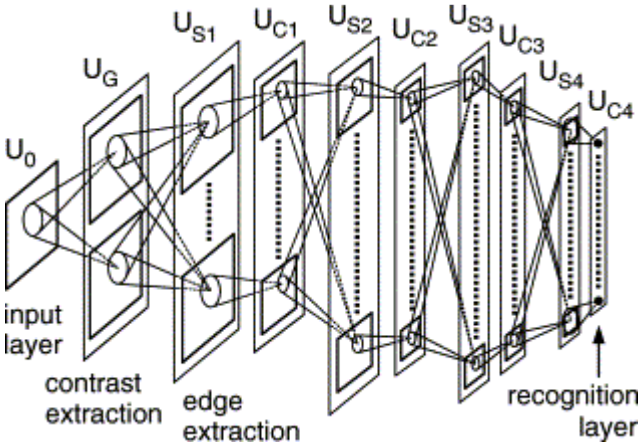

Figure 5.4: Neocognitron network used for handwritten digits classification (taken from (Fukushima, 2003)).

Riesenhuber et al. & Serre et al. (HMAX)

A model presented by Serre et al (Serre et al., 2007a; Serre et al., 2007b) is a recent member of the hierarchical and strictly feed-forward members of networks, and strongly related to the *Neocognitron*. The model aims to extend the neocognitron-idea with current neurobiological views, conceptual proposals and ideas from computer vision, to make it more natural on one hand but also more robust in a specialized categorization task on the other hand. The model attempts to quantitatively account for recent anatomical and physiological data. As the original *Neocognitron*, the model builds on units that mimic simple- and complex cells, which are arranged in hierarchical layers (***Figure 5.5***). The model in that way strongly resembles the ideas of Hubel & Wiesel, i.e. simple and complex cells in a multilayered architecture. It uses unsupervised learning up to a stage which is assumes to reflect the monkey inferotemporal cortex, and then switches to supervised (based on linear classifiers, e.g. linear *SVM*) learning for stages related to task-dependent learning, e.g. *PFC*. Beside of a number of agreements with biological findings, the activity of the network units predict a *max-operation* in some of the complex cells in earlier stages, which could be confirmed experimentally in the *V1* and *V4* of cats. The experiments showed that in many of the measured complex cells, the responses closely approximated a *max-operation*. The *MAX*-model states that the response to two bars is equivalent to the larger response for individual bars. Many cells performed a "soft-*MAX*". The degree of nonlinear summation varied from cell to cell and varied within single cells from one stimulus configuration to another but on average fit most closely to the *MAX* model (Lampl et al., 2004). In addition the Serre-model reproduces some of the invariant properties found in monkey *IT* cortex.

The model was successfully applied to a specialized categorization task, i.e. ultra-fast categorization into animal/no-animal according to experiments by Kirchner & Thorpe (Kirchner and Thorpe, 2006), which is assumed to be predominately being solved by fast feed-forward information processing. The model acuity performance is in agreement with psychophysical results.

The Serre-model is the most recent exponent of object recognition models developed in Tomaso Poggio's lab (Riesenhuber and Poggio, 1999). The model solves categorization tasks where the amount of clutter does not extend beyond a certain limit. However as the authors state themselves, the model is intended to show the capacity of purely feed-forward information processing. It neglects the extensive feedback signals and horizontal projections found in the mammalian cortex, and additionally, in its original formulation does not account for temporal structures in neuronal responses. The model is a strong member of feature based models which build up a dictionary along the hierarchy which represents the stimulus input space, does however not allow conclusions on the function of a major fraction of the projections in the visual cortex, i.e. horizontal and feed-back connections.

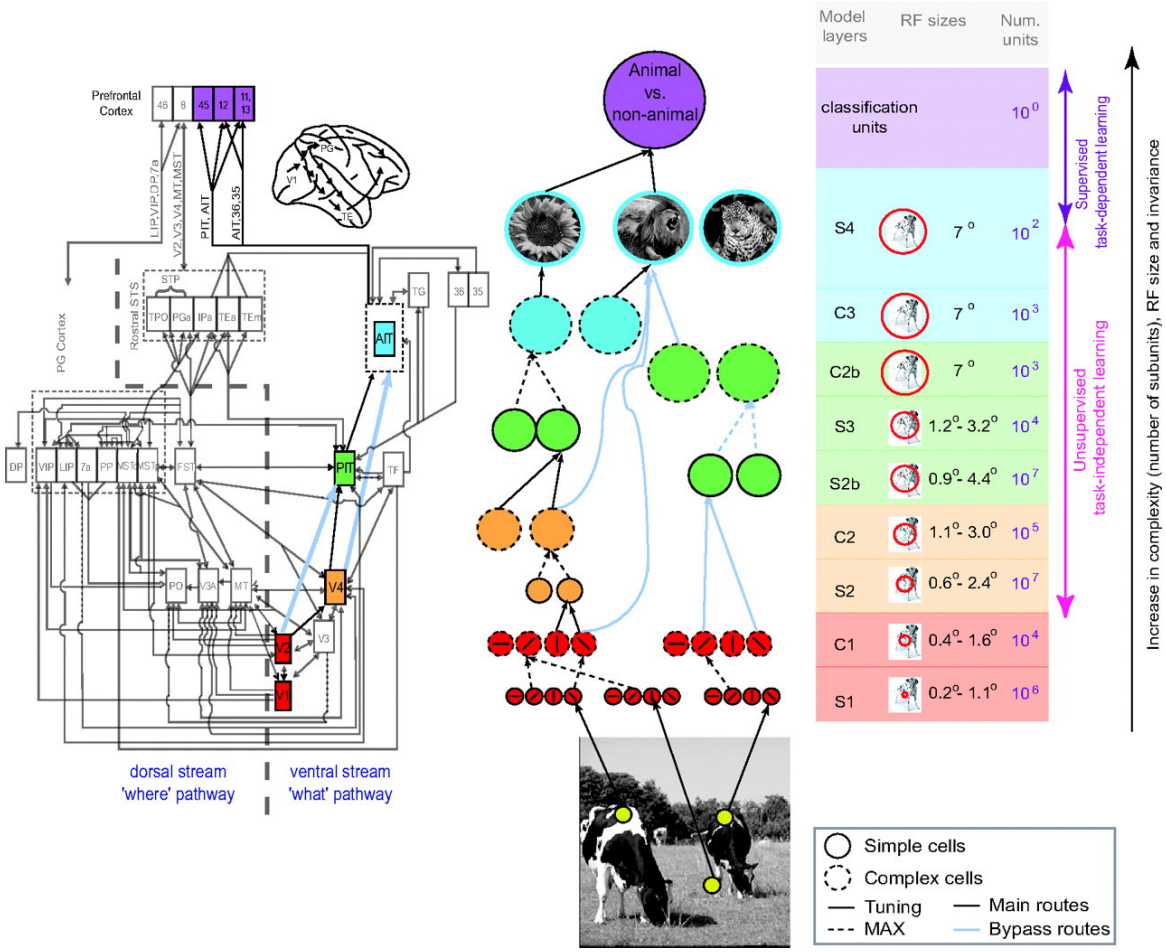

Figure 5.5: Sketch of the a recent implementation of the *HMAX*-model: The model accounts for some cortical mechanisms responsible for object recognition, i.e. an increase of invariance from *V1* to *IT*, accompanied by an increase of receptive field size and the complexity of receptive fields (figure taken from (Serre et al., 2007a)).

Masquelier & Thorpe et al. (SpikeNet)

Another member of feed-forward object recognition networks was presented by Masquelier et al. (Masquelier et al., 2007). As the *HMAX* model it is strongly related to the ideas implemented in the Neocognitron. As *HMAX* the model combines simple cells which gain selectivity by a sum operation with complex cells that gain shift invariance by a *MAX* operation (***Figure 5.6***). The network comprises four cell layers, i.e. S1, C1, S2 and C2, organized in a feed-forward hierarchy. Whereas the layers S1, C1 and S2 are retinotopically arranged, C2 cells take the maximum response of S2 cells over all positions and are thus shift-invariant. For each processing scale (various scaling of the input image) there is a separate S1-C1-S2 pathway. In the final stage a classification based on C2 response is performed. Individual spiking cells are modeled as non-leaky integrate-and-fire cells.

In contrast to *HMAX* the model presented by Masquelier et al. directly builds on spiking activity of individual neurons (for control reasons a non-spiking hebbian-learning-based implementation exists, but is not considered here). In the most recent version of the network, learning is performed by a *STDP*-rule between S2 and C2 layers. The learning considers the earliest spike of an individual cell as the *strongest response*. In conjunction with spike time dependent plasticity neurons in the higher stages gradually become selective to frequently occurring feature configurations. The implementation of the-first-spike-idea reflects an earlier statement made by Thorpe. He states that due to the ultra-fast object recognition capabilities of humans, the processing in an individual processing hierarchy can only be based on very few, probably only a single spike (Kirchner and Thorpe, 2006).

The model contains a number of, in part, non-local operations which are not directly performed by the network. On S1-level only the best matching orientation is propagated. In addition in S2 the similarity between the current input and the stored prototype is computed based on the common early spikes. Only the strongest response is used in the C2 layer. The final classification based in C2-activity is done by an *RBF*-network, which is used in a binary- or a one-versus-all classification approach.

With this arrangement the model was successfully applied to object recognition tasks in real-world images. The presented model resembles strongly the concepts in *SpikeNet (Thorpe, 2008),* the commercial branch of object recognition systems developed under guidance of Thorpe. As the presented model *SpikeNet* uses rank order coding as well, i.e. variation in spike latencies, to code stimuli.

The use of *STDP*-learning in a time-to-first-spike approach represents an interesting extension of the Neocognitron idea, and makes the model more biologically plausible. However several operations are not directly performed by the spiking network, and are in parts not based on local information.

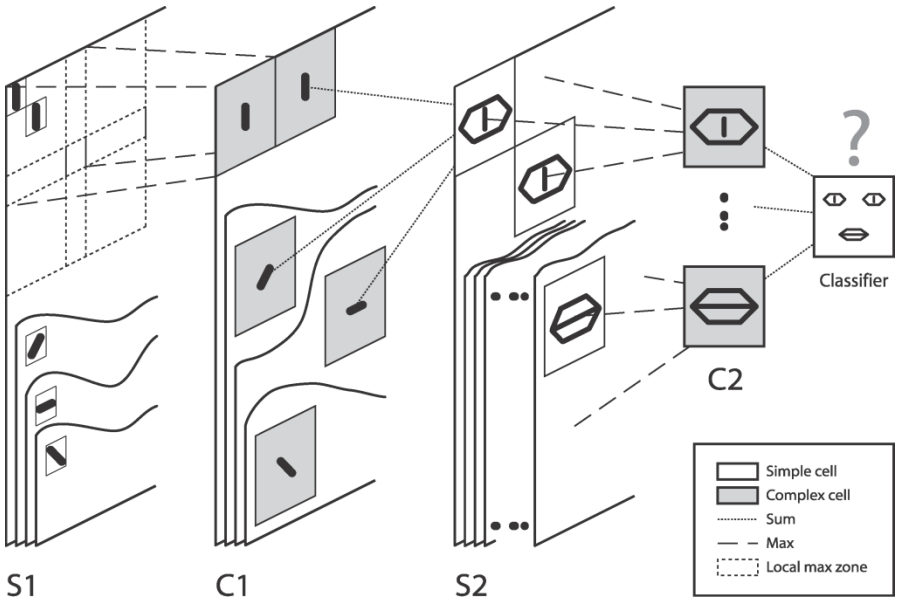

Figure 5.6: The object recognition network proposed my *T. Masquelier* and *S. J. Thorpe*: As in *HMAX*, simple cells (gain selectivity through sum operation) and complex cells (for shift and scale invariance through a *MAX* operation) alternate, to produce cells with increasingly complex optimal stimuli in higher layers. The network comprises spiking neurons and uses spike time dependent plasticity to learn visual features in an unsupervised manner (figure taken from (Masquelier et al., 2007)).

Rolls et al (Visnet)

VisNet (Wallis and Rolls, 1997; Rolls and Milward, 2000; Stringer et al., 2006) is a rate-based hierarchical feed-forward model comprising inter-areal convergence and inner-areal inhibition as exhibited in the mammalian visual pathway (***Figure 5.7***). A recent version consists of four hierarchical competitive networks with local graded inhibition. Due to the connectivity pattern the receptive field size is increased along the visual hierarchy. The forward connections to individual cells are derived from a topologically corresponding region of the preceding layer, using a *Gaussian* distribution of connection probabilities. The hierarchical steps are considered to model the steps *V2*, *V4*, *TEO* and *TE* (both part of *ITC*) of the visual cortex. The model uses a threshold parameter to control the sparseness of firing rates in each layer. The parameter is set to a layer specific fixed value in advance. To model experience related changes the model uses a non-supervised, hebbian-based learning rule to implement Continuous Transformation (*CT*) learning. *CT*-learning utilizes spatial continuity inherent in how objects transform in real world, combined with associative learning of the feed-forward connections weights. The idea behind assumes that between two transformations, e.g. small shifts or 3D-rotations, many of the neuronal units get a similar input as before the shift. Only at the object edges significant changes appear. Due to the learning neurons in the subsequent layer are able to generalize over these small distortions to form a stable percept.

With these concepts the model is able to produce view independent cell activations in the last stage. Some neurons in the last layer are for example able to distinguish rotated cubes and tetrahedrons.

An extended version of the *Visnet* (Deco and Rolls, 2004) model explores the effect of feedback connectivity in a network based on *CT*-learning. The top-down signaling stream models the control of attention in biological systems. In addition it incorporates mechanisms to select single targets in situations where several objects are presented simultaneously.

The model is in its latest version starts to leave the pure feed-forward design and uses more biological plausible architectures, e.g. feedback signals, cortical magnification and a *where*-pathway. However it neglects the temporal structure of neuronal responses and does not account for the function of the extensive excitatory inner-areal connections exhibited by the stages in the mammalian visual pathway.

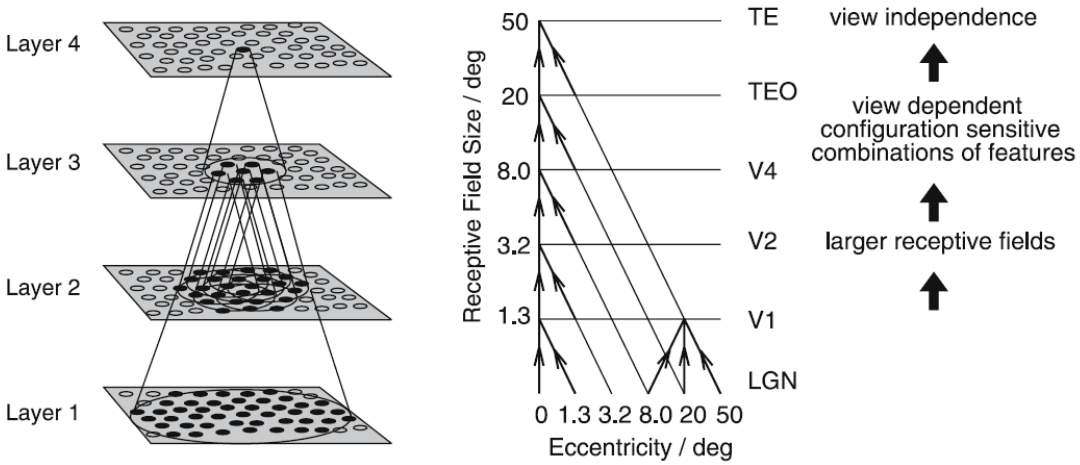

Figure 5.7: Model proposed by *Rolls*: Units in the layers exhibit progressively larger receptive fields, with *Layer 4* units revealing view independence by selectively summing up the information over the whole visual field of the retina (picture taken from (Stringer et al., 2006)).

5.2.2 Non-hierarchical models

Bohte et al. (unsupervised clustering with spiking neurons)

A specialized network for clustering of visual real world input was presented by Bothe al. (Bohte et al., 2002). They show that a neuronal model that encodes information by spike-times is capable of computing and learning clusters in an unsupervised manner. The network filters the input by a set of *RBF* functions, and sends the output to a layer of spiking neurons (***Figure 5.8***). Neurons are modeled as leaky-integrate-and-fire cells, and considered to spike if an internal variable, representing the membrane potential exceeds a threshold value. The spiking output of the layer is sent via a fully connected architecture to the subsequent stage, which also contains spiking neurons. The coupling between two spiking neurons comprises of a set of individual connections, each with an individual delay.

The network uses a winner-take-all approach to update the weights between source neurons and the neuron first to spike in the target layer. The underlying learning rule is an unsupervised time-variant of the Hebbian algorithm, resembling *STDP*-learning. If the presynaptic potential slightly precedes the postsynaptic spike, the weight of the synapse is increased, in all other cases lead to a decrease of the weight. Only the first spike of the output neurons is considered for the learning.

The authors show that the input patterns are encoded in spike times in the input spiking layer, and that through the hebbian learning rule neurons in the subsequent layer are trained to certain spike patterns. The neuron reflects the distance of the evaluated pattern to its learned input pattern by the firing time, and thus implements a kind of *RBF* neuron. The model can be extended by further layers to implement hierarchical clustering. The model is even extendable with reciprocal lateral connections to enhance the clustering capabilities.

The model is an abstract but interesting approach to perform an unsupervised clustering of real-world data via *RBF*-networks and spike time dependent learning. As the results reveal the network is able to classify certain data sets with a performance of k-nearest neighbor algorithms. However the network does not include anatomical considerations, and does not exhibit the invariant properties of biological cells which would be comparable to the clustering neurons, i.e. *IT* neurons.

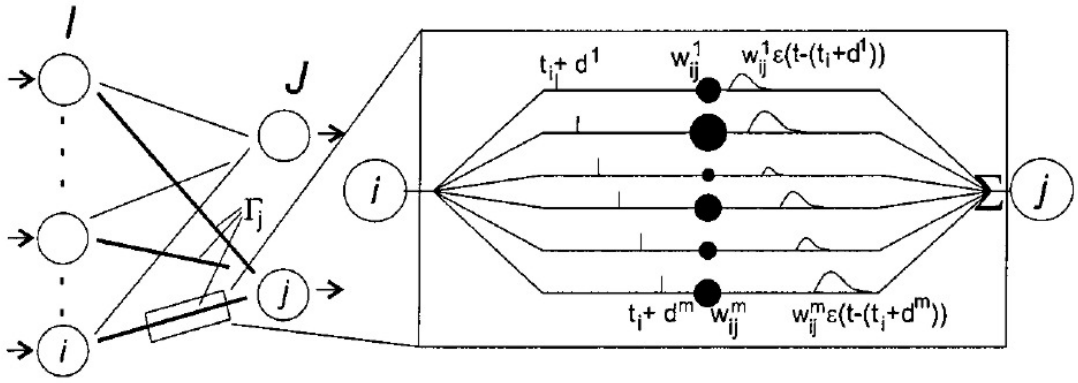

Figure 5.8: Unsupervised learning model proposed by *Bohte et al.*: A collection of connections between input (*i*) and output units (*j*), covering a full range of transmission speeds, transport spike-based encoded stimulus information to subsequent units (*j*) which act as coincidence detectors and change the synapses according to a spike-time-delay based plasticity rule (figure taken from (Bohte et al., 2002)).

Merzenich, Buonomano (temporal coding)

In 1999 Buonomano showed that a network comprising center feed-forward and lateral inhibition can modulate both the firing rate and temporal features (Buonomano and Mezernich, 1999). The network transforms presented patterns into onset latency histogram (***Figure 5.9***). Due to the symmetric connectivity pattern, the latency histograms exhibit position invariance. The model generates robust temporal codes for simple shapes like '+' or 'L', but also produces good results for handwritten digits. In a later model Buonomano shows that these temporal codes can be decoded by means of plastic synapses (Buonomano, 2000). He shows that the temporal tuning of cells can rely on long-term changes in synaptic strength and does not require changes in the time constants of the cell's temporal properties. In a large population cells exhibited a broad range of temporal selectivity ranging from no interval tuning to interval-selective tuning.

The model shows that connectivity patterns found in the visual cortex transforms stimuli into invariant temporal representations. The *TPC* model uses and extends this idea to lateral excitatory connections (Wyss and Verschure, 2003).

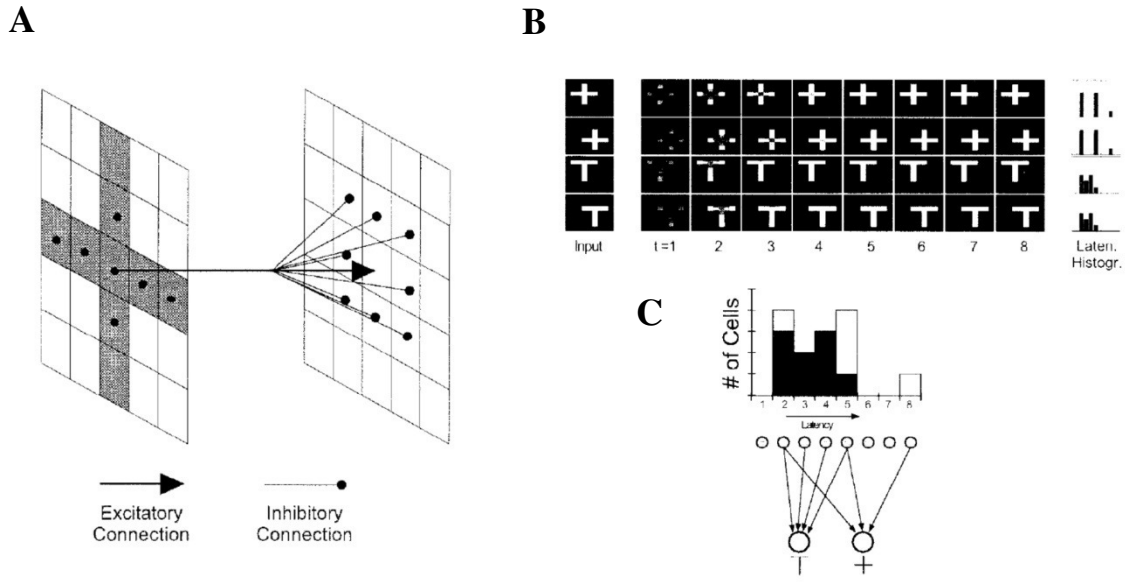

Figure 5.9: The position invariant encoding model proposed by *D.V. Buonomano and M. Merzenich*: Feed-forward excitatory connections surrounded by inhibitory projections (*A*) produce pattern specific latency diagrams in the subsequent neuronal layer (*B/C*). Since the connectivity patterns uniquely exploit relative geometrical properties, independent from the absolute position of the stimulus, the latency diagram is *position-invariant* (figure taken from (Buonomano and Mezernich, 1999)).

Maass et al. (Liquid State Machine – LSM)

Recently Maass presented a generic computational model, i.e. the *Liquid State Machine (LSM)* that performs its computations based on continuous data streams, which contrasts other dynamical system models, e.g. Turing machines and attractor-based models (Maass, 2009). Both inputs and outputs of a LSM represent streams of data in continuous time, which are modeled as functions. These functions are usually multi-dimensional and typically model spike-trains from many different input and output neurons. The LSM is a model for adaptive computation that separates the data processing and the learning into two distinct stages, i.e. the *Liquid* and the readout stage (***Figure 5.10***). The Liquid usually comprises a diversity of recurrently connected units that serve as a pre-processing stage which carries and amplifies the possible input functions, subsequent readout neurons cam learn. One *Liquid* thereby represents an input pool for many readout neurons which learn and emphasize various aspects of the received data streams. The input a readout neuron receives at a particular point in time is usually termed the *liquid state*. The adaptive stage is usually kept as simple as possible, i.e. a readout neuron only learns to map an isolated *liquid state* onto a target value (output) without the capability to integrate over many different time points. This memoryless readout where the output at time *t* only depends on the values of the input stream at the same time point *t* requires that the *Liquid* performs all temporal integration needed to represent the complete information history in the *liquid state* at each time point *t*. In this view the *Liquid* could be adaptive as well, but not optimized to solve a single computational task, rather it pre-processes the data for a large range of specialized task-driven readout neurons. The ability of continuous data integration makes the LSM to a member of an *online computational model* that does not require that all relevant information is available at the start of the computation.

The features of the LSM, i.e. computation based on time continuous data streams, temporal integration of information by virtue of recurrently connected units into *liquid states*, and the adaptive and computational power made the approach appealing as model to understand the computations carried out in cortical microcircuits. LSM derivates based on randomly connected Liquids comprising spiking units and biological inspired synapses were used in speech recognition tasks, and performed as well as state-of-the-art algorithms (Schrauwen et al., 2008). Recently a Liquid State Machine was also used to decode the output of the model that was used as a starting point in this thesis, i.e. *Temporal Population Code (TPC) (Knusel et al., 2004).*

The LSM with its ideas and concepts is related to the *Temporal Population Code.* Both are based on processing of continuous data streams. The two models however emphasize different aspects of computation in recurrently connected neuronal pools. The *TPC* model demonstrates how a model with biologically inspired connectivity patterns and model units robustly transforms spatially distributed information into a non-topological temporal representation, which co-exists with topologically organized information carried by local filters, e.g. output of retinotopically organized neurons tuned to certain orientations. The *TPC* in its original formulation does not make direct

predictions how these temporal fingerprints are readout by subsequent stages, e.g. whether it is performed in a memoryless manner or with temporal integration. The *Liquid* in the LSM focuses on the function of the *bulk* as a pool of units that pre-processes the information in a way that 1) the complete history carried by the input information stream is represented at each time in the Liquid state, and that 2) as many functions as possible are represented and amplified in the pool which can be readout by task-dependent neurons in the subsequent memoryless adaptive stage.

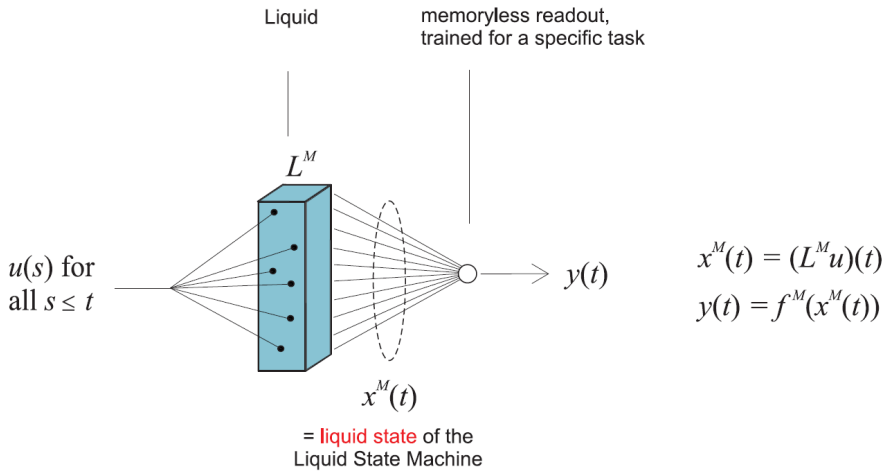

Figure 5.10: The principle of a *Liquid State Machine (LSM)*, which transforms an input stream *u(s)* into output stream *y(t)*. L^M denotes the *Liquid*, and $x^M(t)$ the *liquid state* of the system. The *Liquid* performs the temporal integration of the information, in a way the output at each time point carries the relevant information history in its *liquid state*. The *liquid state* is read out by subsequent neurons trained to a specific task in a memoryless manner (figure taken from (Maass, 2009)).

5.2.3 The model presented in this thesis (the *enhanced TPC* model)

Based on the ideas of population coding and transformation of spatial information into temporal patterns, Reto Wyss presented a model which uses the horizontal connections in combination with distance related delays (Wyss et al., 2001; Wyss and Verschure, 2003) to produce a distributed stimulus representation. The crucial part of the network are the excitatory horizontal connections which comprise distance related delays. Neurons connected in this way transform spatial stimulus information into temporal population activity, which allow fast and robust object classification. The code revealed to scale up to several hundreds of classes and exhibited translation and rotation invariance.

The model we present here develops this idea further. We show that a biologically meaningful readout mechanism based on fast feed-forward connections in combination with modulation of dendritic signal integration, is able to produce a position-specific temporal population code, that allows scene segmentation and still exhibits the robustness of the previously presented *TPC* model. The optimal speed of the feed-forward connections reveals to be similar to the ones measured in monkey primary visual cortex (Angelucci and Bullier, 2003). The modulation of dendritic integration is modeled according to acetylcholine (*ACh*) mediated changes in the muscarinic receptor, which leads to alterations in the effective electrotonic length of the dendrite. Cholinergic projections from the basal forebrain as one of the large modulatory systems are known to have widespread targets in the mammalian brain. As shown in previous studies the input has the capacity to alter contextual integration, similar to changes during attention related tasks (Roberts et al., 2005).

The model thus incorporates two additional aspects of cortical connectivity, i.e. the fast-feed-forward connections with distance related transmission delays and modulatory feedback input, to produce a robust position specific distributed temporal representation of the stimulus. In addition we show that the model not only generalizes over prototype distortions but also has the capacity to be very specific, i.e. the model is able to perform in a *Vernier line discrimination task* with hyperacuity.

Finally, we show that the enhanced temporal population code can be used in combination with plastic synapses to learn specific patterns in a subsequent processing layer.

Model details and assumptions

Stimulus preprocessing

Input is projected on a regular grid of linearly activated units, resembling the retinal photoreceptors. The produced output is subsequently projected over topographic excitatory projections to an *LGN*-like stage. The *LGN* units are again orderly distributed in a regular grid and perform edge detection based on *DOG* (difference-of-*Gaussian*) receptive fields with center- and surround-radii gathered from biology.

Coding

The subsequent layer (*V1*) with the first spiking neurons in the model receives the processed *LGN* information as excitatory tonic input. The *V1* neurons are modeled as noisy conductance-based leaky-integrate-and-fire neurons and exhibit a soft-refractory period, in which it is more difficult to elicit an action potential (due to voltage dependent potassium channels). Each neuron has in addition a given orientation preference modeled in conformance to cortical simple cells (Marcelja, 1980), i.e. the receptive fields have *gabor*-patch-like shapes with meaningful sizes. Neurons cover all orientations from 0-π whereas units with similar orientation preference are grouped in separate layers without connections between the layers.

The *V1* layer represents the first part of the coding stage. By virtue of the recurrent horizontal connections the incoming information reverberates within the layer. The transmission delays between the neurons (Angelucci and Bullier, 2003) and the anisotropy of the connections along the preferred orientation (Chisum and Fitzpatrick, 2004) (preferred orientation ± 30°) reveal to be similar to the ones measured in the primary visual cortex of monkeys. Since the emphasis in this stage lies on the coding power of the horizontal projections, only the recurrent excitatory connections between pyramidal neurons were modeled, rather than the full cortical inter-layer connectivity. It is assumed that each *V1* unit reflects the population activity in vertical column.

In addition to feed-forward and recurrent horizontal connections each neuron receives modulatory feedback, which models cholinergic input from the forebrain (Roberts et al., 2005). The modulatory input has no direct influence on the membrane potential. Rather acetylcholine (*ACh*) acts over the muscarinic receptor and affects dendritic integration signals (Verschure and Konig, 1999). The dendrite of each unit is modeled as an equivalent cylinder (Rall, 1969), characterized by a attenuation factor (Zador et al., 1995). The cholinergic input directly acts on the signal attenuation, by a transient onset of high attenuation after a relaxed initial phase (see **Figure 6.3** in *Results* section)

The second stage of coding is represented by fast feed-forward connections which readout the population activity in the *V1* layer. Their transmission speeds are comparable to the ones measured in monkey cortex (Angelucci and Bullier, 2003). Due to the distance

related transmission delays they readout a position related code of the projected stimuli. This allows analysis of scene details or the segmentation of target stimuli from distractors. It is important to note, that the mechanism does not build on bottom-up mechanisms, e.g. pop-out of salient stimuli. Rather it allows top-down signals to influence the signal processing in early visual stages, to guarantee for optimal coding. In this sense it is the distinction between the two terms *segmentation* and *binding* of features, under control of feedback signals.

Up to now all the coding was performed without learning. The results emphasize the point that anatomically and physiologically plausible model properties lead to a transformation of spatial stimulus features into a temporal representation which generalizes over stimulus classes but is very specific at the same time. Here we show that this temporal representation can be used in combination with plastic synapses to produce stimulus specific cells. The output of the *V1* layers which are tuned to individual preferred orientations are collected and subsequently transmitted to learning units which perform a binary classification. The learning is based on calcium controlled synapses, which reproduce several experimental findings (Castellani et al., 2001; Shouval et al., 2002b; Castellani et al., 2005), i.e. similar weight changes as in pairing experiments, frequency dependence of the weights, and SDTP-learning windows

Conclusion

The presented model incorporates a number of fundamental anatomical patterns found in mammalian brains, i.e. fast feed-forward connections, slower anisotropic horizontal projections and widespread modulatory feedback. With these patterns and biologically constraint neuronal models the network proofs to produce several experimentally measured benchmarks, i.e. categorization of stimuli in attention-related tasks, hyperacuity in a *Vernier line discrimination task* and dot pattern classification. It is one of the few examples which attributes a clear function to the horizontal connections, since it shows that the recurrent excitatory connections transform spatial information into a temporal representation. In addition it links the previously presented model (Wyss et al., 2003a) to the feed-forward and modulatory feedback connections, and shows that the merged model circumvents the weaknesses of the previous design, i.e. breakdown of the temporal code due to horizontal interactions of the target stimulus with distractors, and complete loss of positional information in the temporal code.

The model therefore allows new insights into the functional properties of anatomical structures, and argues for the importance of temporal coding in a mixture of non-hierarchical and hierarchical feature-based networks.

Chapter 6

Segmentation in a biophysically restricted population code model

6.1 Management summary

Primates excel in their ability to recognize objects or parts of it under various viewing and illumination conditions. As psychophysical experiments reveal the recognition is not only highly accurate but also very fast at the same time (Kirchner and Thorpe, 2006). The neural mechanisms underlying these abilities are still highly debated. However, the increased knowledge from studies in recent years shed more light on what the neural substrates could be, and how the neuronal and network properties could allow the speed and accuracy in object recognition tasks. A special requirement of systems performing recognition tasks in cluttered scenes is the need to separate a target stimulus from distractors or the background.

6.1.1 Previous knowledge

Anatomical studies revealed a series of cortical areas related to vision in the mammalian cortex. Beside of inter-areal feed-forward connections many mammalian species exhibit extensive excitatory lateral connections which seem to distribute information between neurons with similar properties. The neural units are thereby arranged in overlapping functional maps, e.g. orientation and ocular dominance maps, where neighboring neurons within a region surrounded by sharp boarders tend to share similar features. Emphasize of early physiological studies on the properties of single neurons and the inter-areal feed-forward connectivity, lead to the development of hierarchical models of visual scene processing. In these models visual scenes are first decomposed into small fragments, represented by the activity of single units in the early stages of the visual pathway. In later stages the activities are combined to form more and more complex feature representations culminating in formation of coherent percepts of whole objects in the late pathway areas like the inferotemporal cortex. This hierarchical view was supported by computational models which reveal the strength of hierarchical feed-forward models in object recognition tasks.

Most of these approaches however neglect the existence of the strong horizontal connectivity and the feed-back modulatory inputs found all over the cortex. Recently Reto Wyss et al. proposed a non-hierarchical model approach which encodes visual stimuli by virtue of extensive lateral connections. The computational model utilizes distance related transmission delays between recurrently connected neurons to transform spatial stimulus features into a temporal population activity representation. The model

matched the performance of the best hierarchical models in a hand written digit recognition task, and additionally exhibited translation and rotation invariance. The model clearly shows that the horizontal connectivity can deserve as a neural substrate to solve object recognition and classification tasks. The extensive long-range horizontal connections are however its weakness at the same time. The model is not able to control contextual influences and consequently cannot segment target stimuli from distractors. Any distractor closely positioned to the target perturbs the temporal code formation and leads to sever performance drawbacks.

6.1.2 New contributions

In this chapter we present several extensions to the model presented by Wyss et al. The enhanced model augments the capacity of the original proposal by allowing modulation of contextual influences. This is achieved mainly by two biologically meaningful model components, i.e. a dedicated readout mechanism that collects the population activity produced by laterally connected neurons, and modulatory input which mimics cholinergic feed-back input to cortical regions. By virtue of modulation of dendritic signal integration and the resulting changes in the effective connectivity of laterally coupled neurons the model controls contextual influences in cluttered scenes.

We show that the model successfully recognizes objects in situations where the target is presented with closely positioned distractors. The new model clearly outperforms the original one, and even stays significantly above chance level when the target stimulus overlaps with the distractor. Furthermore the model reveals to encode the stimuli faster than the original one, and also exhibits a better maximum performance for the used stimulus set.

In summary, while the previous model of Wyss et al. focused uniquely on recurrent inner-areal connections the new model assigns clear functions to two additional connectivity patterns found all over the cortex, i.e. fast inter-areal excitatory feed-forward connections, and modulatory top-down projections. The feed-forward connections collect position related population activities and transports them to the next stages. The modulatory input regulates contextual influences in the visual scene, and in this way controls between binding and segmentation of scene components. The model satisfies both performance criteria found in psychophysical experiments, it is fast *and* accurate given its 97% correctly categorized stimuli around 50 ms after stimulus presentation. With the extensions the network combines properties of the recurrently connected *TPC* model with the features of hierarchical feed-forward models, and further demonstrate how top-down modulation augments the performance in object recognition tasks.

6.2 Introduction

Sensory perception and subsequent processing of information are the basis for the remarkable ability of animals to react fast and accurately to external stimuli. In primates, vision is a fundamental source of information about the external environment. Accurate responses require classification or identification of features or objects in the visual scene under large variations in viewing conditions. Moreover, the behavioral relevance of visual objects may vary with task and context. Thus, initial encoding mechanisms have to be able place dynamic segmentation borders in the scene (Zhou et al., 2000; Roberts et al., 2005). They must be able to segregate objects from background, and separate relevant targets from distractors.

Beside of being highly accurate and flexible, the processing machinery has to be very fast as well. In a visual discrimination task, in which human subjects had to identify human faces and respond with eye movements, the minimum saccadic reaction time was 120 ms, with an associated accuracy of 85.9% (Kirchner and Thorpe, 2006). 200 ms after stimulus presentation, the accuracy reached 90.1%. Comparable reaction times were also observed in monkeys (Fabre-Thorpe et al., 1998). This is remarkable since the feed-forward circuitry of the network involves at least 8 synapses until the inferotemporal (*IT*) cortex, where cells respond to specific objects (Hung et al., 2005; Quiroga et al., 2005a).

The spatial accuracy of the visual system is also remarkable. A large number of psychophysical studies showed that relative positional information is more precise than the retinal receptor distance (Westheimer and McKee, 1977a; Poggio et al., 1992b; Fahle et al., 1995b), a phenomenon known as hyperacuity.

The neuronal mechanisms and cortical structures responsible for these amazing performances are still debated. Anatomical studies revealed dense lateral connections within all visual areas, and sparse connectivity between them (McGuire et al., 1991; Bosking et al., 1997a; Binzegger and Douglas, 2004; Vezoli et al., 2004; Tanigawa et al., 2005b). As expected in light of the short reaction times in visual categorization tasks, feed-forward connections are fast and outperform the speed of the horizontal connections (Angelucci and Bullier, 2003). The existence of dense lateral connectivity, however, is in contrast to predictions of perceptron-like models, which focus primarily on feed-forward- and feedback connections to encode stimuli (Riesenhuber and Poggio, ; Serre et al., 2007b).

Recently is was shown that networks that incorporate dense intra-areal lateral connections transform spatial stimulus features into a temporal population code (*TPC*) (Wyss et al., 2003b). The *TPC* supports rapid invariant classification, has a high capacity and is robust to noise (Wyss et al., 2003b; Wyss and Verschure, 2003; Knüsel et al., 2004). *TPC* exploits the dynamics of densely coupled neuronal networks with time-delayed connections. These transduction delays result from the physical distance between connected neurons, and a finite transduction speed of about 0.1-0.4 m/s for horizontal

connections (Angelucci and Bullier, 2003). In addition, transduction delays can be actively regulated with respect to the particular features the neurons are processing. Evidence for such a regulatory process has been observed in the auditory system (Skottun, 1998; McAlpine and Grothe, 2003), or in peripheral projections in the electro-sensory organ of the weakly electric fish (Benda et al., 2006; Carlson and Kawasaki, 2006).

The characteristic physiological signature of the *TPC* is the introduction of phase lags in the responses of different neurons. The pattern of phase lags is stimulus specific. This has been observed in the primary visual cortex (Gray et al., 1992; Konig et al., 1995). Recently, similar dynamics in the processing of olfactory stimuli in the insect antennal lobe were observed (Knuesel et al, In Press).

Although *TPC* is consistent with cortical anatomy and physiology, its reliance on the dynamics of cortical activity as a representational substrate is also its main weakness. There are no inherent mechanisms in the *TPC* that prevent spatial and or temporal mixing of signals elicited by different objects. In other words, the presence of a distractor interferes with the response to the target, and could impair classification performance. Indeed it was shown that the presentation of targets in the presence of distractors leads to a rapid decline of classification performance (Wyss et al., 2003b). This raises the following question: Which aspects of cortical networks can complement those captured in the *TPC* in order to perform segmentation together with fast and robust classification.

Given the dependence of the *TPC* on lateral connectivity, we hypothesize that segmentation could be achieved by introducing mechanisms that regulate the effective connectivity. In cortical networks, signal integration in the dendritic tree is known to be modulated amongst others by acetylcholine (*ACh*) (Sillito and Kemp, 1983; Kimura, 2000; Roberts et al., 2005). In an earlier theoretical study, it was shown that active dendritic properties allow local features to be bound into synchronously active neuronal sub-assemblies (Verschure and König, 1999). Moreover, a recent in vivo study shows that acetylcholine selectively reduces the efficacy of lateral cortical connections via a muscarinic mechanism, while boosting the efficacy of thalamocortical/feed-forward connections via a nicotinic mechanism (Roberts et al., 2005). The application of *ACh* in primary visual cortex of marmoset monkey reduces the extent of spatial integration while simultaneously making cells more reliant on feed-forward information, as assessed by recording neurons' length tuning.

Here we show that by combining active dendritic properties with dense lateral coupling, we can resolve the *TPC* segmentation problem while retaining its robust and fast classification properties. We show, however, that this extension requires a novel readout mechanism that generalizes the *TPC* hypothesis to hierarchically structured perceptual systems. This readout mechanism is consistent with the known anatomy and physiology of the visual cortex.

6.3 Methods

We analyzed the classification of visual stimuli in the presence of distractors.

The inputs to the network are artificially generated patterns (***Figure 6.1***) that are generated following a stochastic procedure already used in earlier work (Wyss et al, 2003). In short the prototype for each stimulus class is generated by randomly placing 4 points in a plane of 40 by 40 pixels. Subsequently each pair of points is connected with probability 0.3. Each of the 11 stimulus classes, consisting of 200 exemplars is generated from the prototypes by jittering its end-points. Before being presented to the model cortical network each stimulus was passed through an edge detection and rectification stage approximating thalamic processing.

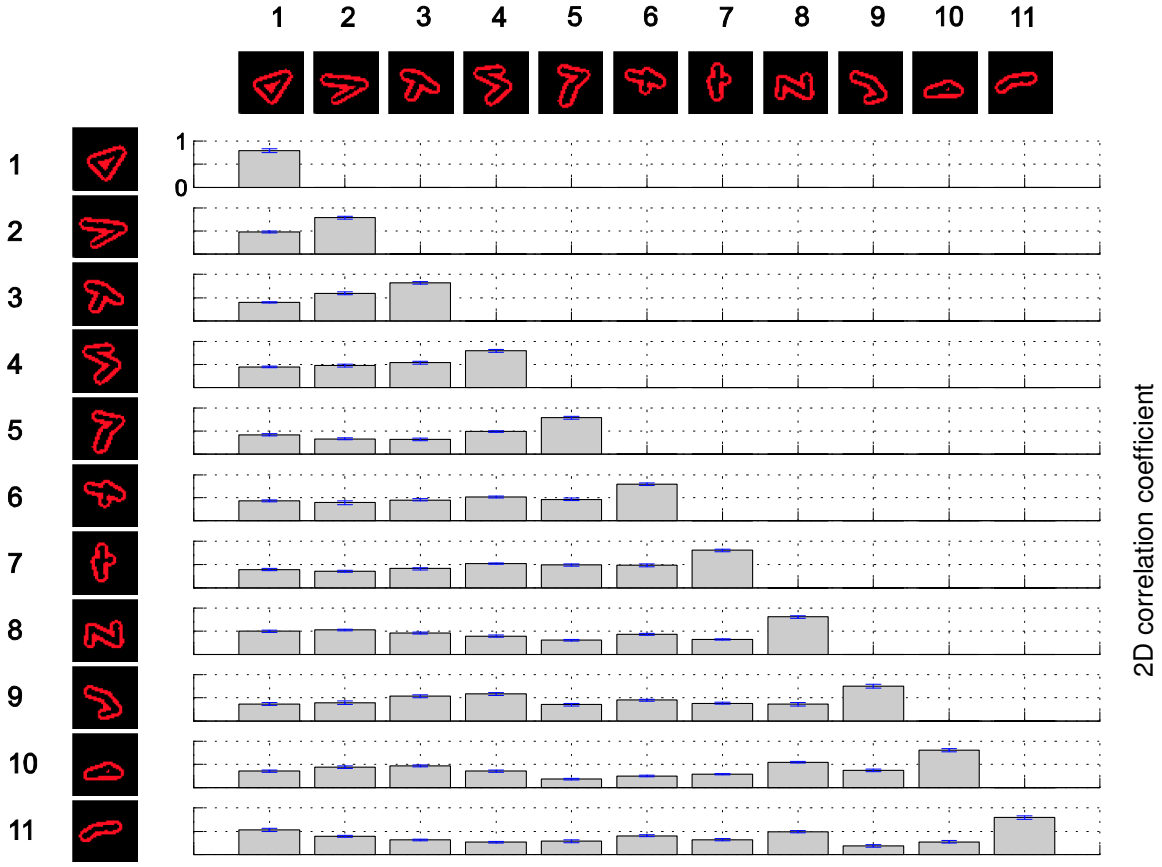

Figure 6.1: The stimuli: 11 artificially generated patterns of 40x40 pixels (following the algorithm proposed in Wyss et al 2003) were used as prototypes to create 11 stimulus classes. 200 stimulus exemplars were produced by distortions of these prototypes. Each of 4 vertex locations was randomly jittered using a two dimensional *Gaussian* distribution (σ=1.2 pixels). The bars and error bars reveal mean 2D-correlation coefficients and standard deviations for all possible stimulus pairs between two stimulus classes.

The network (***Figure 6.2***) consists of an input layer with topographic excitatory connections (driving conductance v=2.8 nS) to 80x40 integrate-and-fire cells (encoding layer). The encoding layer contains symmetrically arranged excitatory lateral connections (driving conductance v=0.05 nS) where each of the cells receives input from a circular neighborhood (r=13 cells), using synapses with instantaneous conductances and transmission delays of 1.03 ms per unit cell-cell distance.

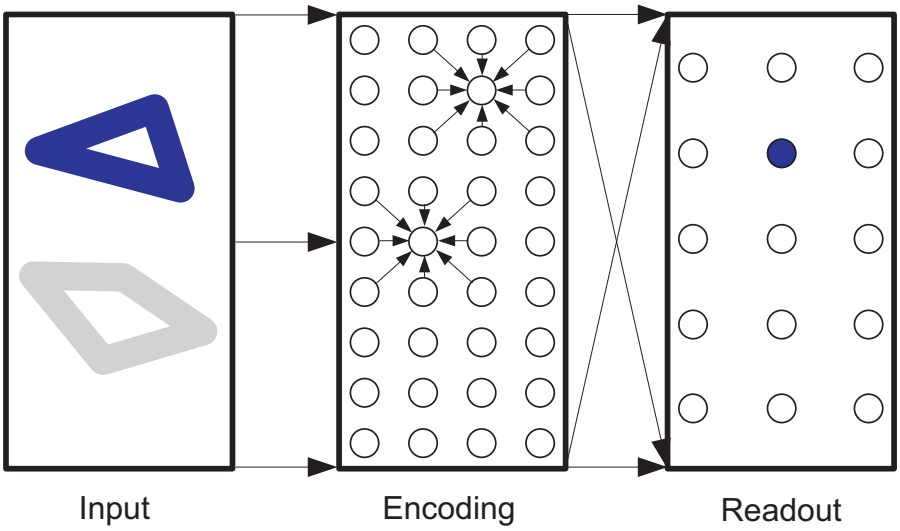

Figure 6.2: Circuit properties and topology of the *enhanced TPC* network: Preprocessed stimuli (see figure 1) are projected on an 80x40 input layer (*input*), with topographic (1-to-1) connections to the 80x40 encoding layer (*encoding*). The encoding layer contains conductance based integrate-and-fire neurons, whereas each neuron receives uniform and delayed excitatory input from a circular neighborhood. The neuronal activity of the encoding layer is projected onto a fully connected 5x3 readout layer (*readout*) with linear activation properties. These connections are subject to a distance related transmission delay and are of equal strength. The segmentation task: Two stimuli are projected simultaneously on the input layer. The goal is to identify the individual stimuli by comparing their summed population response to the temporal population code that was recorded during the training phase when one stimulus was presented at a time.

Dendrites of all cells in the encoding layer are modeled as equivalent cylinders as described in (Verschure & König, 1998). The position on the dendrite of an afferent synapse that originates in the encoding layer is linearly dependent on the distance between efferent and afferent cells: synapses of more distal afferent cells are placed more distally on the dendrite and vice versa. The excitatory postsynaptic potentials propagating towards the soma are attenuated with the attenuation factor *a* (**Figure 6.3**). In our model the attenuation factor *a* can be modulated through mechanisms similar to *ACh*-dependent signal modulation, i.e. the I_m current, known to take place in pyramidal neurons (Verschure and König, 1999; Roberts et al., 2005).

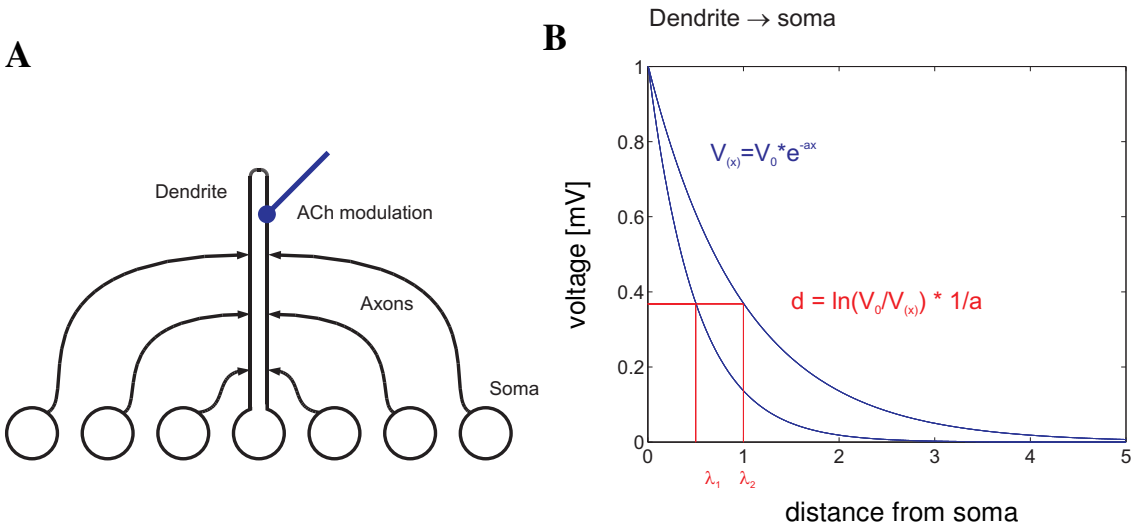

Figure 6.3. Modulation of dendritic signal integration: The local circuit properties of the model shows (*A*) the distance related connectivity pattern of the lateral projections (*black arrows*) onto the dendrites (for clarity reasons only one dendrite is shown). Axons from more distant neurons connect more distally on the target dendrite and vice versa. The electrotonic length of the dendrite can be changed by altering the attenuation of the signals along the dendrite via *ACh*-like modulation (*blue arrow*). (*B*) The electrotonic distance *d* describes the exponential decay of the signal along the dendrite. It can be modulated by a dynamic *ACh*-mediated attenuation factor *a*. The length constant λ is defined as the distance where the original voltage V_0 decayed by 1/e. Two length constants (λ_1, λ_2) for a=1 and a=2 are shown.

The goal was to minimize perturbation by distractors by means of the attenuation, while at the same time maximizing the encoding of the target stimulus by means of the lateral connectivity. In our model the dendritic attenuation (*a*) is set to a base value of 0.84 during the period from 1 to 35 ms after stimulus onset. After that the attenuation is transiently increased leading to a full uncoupling of the neurons in the encoding layer.

The activity of the encoding layer is collected for the first 100 ms after stimulus onset by linearly activated read out cells (readout layer). Cells of the encoding layer are fully connected to the readout layer. Transmission delays between the two layers are also distance dependent using a transduction delay of 0.62 ms per unit cell-cell distance.

During training, an 80x40 pixel plane containing the training stimulus is projected onto the input layer. The output is collected from a readout neuron that is centered on the stimulus. In the test phase a second plane containing a randomly selected distractor stimulus is simultaneously presented with the test stimulus, whereas the Euclidean distance between the centers of the two planes varies between 0 and 45 neurons. During this phase the responses of the readout neuron centered above the target stimulus are collected and subsequently used for the classification. Each target exemplar response is compared to the mean response (***Figure 6.4***) of each training class. A target sample is

assigned to the response class with the highest temporal correlation. Since we are only interested in the temporal evolution of the *TPC* generated by the encoding layer, the collected network responses are normalized to set the peak activation equal to one.

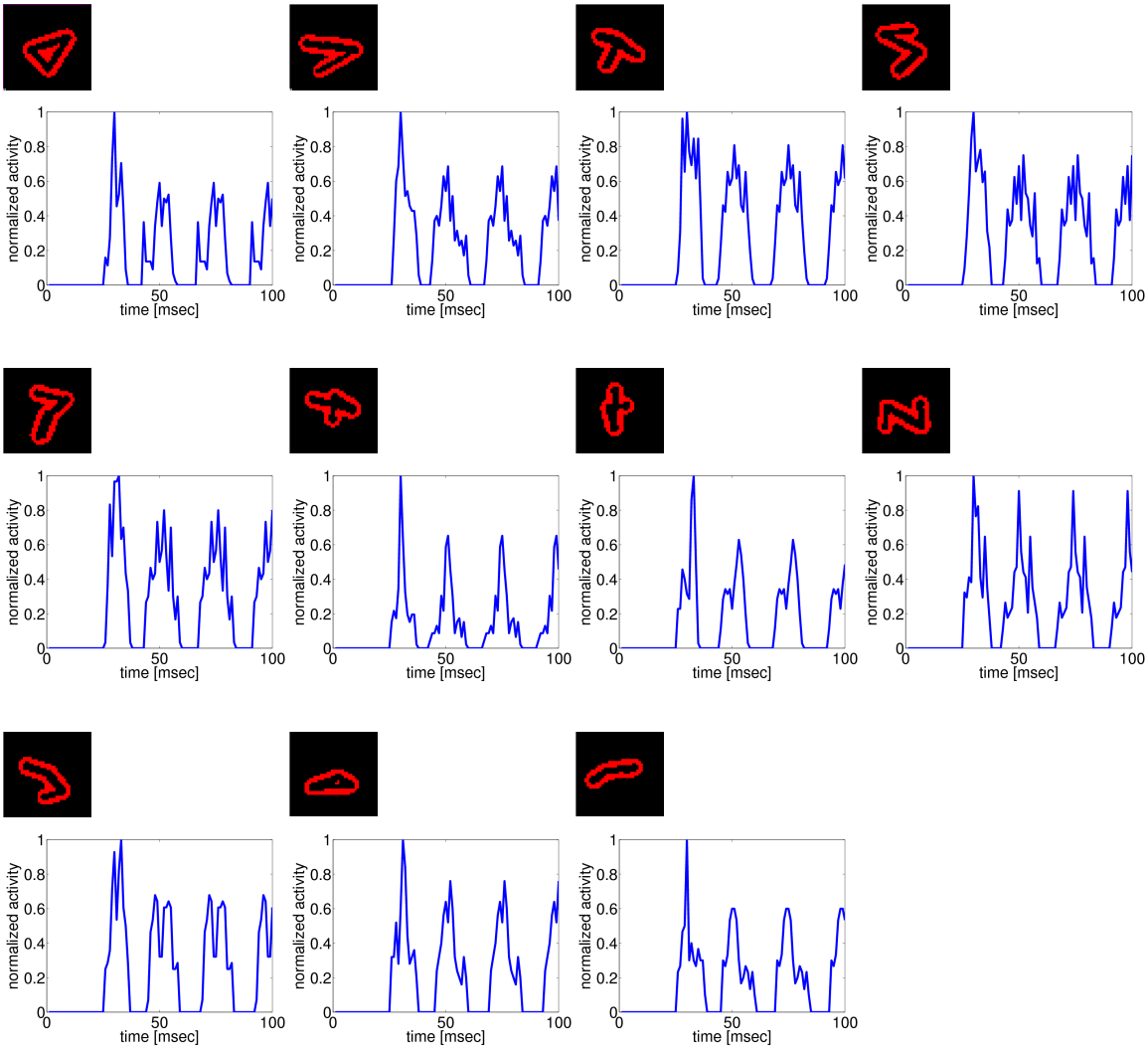

Figure 6.4: Example activity traces in a control condition, e.g. without distractor: The mean activity generated by 100 exemplars of each class (see Figure 6.1) is shown. The stimulus was presented at time = 0 msec.

6.4 Results

With the *TPC* model we want to investigate whether segmentation and binding can be achieved in a model of a cortical circuit that includes active dendritic properties, i.e. modeled cholinergic modulation of dendritic attenuation, and a dedicated readout stage. Hence, we first want to assess whether these changes, in particular the dynamic uncoupling of the encoding units, affects the *TPC* (***Figure 6.4***). When we inspect the average *TPC*s generated for each stimulus class it still follows a characteristic dynamic. In all cases the first spikes appeared at the readout layer around 26 ms after stimulus onset. The decoupling of the neurons at 35 ms after stimulus onset leads to a stereotypical response in the encoding layer that appears to be specific for the different stimuli.

The performance of *the enhanced model* in the classification task was calculated by presenting a target stimulus together with a variably positioned distractor. The resulting classification performance curve as a function of distractor position reveals that the network produces a distractor robust classification (***Figure 6.5***). For distractors that touch or even overlap with the target stimulus, 76% of the target stimuli are still classified correctly. This is much better than the performance of the control model (Wyss et al., 2003b) that uses neither dendritic attenuation nor position related readout delays and that classifies 25% of the test patterns correctly with a chance level of 9.09%.

For distractors further away from the target, the performance of the enhanced model reaches an upper limit of 97% which is equal to the classification performance without distractor. This is significantly better than the performance of the control model that shows an upper limit of 79% for the same stimuli, in situation without distractor.

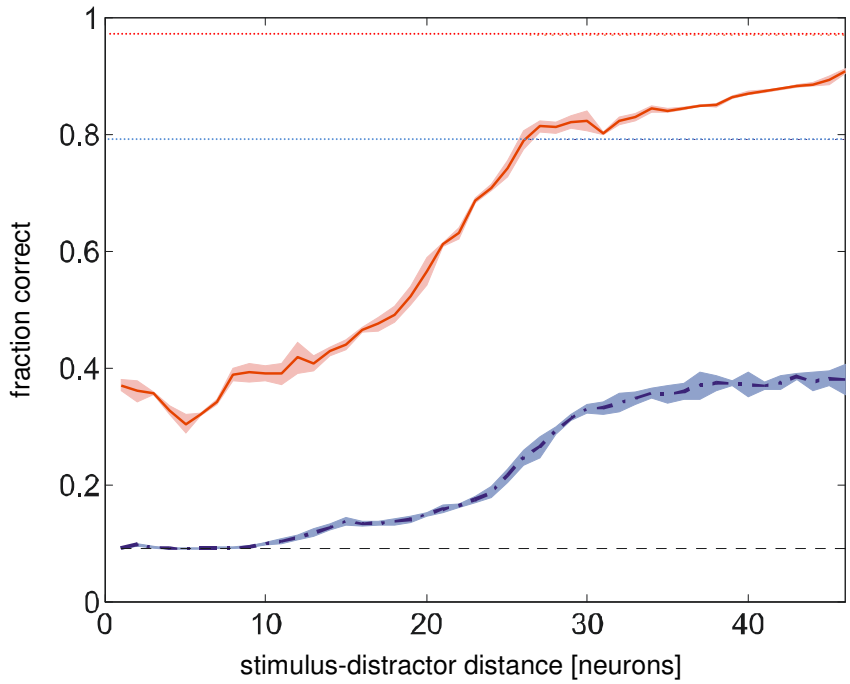

Figure 6.5: Classification performance with a closely positioned distractor: Classification performance in the segmentation task (x-axis denotes distance between stimulus centers, i.e. 0 = completely overlapping, 25 = touching or slightly overlapping). The model had to classify a target stimulus (100/class) in presence of a randomly selected distractor. The red curve shows the performance for the model with active dendrites and transmission delays between encoding and read out layer (*enhanced model*). The dot-dashed blue curve shows the performance for a model without dendrites and readout transmission delays (*control model*). Shaded areas denote the standard deviation for five repetitions. The fraction correct denotes the maximum value of the classification performance time course for increasing *TPC* trace lengths in the interval [1 100] msec. Dotted horizontal lines denote upper performance limits, i.e. fraction correct without distractors. Chance level for the classification task is 9.09%.

To further illustrate the properties of the enhanced network we calculated the classwise classification performance for distractor distances (distance between the stimulus centers in # of neurons) of 45 (***Figure 6.6*** *A*) and 25 (***Figure 6.6*** *B*) cells. For the more distant distractor the mean classification performance is 89% correct, with very low variation between the classes. For the closer distractor the variability between classes is increased and the overall classification is decreased to 76%. For this close distractor case, some classes still show a performance around 100% correct, whereas others like class number 5 fall to 30%. In the latter case, the network confuses the target with stimuli of the classes 2 and 9 (for class prototypes see ***Figure 6.1***). These results again confirm that the *TPC* conserves the similarity among stimulus patterns as defined by the specifics of its lateral connections. The variation in the classification performance between the classes

is also reflected in the mutual information that specifies how much knowing the predicted class reduces our uncertainty about the effective class. The theoretical maximum for the mutual information with 11 equally probable classes is 3.56 bits. In a simulation without distractor the mutual information is 3.21, while with distractors separated by 45 or by 25 neurons the information measure is reduced to 2.83 and 2.25 respectively.

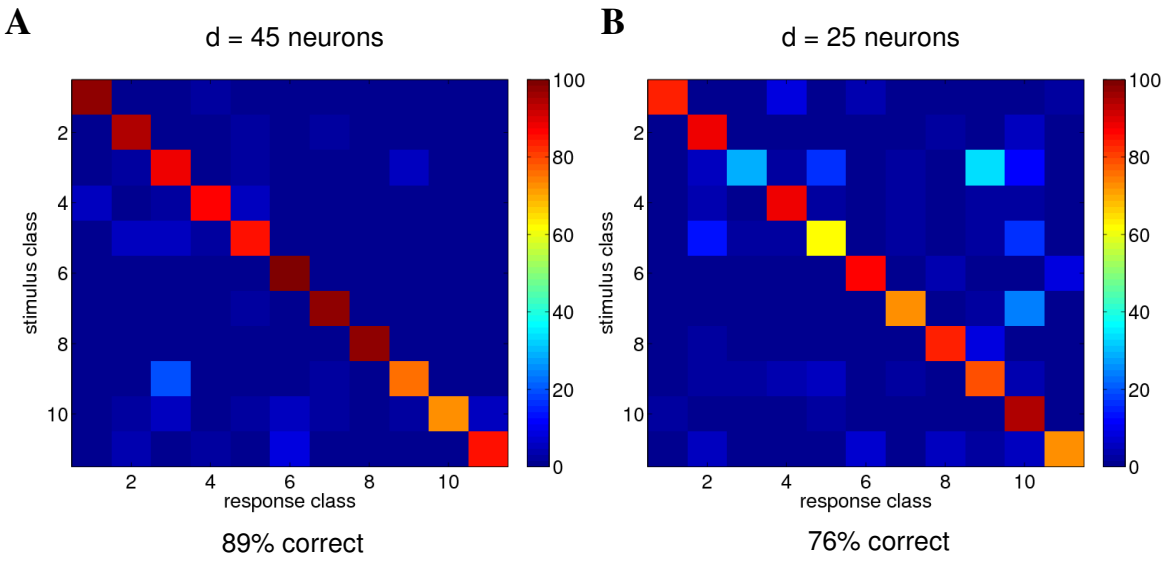

Figure 6.6: Classification hit-matrices: Hit-matrix revealing classwise performance in the segmentation task, 100 target stimuli of each class were simultaneously presented with a randomly chosen closely positioned distractor. The separation of stimulus centers was equal to 45 neurons (*A*), and 25 neurons (*B*). The latter corresponds to touching or slightly overlapping of the stimuli. The y-axis denotes the presented class and the x-axis the response class given by the network.

To investigate the importance of individual *TPC* parts produced by the enhanced model we calculated the classification performance for variable time windows (***Figure 6.7*** *A*). The analysis revealed that very early components represent already a highly accurate and robust encoding. In the non-distractor case the first 15 ms after the initial spike allow a classification performance of 85% correct (***Figure 6.7*** *B*). This value can be increased by using a bigger fraction of the *TPC* trace. The first 46 ms after the initial spike produce a maximal performance of 97%. In the distractor case later *TPC* parts are perturbed by the additional stimulus, which leads to a decrease of performance for larger time windows (***Figure 6.7*** *C/D*). The perturbation is more pronounced for close distractors than for more distant ones.

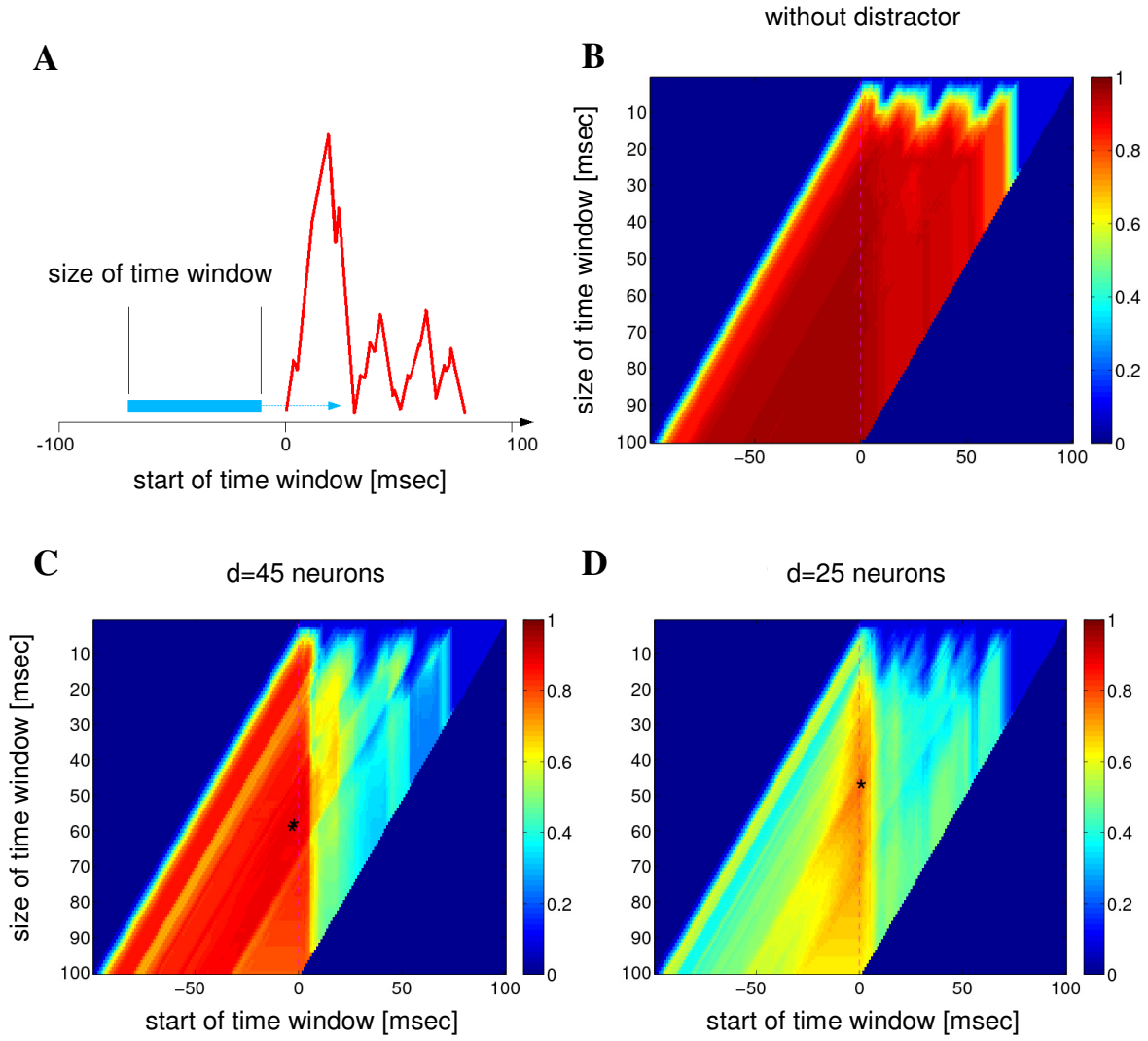

Figure 6.7: Classification performance for variable readout intervals: A sliding time window is shifted along the *TPC* (*A*). For each position and size of the window we calculate the classification performance. The three plots show the performance for a control without distractor (*B*), a distractor positioned 45 neurons (*C*) and 25 neurons (*D*) from the target stimulus. For classification, the leading zeros of all traces were omitted, and their peak activity was normalized to 1.

To illustrate these results the influence of the distractor on the spiking behavior of individual cells in the encoding layer was investigated. The results show that dynamic increase of dendritic attenuation after a short encoding frame can reduce the perturbation of the *TPC* by distractors. The increased attenuation leads to a functional uncoupling of the laterally connected neurons. Perturbations are no longer propagated over the whole layer, but are restricted to a small area surrounding the distractor (***Figure 6.8***). Hence a large part of the target stimulus is not affected and produces an unperturbed representation. In the subsequent stage, readout neurons centered above the target

stimulus produce the 'best local guess' and deliver not only the stimulus class but also the position of the target pattern.

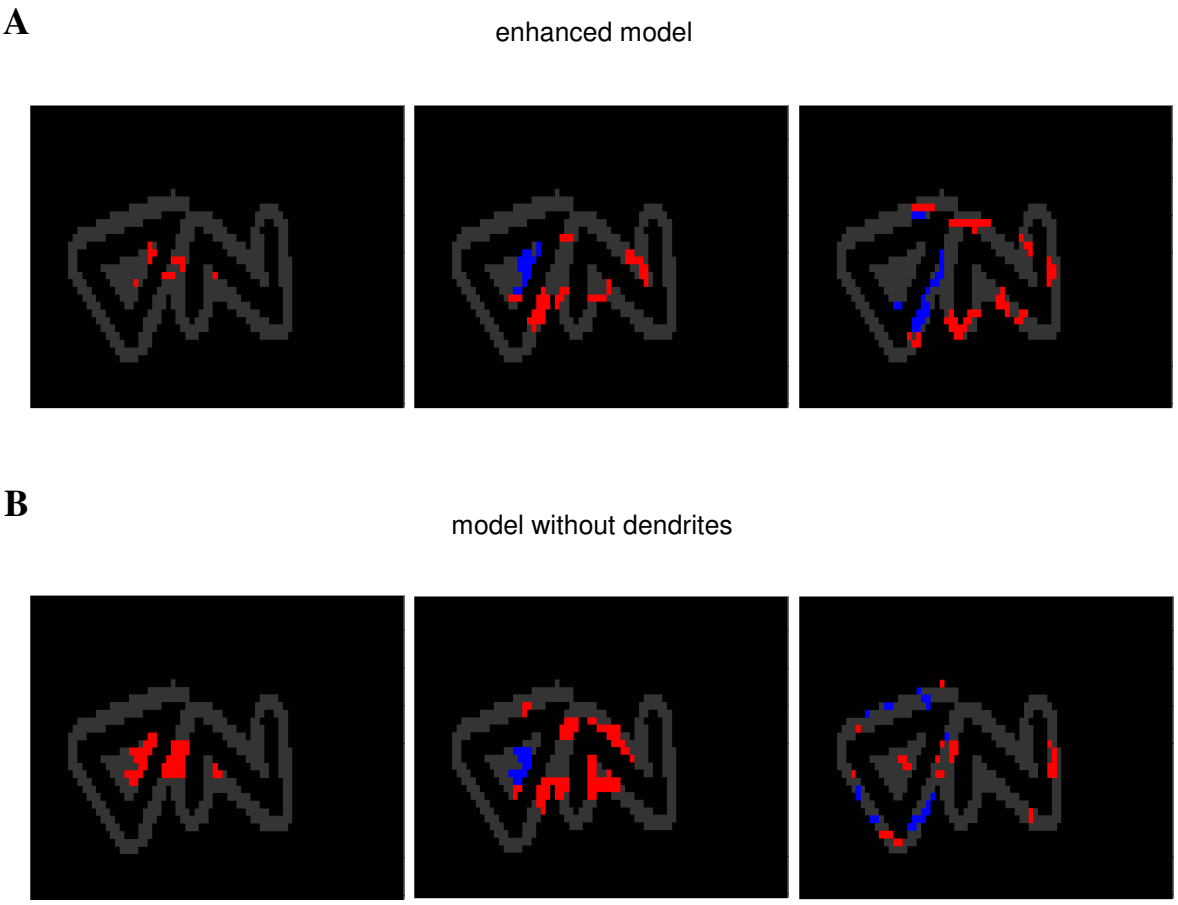

Figure 6.8: Cell activity differences: Neuronal activity in the enhanced network in presence of a closely positioned distractor (*A*), and a control network without dendrites (*B*). In the image series the activity difference between training- (only target stimulus presented to the network) and test-phase (target stimulus and distractor presented to the network) at three time points is shown. Color code: *Red* shows cells that are active in the test but not in the training phase, *blue* is for cells that are active in the training but not in the test phase at the corresponding time. *Grey* areas denote placeholders for the stimulus projections, where the left triangle-shaped stimulus is considered as the target stimulus and the right N-shaped stimulus is considered as the distractor.

To further investigate the *TPC*, i.e. the influence of the biophysical parameters we calculated the classification performance in the segmentation task as a function of the readout delay (***Figure 6.9*** *A*) and dendritic attenuation (***Figure 6.9*** *B*). Classification performance as a function of dynamic attenuation reaches its maximum for an increase of attenuation 35 ms after stimulus presentation. Performance for earlier and later onsets is mainly dominated and compensated by the read out delay encoding scheme.

Variation of the read out delay has a more profound effect on classification performance (***Figure 6.9*** *A*). The maximal performance is reached for a delay of 0.62 ms between neighboring neurons. For shorter delays the performance is decreased dramatically since target stimulus activity is more and more mixed with activity peaks belonging to the distractor.

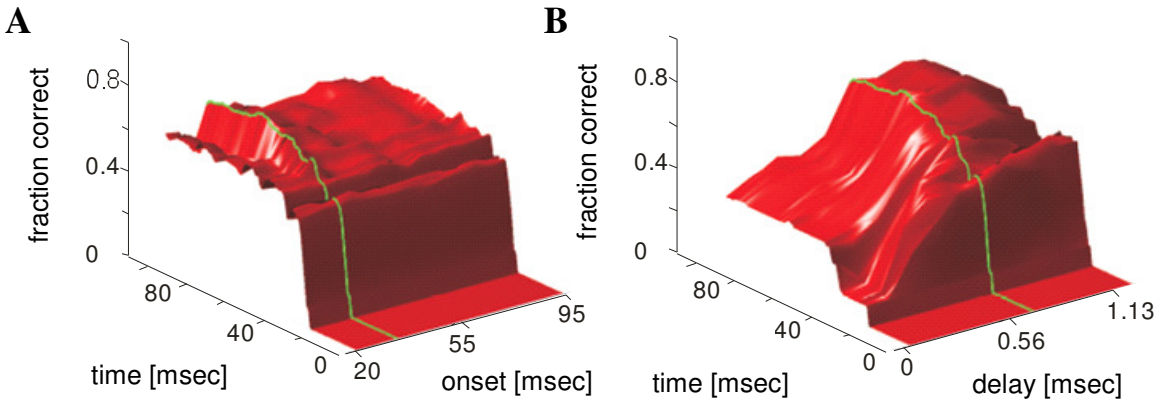

Figure 6.9: Classification performance dependencies: Classification performance time courses as a function of dynamic dendritic attenuation on neurons in the encoding layer (*A*) and as a function of distance related delays between encoding and readout layer (*B*). Classification performance was calculated for increasing time windows starting at t=0 ms (stimulus onset) with a closely positioned distractor (stimulus center distance = 25 neurons). For (*A*) the transient onset of high attenuation was varied between 20 and 95 msec. The performance reaches a maximum (green line) at a delay of 35 ms (76% correct, after 72 ms). For (*B*) the readout delay was varied between 0 ms and 1.125 ms per unit cell-cell distance. The performance reaches a maximum (green line) at a delay of 0.62 ms per cell (76% correct, after 72 ms).

The used read out mechanism is an encoding scheme itself. Activities produced by close edges will reach the readout neuron earlier than distant ones. To further investigate this, we calculated the time course of the classification performance for several network configurations without distractors (***Figure 6.10***). The results show that both parts, e.g. the lateral connectivity and the readout delays between encoding and readout layer, are able to produce a highly accurate stimulus class specific representation. The read out delay based representation is a very fast stimulus class specific trace. The performance can be improved by the recurrent lateral connectivity. The combined model reaches its classification performance maximum about 30 ms after the first spike.

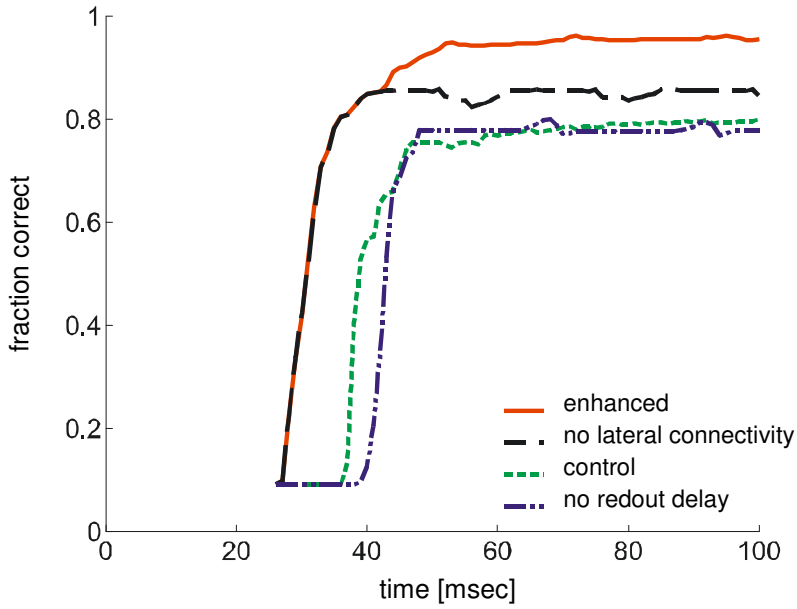

Figure 6.10: Time course of classification performance in a control condition without distractors: Four model configurations were tested: A control model without dendrites and readout delays (short-dashed green curve), the enhanced model with optimized dynamic attenuation and readout delay (solid red curve), a model without lateral connectivity (long-dashed black curve) and a model without readout delay (dot-dashed blue curve). The data reveal that the enhanced model shows the best performance. During the first 10 milliseconds after the initial spike the performance resembles that of the model without lateral connectivity, but later improves through the encoding produced by the recurrent lateral connectivity. The control model (green) and the model without readout delay but dendrites and dynamic attenuation (blue), show similar performance in this non-distractor case.

The same network in the non-segmentation-mode, i.e. with relaxed log-attenuation factor (*a* at base level = 0.84), classifies dot patterns which resemble the properties of stimuli used in human psychophysics with high accuracy (***Figure 6.11***). In the simulations a collection of 11 dot-pattern classes had to categorized based on the temporal output the network produced. Each stimulus class was built out of distortions of randomly generated prototypes. The class members were generated by jittering each dot position along a two-dimensional *Gaussian* distribution. To avoid classification purely based on the delay to the first spike, which would need internal knowledge about the exact stimulus onset, the spike trains were aligned on the first spikes. The network performs with 75% correct 15 ms after the first spike, and reaches a maximum of 97% correct after 100 ms.

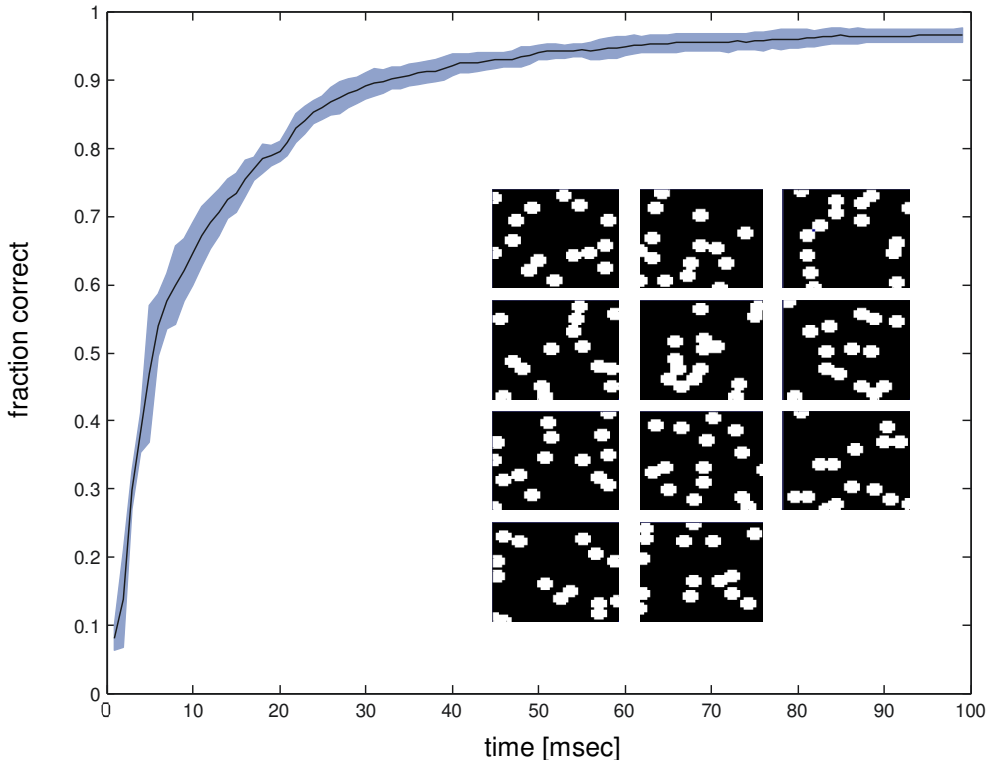

Figure 6.11: Dot patterns classification performance: The same network in the non-segmentation mode, i.e. with relaxed log-attenuation factor, classifies *dot patterns* (see figure inlays for a set of 11 class prototypes) as used in psychophysical experiments without problems. The curve shows the mean classification performance (*y-axis*) based on the temporal correlation, for increasing network output lengths (*x-axis*). It reaches a mean classification performance of 97% correct for an output trace of 100 ms. Shaded areas denote the standard deviation for 5x11 dot pattern collections. Each class is constructed out of a prototype in which vertices are jittered along a two-dimensional *Gaussian distribution*. In each of the five sessions, 11 classes each with 200 examples are presented to the network. The first 100 examples are considered as the training set, the latter 100 as the test set. The classification is performed according to the method used in the *segmentation* simulations, i.e. output of the exemplars are compared to the mean output of the training classes.

6.5 Discussion

With the *enhanced TPC* model we wanted to investigate whether segmentation can be achieved in a model of a cortical circuit that includes active dendritic properties, i.e. cholinergic modulation of dendritic attenuation, and a dedicated readout stage. In particular we wanted to assess whether the dynamic uncoupling of the encoding units affects the *TPC*. When we inspect the average *TPC*s generated for each stimulus class it still follows a characteristic dynamic. 97% of stimuli presented in a non-distractor case are classified correctly. The decoupling of the neurons at 35 ms after stimulus onset leads to a stereotypical response in the encoding layer that is specific for the different stimuli. The model is able to successfully classify 76% of the stimuli in the presence of closely positioned distractor (***Figure 6.6***).

The *enhanced TPC* model uses a manually set dendritic attenuation to get an optimal segmentation performance. It is assumed that this attenuation signal is part of a top-down signaling pathway which tunes the system either to binding of features into a coherent unambiguous object representation, or to segmentation, i.e. analysis of object details. Recent in-vivo studies show that *ACh*-mediated modulation of dendritic attenuation via the muscarinic pathway directly influences the spatial summation properties of the primary visual cortex cells in the marmoset monkey (Roberts et al., 2005). As in other mammals these cortical cells show an extensive amount of lateral connections whose efficacy seems to be dependent on the local *ACh* concentration. The natural release of *ACh* seems to be strongly linked with states of arousal and attention. A view which is supported by results of earlier studies that relate the reduction of contextual influences in the primary visual cortex to attention and perceptual learning (Ito et al., 1998). The hypothesized effects of *ACh* on contextual effects require a spatial and temporal regulation of acetylcholine concentration. A variety of studies show that spatial specificity of *ACh* release is higher than originally thought (Price and Stern, 1983; Carey and Rieck, 1987; Fournier et al., 2004). This study now shows that a simple transient increase of the *ACh*-mediated attenuation 35 ms after stimulus onset produces a highly distractor robust system, which provides better performance than a laterally uncoupled- or a completely coupled system (***Figure 6.9, Figure 6.10***).

Regulating the contextual effects of the lateral connections by virtue of attenuation is only part of the reasons for the distractor robustness of the enhanced *TPC* model. The simulations also emphasize the importance of a dedicated readout stage, based on distance related transmission delays. Inspecting the optimal speed of the modeled connections reveals that the model feed-forward projections are 1.7 times faster than lateral ones, which leads to a fast development of the *TPC* in the subsequent readout layer (***Figure 6.7, Figure 6.9, Figure 6.10***). Direct measurements of the transmission speeds in macaque monkeys reveal similar speed relations between part of the horizontal and feed-forward connections (Angelucci and Bullier, 2003). But on average the in-vivo feed-forward connections are about 10 times faster than the lateral ones. This discrepancy

could point to a system where different feed-forward transmission speeds are related to specific information contents. While slow to medium fast connections carry most of the information about the class relationship of an object, the very fast connections mostly reveal the location of stimulus, which can be used to provoke a saccade or to set attention by a top-down mechanism. This would explain how a certain readout channel, i.e. a specific readout neuron in the model, can be selected, based on the location and the saliency of the stimulus.

Taken together this is in line with psychophysical studies in humans (Kirchner and Thorpe, 2006) (***Figure 6.12***) and electrophysiological experiments in monkeys (Hung et al., 2005) (***Figure 6.13***) which suggest that a first fast feed-forward wave of cortical processing carries enough information to trigger useful behavioral responses. The recordings in monkey *IT* cortex showed that only 125 ms after stimulus onset a classification based on spikes in a very small time bin of only 12.5 ms allowed stimulus classification with an accuracy of 70%±3%.

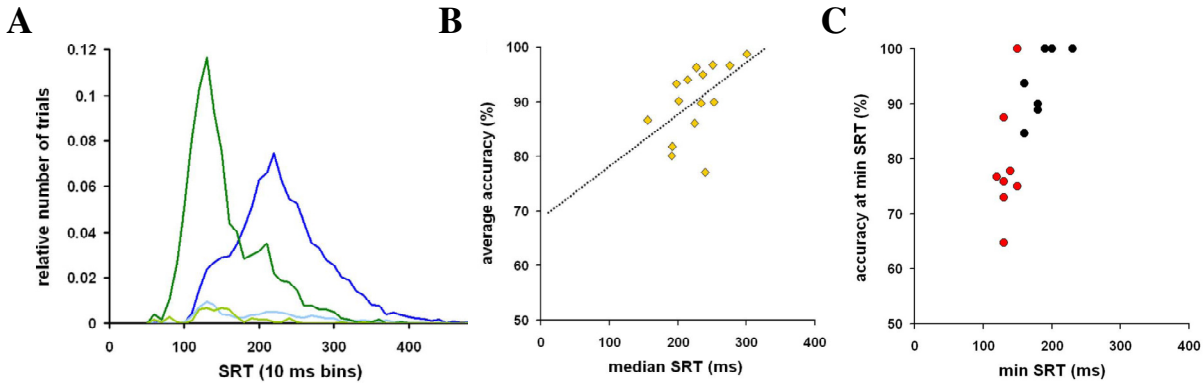

Figure 6.12: Human psychophysical data for a *2-afc* classification task where the category *animals* had to be detected and signaled by eye saccades (adapted from Kirchner & Thorpe (Kirchner and Thorpe, 2006)). (*A*) Pooled saccadic reaction time (SRT) histogram (n=15 subjects) for the condition where only one image was shown (blue), and for the condition where two images where shown simultaneously whereas only the target contained an animal in the scene. Median (*B*) and minimum SRTs (*C*) as a function of average accuracy for individual subjects. Subjects were able to signal the target image with very high accuracy around 250 ms after stimulus onset (with a median of 228 ms). The eight fastest subjects had reaction times below or equal to 150 ms.

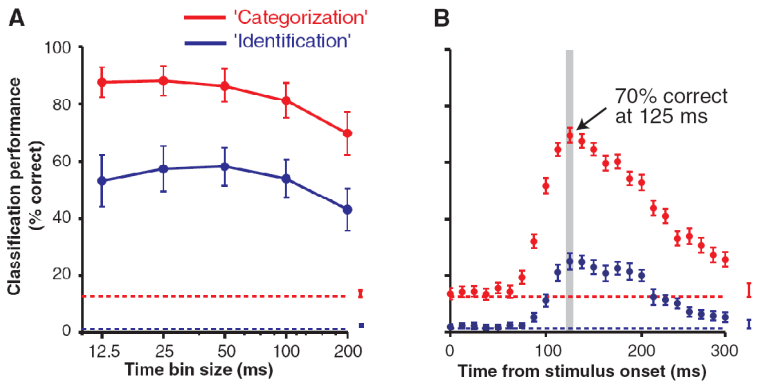

Figure 6.13: Classification performance based on electrophysiological recordings in monkey *IT* cortex, adapted from Hung et al. (Hung et al., 2005). *(A)* Classification performance (n=128 sites) as a function of the bin size, i.e. temporal resolution. (B) Classification performance based on a single bin of 12.5 ms at various latencies. Already very small time bins at a latency of only 125 ms after stimulus onset allow for a classification performance of 70% correct.

The original *TPC* model (Wyss et al., 2003b) produced a position- and rotation-invariant neural representation of the stimulus. The enhanced model presented in this thesis however by virtue of its distance related feed-forward transmission delays produces a position-specific representation. The collected population code varies as function of the stimulus position and the readout neuron(s) used as output channels. This position dependent encoding of stimulus information is biologically plausible, though. In several experiments the dependency between object recognition performance and spatial attention was demonstrated. In spatial attention information is selected based on saliency information in the image (bottom-up) and on prior knowledge about the scene or the task (top-down). It was argued that the region-dependent gating of information is the key component to solve object recognition tasks in highly cluttered scenes (Rutishauser et al., 2004).

A recent member of a biologically inspired attention model (Itti et al., 2005; Walther and Koch, 2006) proofed to produce eye saccade traces that resemble the properties of human observers. The model does not only provide the coordinates of the most salient points, but exact timing information as well. A visual scene is first processed for low-level features. Resulting feature maps are then combined into conspicuity maps, and finally into saliency maps. Based on this information a winner-take-all (WTA) neural network determines the most salient location. Combined with an inhibition-of-return mechanism the model sequentially selects biologically plausible target locations. Advanced versions of the model even deal with continuous video input. The model is able to foveate or pay attention to objects or features irrespective of their initial position in the visual scene.

This biologically plausible attention mechanism could be used to extend the *TPC* model presented in this thesis. The encoding of stimulus information in the presented *TPC* model depends on the stimulus features and on the position of the stimulus within the encoding layer with respect to the output channel (readout neuron used to collect the activity pattern of the encoding layer). A position invariant encoding requires either to foveate the stimulus or to shift the attention of the network to the presented stimulus, which is equal to switching the output channel. These are exactly the features of the saliency based attentional framework presented by Walther & Koch. Future experiments will reveal whether a *TPC* model that incorporated both *ACh*-mediated segmentation features and saliency visual attention properties is able to produce position and rotation invariant stimulus representations, even in cluttered scenes.

Further, an open question is how the dendritic attenuation, depending on time, the presented stimulus and possibly other parameters can be optimized in a neural system. Future investigations should show whether it is an unsupervised perceptual-learning-like mechanism or if an external reward system is necessary, i.e. a supervised top-down mechanism.

6.6 Appendix

The Encoding Neuron

The time course of the leaky integrate-and-fire neuron's membrane voltage *V(t)* is described by the differential equation:

$$Cm\frac{dV}{dt} = -(I_{exc}(t) + I_K(t) + I_{leak}(t)) \qquad (5.1)$$

Where C_m is the membrane capacitance (C_m=0.2 nF), and $I_{exc}(t)$, $I_K(t)$ and $I_{leak}(t)$ represent the transmembrane currents. The currents are computed by the equation $I(t) = g(t)(V(t)-V_{rev})$ where g is the conductance and V_{rev} is the reversal potential of the conductance (V_{exc}^{rev} = 60 mV, V_K^{rev} = -90 mV, V_{leak}^{rev} = -70 mV).

Cells in the encoding layer are laterally coupled, whereas the transmission delays are related to the Euclidean distance between the pre- and post-synaptic cell, with a proportionality factor of τ = 1.03 ms/cell. In addition the synapses of the lateral connections connect in a distance related manner on the dendrite, where x, the distance between the synapse and the soma of the postsynaptic cell equals the Euclidean distance between the two cells.

The excitatory input current $I_{exc}(t)$ originating from synapses of the lateral connections is attenuated while traveling along the dendrite, such that the effective current reaching the cell soma is equal to:

$$I_{exc}^{soma}(t) = I_{exc}(t) * e^{-a(t)x} \qquad (5.2)$$

Where $I_{exc}^{soma}(t)$ is the effective current integrated at the cell soma at time *t*, $I_{exc}(t)$ is the input current produced by the excitatory synapse, *a(t)* the attenuation factor along the dendrite and *x* the distance between synapse and soma of the postsynaptic cell. The optimal time course of attenuation *a* was revealed by a genetic algorithm. It is 0.84 from 0 ms to 35 ms after stimulus onset, and is then transiently increased to a value of 1000 for the rest of the data acquisition, which completely uncouples the horizontal connectivity.

The neuron's activity at time t, $A(t)$, is given by $A(t) = H(V(t) - \theta)$ where H is the Heaviside function and θ is the firing threshold (θ = -55 mV). Each time a spike is emitted, the neuron's potential is reset to $V_{rest} = V_{leak}^{rev}$. The constant leak conductance g_{leak} is 20 nS. The synaptic interactions are 'instantaneous', such that the total input current at time t is the linear sum of all effective input currents at the cell soma at time t.

In the discrete-time simulations, the equations above are integrated with Euler's method and a temporal resolution Δt of 1 msec.

Clustering Algorithm

The responses of the readout neuron centered above the target stimulus to 11 stimulus classes $S_1, S_2, \ldots, S_{11}$ are assigned to *11* response classes $R_1, R_2, \ldots, R_{11}$ yielding a *11 x 11* hit-matrix $N(S_\alpha,R_\beta)$. As a distance measure, the temporal correlation ρ of the target response with the mean response of each training class is used:

$$\rho = \frac{cov(i,j)}{\sqrt{cov(i,i)\ cov(j,j)}} \quad (5.3)$$

Where ρ is the correlation coefficient, i the mean response to the i-th training class, and j the response of the j-th test exemplar. A target exemplar is assigned to the response class with the highest correlation. Since we are only interested in the temporal evolution of the *TPC* generated by the encoding layer, the collected network responses are normalized to set the peak activation equal to one.

The mutual information I is calculated by:

$$I = \frac{1}{N_{tot}} \sum_{\alpha,\beta} N(S_\alpha, R_\beta) \left[\log_2 N(S_\alpha, R_\beta) + \log_2 N_{tot} - \log_2 \sum_a N(S_a, R_\beta) - \log_2 \sum_b N(S_\alpha, R_b) \right] \quad (5.4)$$

where N_{tot} is the total number of stimuli and $N(S_\alpha,R_\beta)$ the hitmatrix. For 11 equally probable classes, random classification corresponds to $N(S_\alpha,R_\beta)=N_{tot}/11^2$, where $I=0$. For perfect classification of the 11 stimulus classes, the mutual information becomes maximal, i.e. $I=log_2(11)=3.56$.

Chapter 7

Line discrimination task solved by the population code model

7.1 Management summary

In the previous chapter aspects of neural processing in visual object recognition were discussed. Another benchmark to describe the primate visual system is constituted by its visual acuity. In visual acuity the discrimination threshold for separations of visual elements is measured. A special and in psychophysics probably the best investigated task is the *Vernier line discrimination task*. In this task observers have to judge whether a vertical line segment is displaced to the right or the left compared to a reference segment. With a few seconds of arc which is clearly below the minimal retinal receptor distance the human perception threshold is amazingly low, and often termed *hyperacuity*. The amazing performance and the paradoxical fact that the perception threshold in *Vernier* tasks is below the minimal retinal receptor distance brought the psychophysical results into the center of interest of many physiological and computational modeling studies. Surprisingly after decades of research in this field it's still debated how the underlying neuronal mechanisms work. In this chapter we investigate, whether the model presented in the previous chapter is able to perform with hyperacuity in simulations resembling the *Vernier line discrimination task*.

7.1.1 Previous knowledge

A whole bunch of psychophysical studies undertaken during the last decades revealed detailed descriptive insight how humans perform in visual acuity tasks, and how the performance changes with training. Already shortly after the discovery of the hyperacuity phenomenon in the nineties of the 19th century researches postulated that the underlying mechanisms are probably based on an averaging process along the stimulus lines. This was questioned however with the discovery that hyperacuity is also observed if only dot pairs instead of whole line segments are used for the task. However theories which explain the phenomenon with pooling of information of single units in the early visual pathway are still alive and the core of all actual explanation attempts. Current theories mainly focus on the question how the neural system is able to learn the tiny differences between the two stimulus categories, i.e. left/right side displaced. This mainly breaks down to the question how the neural system is able to assign higher weights to units carrying differential responses for left/right displacements, even though their response amplitude is much smaller than the one for units without differential responses and where in the visual pathway it takes place (see introduction and results sections for more details).

The results show that the responsible mechanisms probably are mainly located in the early visual pathway, since training effects are not transferred between the eyes and different line segment orientations. Computational modeling approaches further revealed that the problem of weighing single unit outputs correctly to gain hyperacuity, can be solved in supervised learning paradigms and in an unsupervised manner.

7.1.2 New contributions

Pervious modeling approaches revealed more insight how hyperacuity in *Vernier* acuity tasks, is gained during training. However, most of the models neglected the spiking nature of neural output and did not incorporate the predominant connectivity patterns of the early visual cortex, the substrate they tried to model. Here we show that a model, which is based on the approach of the previous chapter and incorporates the fundamental projections patterns of the early cortex, i.e. extensive excitatory horizontal connections, and fast feed-forward projections, together with modulatory top-down input, performs with hyperacuity in a *Vernier line discrimination task*. In contrast to previous approaches we use spike-based neuronal model, and analyze the temporal structure of the network output to compute the task performance. We further demonstrate that our model reveals dependencies on various stimulus parameters that resemble the ones gained in psychophysical experiments. Together this supports the notion that the coding principle which relies on the lateral connectivity in combination with feed-forward and feed-back components as a coding substrate captures a main principle of how information is processed in the visual cortex.

7.2 Introduction

One of the amazing performance benchmarks in the primate visual system is its ability to perform with hyperacuity. Perception thresholds in line discrimination and bisection tasks typically reach values of a few seconds of arc (Westheimer and McKee, 1977a; Harris and Fahle, 1995). This is much less than the photoreceptor spacing in the retina which is about 30''. In addition the smallest receptive field center diameter measured in primates is around 2'. The performance seems not to be determined by the receptor distance or the receptive field dimension. Already in 1899, shortly after Wülfing (1892) first described the phenomenon, Hering postulated that hyperacuity is reached by an averaging process along the stimulus line. Later however it was shown that hyperacuity can also be observed in discrimination tasks where only dots instead of lines are used (Yap et al., 1987). Several studies hypothesized about the nature of the pooling or interpolation process (Fahle and Poggio, 1981; Wilson and Gelb, 1984; Wilson, 1986; Poggio et al., 1992; Poggio et al., 1992b; Weiss et al., 1993; Fahle et al., 1995a; Fahle, 2004). They support the notion that information of neighboring elements is combined and that the known spatial and frequency tuned mechanisms can provide the basis for hyperacuity.

The discrimination performance often improves with training. But the improvement is specific for the exact task, the stimulus location and orientation, and the training effect is not transferred between the eyes (Fahle, 2004). Although some aspects of hyperacuity learning seem to be dependent on feedback and attention (Herzog and Fahle, 1997, 1999), the specificity of the effect pinpoints the responsible mechanisms to the early stages in the visual pathway, where orientation sensitive monocular cells are located.

Recently a model for information encoding in the primary visual cortex was proposed, which uses precise spike timing properties produced by the dense lateral connectivity between cortical neurons as an encoding substrate. The so called temporal population code (*TPC*) supports rapid invariant classification, has a high capacity and is robust to noise (Wyss et al., 2003b; Wyss and Verschure, 2003; Knüsel et al., 2004). *TPC* exploits the dynamics of densely coupled neuronal networks with time-delayed connections. These transduction delays result from the physical distance between connected neurons, and a finite transduction speed for horizontal connections (Angelucci and Bullier, 2003). The characteristic physiological signature of the *TPC* is the introduction of phase lags in the responses of different neurons. The pattern of phase lags is stimulus specific. This has been observed in the primary visual cortex (Gray et al., 1992; Konig et al., 1995). Recently similar dynamics were observed in the processing of olfactory stimuli in the insect antennal lobe (Knuesel et al, In Press). In addition an extended version of the model (*enhanced TCP model*, presented in this thesis) which incorporates fast inter-areal feed-forward connections and introduces mechanisms that regulate the effective lateral connectivity by dynamic dendritic attenuation, has proven to

be able to segment several simultaneously presented stimuli, while retaining the advantageous properties of the original *TPC* model (submitted).

Given the classification properties of the *TPC* code, the question arises whether a network model based on *TPC* principles does not only produce robust stimulus-categorization dependent signals, but also very specific responses needed in object identification and visual acuity tasks. We show that in a special acuity task, i.e. line discrimination task the *enhanced TPC model* presented in this thesis exhibits discrimination thresholds below receptor distance, i.e. performs with hyperacuity, and further reflects similar threshold dependencies on various stimulus parameters like line length and line separation, as gained in human psychophysical tasks (Westheimer and McKee, 1977a). In line with earlier results (Wilson, 1986) we show in addition that the performance depends on the correct weighting of responses originating from cell populations with different preferred orientation tunings and receptive field sizes.

7.3 Methods

Task

We analyzed the classification of artificial visual stimuli in a *Vernier* discrimination task. In the task two line segments are presented either with a left- or right-sided displacement. Based on the network response a discrimination threshold is calculated.

Stimuli

Two vertical line segments each with a width of 1' are presented with the constant stimuli method to the network. In the simulations line segment displacements are varied between +/- 30'' (left-/right-displaced) with a step size of 1.2''. Displacements smaller than the receptor distance are simulated by setting the contrast level in each receptor proportional to the area covered by the stimulus, e.g. 1 if the whole receptor is covered or 0.9 if 90% are covered. For each displacement level network responses to 200 stimulus repetitions are collected. All stimuli have a contrast of 1 (all stimulus pixels set to 1, background set to 0). Discrimination thresholds for various line segment lengths between 30'' and 10' and line separations between 0 and 5' were calculated.

Network

The network consists of a 40x40 input layer (*input layer*) with topographic excitatory connections to a subsequent layer of equal size (*LGN layer*), containing neurons with a linear activation function, which perform *LGN*-like edge detection. The *LGN* neurons have circular *DOG* receptive fields, with an excitatory center width of 30' and an outer width of 1.5' (***Figure 7.1***).

The resulting activity is transmitted to the *V1* stage (*V1 layer*). *V1* consists of 36x40x40 leaky integrate-and-fire neurons. The receptive field of each neuron is modeled as an oriented *gabor*-patch shaped weight map (Wandell, 1995). The 36 *V1* layers with their orientation tunings cover the whole angular interval [0 2π] with a step size of $\pi/18$. According to the task, the receptive field diameter is varied between 7.5' and 15', with a center size of 2' and 4' respectively. The sizes match physiological data of *V1* receptive field sizes measured in monkeys (Wandell, 1995; Bosking et al., 1997b; Angelucci and Bullier, 2003).

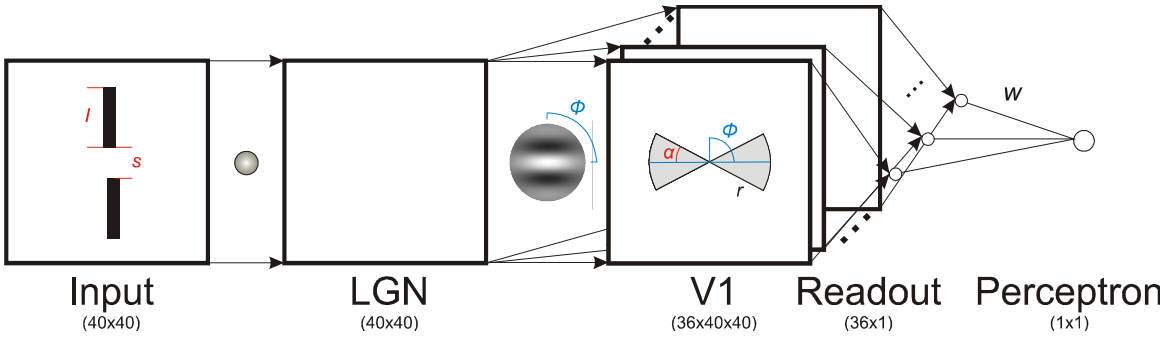

Figure 7.1: Network model used for the *Vernier* localization task: The *Vernier* stimuli with line segment length *l* and line separation *s* are projected on an input layer of linearly activated neurons. Subsequent *LGN* neurons with *DOG*-receptive fields perform edge detection, and send the resulting activity to 36 *V1* layers covering the preferred orientations from 0 to 2π. *V1* neurons are modeled as conductance based leaky-integrate-and-fire neurons with receptive fields formed by an oriented (*Φ*) *Gabor* filter. Each of the *V1* neurons gets in addition to the feed forward input excitatory input from other *V1* neurons of the same layer, lying within ±*α* (±*30°*) along the preferred orientation and within radius *r (0.3)*. The population activity is read out by 36 fully connected and linearly activated neurons centered above the *V1* layers. The frequency output of the read out neurons is used as input to a perceptron which reveals the optimal weights (*w*) to calculate the weighted sum of the temporal population activity which is subsequently used for the *ROC*-analysis.

Within each of the *V1* layers neurons get excitatory input from neighboring neurons located along the preferred orientation within segments of a circle with a diameter of 18’ and an angle of ±30°. The connections exhibit cell-cell distance related transmission delays. There are no connections between the layers. In addition each of the *V1* neurons is a source of noise modeled as a *Poisson* spike train of independent events, with a common spiking frequency of 5 Hz.

The resulting activity is readout by 36 fully readout neurons (*readout layer*) with linear activation functions. Each of these neurons corresponds to one preferred orientation and is fully connected to the corresponding *V1* layer with distance related transmission delays. In a subsequent supervised learning stage with the goal to optimize the discrimination performance, the frequency output of the readout neurons is used as input to a perceptron network. The learned optimal weights are used to build the weighted sum of the temporal population activity output of all readout neurons. The resulting activity trace is used to calculate the final discrimination thresholds.

For all presented stimulus exemplars the network activity is measured for a period between 0 and 100 ms after stimulus presentation.

Threshold

For the threshold calculation the 200 network responses per displacement level are divided into a training set and a test set.

In the subsequent *ROC* analysis (receiver-operator-characteristics) the network responses to 100 stimulus exemplars (training set) collected for a specific displacement level are compared to the pooled responses (25x100 exemplar responses – test set) for left- and right-displacement respectively or to corresponding equal displacement levels of the test set (e.g. *test*: 100 responses to 30''-displaced line segments are compared to *train*: 2x100 responses to ±30''). The temporal correlation between all possible response pairs delivers two distributions (match vs. non-match). The approximately normal z-transformed distributions are used to calculate the true-positive (*TP*) and false-positive (*FP*) rates to plot the *ROC* curve. The area under the *ROC* curve is considered as the performance for the selected displacement level. The procedure is repeated for each displacement level between 1.2'' and 30'' and for both sides (right-/left displacement), and the resulting data points are subsequently fitted by a logistic function. The fitting procedure which reveals the perception threshold and confidence intervals was performed with the psignifit framework (Wichmann and Hill, 2001b, a).

7.4 Results

With the current implementation of the *enhanced TPC* model we want to investigate whether the network response to *Vernier* stimuli provides a basis to achieve hyperacuity in a line discrimination task. Specifically we want to investigate whether the stimulus specific phase lags in the activity trace produced by the dense lateral coupling of the orientation tuned layers in *V1* allows classification of *Vernier* line stimuli under noisy conditions. The analysis should reveal the optimal weighting of the various orientation filters. In addition the discrimination thresholds should show similar stimulus property dependencies as the ones measured in human psychophysical experiments.

If we compare the mean output of orientation tuned neuronal responses for different *Vernier* stimuli, we see that the network produces a differential output for left- versus right displaced line segments (***Figure 7.2***, ***Figure 7.3***). ***Figure 7.2*** shows the normalized mean responses for abutting line segments each with a length of 2.5' for left and right side displaced stimuli. If we compare left versus right mean responses for corresponding displacement levels we see that the differential response increases with the displacement magnitude. It is the largest for a displacement of 30'' and is close to 0 over the whole recording period for 1.2'' (***Figure 7.3*** *A*). The mean response for 30'' left displaced stimuli is closer related to displacement levels of the same side than to the ones of the opposite side, i.e. the response difference to the left side displacements is smaller than the difference to the right side displacement levels (***Figure 7.3*** *B*).

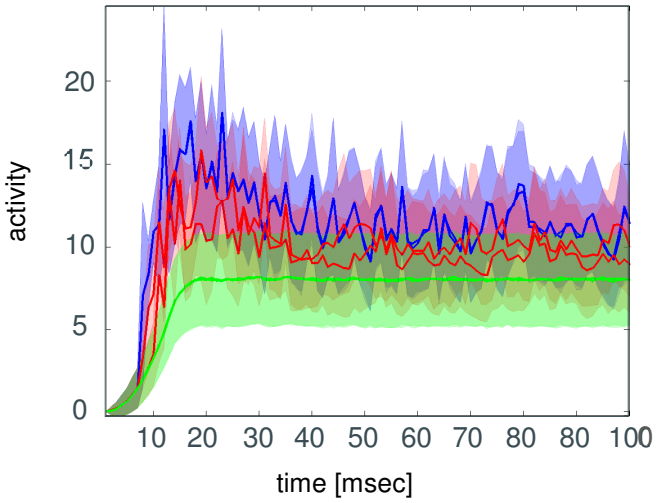

Figure 7.2*:* Population activity traces in the *Vernier* localization task: Activity of the read out neurons for the preferred orientations 0 (blue), π/9 (red) and π/2 (green) under noisy conditions. The two solid lines per orientation denote mean responses for left- and right-displaced segments respectively. Shaded areas denote the standard deviation of the activities collected for 5000 exemplars from 2x25 displacement levels [0 ±30'']. The activity for π/9 (red) shows intermediate amplitude but a large differential response between left- and right-displaced segments.

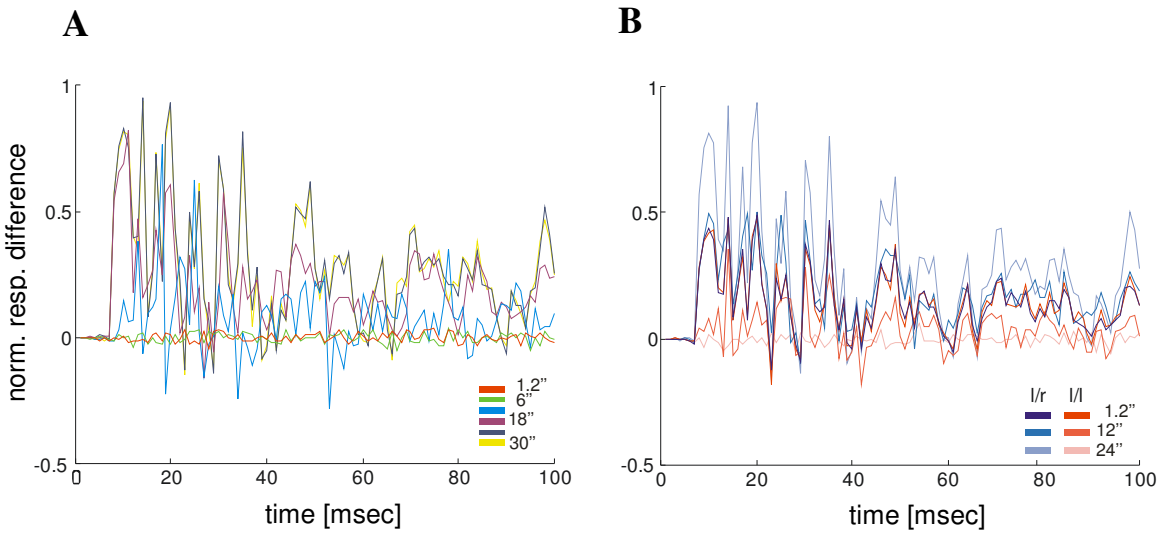

***Figure 7.3**:* Mean normalized readout neuron response differences between stimulus classes of the same or different displacement sides (left/right)/(left/left): (*A*) Response differences between corresponding left- vs. right displacement levels. The traces denote the mean normalized activity differences at each time point for an optimally weighted network output. Larger displacement levels (yellow) reveal larger response differences than small displacements (red). (*B*) Normalized mean response differences of the optimally weighted network output between 30’’-left-displaced and other displacement levels. The response difference between activities of the same displacement side (l/l – red) is smaller than the difference between activities of opposite displacement sides (l/r - blue).

The dependency of the discrimination threshold on the line segment length (***Figure 7.4** A*) reveals similar relationships as observed in human psychophysical experiments (Westheimer and McKee, 1977a). The threshold stays nearly constant at a low level around 15’’ for line segments bigger than 1’ and is elevated to 33’’ only for very small segments, i.e. 30’’ line segment length. The network is also able to reproduce characteristic responses in a situation where a gap between the line segments is present. However, to get optimal results bigger *V1* receptive field have to be used. This makes sense since smaller receptive fields are no longer able to produce a differential response if the gap between the line segments becomes too big. The simulations for line segments with vertical separation were performed with receptive fields of 15’ in diameter with an excitatory center of 4’. The thresholds show a almost linear increase for larger vertical separation levels, a fact which was also measured in human observers (Westheimer and McKee, 1977a) (***Figure 7.4** B*).

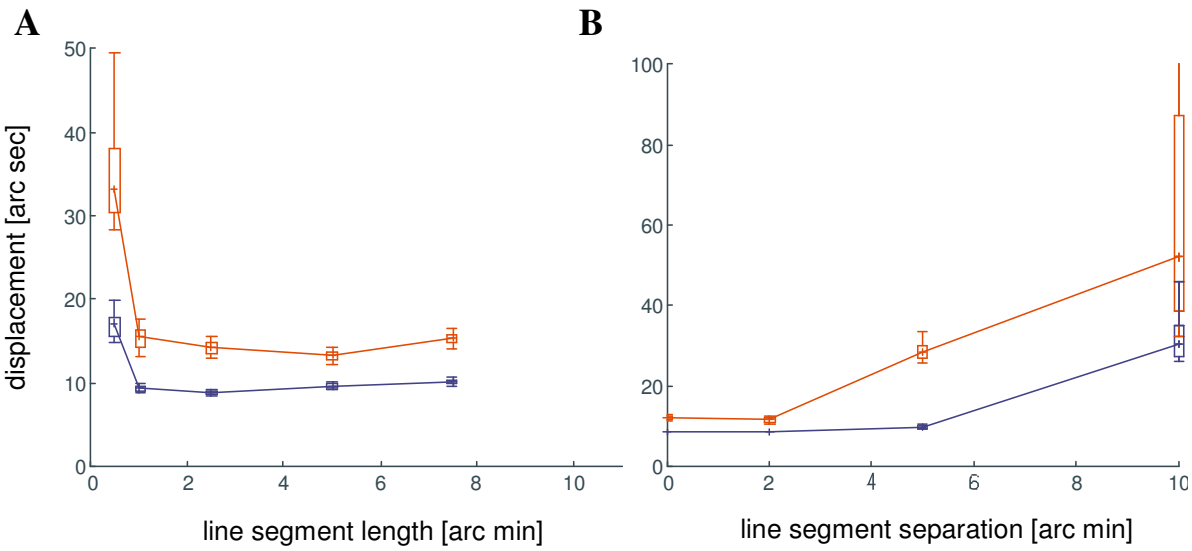

Figure 7.4: Dependence of localization performance on stimulus properties: Performance as function of line segment length and line segment separation. Red lines denote thresholds if responses of individual displacement levels are compared to the pooled responses of left- and right-displacements respectively. Blue lines show thresholds for the comparison of left-/right-displacement levels of equal magnitude. Each data point is the result of a *ROC*-analysis and subsequent fitting by a psychometric function. The network is considered to perform with hyperacuity if the threshold stays below 30''. (*A*) Threshold as function of line segment length. The performance stays nearly constant around 9'' and 15'' respectively, only very small line segments lead to an increase of the threshold. (*B*) Threshold as a function of line segment separation for a line segment length of 2.5'. The performance is getting weaker with increasing line separations.

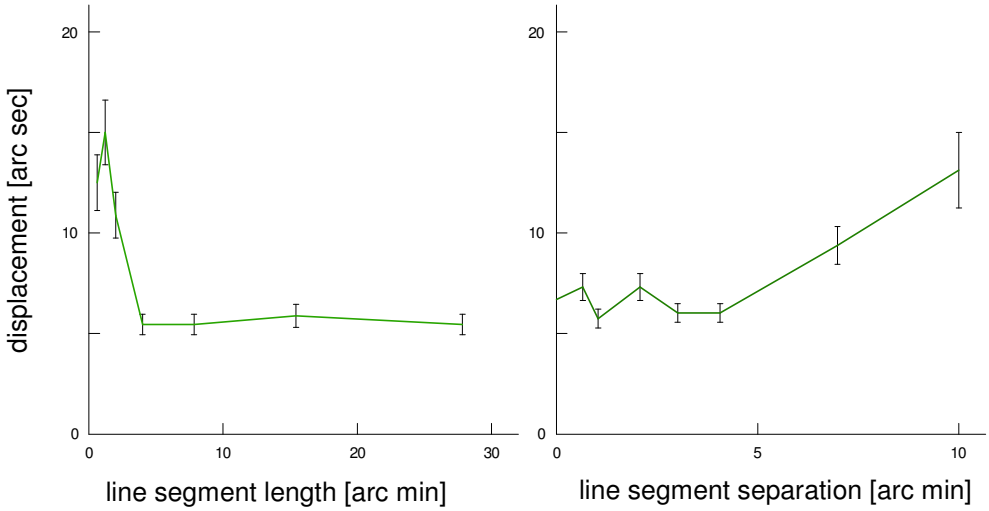

Figure 7.5*:* Dependence of localization performance on stimulus properties measured in human subjects: The human observers exhibit similar perception threshold changes as the *enhanced TPC* model (data for a single observer, figures based on data from (Westheimer and McKee, 1977a)).

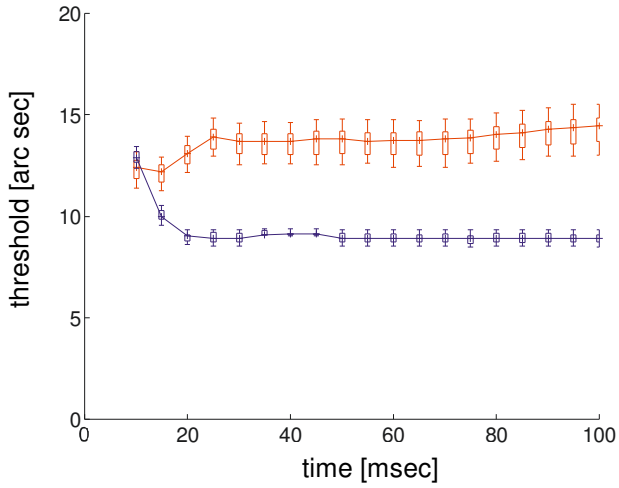

Figure 7.6: Time course of the threshold: Threshold at various time points after stimulus presentation for abutting line segments with a length of 2.5'. Red lines denote thresholds if responses of individual displacement levels are compared to the pooled responses of left- and right-displacements respectively. Blue lines show thresholds of the comparison between displacement levels of equal magnitude. Each data point is the result of a *ROC*-analysis and subsequent fitting by a psychometric function. The network is considered to perform with hyperacuity if the threshold stays below 30''. 25 ms after stimulus presentation the threshold stays approximately constant at hyperacuity level.

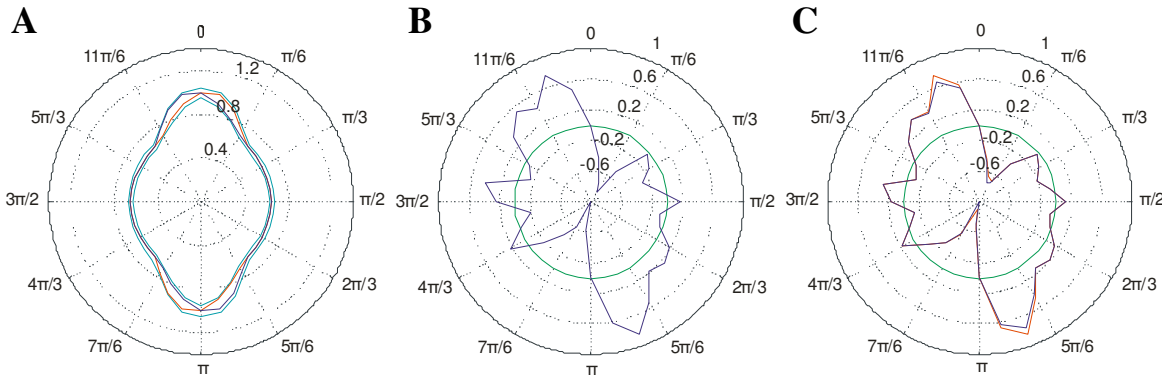

Figure 7.7: Optimally weighted network output: (***A***) Polar plot of the normalized mean rate output of readout neurons representing various preferred orientations between 0 and 2π. The *blue* line denotes the output for left- and the *red* line for right-displaced line segments. Cyan corresponds to the common standard deviation. The network produces a differential output for several preferred orientations. (*B*) Normalized optimal weights revealed by a perceptron network. Green line denotes the zero iso-curve. (*C*) Optimally weighted network output calculated by multiplying the output of *A* with the weight matrix of *B* and normalizing it. The *blue* line denotes the output for left- and the *red* line for right-displaced line segments. Green line denotes the zero iso-curve. The final network output used in the *ROC*-analysis corresponds to the sum of all weighted activities in *C*.

The time course of the threshold for abutting line segments of 2.5' length reveals an asymptotic decrease which reaches its minimum 25 ms after stimulus onset (***Figure 7.6***).

If we closer investigate the network output (***Figure 7.7***), we see that the *Vernier* stimuli produce differential responses for slightly tilted receptive fields. The difference between left- and right-displaced line segments is maximal around an angle of ±10° from the aligned orientation. This difference is captured by the perceptron which emphasizes output produced by neuronal populations with tilted receptive fields, to calculate the weighted sum.

7.5 Discussion

With the current implementation of the enhanced *TPC* network we wanted to investigate whether the model is able to perform with high accuracy in a *Vernier line discrimination task*. We show that the model performs with hyperacuity, meaning that the perception threshold is below the receptor distance, and that the dependencies of the threshold on various stimulus parameters, like line segment length or line segment separation are similar to the ones in human psychophysical experiments (Westheimer and McKee, 1977a). With a receptor distance of 30'' the model performs at best with a threshold of 9'' (**Figure 7.4**). Threshold levels are only increased for very small line segments or if the vertical line separation is increased. The results show that a network based on the fundamental cortical connectivity architecture produces a population activity trace which can be used to classify *Vernier* stimuli with hyperacuity.

In the presented model line segment shifts below the receptor distance are simulated by reduction of the contrast in the affected receptors. The contrast transmitted by a receptor is proportional to the area that is covered by the stimulus. The stimuli contain no external noise, i.e. they were perfect vertical line segments. The internal noise of the system is produced exclusively by the *V1* neurons which fire *Poisson* spike trains. The rate of the spontaneous spiking was set to a plausible frequency of 5 Hz according to measurements in the primary visual cortex of macaque monkeys (Ringach et al., 2002). To model internal noise while neglecting external sources is in line with results of human psychophysical experiments which show that the perception performance is mainly restricted by internal random noise, not stimulus dependent systematic noise (Li et al., 2006).

For a long time it was unclear how the primate visual system can perform with hyperacuity given the facts that the receptor distance is around 30'' but the smallest receptive fields in *V1* exhibit center excitatory regions with a diameter of 2'. Theoretical studies revealed that hyperacuity can be reached given these receptive field dimensions (Wilson, 1986; Weiss et al., 1993). The results of the current study point out that if the

precise spiking dynamics are taken into account, i.e. the stimulus specific phase lags in the population of orientation selective *V1* neurons, not necessarily responses of neurons with the smallest receptive fields serve as the basis for the best performance. In the simulations with vertical separation of the line segments bigger receptive fields than the ones used in the abutting line simulations perform clearly with hyperacuity, while the smaller receptive fields fail to produce differential responses (data not shown).

During the simulations the population activity of *V1* neurons is readout in a position related manner. A manually positioned readout neuron centered above the midpoint between the line segments (***Figure 7.1***) collects the spike responses of the neurons with distance related transmission delays. The position of the readout neuron is selected according to the position of *V1* cells which will expectedly produce the biggest differential response for left- versus right displaced line segments. The position and the results of the optimization procedure which reveals that not the neurons with the biggest response, i.e. with receptive fields aligned with the line segments, but neurons with slightly tilted receptive field orientation produce the maximum differential response (***Figure 7.7***) are in line with earlier theoretical considerations (Wilson, 1986). From this we would predict, that human observers will not asses to the whole stimulus equally, but instead will pay more attention on the central part around the midpoint, which will presumably produce the differential response. This is in line with recent findings in human psychophysics which state that observers in a position discrimination task weight the proximal parts of two segments more than the distal parts (Li et al., 2006). Future studies have to show whether the location of the readout neuron should be seen as a learned process or can be explained purely by stimulus statistics. Future psychophysical experiments and currently existing attention models like the one of *Itti et al.* could give deeper insights.

The supervised learning based optimization process and the subsequent *ROC* analysis for the temporal population activity traces shows that the used *Vernier* task represents a linear separation problem, where differential responses of orientation selective neurons are subtracted from one another. Future studies have to reveal whether the known architecture of the primary visual cortex in combination with appropriate learning rules lead to an unsupervised optimization of the perceptual performance revealing similar weights as in the above learning process.

7.6 Appendix

LGN Neuron

Input to the network passes through an edge detection stage by convolving it with a difference of *Gaussian* (*DOG*) kernel given by

$$k_{ij} = e^{-16r^2} - 1/4e^{-4r^2} \text{ with } r = \frac{\sqrt{i^2 + j^2}}{3} \text{ for } i, j \in \{-3,...,3\} \quad (5.5)$$

The resulting image is cropped to the original size and represents the activity in the *LGN layer*. *LGN* neurons have topographic excitatory connections to the *V1 layer* with an input conductance of 1.25 nS.

V1 Neuron

The time course of the leaky integrate-and-fire neuron's membrane voltage $V(t)$ is described by the differential equation:

$$Cm\frac{dV}{dt} = -(I_{exc}(t) + I_K(t) + I_{leak}(t)) \quad (5.6)$$

Where C_m is the membrane capacitance (C_m=0.2 nF), and $I_{exc}(t)$, $I_K(t)$ and $I_{leak}(t)$ represent the transmembrane currents. The currents are computed by the equation $I(t) = g(t)(V(t)-V_{rev})$ where g is the conductance and V_{rev} is the reversal potential of the conductance (V_{exc}^{rev} = 60 mV, V_K^{rev} = -90 mV, V_{leak}^{rev} = -70 mV). The neuron's activity at time t, $A(t)$, is given by $A(t) = H(V(t) - \theta)$ where H is the Heaviside function and θ is the firing threshold (θ = -55 mV). Each time a spike is emitted, the neuron's potential is reset to $V_{rest} = V_{leak}^{rev}$. The constant leak conductance g_{leak} is 20 nS. The time course of the potassium conductance is described by $\tau_K dg_K/dt = -(g_K(t) - g_K^{peak}A(t))$, with τ_K = 40 ms and g_K^{peak} = 200 nS. The synaptic interactions are 'instantaneous', such that the total input current at time t is the linear sum of all effective input currents at the cell soma at time t.

The neurons have receptive fields modeled by a *Gabor* patch shaped weight map which is characterized by its orientation (Φ), spatial frequency selectivity (v) and size (r). The activity in one column is defined by the absolute of the complex sum

$$a(\vec{x},\phi,v)=\left\|\sum_{\|\vec{y}-\vec{x}\|<r_{\max}^{v}}\exp(-(2\|\vec{y}-\vec{x}\|/r_{\max}^{v})^{2})\times\exp(i\vec{\phi}(\vec{y}-\vec{x})3\pi r_{\max}^{v})\right\| \qquad (5.7)$$

where $\vec{\phi}$ is the unit vector with angle ϕ, $r_{\max}^{v}$ is the normalized radius of the receptive field which is 0.15 or 0.3 respectively.

1600 Neurons sharing the same orientation preference are grouped in a 40x40 regular grid layer that spans the unit plane $[0\ 1]^2$. 36 topographically arranged layers containing neurons with corresponding receptive field centers and equal receptive field sizes but which differ in their preferred orientation cover the whole angular interval $[0\ 2\pi]$ with a step size of $\pi/36$. Depending on the experiment the receptive field size was either r=0.15 or r=0.3, with respect to the unit plane.

The neuronal units are laterally coupled. Each neuron gets excitatory input from neighboring neurons of the same layer, along the preferred orientation within segments of a circle with a diameter of 13' and an angle of ±30°. The transmission delays are related to the Euclidean distance between the pre- and post-synaptic cell, with a proportionality factor of τ = 1.03 ms/cell. In addition the synapses of the lateral connections connect in a distance related manner on the dendrite, where x, the distance between the synapse and the soma of the postsynaptic cell equals the Euclidean distance between the two cells. The excitatory input current $I_{exc}(t)$ originating from synapses of the lateral connections is attenuated while traveling along the dendrite, such that the effective current reaching the cell soma is equal to:

$$I_{exc}^{soma}(t)=I_{exc}(t)*e^{-a(t)x} \qquad (5.8)$$

Where $I_{exc}^{soma}(t)$ is the effective current integrated at the cell soma at time t, $I_{exc}(t)$ is the input current produced by the excitatory synapse, $a(t)$ is the attenuation factor along the dendrite and x is the distance between synapse and soma of the postsynaptic cell. For all simulations attenuation a is set to a constant value of 0.84.

There are no connections between neurons with different preferred orientation.

Each preferred orientation layer is fully connected to a readout neuron with a linear activation function. The transmission delays of the excitatory connections are distance related with a proportionality factor of $\tau = 0.62$ ms/cell

In the discrete-time simulations, the equations above are integrated with *Euler's* method and a temporal resolution Δt of 1 msec.

Optimal weights

The weighted sum of the 36 readout neuron responses represents a temporal population activity trace which is used in the subsequent *ROC* analysis. The optimal weights to make the binary choice whether a given response comes from a left- or right side displaced stimulus are revealed by a supervised learning algorithm, where the frequency outputs of the 36 readout neurons are used as input to a perceptron network. The perceptron has 36 input elements and one output neuron. Rate responses of 2x2500 stimulus exemplars from 25 displacement levels on each side are pooled in two groups and serve as input. The network uses a weight and bias learning function with 100 epochs and random presentation order of the input vectors in each epoch. The revealed optimal weights are used to build weighted sums of the 36 readout responses at each time point of the 100 ms recording period, resulting in the final population activity traces used in the *ROC* analysis.

Figure 7.7 shows the optimal weights for an example of abutting line segments each with a length of 2.5'.

Chapter 8

Vernier acuity with the enhanced model and *Ca²⁺*-controlled *NMDA*-synapses

8.1 Management summary

In the model we presented in the previous chapters we analyzed the network output based on precise spike timing. In an extended model of the coding-by-lateral-connections principle we achieved *Vernier* hyperacuity by exploiting the temporal and rate properties of the network output. The optimal weighing of the orientation filter banks was thereby achieved by a perceptron, which however did calculate the optimal weight matrix on the rate output only. Even though most of the current computational network models for object recognition and visual acuity are based on rate coding, from a biological point of view a spike timing correlation based learning algorithm would be preferable.

8.1.1 Previous knowledge

A number of interesting spike correlation based learning algorithms were developed in recent years. Some of them directly resemble the weight change dynamics measured in neural pairing experiments. A very promising model which reproduces learning dynamics of *NMDA*-synapses was recently presented by Shouval et al, aka *the calcium control hypothesis*. The model uses spike related calcium concentration changes at the postsynaptic receptor to control synaptic efficacy. The model goes far beyond pure *STDP* learning and reproduces a number of learning properties measured in physiological experiments.

Due to the inherent difficulties to describe and control spike time related learning on a network level, not many current object recognition or visual acuity network models make use of the biologically plausible learning algorithms. *SpikeNet* of Masquelier & Thorpe and the unsupervised clustering network of Bohte et al. are the exception here.

8.1.2 New contributions

With the introduction of the calcium control hypothesis of Shouval et al. into the model presented in this thesis we make the first steps to perform spike based object recognition with the model presented in the previous chapter of this thesis. We show that the temporal aspects of the code produced in the encoding stage of the model can be captured by the *NMDAR*-model in a non-trivial manner, and that the resulting weight changes can be used to solve simple object recognition tasks. In addition we show that the same model performs with hyperacuity in the *Vernier* task. The learning is thereby in

both tasks under control of modulatory feed-back signals which mimic cholinergic input originating from the basal forebrain. We interpret the results and postulate that the cholinergic top-down signal not only has attentional functions as described and measured by Roberts et. al in visual areas of cats, but that it may represent an integral part in the supervised control of learning along the visual pathway.

8.2 Introduction

In the previous chapters we presented a model which allows classification of objects in bounded regions in a visual scene, i.e. scene segmentation by virtue of an *ACh*-model resembling attention-related mechanisms. In addition we have shown that an extended version of the principle, i.e. a combined code sharing temporal and rate properties, which uses orientation selectivity as found in the primary visual cortex, is able to solve a *Vernier line discrimination task* with hyperacuity. In this version of the model we used a preceptron to decode the information contained in the output spike trains of the model. The perceptron however did not consider the exact temporal structure of the spike trains, but used the time-averaged population rate to calculate the optimal weight matrices. Whether this is a plausible biologically model of learning and decoding of information in spike trains is questionable. It is for example unclear how the backpropagated error signal, the perceptron roots on, is represented in natural neural networks. In addition the preceptron learning procedure neglects the temporal information contained in spike trains.

The question arises whether the code produced by the transmission delays of the lateral and fast feed-forward connections can be used in combination with biologically more plausible correlation based, i.e. hebbian-like learning mechanisms, to solve visual pattern classification tasks. To connect this thesis section with the previous chapter, we again used *Vernier*-like bar stimuli. We present that our model, in combination with a biologically plausible *NMDA*-synapse model, is able to decode spike-based information, and performs with hyperacuity in the *Vernier* localization task. The results represent the first steps towards a network which learns object recognition based on precise spike timing.

The *NMDA*-synapse model we have chosen was recently presented by *Shouval et al* (Shouval et al., 2002a). It exploits the notion that the efficacy alterations in *NMDA*-synapses are correlated with calcium concentration changes during learning – the reason why the model is also termed *calcium controlled hypothesis*. The model goes beyond pure *STDP*-like learning, and shows various signal transmission properties as observed in physiological experiments, e.g. the dependence of the synaptic efficacy on the presynaptic spiking frequency, or the postsynaptic membrane potential. The detailed physiologically rooted synaptic model covering membrane potential, frequency and spike timing

dependencies made the synapse to an ideal candidate to explore its capacity to reflect temporal structures of the *TPC* traces produced by the model presented in this thesis.

We show that the working mode of the synapse, i.e. potentiation or depression, can be controlled by the same modulatory cholinergic top-down signal we proposed in the previous chapters. In this learning scheme the modulatory input represents a supervisor signal which selects neuronal groups, which represent the input stimulus by forcing surrounding populations into the depression learning mode. After many stimulus repetitions the synaptic efficacies converge and lead to a situation where cells predominately respond to their target stimuli. The final weight is thereby not only dependent on the presynaptic rate, but is also sensitive to the fine temporal structure of the input spike train.

8.3 Methods

Task

We investigated whether stimulus features encoded in the proposed *enhanced TPC* model can be learned and decoded by neural structures which comprise biologically plausible plastic synapse model, i.e. the calcium controlled synapse (Shouval et al., 2002a). The first group of the simulations performs a binary classification of spatial patterns, i.e. an *A*- or *B*-task paradigm, where two output neurons are trained to individual target bar-patterns. The second group investigates the question whether the principle can be applied to the *Vernier* acuity task, presented in the previous chapter. Specifically we want to answer the question whether the fully spike based model performs with hyperacuity.

Stimuli

Simple spatial patterns were used, i.e. bars with various inter-stimulus angles, and *Vernier* line segment stimuli. The *Vernier* stimuli were identical to the ones used in the previous chapter.

Network

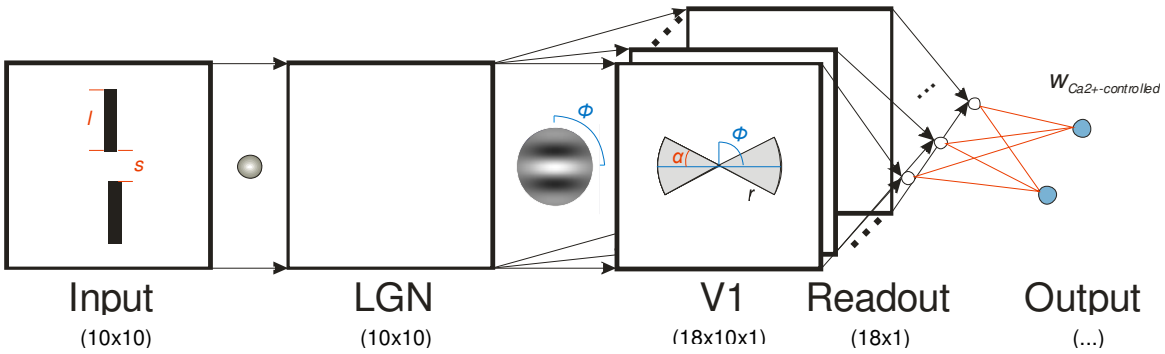

Figure 8.1: Network model used for the *Vernier* localization task in combination with *NMDA*-synapses: Network used to produce pattern specific cells, i.e. units with increased activity for trained target-stimuli and decreased activity for non-targets. The network equals the proposal in chapter 5 (*Vernier line discrimination task*) with the exception of the learning approach. In the final step fully connected output neurons receive input from the readout neurons (*red projections*), which collected the temporal population activity from feature selective cells in *V1*. The synapses adopted from Shouval et al. (calcium controlled synapses (Shouval et al., 2002a)) use the various properties of the pre- and postsynaptic cells to perform weight changes.

The formation of the stimulus specific spike code is equal to the proposal in the previous chapter. Spatial patterns are projected onto input layer representing the retina, which projects to an *LGN* layer which performs edge detection by *DOG*-receptive fields. Feed-forward connections send the resulting activity to populations of orientation selective neurons, comprising *Gabor* patch like receptive fields. Each of these neurons gets input from other neurons with the same orientation selectivity, located within a given radius and along the preferred orientation. The layers containing the orientation sensitive neurons cover the whole range from *0* to π with a step size of $\pi/18$. The temporal population code produced by the horizontal connections is read out by fast-feed-forward connections with distance related transmission delays. Unlike the model in the previous chapter the output of the readout neurons is not sent to a perceptron, which performs a binary classification, but to a fully connected population of neurons comprising calcium-controlled plastic synapses (for a detailed description of the neuron model, topology and formation of the temporal population code refer to methods and appendix of chapter 7, and ***Figure 8.1*** of this chapter). Each neuron is trained to a single pattern or to a stimulus class, with the goal that output units signal the identity of the trained pattern by their increased activity, i.e. on a rate basis.

Network parameters		
Layers		
INPUT (10x10 cells) - linearly activated units		
LGN (10x10cells) - linearly activated units		
V1 (10x10x18) - conductance-based LIF-units		
membrane resting potential (V_{rest})	=	-70 mV
spiking threshold (θ)	=	-55 mV
membrane capacitance (C_m)	=	0.2 nF
potassium peak conductance (g_K^{peak})	=	200 nS
potassium conductance time constant (τ_K)	=	40 ms
leak conductance (g_{leak})	=	20 nS
leak conductance reversal potential (V_{leak}^{rev})	=	-70 mV
exc. conductance reversal potential (V_{exc}^{rev})	=	60 mV
pot. conductance reversal potential (V_K^{rev})	=	-90 mV
relaxed dendr. log-attenuation factor (a)	=	0.84
Poisson spike rate ($v_{Poisson}$)	=	5 Hz
V1-readout (18 cells) - conductance-based LIF-units		
relaxed dendr. log-attenuation factor (a)	=	0
Poisson spike rate ($v_{Poisson}$)	=	0 Hz
rest of parameters as in V1		
$OUTPUT_{Ca2+\text{-}controlled}$ (2 cells) - conductance-based LIF-units		
relaxed dendr. log-attenuation factor (a)	=	0
tense dendr. log-attenuation factor (a)	=	10
Poisson spike rate ($v_{Poisson}$)	=	0 Hz
rest of parameters as in V1		
Connections		
INPUT→LGN		
DOG-filter [4.0/3.0(exp(-sqr(r/0.25))-0.25*exp(-sqr(r/0.5)))]*		
Radius (r)	=	0.1
LGN→V1		
oriented Gabor-patch (Φ, v, r) → see (5.7)	=	[0 π], 1/r, 0.6
V1→V1		
radius (r)	=	1
transmission delay (d)	=	1.03 ms/cell
V1→V1-readOut		
full connectivity within same orientation preference		
transmission delay (d)	=	0.62/cell
V1-readOut→OUTPUT		
full connectivity (NMDA-synapses), no transmission delays		
CHOLINERGIC→V1 / OUTPUT		
full connectivity, no transmission delays		

Table 8.1: Network parameters of the enhanced model including *NMDA*-synapses.

Synapse

Synapses in the brain are bidirectionally modifiable, i.e. exhibit *LTP* and *LTD*, as demonstrated for example in *CA1*-synapses in the *hippocampus* (Dudek and Bear, 1993). Findings of the past years indicate that the important variable is the amount of integrated postsynaptic *N-methyl-D-aspartate* (*NMDA*) receptor (*NMDAR*) activation during learning (Mulkey and Malenka, 1992; Kirkwood and Bear, 1994; Cummings et al., 1996). Strong *NMDAR* activation induces *LTP* and modest activation leads to *LTD*.

Recently Shouval et al. presented a synapse model for N-*methyl-D-aspartate receptor*-dependent long-term depression and long term-term potentiation (Shouval et al., 2002a). It reproduces *LTP*/*LTD*-dependencies on various biophysical properties of the pre- and postsynaptic cells, e.g. membrane potential of the postsynaptic neuron during presynaptic stimulation, the rate of presynaptic stimulation, and the timing of pre- and postsynaptic action potentials. Thus, the model goes beyond pure *STDP*-learning, since it incorporates various routes in a single model, which leads to biologically meaningful learning modifications at the synapse.

The underlying variable which controls the behavior of the model is the calcium influx through *NMDARs*, and the resulting calcium concentration change in fractions of the postsynaptic cell. The experimentally confirmed assumption is that modest calcium elevation leads to *LTD*, whereas higher concentrations lead to *LTP*. The *STDP* is *NMDAR*- and calcium-dependent as well (Markram et al., 1997; Bi and Poo, 1998) and modeled in a way that postsynaptic back-propagated spikes occurring shortly after a presynaptic action potential lead to a large calcium elevation and therefore to *LTP*, whereas in situation where postsynaptic spikes arrive shortly after presynaptic events lead to *LTD*.

For detailed information about the basic properties of the synapse and equations consider the appendix of this chapter.

8.4 Results

With the implementation of the calcium controlled synapses in the *enhanced TPC* model, we want to deliver a proof-of-concept that the stimulus specific code produced by horizontally connected excitatory neurons, which is collected by fast feed-forward connections, can be used to produce units which exhibit learning-derived stimulus specific activity. Specifically we wanted to investigate the capacity of the units to learn bar patterns in *A-or-B* classification- and identification tasks. The units should signal the target stimulus or class by higher spiking frequency, as compared to the activity for the non-targets. The experiments are in close relation to the results in chapter 7, where a perceptron was used to solve a *Vernier line discrimination task*. Whereas the perceptron used the mean activity of the orientation selective cell populations to obtain optimal weighing of the temporal population code (*TPC*), the learning of the units in this fully spike based network, with the calcium controlled synapses directly use the temporal structure of the *TPC* during the learning procedure, as well.

If we analyze the convergence of the synaptic weights as a function of presynaptic frequency and temporal structure of the input spike stream (***Figure 8.2***), we see that there is no trivial relationship between the input frequency and the converged synaptic efficacy. Even small input frequencies as 3 Hz are able to produce a high weight value. Correspondingly higher input spike frequencies do not necessarily lead to elevated efficacies; they can as well produce very low weights. As ***Figure 8.2*** shows the weight distribution medians (*red line*s) for 1000 trials/frequency decrease up to an input rate of 10 Hz, and then start to increase up to the tested limit of 20 Hz. Intermediate frequencies show a strong tendency to cover the whole range of possible weight values, i.e. whiskers which denote 1.5 times the inter-quartile distance extend from very low (~0.1) to very high values (~0.9) - individual distributions are significantly different with a confidence probability of 5%, when the notches flanking the medians do not overlap. The underlying mechanisms of this competence are illustrated in the appendix of this chapter.

The capacity of the synapse to produce input frequency- and temporal structure dependent efficacies makes the calcium controlled hypothesis a strong candidate to capture and exploit the coding properties of the *enhanced TPC* model. The *enhanced TPC* model transforms spatial stimulus properties into spike based temporal representations. In the exemplary implementation which is based on recurrently connected orientation selective neurons, the *TPC* is collected *feature-bank specific* via a series of output channels. We wanted to test whether a small number of cells and synapses is enough to solve suited *A-or-B* identification tasks, i.e. identification of bar stimuli (well controlled bar pairs and *Vernier* stimuli).

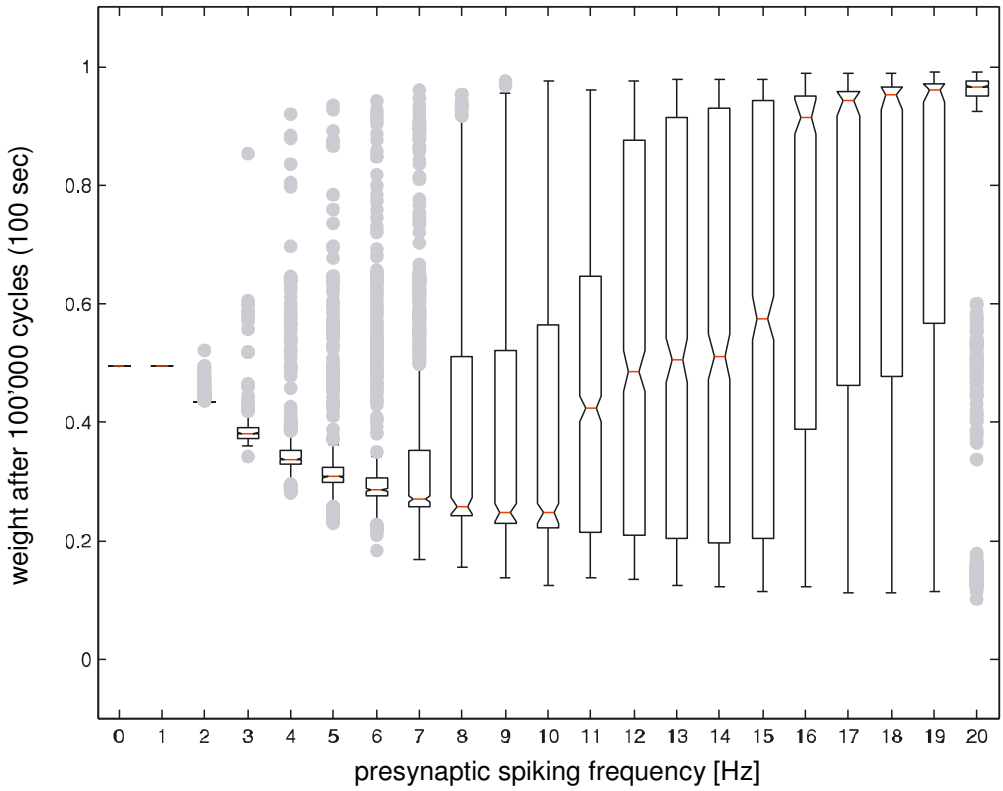

Figure 8.2: Synaptic plasticity for various spike trains: The boxplot data denotes the weight of a single synapse if trained with spike trains of various frequencies and temporal structures. The *red* horizontal line in each box denotes the median of the data points. The two *black* lines of the box represent the upper and lower quartile values, and the whiskers extend up to 1.5 times of the inter-quartile distance. *Gray* dots display outliers with values beyond these limits. For each represented frequency 1000 sequences with a length of 1000 ms, and with exactly the same number of spikes but different temporal structures were used to perform the training. In independent simulations where the postsynaptic cell was allowed to spike each sequence was repeated 100 times before the weight data was collected. The initial weight of the synapse was set to an intermediate level of 0.5 before the training procedure started. The weight shows a non-trivial dependence on the spike frequency. Even very small frequencies are able to produce high weight values when the temporal structure of the spike train is optimal. Higher frequencies tend to converge to higher values but still can produce very low weights, depending on the structure of the action potential sequence.

If we investigate the performance of the model to identify bar patterns separated by a variable angle under noisy conditions (**Figure 8.3**), we see that the *AUC*-value (area under the *ROC* curve) denotes an almost perfect identification down to a separation angle of 30°. Lower angles lead to an adequate identification of the target in only one of the two trained cells, as visible in the large standard deviation in the *AUC*-values of the cells. If the same cells are trained with new patterns, they exhibit again a very good identification performance for the targets. In addition, despite of the small numbers of synapses the cells do not *forget* the previous history. They are still capable to perform the *A-or-B* identification with the old patterns. This is also true when the old and new target are not

highly correlated, which would allow the cell to just maintain and stabilize the gathered synaptic efficacies (see 2D-correlation in figure).

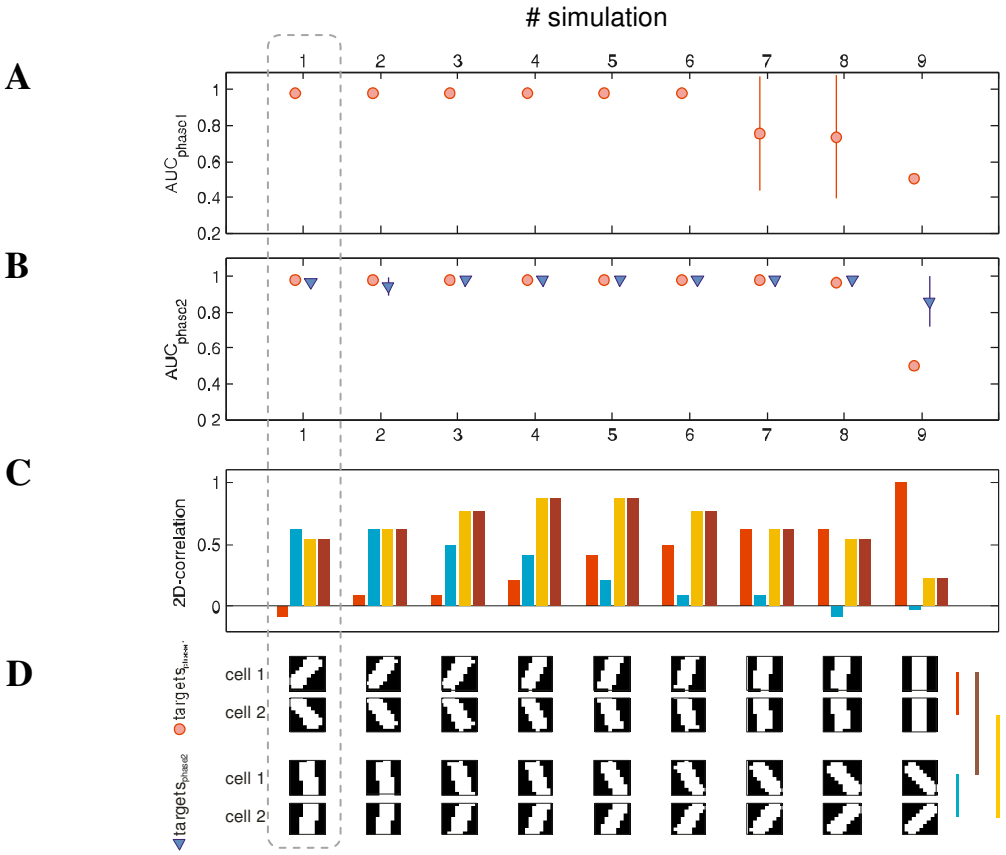

Figure 8.3: Identification performance for 9 neuron pairs trained to bar patterns with various separation angles: Data belonging to one simulation is arranged in columns (see gray dashed box for simulation #1). Each x-axis position in (*A*) and (*B*) denotes an independent simulation where a pair of neurons with Ca^{2+}-controlled synapses and cholinergic modulatory input were trained to bar patterns (*D*). (*A*) *AUC* values for 10 pairs of neurons trained to targets in (*D*, $targets_{phase1}$). *Red dots* denote the mean performance (as *AUC*) of the two cells for each of the 10 binary classification tasks. As expected identical patterns lead to a performance at chance level, i.e. 0.5 which means 50% correct. Already a separation angle of 20° allows a classification with 72% correct, bigger angles are classified almost perfectly. (*B*) *AUC* values for cells trained to patterns in (*D*, $targets_{phase1}$) and subsequently retrained to new targets in (*D*, $targets_{phase2}$). The result shows that the cells learn the new targets (*blue triangles*) and the same time are still able to separate the old patterns (*red dots*). (*C*) The distance between the two target patterns as 2D-correlation. The color coded bars denote the 2D-correlation of pairs of target patterns as notified by the colored lines in (*D*).

If we have a closer look at the effects of an additional learning phase, we see that the temporal structure of the response to the old target is preserved after learning new targets **Figure 8.4**. In a situation where the model first learns to identify two bars separated by 80° and subsequently is trained to bars with an angle of only 10. While the non-target trace reflects a very low activity after the initial learning sequence, it is

increased after the additional training phase. However the overall activity for the old target is still higher than for the old non-target, and the delay to the first spike is smaller for the target pattern, i.e. 11 ms for the old target vs. 13 ms for the old non-target. The new target/non-target stimuli separated by only 10° are harder to separate. However, the model reliably produces higher activity for the new target, than for the new non-target stimulus **Figure 8.4**. Remarkably, the large standard deviation present for 10°-bars with only one training phase (see **Figure 8.3** *A*) is no longer present if the model was trained to bar stimuli separated by a bigger angle before (see **Figure 8.3** *B*)

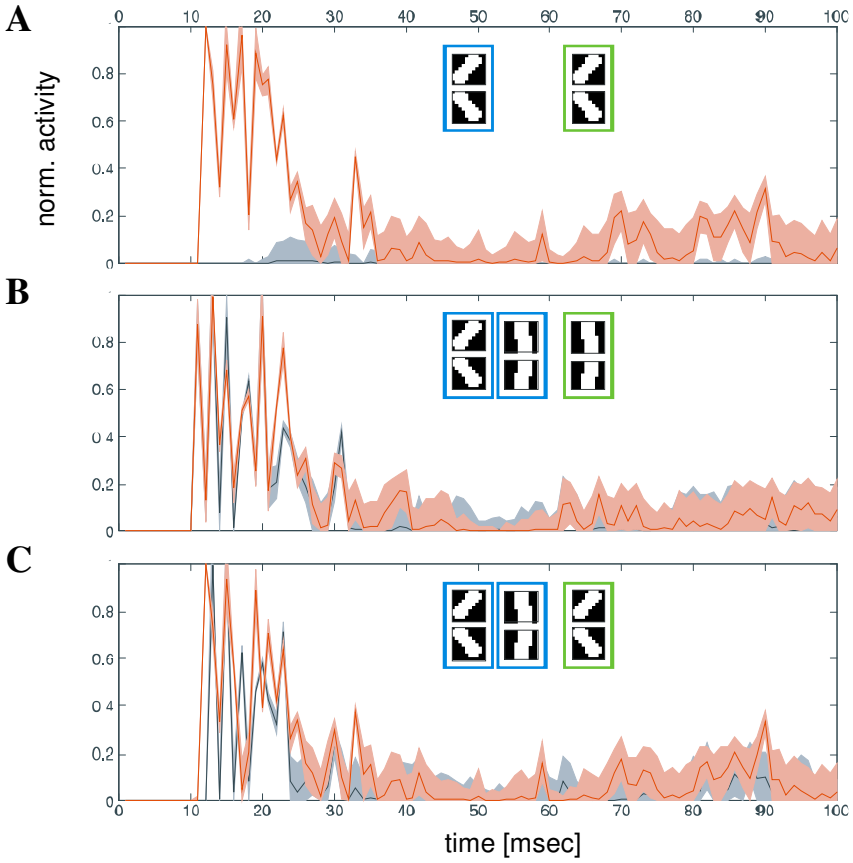

Figure 8.4: Activity traces for trained output cells: Examples of temporal activity traces after the first and the second learning phase (*blue boxes*, upper = target, lower = non-target). The solid lines denote the mean over 2500 trials (tested with patterns in *green boxes*), shaded areas represent the standard deviation. (*A*) in the initial training phase, target and non-target exhibit a separation angle of 80°. After training the cell shows a clear separation between target and non target, i.e. the activity for the target is higher than for the non-target. The delay to the first spike is smaller for the trained compared to the untrained pattern. (*B*) In the second training phase the separation angle between the two bar stimuli is only 10°. The separation in the averaged temporal response is less clear now. But as the previous figure reveals the *ROC* analysis still returns an *AUC*-value of 0.96. (C) shows the responses to the initial patterns after the cell was trained with new target/not-target stimuli. It turns out that the non-target increased its activity. However the response to the target stimulus (*red curve*) is still highly correlated to the initial trace (*red curve in A*). Hence the cell is able to learn new patterns without 'forgetting' previous targets.

Considering the learning dynamics of the system (***Figure 8.5*** and ***Figure 8.6***) we see that the model reveals an initially steep learning curve. Starting with a uniformly distributed weight matrix, i.e. initially all weights at 0.25, with learning, targets units exhibit a higher activity compared to non-targets even after a few pattern presentations. For bars separated by 80° (***Figure 8.5***), the non-target response is lowered, while the target activity is boosted to an upper frequency around 120 Hz, reached after about 50 randomly selected pattern presentations (corresponds to 50'000 cycles or 50 seconds). The situation is similar for bars separated by only 50° (***Figure 8.6***); the maximum frequency of about 120 Hz for target stimuli is reached for both cells around 50 randomly chosen presentations. However, as revealed by the non-target activity traces, the opposing learning regimes lead to fluctuations of the activity for non-target stimuli. This is plausible since for a given cell and synapse the presentation of the target leads to an increase of efficacy, and the correlated non-target to a decrease. In situations where both inputs are comparably effective the synaptic efficacy starts to oscillate around an intermediate value. If the non-target reveals more effective input for this synapse it will lower the efficacy to very low values.

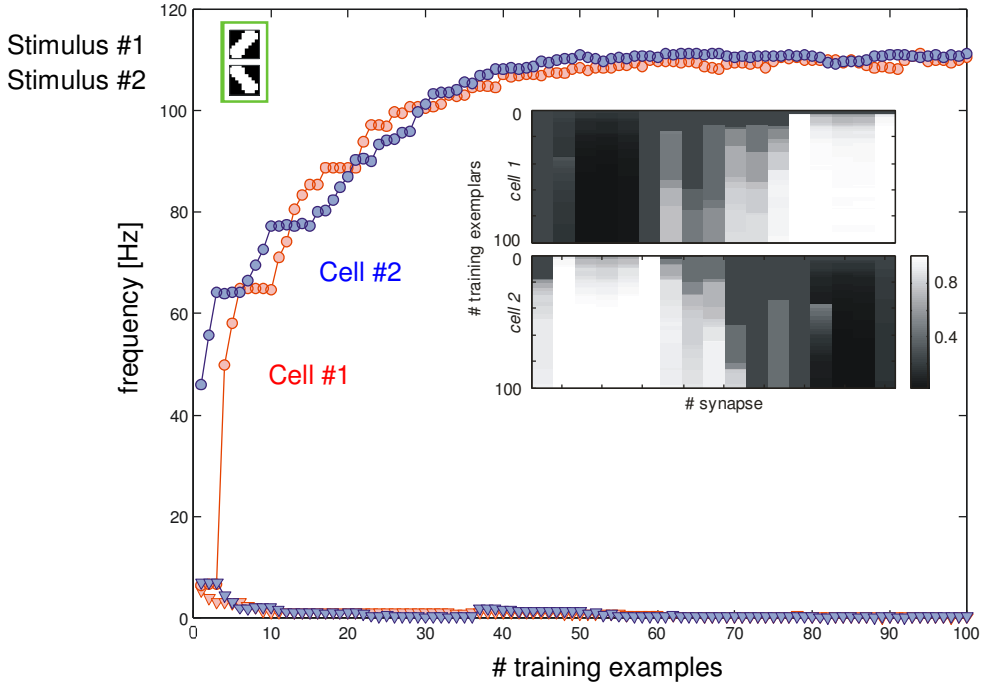

Figure 8.5: Learning dynamics of trained output cells I: Learning dynamics for two cells trained and tested with target/non-target bar stimuli separated by an angle of 80° (*green box*). Color coded is the output frequencies of the two cells (*red* equals *cell #1- trained to stimulus #1*, *blue* equals *cell #2 – trained to stimulus #2*). The markers separate the target (*dots*) from the non-target (*triangles*). The network was trained by showing 100 randomly chosen target/non-target stimuli. After each presentation which lasted 100 ms, the output frequencies of the network were collected by presenting 5000 exemplars of the target and non-target. The small inlay indicates the development of the weights over the whole training session. Both cells are able to indicate the membership of the presented stimulus by their output frequency. According to the large separation angle of the target/non-target bars the synapses develop high or low weights.

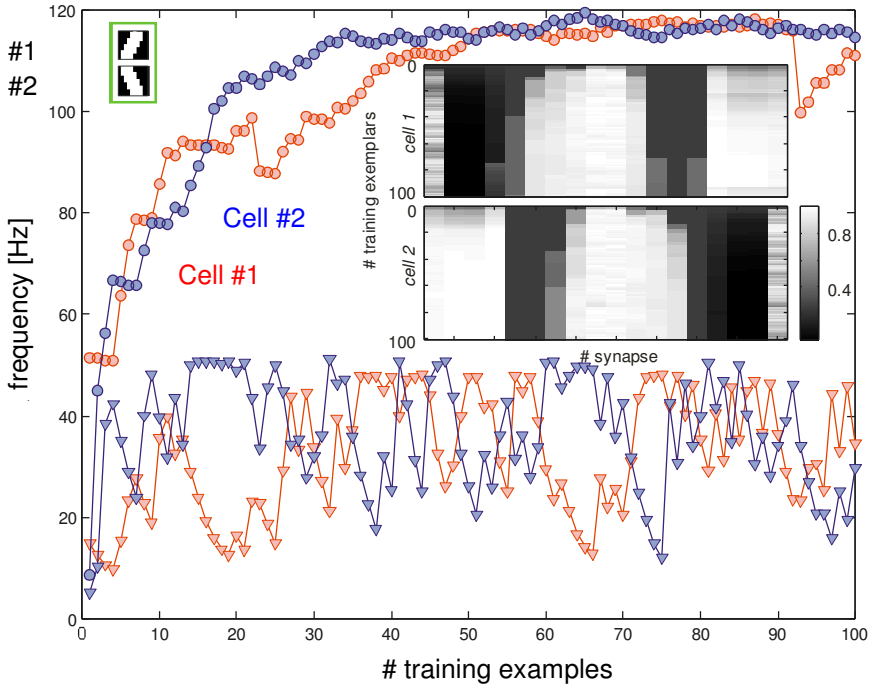

Figure 8.6: Learning dynamics of trained output cells II: Learning dynamics for two cells trained and tested with target/non-target bar stimuli separated by an angle of 50° (*green box*). Color coded is the output frequencies of the two cells (*red* equals *cell #1- trained to stimulus #1*, *blue* equals *cell #2 – trained to stimulus #2*). The markers separate the target (*dots*) from the non-target (*triangles*). The network was trained by showing 100 randomly chosen target/non-target stimuli. After each presentation which lasted 100 ms, the output frequencies of the network were collected by presenting 5000 exemplars of the target and non-target. The small inlay indicates the development of the weights over the whole training session. Both cells are able to indicate the membership of the presented stimulus by their output frequency. However, due to the limited separation angle target start to compete for certain synapses. The weights and as a consequence the output frequency start to oscillate during the learning procedure. This is especially visible for the output corresponding to the non-targets (*triangles*).

As shown the network is able to solve the *A*- or *B*-identification task with simple bar stimuli under noisy conditions. The question arises whether it is also able to generalize over several bar stimuli to form a class percept, as needed in *Vernier* acuity tasks, where right- and left- displaced stimuli have to be grouped into two classes. If we investigate the performance and learning dynamics of the network in the *Vernier* acuity task, where in each trial the winner output neuron is chosen based on its response frequency, we observe that the output cells are able to signal the line displacement side with hyperacuity (***Figure 8.7***). Hence, the cells with the *NMDA* synapses, in combination with the modulatory top-down signal are able to exploit the code of the input streams to generalize over several stimuli and form class percepts. Considering the learning dynamics and the transfer between presentation angles, we see that the network improves its performance the number of presented stimuli, resembling the learning characteristics

of human observers (Fahle, 2004). Additionally we see that that the learnt improvement is not transferred between presentation angles. When vertical *Vernier* stimuli after 100 random stimulus presentations, are rotated by 90° (corresponding to 100'000 cycles), performance drops to the pretraining level, from where it again reaches hyperacuity after 100 additional stimulus presentations.

The spike raster plots for various time points during learning reveal that the cells encode the *Vernier* stimuli in a period between 10 and 30 ms after stimulus onset, by virtue of only a few spikes. After 100 random presentations, with a displacement magnitude around threshold, even the first spike is enough to reliably detect the stimulus class (***Figure 8.8***). Hence, averaging over many output cells (in the current network only one unit per class is used) would allow to decode the *Vernier* stimulus after about 13 ms with only one spike per cell. In the light of the very fast classification capabilities of primates, i.e. reliable object detection around 100 ms after stimulus onset, this fits quite well to the considerations stated by Kirchner & Thorpe (Kirchner and Thorpe, 2006), which suggest that along the visual hierarchy the processing can only be based on one or a few spikes at each stage.

As already shown, highly correlated input turns out to be difficult to identify with only two output cells and a small number of synapses, since all the synapses are subject to competition between both, target and non-target stimuli. This can lead to oscillations of the output activity, depending on the learning sequence and the noise in the system. However, this and the fact that noise can override small differences between target/non-target output activities can be overcome with averaging over larger ensembles of neurons. The comparably small number of stimulus representing input neurons together with the high noise level in the *TPC*-producing neurons puts hard requirements to the learning network. We show that a simple and plausible increase of the number of neurons is able to overcome the difficulties and to produce meaningful performance in the *Vernier line discrimination task*.

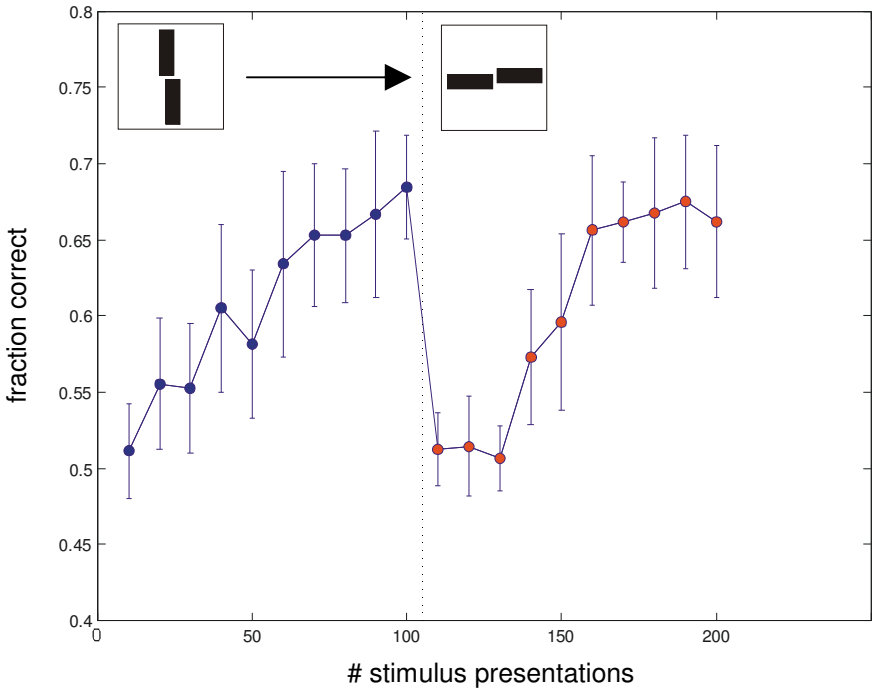

Figure 8.7: Learning Dynamics of the network for various *Vernier* stimuli: The curves show the mean performance (fraction correct for *Vernier* stimuli 0'' to ±30'' displacement) of the two trained cells in the *Vernier* acuity task for various training periods and training situations. *Blue circles*, performance progress for an initially equal weight distribution, for vertically oriented *Vernier* stimuli. *Red circles*, performance dynamics with training for horizontally oriented *Vernier* stimuli for a network previously trained to vertically oriented stimuli. Dashed line after 100 random stimulus presentations (corresponds to 100'000 cycles) denotes the switch from the vertically oriented to the new tilted *Vernier* stimuli. The last data point after 200 # training stimulus presentations corresponds to a perception threshold of 17.62 arc sec, as revealed by fitting the displacement level dependent *AUC*-values to a psychometric function (for detailed method see chapter 7).

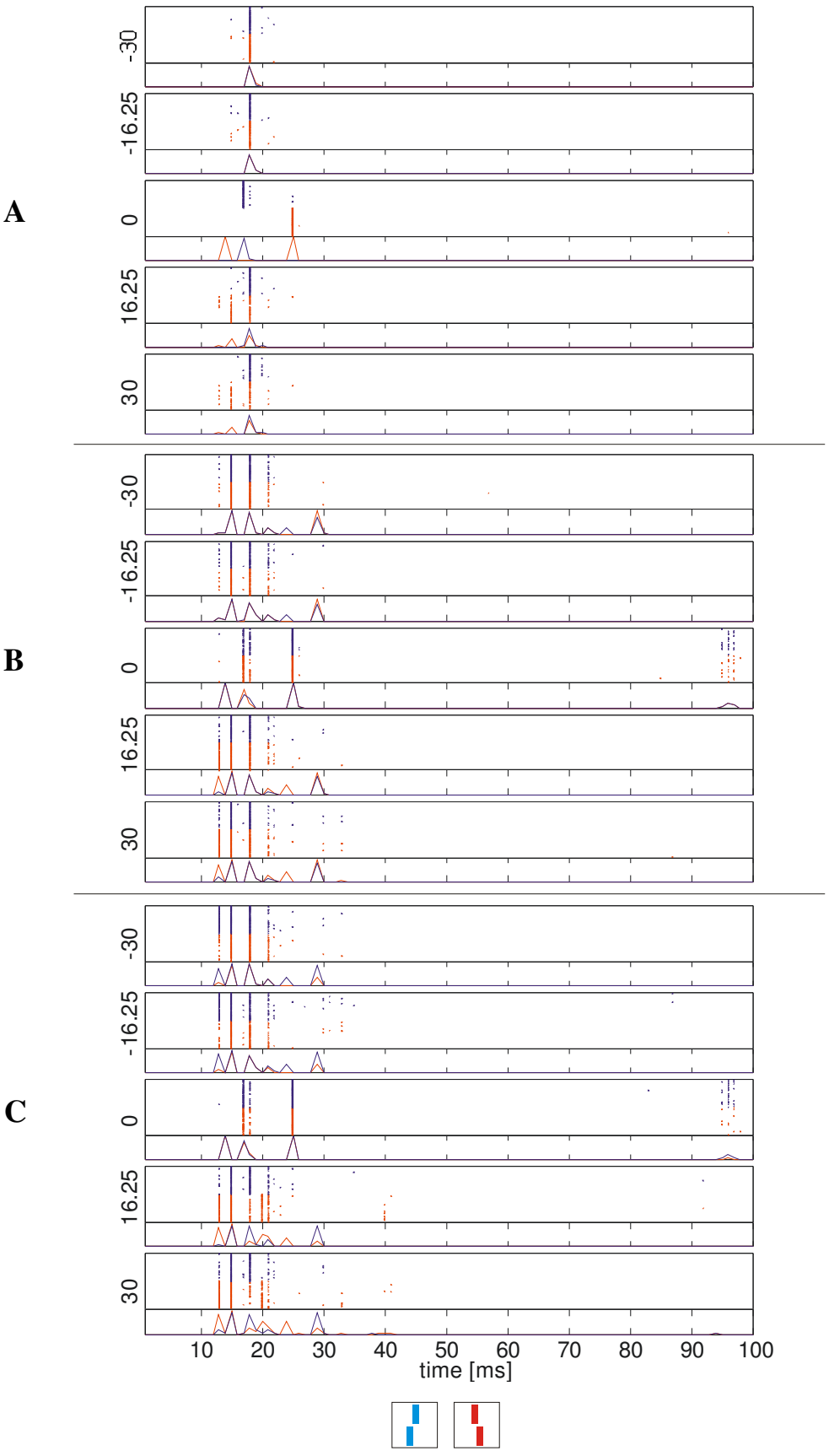
A
B
C
-30
-16.25
0
16.25
30
10
20
30
40
50
60
70
80
90
100
time [ms]

Figure 8.8: *(figure on previous page)* Spike raster-plots for various training periods and line segment displacement levels: Upper part of each row denotes the single spike events for the trained neurons (*red – trained to left displacement/blue – trained to right displacement, see small inlays at the bottom*) for the first 100 ms and 100 stimulus repetitions under noisy conditions. Lower part in each row denotes the mean normalized response of the two output units for the same period. The three figure groups denote the responses for 5 displacement levels, i.e. 30'', 16.25'', 0'', -16.25'' and -30'' after 10'000 training cycles (*A*), 60'000 training cycles (*B*), and after 100'000 trainings cycles (*C*), whereas during training each *Vernier* stimulus with a random displacement level was presented for 1000 ms. The network learns to distinguish the two displacement sides, as can be seen in the progressively bigger response differences between the output neurons. After 100'000 cycles the first spike allows a separation between the two stimulus classes, given that the line segment displacement magnitude exceeds a certain level.

8.5 Discussion

With the current network we wanted to investigate whether the stimulus specific code produced by our model can be exploited by a combination of the previously introduced modulatory feedback mechanism which mimics cholinergic top-down input, and a recently proposed biologically meaningful calcium controlled synapse model (Shouval et al., 2002a). Amongst other bar-composed stimuli, we again used *Vernier* line stimuli. *Vernier* stimuli comprise rotation symmetry and therefore are not coded differentially by the original formulation of the proposed *TPC* network, with its invariant properties (Wyss and Verschure, 2003). Hence, the *Vernier* stimuli could not be decoded by neurons in later stages of the neural processing machinery. With the model presented in this chapter we demonstrate how the original *TPC* can by extended by biological plausible and well defined mechanisms, to produce differential codes for right- and left displaced bar segments. The network decodes the ciphered information by means of a synaptic model resembling the properties of *NMDA*-receptors, which are known to play an important role in neural plasticity during conditioned learning. The network exploits the stimulus statistics, the bidirectional learning properties of the synapse, i.e. *LTP* and *LTD*, in combination with a modulatory top-down signal to solve the *Vernier* task with hyperacuity.

The decoding stage of the network strongly exploits the properties of *NMDA*-synapses to achieve a separation of highly correlated input information, i.e. *Vernier* stimuli separated by only a few *arc sec*. In the noisy environment of the coding stage the two stimulus classes, represented by the two line-segment displacement sides, will produce highly overlapping rate distributions at the output neurons. However as our biophysically restricted *enhanced TPC* model proved (see chapter 6), cortical networks are able to encode stimulus information in the temporal domain, as well (Wyss et al., 2001). When we inspect the capacity of a single synapse to reflect the temporal structure of an input spike train, we see that the model is able to reflect the input in a non-trivial

manner, i.e. low *and* high frequency input is able to produce weights at various high and low values (***Figure 8.8***). This property is a necessary requirement for a model exploiting temporal aspects of stimulus representations and not just averaged rate activities.

In an *A-or-B* identification task, in a situation where only two cells with 18 synapses each are trained to detect bar stimuli separated by various angles, the model exhibits almost perfect classification down to a separation angle of 30° (**Figure 8.3**). Even with the small number of synapses the system is able to learn additional patterns without losing the capability to identify the previously presented pattern pair. Furthermore, the newly trained targets are separated with high reliability (**Figure 8.4**). For the exemplary bar stimuli the output neurons asymptotically reach an upper output frequency of about 120 Hz, after circa 50 randomly chosen training patterns. This relatively slow learning in combination with the asymmetric bidirectional learning properties, i.e. *LTD* is slower than *LTP*, stabilizes already learnt information.

In the recent years many studies illuminated various aspects of primate object learning and recognition (Kourtzi and DiCarlo, 2006). Parts of it deal with plasticity in early stages of the visual pathway which presumably underlie the performance improvements in various psychophysical tasks, e.g. *Vernier* acuity tasks. The reasons for pinpointing the functional changes to the early stages like *V1*, comes from psychophysics. As Fahle & Morgan (Fahle and Morgan, 1996; Fahle, 2004) and others showed, the acquired performance improvements in line discrimination tasks are not transferred between eyes, presentation angles or retinal positions. Thus, the restricting cells exhibit presumably ocular dominance, reveal orientation specificity and restricted receptive fields. Attributes which are known to be fundamental functional aspects of the early visual pathway, since Hubel & Wiesel made their seminal statements about the structure and properties of mammalian visual cells and networks (Hubel and Wiesel, 1959). As others showed the capability to improve the performance with the number of trials is strongly related to error feedback. Subjects who do not get an external error signal, or receive mismatched feedback, do not or only marginally improve their performance in *Vernier* tasks (Herzog and Fahle, 1997). Previous models which tried to reproduce the remarkable performance of human subjects in *Vernier* acuity tasks, all exploit the rate-based output characteristics of orientation selective neurons, resembling the properties of filter-banks in the early visual cortex, to produce differential responses for *Vernier* stimuli (Wilson and Gelb, 1984; Wilson, 1986; Herzog and Fahle, 1998). The optimal linear combination of the filtered output is computed by an error minimization between the actual classification output of the network and the desired output. The main goal of the models is to reduce the efficacy of units which do not deliver differential output for the *Vernier* stimuli, i.e. the ones with receptive fields aligned with the stimulus, and to increase the importance of the cells producing differential output, i.e. the slightly displaced and tilted ones. To overcome the problem that aligned units produce at least as high rate output as the tilted and displaced ones the models propose distinct mechanisms, i.e. preceptron like approaches or random scans of the output space. While the first

approach assumes a backpropagation of an output error through a hierarchical biological spike based neural network, which is hypothetical and disputed, the latter seems to be quite inefficient. The question arises, whether our network which is spike based and exhibits biophysical constraint properties, can achieve hyperacuity in a *Vernier* acuity task. The hypothesis is, that the coding properties of the network, and the bidirectional learning properties of *NMDA*-synapses, in combination with a biologically meaningful teacher signal, which resembles the properties of cholinergic input originating from the basal forebrain, lead to synaptic weights at the output neurons which allow reliable classification even for highly similar stimuli – without the need of complex top-down signals or scans of the error space.

When we inspect the performance of our model, we see that it clearly reaches hyperacuity, i.e. with a threshold around 18'' arc sec. The network exhibits learning dynamics resembling the speeds of human observers (Herzog and Fahle, 1997), and shows the angular dependence of the performance, i.e. the performance improvement is not transferred between presentation angles (***Figure 8.7***). Given the difficulty of the task, it is remarkable, that the output neurons on average signal the class membership of the *Vernier* stimulus already with their first spike which at threshold appears about 13 ms after stimulus onset (***Figure 8.8***). This highly efficient coding fits well to the speed restrictions to more complex stimulus set by psychophysical and physiological classification experiments. Human and primates signal class membership in trained stimulus sets with a delay of only about 100 ms, which allows the conclusion that the processing in the various stages along the visual hierarchy can only be based on one or e few spikes (Fabre-Thorpe et al., 1998; Kirchner and Thorpe, 2006). It is unclear however whether this result would hold in a situation where cells covering a whole range of receptive field sizes and preferred spatial frequencies are present. The current model configuration guarantees that the cells with stimulus-aligned receptive fields do not produce output activities which exceed the slightly tilted ones by a large magnitude.

In conclusion, we have shown that our approach learns bar stimuli, and is able to perform with hyperacuity in a *Vernier* task. It does not assume abstract error backpropagation in rate coded systems or an inefficient random scan of the error space, represented by the distance by the desired output and the actual outputs. We show that the problem of weighing the feature outputs can be solved by exploiting the coding capacities of our *enhanced TPC* model and distinct learning properties of the *NMDA*-synapses, which are controlled by modulatory top-down signals.

The quality of a model is reflected in its predictive power and as important in the plausibility of its assumptions. With respect to cortical models, the plausibility can be judged by investigating all the components of the network, e.g. neurons, connection patterns, synaptic and signal properties, and comparing them to biological data. The plausibility of the inner-areal lateral projections and the faster feed-forward connections was discussed in the previous chapters. Hence we concentrate on the remaining network

parts in this section, i.e. the modulatory top-down signal, resembling the effect of acetylcholine, and the incorporated *NMDA*-synapse model.

As mentioned earlier learning in psychophysical tasks often depends on externally delivered feedback signals. The functional implications and anatomical substrates of feedback signal processing are still unclear. However, as various recent studies show the cholinergic system originating in the basal forebrain may play an important role in object learning and recognition. Cholinergic projections are broad and target regions throughout the cortex. Although the connectivity as a whole is very widespread the projection of individual cells seems to be limited to a small cortical area of 1-1.5 mm in diameter only (Price and Stern, 1983). *Nicotinic* and *muscarinic* receptor antagonists, like *scopolamine* or *atropine*, are known to strongly reduce sustained attention performance, where subjects know where to expect what type or what modality of a stimulus (Sarter et al., 2001). Recent studies in addition speculate that acetylcholine (*ACh*) is the biological effector for attention related observations made in cat early visual cortex (Roberts et al., 2005). *ACh* affects the signal processing in the primary visual cortex similar to what was observed and expected in attentional tasks, i.e. it strongly suppresses intracortical connections and boosts feed-forward projections, which in the sum reduce the contextual influences in a visual scene (Kimura et al., 1999; Kimura, 2000; Roberts et al., 2005; Zinke et al., 2006). In our model we use the modulatory effect at two stages. First in the laterally coupled part, resembling the properties of the striate cortex (*V1*) and second in the plastic output neurons with the *NMDA* synapses. As suggested by physiological experiments the signal is dynamic and modulatory, and does not introduce direct excitation or inhibition, but changes the dendritic signal processing properties. To reflect and exploit this behavior we dynamically change the log-attenuation factor over time and with that alter the electrotonic length of the dendrites. The function is two-fold; as we have shown in chapter 6, a transient signal increase after a few tens of milliseconds mimics attentional effects, and can be used to segment the visual field, to reliably code target locations and objects in cluttered scenes. Here we show that the same mechanism can be used to decorrelate output signals during a supervised learning paradigm. While we leave the log-attenuation factor of the laterally coupled neurons in a relaxed state, we exploit the bidirectional learning properties of the *NMDA*-synapses by our modulatory feedback signal. As in the previous case, the modulatory signal itself reveals a quite simple structure, i.e. a low attenuation factor to signal target stimuli, and a high level factor for distractors. Hence no implausible, complicated top-down signal machinery, which would have to be hyperfast, to fulfill the speed requirements, is needed. The complicated processing is done locally by the connectivity patterns, synapse properties, and the stimulus statistics. The top-down signal, serves as a switch, and only forces the local units into different processing and learning regimes, which allows them to differentially exploit the encoded stimulus information. A crucial part in this view is attributed to the plastic synapses, i.e. the *NMDA*-synapses.

NMDA-synapses belong to the ionotropic glutamate receptors and are suspected to represent an important substrate for observed learning properties of biological systems. Activation of the receptor results in the opening of a non-selective *cation-channel*, which allows Na^+ and small amounts of Ca^{2+} to penetrate into the cell, and K^+ out of it. In the recent years evidence accumulated that the actual amount of activated *NMDA*-receptors (*NMDAR*, *N-methyl D-aspartate receptor*) is the important parameter which controls the bidirectional behavior, i.e. depression and potentiation, during conditioned learning. Beside of glutamate various other chemicals activated and modulated the *NMDA*-receptors e.g. *polyamine*, *glycine* and Zn^{2+}, which are all present throughout the brain. The receptor is both, ligand-gated and voltage-dependent. The calcium influx and the resulting concentration change within the postsynaptic cell is thought to play a critical role in the activation of the *NMDA*-receptor, and is considered to constitute a cellular mechanism for learning and memory, as for example shown in Schaffer collateral/CA1 synapses in the rat hippocampus, which exhibit long term potentiation (*LTP*) if trained and tested with a shock and a tetanus stimulus respectively. The same synapses produce long term depression (*LTD*) if faced to continuous small input (Cooke and Bliss, 2006).

The recently presented *NMDAR*-model of Shouval et al. and Castellani et al. (Castellani et al., 2001; Shouval et al., 2002a; Shouval et al., 2002b; Castellani et al., 2005) reproduces the bidirectional behavior of *NMDA* synapses. The alteration of the synaptic efficacy is dependent on the calcium concentration change, which is a consequence of ligand-driven *NMDAR*-activation and voltage dependent ion currents. The complex signaling chain that is triggered by calcium and leads to changes in the synaptic efficacy is not fully understood. The biophysical processes that control the channel opening are quite clear however (Lisman, 1989). Hence, instead of modeling the calcium dependent signaling cascade the authors adopted a phenomenological approach, where the intracellular calcium concentration controls the synaptic weight changes. The resulting synapse model describes the *NMDA* receptor as a complex coincidence detector which goes beyond pure spike time delay plasticity.

As mentioned before, the introduced cholinergic modulatory top-down signal, introduces a learning mode switch in the *NMDA* synapses. To switch from potentiation (*LTP*) to depression (*LTD*) the network regulates dendritic signal integration and in that way exploits the bidirectional weight change properties of the synapse. Increasing the log-attenuation factor keeps the membrane into a predominately depolarized state, and consequently forces the synapse into *LTD*-mode. The temporal code produced in the feature banks is collected by a series of readout neurons and transported to the efferents. Due to the learning mode switch stimuli compete for the synapses. If a target stimulus produces a more *efficient* code than the non-target (distractor), it will boost the synaptic efficacy to high levels. If the non-target is more efficient the weight will be decreased, in the extreme case to almost 0. *More efficient* in the complex response behavior of the synapse does not simply mean, a higher input rate. The temporal structure of the input spike train is important as well. After many stimulus repetitions, the competition leads to

distinct weight matrices, which allow an efficient decoding of the input information streams, i.e. output neurons which signal stimulus class membership.

The presented network is still very simple and performs only a binary classification. However, it reproduces performance measures of a psychophysical task, investigated in great detail during the last decades, the *Vernier acuity* task. The task is interesting since a lot of psychophysical data is available and the underlying mechanisms can be attributed to the early regions of visual hierarchy, which restricts the possible neural substrates, and allows the construction of detailed models without too many assumptions. Given the simplicity of the stimuli and the task, and the enormous number of studies in various areas of brain research, e.g. physiology, psychophysics and modeling, it is surprising, that the underlying mechanisms, especially when dealing with the decoding stage, are still quite unclear. We presented a biophysically constraint cortical model which is able to solve both the encoding and decoding stage, by virtue of plausible model elements resembling the visual processing machinery. We have shown that a system exploiting local processing power, with feedback signals acting only as modulatory switch is able to solve this task. No complicated top-down signal machinery with processing in each hierarchical step or random exploration possible weight combinations is needed. However, as stated above, additional investigations are necessary to whether this result represents the exception, or if it holds for other receptive field properties.

Together with the proven encoding capabilities of the original *TPC* proposal, augmented with the attentional and position-specific properties of the model presented in this thesis, this offers an entry point for more complex tasks, where the task is scaled to a larger number of classes, or where the output units have to generalize over larger distortions. In the present proof-of-concept simulations we used a small number of only 18 synapses, one for each orientation preference. As the experiments show the small number is enough to produce bar pattern specific output neurons. Further it reveals to be highly specific since it solves the *Vernier* acuity task with hyperacuity. It is unclear where the scaling limits of this restricted model are. However, given the small number of synapses it cannot be assumed that the network scales to a large number of classes. Several model extensions that possibly improve the scaling properties are conceivable. The reader is referred to the final conclusion for a discussion of possible model enhancements.

8.6 Appendix

Assumptions and equations of the calcium controlled synapse

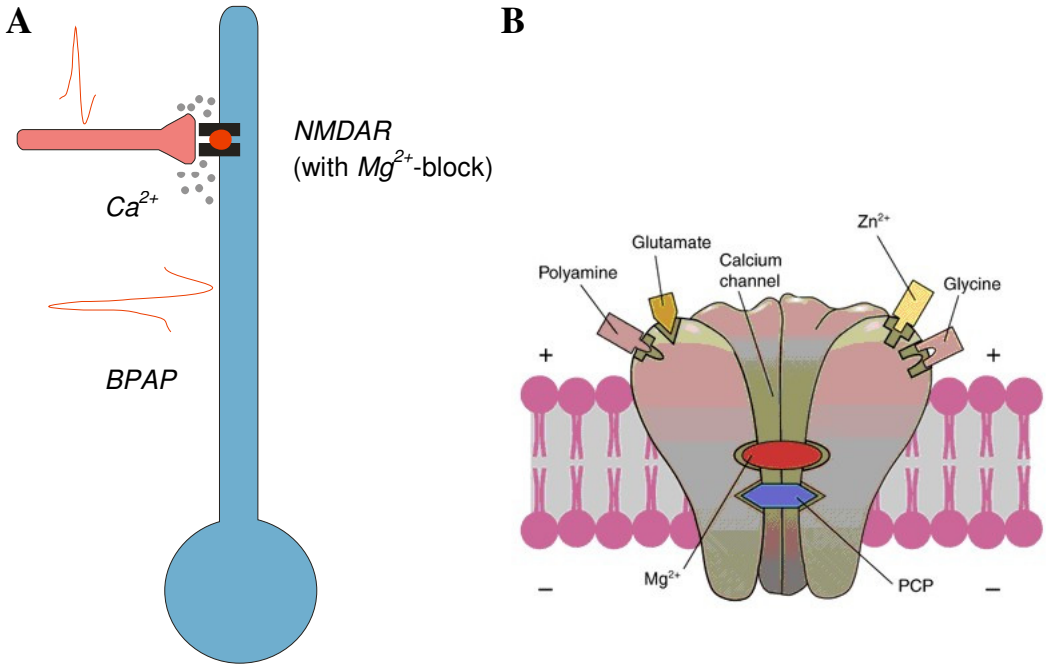

Figure 8.9: Schematic drawings of a cell with *NMDA*-synapses: (*A*) The calcium control hypothesis models synaptic plasticity based on calcium concentration changes induced by Ca^{2+}-ion influx through *NMDA*-receptors (*NMDAR*, *black bars in figure*). *NMDA*-receptors belong to the ionotropic receptor family. They are both ligand-gated and voltage dependent. Before Ca^{2+} can pass through the receptor channel the Mg^{2+}-block (*red dot in figure*) has to be expelled from the channel. The release of the block is more likely if the surrounding membrane is depolarized. (*B*) Beside of the voltage dependence and the glutamate ligand several other modulators, e.g. polyamines, glycine and zinc, affect the *NMDAR* activity. They are not explicitly modeled in the calcium control hypothesis, but find indirect representation as for example in the Ω function (schematic channel illustration taken from web).

The synapse model of Shouval et al. (Castellani et al., 2001; Shouval et al., 2002a; Shouval et al., 2002b) uses the calcium concentration which is dependent on the *NMDAR*-activation to change the synaptic efficacy (***Figure 8.9***). The model is bidirectional, i.e. it allows depression and potentiation. The core of the model is constituted by three parts, i.e. the temporal dynamics of the calcium concentration change as a result of various factors (input, postsynaptic potential, *BPAP* and history of the *NMDAR*), and the calcium concentration dependent *Ω-function* and the learning rate function (η). The *Ω-function* introduces an upper and lower [Ca^{2+}]-boundary denoting the limits for no-efficacy-change, depression, and potentiation. Both, the *Ω-function* and *η-function* are biologically plausible and can be derived based on biophysical properties of *NMDA*-receptors. The

synapse model goes far beyond pure spike latency based SDTP-learning. It exhibits realistic behaviors as gathered in physiological experiment, i.e. membrane potential dependence (*pairing* experiments), presynaptic activity dependence and spike timing dependent properties.

The calcium control hypothesis assumes that different calcium levels lead to different types of synaptic plasticity, i.e. *LTP* or *LTD*. This was formulated as:

$$\dot{W}_j = \eta\Omega\left([Ca]_j\right), \tag{5.9}$$

where $\dot{W}_j$ represents the weight change, i.e. synaptic strength of the synapse *j*, η is the learning rate, and $[Ca]_j$ is the calcium concentration at synapse *j*. A calcium concentration below a lower threshold θ_d does not lead to a modification of the weight. If the concentration is between the lower threshold θ_d and the upper threshold θ_p the weight is depressed and if the concentration is above θ_p the synaptic strength is potentiated. The Ω-function expressing this has the form:

$$\Omega = 0.25 + sig(Ca-\alpha_2,\beta_2) - 0.25 sig(Ca-\alpha_1,\beta_1), \tag{5.10}$$

where $sig(x,\beta) = \frac{e^{\beta x}}{1+e^{\beta x}}$ with α_1=0.35, α_2=0.55, β_1=80 and β_2=0.45.

To stabilize the growth of synaptic strength without introducing absolute saturation limits into the model a weight decay term is added to model:

$$\dot{W} = \eta\left([Ca]_j\right)\left(\Omega\left([Ca]_j\right) - \lambda W_j\right), \tag{5.11}$$

where λ (=1) denotes a decay constant. The weight decay term avoids that the synaptic strength increases or decreases infinitely. The calcium concentration dependency of the learning rate η (***Figure 8.10***) is necessary since otherwise the weights would rapidly converge back to their initial values when the Ca^{2+}-concentration returns to the basal level. η has the form:

$$\eta = 1/\left(\frac{P_1}{P_2 + (Ca)^{P_3}} + P_4\right), \tag{5.12}$$

where P_1 =0.1 sec, $P_2 = P_1 /10^4$, P_3 =3 sec and P_4 =1 sec. The dependency described in equation (5.11) can be derived from the biophysical properties of the biochemical machinery following *NMDAR* activation (for details refer to (Shouval et al., 2002a)).

The model assumes that in situations where presynaptic activity is paired with postsynaptic depolarization, the primary sources of calcium influx into the postsynaptic spines are the *NMDAR*s (Malenka and Nicoll, 1999; Sabatini et al., 2002). This view is supported by experimental findings showing that *NMDAR*-activation is crucial for many forms of calcium dependent *LTP* and *LTD* (Malenka and Nicoll, 1999). The calcium current through the NMADR was modeled as:

$$I_{NMDA(t_i)} = P_0 G_{NMDA} \left[I_f \theta(t_i) e^{-\frac{t_i}{\tau_f}} + I_s \theta(t_i) e^{-\frac{t_i}{\tau_s}} \right] H(V), \tag{5.13}$$

where P_0 (=0.5) is the fraction of *NMDAR*s that shift from the closed to the opened state after a presynaptic spike, and G_{NMDA} is the peak *NMDAR* conductance (=-1/500 [μM/(ms*mV)]), and I_f (=0.5) and I_s (=0.5) are the relative magnitude of the fast and slow *NMDAR* current, and θ is threshold function which is 0 when t_i is negative and 1 if it is above zero. The two time constants τ_f and τ_s are set to 50 ms and 200 ms respectively. $H(V)$ describes the voltage dependence of the current and has the form:

$$H(V) = B(V)(V - V_r), \tag{5.14}$$

where $B(V)$ describes the effect of the magnesium block, and V_r (=130 mV) is the reversal potential of calcium. $B(V)$ has the form:

$$B(V) = \frac{1}{1 + e^{-0.062V} \left(\frac{[Mg]}{3.57} \right)}, \tag{5.15}$$

where $[Mg]$ is assumed to be equal to 1.

The change of the calcium concentration is given as:

$$\frac{d[Ca(t)]}{dt} = I_{NMDA}(t) - \left(\frac{1}{\tau_{Ca}} \right) [Ca(t)], \tag{5.16}$$

where $\left[Ca(t)\right]$ is the calcium concentration at the spine at time *t* and τ_{Ca} is the decay constant (=50 ms).

The pre- and postsynaptic cells were modeled as conductance based leaky-integrate-and-fire neurons (see chapter 5 for detailed equations). In addition to the instantaneous effects modeling EPSPs the membrane potential at the postsynaptic site was influenced by a back-propagated action potential (*BPAP*) modeled as:

$$BPAP(t) = 100 * \left(I_f^{bs} e^{-\frac{t}{\tau_f^{bs}}} + I_s^{bs} e^{-\frac{t}{\tau_s^{bs}}} \right), \qquad (5.17)$$

where I_s^{bs}=1-I_f^{bs}, with I_f^{bs}=0.75, τ_f^{bs}=3 ms and τ_s^{bs}=25 ms. In the simulations it was assumed that the *BPAP* arrives at all synapses at the same time, with a delay of 1 ms after the generation in postsynaptic cell's soma.

The resulting dynamics are illustrated in ***Figure 8.2*** and **Figures 8.11-2**.

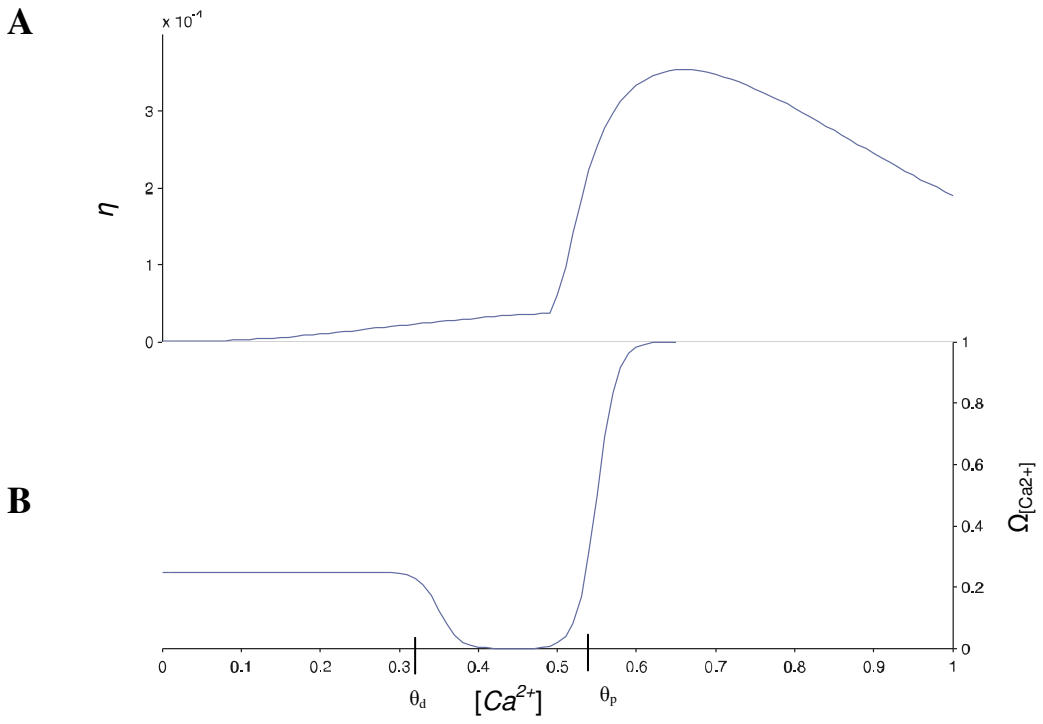

Figure 8.10: Learning function η and Ω function: (*A*) The learning rate (η) is calcium concentration dependent. The asymmetry avoids that the synaptic weight returns to base level during the transition from high to low calcium concentrations. (*B*) The Ω function introduces a lower (θ_d) and an upper threshold (θ_p), which set the boundaries for *no-weight-change* (below θ_d), *LTD* (between θ_d and θ_p) and *LTP* (above θ_p).

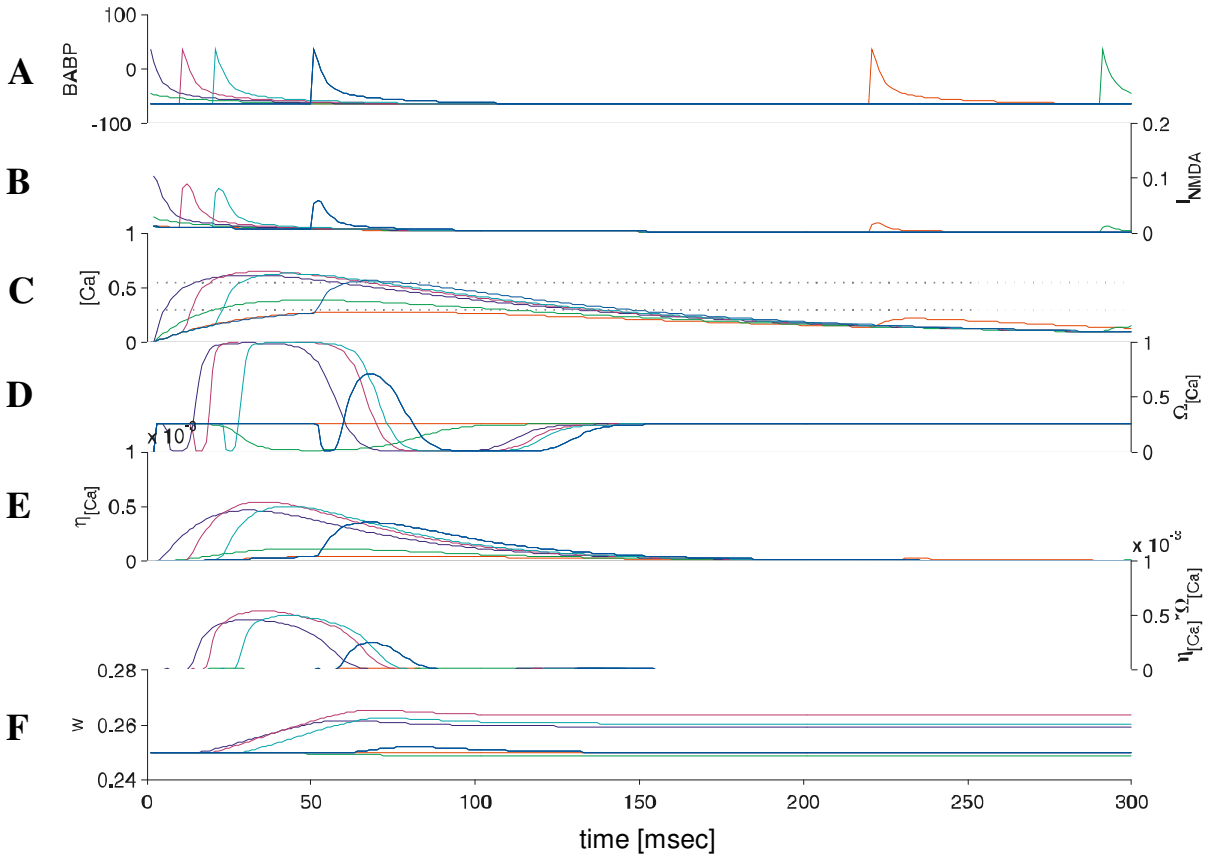

Figure 8.11: Dynamics of weight changes during presynaptic activity and back-propagated action potentials (*BPAP*): (*A*) An incoming presynaptic spike is assumed to occur at t=0 ms. The color coded curves denote *BPAPs* at different time points before and after the presynaptic spike (*green* is used in two cases, a *BPAP* shortly preceding the presynaptic spike, and one with a delay of ~300 ms after the presynaptic activity). (*B*) The resulting calcium current through the NMADR is delay specific. The bigger the delay between the pre- and post-activity the smaller the Ca^{2+}-current. (*C*) Only *BPAPs* shortly after the presynaptic action potential manage to increase the calcium concentration above the upper threshold (θ_p, *upper dotted line*). Shortly preceding or later *BPAPs* stay between θ_d and θ_p, or result in low Ca^{2+}-concentrations (below θ_d, *lower dotted line*). (*D-F*) The calcium concentration dependent functions Ω (*D*) and η (*E*) control the weight change. (*F*) *BPAP*-dependent synaptic weight change with an initial weight of 0.25: Only *BPAPs* occurring shortly after the presynaptic spike lead to a weight increase (*LTP*). *BPAPs* shortly before the presynaptic action potential result in a small decrease (*LTD*) of synaptic efficacy (*green curve*). *BPAPs* occurring at other time points do not or only marginally change the synaptic weight.

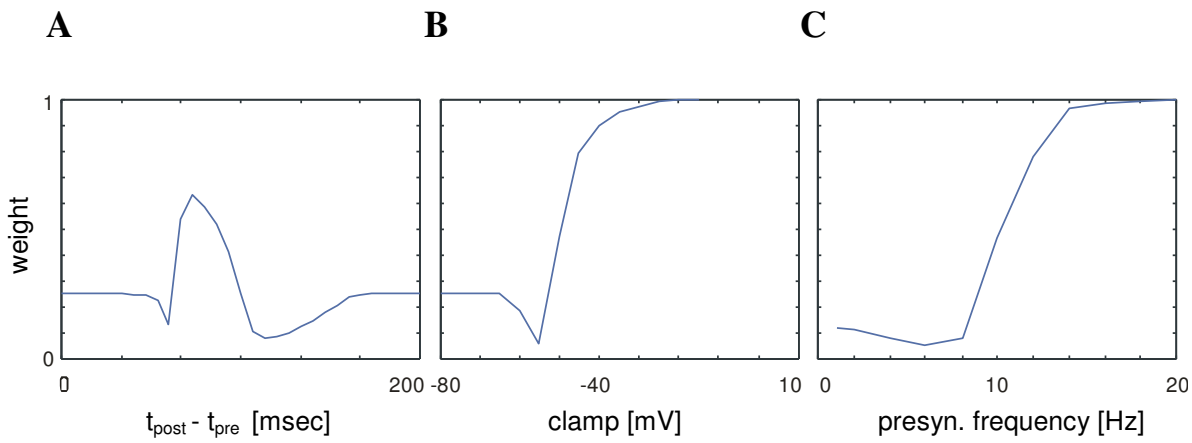

Figure 8.12: Weight convergence as a function of various experimental conditions: (*A*) Weight convergence as a function of spike-time delays (*STDP*): The calcium controlled synapse model reveals *LTD* and *LTP* regions for the time delays between pre- and postsynaptic action potential. Postsynaptic action potentials shortly preceding the presynaptic spikes leads to depression. Spikes with a small positive delay lead to potentiation. Weights converged for a presynaptic frequency of 1 Hz and 1000 repetitions. (*B*) Weight convergence in a simulated pairing experiment: In pairing experiments the change of synaptic efficacy during low frequency presynaptic stimulation and clamped postsynaptic membrane potential is analyzed. The data was collected for a stimulation frequency of 1 Hz and various clamping between -80 and 10 mV. Clamping potentials around the resting potential of the cell (-70 mV) do not change the initial weight with a value of 0.25. Slightly more depolarized membranes result in depression, while voltages of ~-50 mV or higher potentiate the synaptic efficacy. (*C*) Synaptic plasticity as a function of presynaptic activity: The data points represent weights after 1000 repetitions of spike sequences of various rates and a length of 1 sec. With an initial weight value of 0.25 the model reveals a *LTD* region for low rates up to about 9 Hz, and *LTP* for higher frequencies. The data was collected without postsynaptic spikes.

Chapter 9

Discussion & Conclusion

Due to the mainly descriptive nature of the software framework documentation in the appendix of this thesis this final conclusion chapter 9 will mainly discuss and evaluate the results of the chapters 6 to 8.

9.1 Considerations about modeling of brain functions

In the last decades the methods to analyze brain functions have made large advances. A large body of anatomical studies investigated the shape and connectivity patterns of cortical neurons. Intracellular recordings deliver precise data about the activity of single neurons with sub-millisecond time resolution over several hours. Chronic electrode arrays record extracellular signals of dozens of units, and can extend the recording period to several month or even years (Lebedev and Nicolelis, 2006). The latest imaging techniques reveal population activity with single-cell and single-action-potential resolution, i.e. calcium imaging, or non-invasive observation of the state of many brain areas via the *BOLD*-signal, i.e. *fMRI*, or via electromagnetic potentials collected on the skull, i.e. *EEG*. However, none of the current methods allows the precise recordings up to the network or system level, where thousands of cells or even several brain areas communicate together during the information processing. Here, computational modeling comes into play. It represents a way to close the gap between the anatomical structure of brain networks and their putative functions. However, the models have to be designed carefully. A model which reproduces some behaviors of biological nerve systems does not necessarily have to reflect the situation and working principles animals use to produce their remarkable behaviors. Many theoretical approaches can lead to similar results, especially if one deals with a big number of free parameters, which can be tuned to gain a certain network behavior. Hence, computational models of brain functions have to, as any other model of natural systems stay as close to the available measured data as possible, and should at the same time operate with a minimal number of free parameters to reduce the assumptions that have to be drawn. Ideally, a computational brain model should not try to mimic a desired function, but should naively incorporate the *important* biological facts about anatomy, biophysical properties of the neurons, and the connectivity patterns to produce a model network whose output can be analyzed and compared to their natural prototype. This process does try to avoid investigator based biases and introduction of external knowledge, which can lead to misperceptions, and wrong conclusions and predictions. To follow this path is hard however. In theoretical brain research one has to rely on data gathered in biological experiments, which are due to the methodological restrictions far from perfect. Even worse, these restrictions often make it hard or impossible to evaluate the conclusions drawn in the modeling studies in their biological

counterparts. Therefore, in recent times a whole zoo of modeling studies dealing with brain areas and their putative functions, with sometimes contradictory predictions were developed.

The before illustrated design principles for the modeling of information processing along the visual pathway demand that we restrict ourselves to the main components of the system, and that we do not select and arrange these components according to the possible/desired model function. We should rather embed them in the system in a naive way, based on the biological facts. The reduction of the biological details we incorporate reduces the number of free parameters and necessary assumptions, and prevents our model from the undesired investigator based biases. In this thesis we wanted to investigate the coding related functions and interactions of a subset of long range connectivity patterns found in the visual cortex, i.e. the fast inter-areal feed-forward connections, the slower inner-areal horizontal connections, and the widespread cholinergic modulatory input originating from the basal forebrain. Inhibitory interactions were not considered in this analysis. They may however play a crucial role in future investigations, when one tries to relate the results of this thesis to the functions of the inner-areal cortical microcircuits. With respects to the design of the components we used a biophysically restricted approach, i.e. conductance based leaky-integrate-and-fire units with dynamic dendritic properties, and distance related axonal signal transmission delays, as a model for excitatory pyramidal neurons. The connectivity patterns were designed according to biological data, i.e. topological fast feed-forward projections, fan-like anisotropic horizontal connections along the cells' preferred orientation, and widespread modulatory input affecting dendritic signal transmission. For the plastic properties of the neurons we relied on a detailed *NMDA*-synapse model, following *the calcium control hypothesis*.

9.2 The goals and results of the thesis

The goal of the present dissertation was to study the coding of information in a biophysically constraint model of the cortex. More specific, we wanted to explore the limits and possible enhancements of a recently proposed coding principle published by Reto Wyss et al. (Wyss and Verschure, 2003). The model attributes a clear coding function to the extensively present inner-areal horizontal connections of the neocortex, i.e. it shows that the distance related transmission delays of the horizontal connections are able to transform spatial stimulus properties into a temporal representation. The averaged spiking activity of neuronal groups depicts a robust and stimulus specific temporal code which can be used for classification purposes. It was shown that the code scales to several hundred of artificial stimulus classes, and in addition exhibits invariance for small stimulus distortions and transformations, e.g. rotations and translations. However, several questions remained open. First, there is an intrinsic problem in the usage of the horizontal connections for the coding of stimulus information. The model cannot distinguish

between target objects and distractors. Any stimulus positioned close to the target will, by virtue of the horizontal projections, perturb the produced code. A further constraint of the *TPC* model for solving realistic tasks, as used in psychophysics, is introduced by the biophysical substrate of the rotation and translation invariance. To achieve the desired invariant encoding the model relies on symmetric horizontal connections, which produce identical input/output arrangements at each cell. This arrangement however does not allow a later disambiguation of rotation symmetric patterns, as for example the *Vernier* stimuli, or the decoding of position information, since this information is intentionally not encoded in the temporal information stream. Linked to the invariance is the contradictory requirement of an object recognition system to be specific as well, i.e. the system should not only be able to generalize over small distortions to form perceptual stimulus classes, but should also be able to recognize specific objects in a collection, i.e. perform object identification. The *Vernier* stimuli represent a class of highly similar stimuli, to perform the task with satisfactory acuity the system has to produce highly specific codes - a requirement for which the original *TPC* was not tested before.

We demonstrate that the original lateral-connections-based *TPC* model (Wyss et al., 2001) can be extended by biologically meaningful feed-forward and top-down mechanisms, to produce distractor robust codes and perform with hyperacuity in localization acuity tasks. In addition the enhanced model proves to deliver better classification performance than the original model, in target-stimulus-only paradigm, with a stimulus set already used in the original model. Further the model produces a code which allows classification of dot pattern stimuli similar to those used in psychophysical tasks, which are built by prototype distortions. The model generalizes over these distortions of dot patterns.

In the first part of the thesis, we focus on the segmentation problem of laterally connected networks. Closely positioned distractor stimuli lead to a major perturbation in the temporal population code formation, which results in a reduced stimulus classification performance. Starting from the initial formulation of the temporal population code formation (*TPC*) we explored a possible mechanism to reduce perturbations originating from closely positioned distractors. We show that active dendritic compartments with modulatory input affecting dendritic signal integration are capable to reduce contextual influences in situations where target and distractor stimuli are presented simultaneously. Modulation of dendritic signal integration models the effect of cholinergic input as shown in physiological experiments (Roberts et al., 2005; Zinke et al., 2006). In these studies the authors show that acetylcholine injected into early visual areas resembles the processing changes observed during attentional tasks, i.e. it reduces the efficacy of feedback and intracortical connections via the activation of muscarinic receptors, and increases the efficacy of feed-forward connections via the activation of nicotinic receptors. We show that this principle can be adopted in the formation of temporal coding in populations of neurons. By dynamically increasing the signal attenuation along the dendrite, modeling

activation of muscarinic receptors, we are able to control the influence of closely positioned distractors by virtue of the horizontal connections. In addition we introduce fast feed-forward connections to fully exploit the robust temporal code. Together the two biologically reasonable extensions are able to solve the segmentation problem inherently present in laterally coupled networks. Additionally we show that the enhanced model produces a faster and more accurate classification signal for the used artificial stimuli, than the proposal without active dendrites and specific readout mechanisms. We further show that the same network can be used to produce highly stimulus specific responses for dot-pattern stimuli as used in many psychophysical tasks.

In a second part we investigate the limits of the proposed network in a widely used psychophysical task which requires highly specific coding of stimuli, i.e. *Vernier* localization acuity. Localization acuity is one of the best studied psychophysical tasks. Many studies reveal that highly trained human subjects are capable to reach hyperacuity in these tasks, i.e. the threshold to detect the displacement side of two bar segments is below the minimal receptor distance which is around 30 sec arc in the foveal region of humans (Westheimer and McKee, 1977a; Fahle and Poggio, 1981). Training effects in localization acuity tasks are not transferred between eyes, visual positions in a scene, or between presentation angles (Fahle, 2004). This lead to the conclusion, that the responsible processing presumably takes place in very early stages of the visual pathway, where retinotopically organized ocular dominant neurons with small oriented receptive fields are present. Previous models of hyperacuity proposed that slightly displaced and misaligned receptive fields in these stages produce differential responses for right and left displaced bar segments. All of these models did not consider time as a coding domain (Wilson and Gelb, 1984; Wilson, 1986), since they did not exploit spike but rate based coding strategies. We show here that the model presented in the previous chapter, extended by populations of orientation sensitive neurons with biologically meaningful connections patterns, i.e. anisotropic fan-like connections between neurons sharing similar feature properties, are able to encode *Vernier* stimuli in the temporal domain in a highly specific manner, which allows hyperacuity. We observe similar threshold dependence on stimulus properties like the ones measured in human subjects. As in the previously presented models for *Vernier* acuity the optimal code is produced by neuronal populations with slightly tilted receptive fields, as compared to the bar segment alignment. We show that optimal weights can be acquired by a linear perceptron which uses averaged responses of the feature selective banks. Considering the temporal structure of the optimally weighted output we show that already 20-30 ms after stimulus onset we reach optimal classification performance with physiologically meaningful noise levels.

In the third part we extend the view of encoding stimulus features in the temporal domain and along feature-selective channels with a decoding stage. The transformation of the external world into a cortical representation requires the coding of stimuli with spiking neurons as the coding substrate. However, in subsequent stages the new representation has to be decoded again to produce behaviorally accurate responses.

Several attempts were made in the past to exploit the temporal structures of spike trains (Bohte et al., 2002; Knüsel et al., 2004). They apply hebbian-like learning logarithms to non-supervised or supervised learning paradigms, to produce output units capable of decoding inputs which carry information in the temporal domain. We show that our model, which combines coding in the temporal domain with specific multichannel readout-mechanisms, which collect the temporal codes along feature specific paths as observed in the early stages of the visual pathway is able to produce neurons which act as decoders. In proof-of-concept simulations we adopt a recently proposed synaptic model, i.e. the calcium control hypothesis (Shouval et al., 2002b), to solve the previously used *Vernier* localization task. The synapse reproduces several properties of *NMDA*-synapses, e.g. similar weight convergence as in pairing experiments, meaningful dependence on presynaptic spiking frequency and spike time delay dependent behavior as measured in physiological experiments. The synaptic model thus goes beyond pure *STDP*-learning schemes, and promises the capacity to capture temporal structures of input spike trains. We demonstrate that the temporal structure of spike trains is reflected in a non-trivial manner in the weight convergence of the synapse. We further show that by exploiting the previously introduced cholinergic mechanism we are capable to control the switch of the synapse between potentiation and depression. Acetylcholine, the neurotransmitter of the long range basal forebrain projections targeting the cortex, is known to play an important role during learning since it has the capacity to modulate *NMDAR* function, and also interferes with inner-areal lateral information transfer, which makes it to a candidate effector in attentional tasks. Hence, the modulation of plastic properties of *NMDA*-synapses by cholinergic top-down input represents a plausible way how supervised learning paradigms could be implemented in natural brains. We show that the network is able to solve the *Vernier* localization task with hyperacuity, and that the learning dynamics resembles the one observed in human subjects (Fahle, 2004).

9.3 Information processing in the biophysically restricted model – coding schemes and their properties

It is probably save to say that brains do not exclusively employ a non-topological temporal coding strategy, as assumed by the original formulation of the *TPC* and the decoding by a *Liquid State Machine* (Knusel et al., 2004). More realistically, the encoding machinery would also take advantage of the feature selective and topologic properties of the neuronal circuitry. While non-topological temporal coding allows invariant representations of stimulus properties, other aspects like the position of objects or the separation of several stimuli is easier exploited and controlled in topologic coding schemes. In this thesis we propose a balanced system which takes advantage of both strategies. The gist of it roots on the predominant connectivity patterns and cell- and synapse-properties found in the neocortex, i.e. fast feed-forward connections, inner-areal projections coupling units sharing similar feature selectivity, modulatory feedback signals

shaping the response of target areas, and the bidirectional learning properties of *NMDA*-synapses known to be important in conditional learning. To illustrate the principles and performance of the network we have chosen a highly specific task, the *Vernier* localization task, which due to its symmetric stimulus-properties could not be solved by the exclusively non-topological approach proposed in the original *TPC*. The original *TPC* averages the output of neurons in a network which evenly covers the feature space comprising symmetric connectivity patterns. This symmetry generates the desired invariant properties of the network responses, but is also the reason for its inability to generate differential responses for the rotation symmetric stimuli in the *Vernier* localization task. The inclusion of biologically plausible topological features, i.e. dedicated feature- and position-specific readout mechanisms in combination with plastic properties of the readout units, however increases the application range of the network. It is important to notice that the two approaches, the non-topological and the topological, exploit the same code produced in the laterally coupled feature-specific layers. The readout decides whether the whole cell population is averaged or whether a multi-channel approach is chosen, which allows disambiguation of rotation symmetry or position reconstruction. In the multichannel system, invariance can be gained at any later stage by linearly summing up the complete channel information. A non-topological approach as the original *TPC* is theoretically able to transmit the complete stimulus information through one channel, i.e. one cell. The temporal code, i.e. the time points at which spikes occur, is constructed by the laterally coupled neurons, and can be transported over very fast projections to subsequent processing areas. In this light, lateral connections could be an evolutionary optimal solution for a system which suffers from space constraints, and which aims to enforce and speed up parallel processing within several brain areas. Only a small number of long-range inter-areal connections are necessary. In addition the speed of the connections is not restricted. The temporal code is produced by the phase lags of large laterally coupled neuronal populations in the absence of a global synchronization signal. Theoretically the transmission from one stage to the next could be instantaneous without perturbing the temporal code. Since the encoding progresses incrementally, subsequent stages can process the incoming information in parallel, while it is constructed in previous areas. In this parallel processing, later stages may even interfere with the earlier ones by top-down signals, to augment and reshape their responses.

Past studies about the coding strategy of brains draw a controversial picture. Most, especially older studies, report rate coding based on a few neurons. These results have to be judged carefully though, since they are possibly biased by the available techniques at that time, i.e. recordings of a large number of neurons with millisecond time resolution even nowadays are hard to collect. A growing number of recent studies emphasize the importance of temporal and population coding. However the coding strategy seems to be task-specific and area-specific as well. While the very early areas show improved coding accuracy if time is considered as a coding domain, area *IT* seems to code the stimuli mostly with rate based population activities. In this thesis we demonstrate in a simple

network how the temporal structured output can be captured by *NMDA*-synapses to produce decoder units, which signal the presence of target stimuli by an increased activity rate. The network is able to classify simple stimuli in a highly specific manner, i.e. it performs a binary classification of very similar categories represented by *Vernier* line stimuli.

Earlier models of *Vernier* hyperacuity propose that the efficacy of aligned and congruent neurons has to be decreased, while the weights of slightly displaced units with tilted receptive fields have to be increased (Wilson, 1986; Poggio et al., 1992b; Herzog and Fahle, 1998). These rate-based models argue that optimally aligned and congruent units although strongly activated do not produce differential responses for left- and right-displaced line segments, which masks the output of the differential responding neurons. In order to produce the optimal efficacy pattern several mechanisms were proposed which either optimize the response by error-backpropagation (Weiss et al., 1993), or by exploring the weight space in a random order to minimize the distance between the output signal and an external error-signal (Herzog and Fahle, 1998). We demonstrate however that a model exploiting temporal aspects of topologically organized networks resembling the properties of the early visual areas is able to solve the *Vernier* localization task with hyperacuity, without error-backpropagation or random exploration. The temporally structured input to the bidirectional *NMDA*-synapses in combination with a modulatory feedback signal perform with hyperacuity and produce learning dynamics as observed in human psychophysical experiments (Herzog and Fahle, 1997; Fahle, 2004). The result conforms to the view that early units in the visual pathway are responsible for hyperacuity, but emphasizes the importance of temporal encoding. As already mentioned the model, in contrast to the original *TPC*, comprises topological elements, which are necessary to solve the *Vernier* task.

With the topological features our model puts itself between pure non-topological temporal coding of the *TPC* model and hierarchical approaches discussed in the introduction of the thesis. While these hierarchical models which go back to a proposal of Fukushima (*Neocognitron* (Fukushima, 1980, 1987, 2004, 2007)) strongly emphasize the feed-forward connections and neglect the temporal structures of information streams, the model presented in this thesis incorporates two not mutually exclusive coding strategies, i.e. the *TPC* established by the lateral coupling and the temporal code formed by the dedicated delayed feed-forward connections. Both exploit the relative spike timing of ensembles of neurons to encode and decode stimulus information, and reveal the earlier mentioned advantages. In addition our network exploits the distinct properties of information pooling, i.e. firstly keeping information separate in several channels (multichannel approach, where each gets information from one feature selective population), or secondly to average over all features which produces invariant codes (single channel approach). The single channel approach produces invariance in a non-hierarchical manner, by pooling responses of neurons with different features selectivity, which code stimulus information in specific activity phase-lags. The multichannel

approach keeps desired information separate, but exploits in each channel the temporal code as well. It intentionally produces non-invariant codes, which at any later time can become invariant by a simple summation over all channels.

As mentioned earlier the network exploits basically two, complementary coding mechanisms, which are capable to produce temporal codes, i.e. the laterally coupled system, and the feed-forward system, both exploiting distance related transmission delays. The coding schemes can co-exist. The mixture of the two could even be under dynamic control. The cholinergic system could represent a candidate control mechanisms. The recent experimental findings report the modulatory effect of *ACh* on the processing in the early visual areas (Roberts et al., 2005; Zinke et al., 2006). They reveal a down-regulation of lateral information processing, by virtue of activation of muscarinic receptors, and a boosting of efficacy of feed-forward connections, by virtue of nicotinic receptors. By increasing the importance of the feed-forward connections, the system could compensate for the coding impairments produced by the lowered lateral coupling.

The cholinergic projections from the basal forebrain which extensively target structures in the whole neocortex are in the focus of attentional and learning related investigations for a long time. Physiological experiments have shown that acetylcholine (*ACh*) is able to produce similar effects as observed in attention related tasks, which are considered to require a strong top-down information stream which restricts the region of interest in a visual scene (Roberts et al., 2005). Corresponding functions of cholinergic input are known from a long series of psychopharmacological experiments which show the implication of the cholinergic system in sustained attention (Sarter et al., 2001). Lesions in the basal forebrain are sufficient to impair the outcome in these tasks dramatically. We demonstrate that these new findings can be exploited in extensions of the *TPC*-model, to produce distractor-robust encoding of target stimuli, which were selected by top-down signals. Similar to the physiological findings the modulatory cholinergic input reduces the contextual influences of horizontal connections. In biological systems this is achieved by activation of muscarinic receptors, which lead to an increased electrotonic length of the dendritic tree. In addition we demonstrate that the produced temporal population code is optimally readout by fast feed-forward connections which exhibit similar transmission speeds as the ones observed in physiology (Angelucci and Bullier, 2003). We show, that the new model not only is able encode target stimuli in presence of distractors, but also reveals a better performance is target-only situations, as compared to the original model, which comprised only the lateral connectivity but no dendritic structures or realistic feed-forward readout mechanisms.

In our model we attribute clear and biologically plausible functions to the top-down projections. Their function splits into an attentional part which influences the contextual processing within areas similar to cholinergic input in early visual areas, and a part constituting a supervisor signal which selects neuronal ensembles. This selection directly exploits the bidirectional learning properties of the *NMDA*-synapse model, i.e. it

forces units which are not intended to represent the stimulus category into a silent or slightly depressing state, while the category units stay in the potentiation learning mode and exploit the temporal structure of the code. This is somehow the opposite of most other supervisor learning paradigms which select the categorical units by additional excitatory signals. Incidentally this relates it to a theory presented over 20 years ago, which links the cognitive declines in Alzheimer disease (*AD*) and dementia in common, to dysfunctions of acetylcholine containing neurons (Bartus, 2000). A variety of subsequent studies indicated that the cholinergic pathways from the basal and rostral forebrain innervating thalamic and cortical structures play important roles in conscious awareness, attention and working memory (Perry et al., 1999), which fueled the hope that a comparably simple neurochemical abnormality underlies the complex symptoms associated with *AD*.

In our model we offer a mechanism how early impairments of the cholinergic system could affect learning properties, and performance of cortical brain areas. We state that reduced spiking activity of cholinergic neurons impairs the control of plasticity in cortical target areas. The reduced activation of muscarinic receptors leads to a failure to switch between *LTP*- and *LTD*-states in target cell populations. While in the healthy system, by virtue of the cholinergic input, only a subpopulation is allowed to switch to a synaptic *LTP*-mode, in the impaired network large populations of neurons end up in the potentiating mode, and continuously start to learn new input without consolidating already learned relations - which corresponds to a forgetting of previously acquired information.

9.4 Comparison to other models

9.4.1 Object recognition models

To get further details about the models described below the reader should also refer to the section '*Object recognition models'* in the introduction of this thesis.

In recent years a number of models investigating the processing principles in the visual cortex were proposed (as discussed and illustrated in the introduction of this thesis) (Fukushima, 2003);(Serre et al., 2007a); (Masquelier et al., 2007); (Bohte et al., 2002; Stringer et al., 2006); (Maass, 2009). With the exception of the *LSM* introduced by Maas and the clustering approach of Bohte et al. most of them adopt a rate coding paradigm, and are mostly based on, or at least emphasize the feed-forward processing of information along the visual pathway. This notion is appealing since it mostly relies on local information, and tries to solve the object recognition task with an unsupervised paradigm. All these hierarchical approaches are strongly related to the *Neocognitron*, a model presented in the early 1980s by Fukushima. With time some of these biologically inspired network based members became quite powerful, and are currently in a stage where they

are commercialized and can compete with traditional algorithm-based machine vision implementations. However, most of these approaches neglect fundamental aspects and facts of biological neural networks, which question their importance for a deeper understanding of the processing happening in the brain. They for example do not reflect the predominant inner-areal connection pattern found in the mammalian cortex, which are the extensive excitatory long-range projections between pyramidal neurons. If at all, they rather adopt a Mexican hat like profile with local excitation and long range inhibition, to introduce a self-organization-map-like (*SOM*) behavior. In addition most of them do not consider time as a coding domain, i.e. they neglect the temporal aspects of spike trains. Anatomical, electrophysiological and information theoretic considerations however revealed that the information processing in the visual pathway does not follow a simple feed-forward scheme. Rather, the areas in the hierarchy seem to process information in a heavily parallel manner, with an extensive crosstalk between the areas. This is illustrated by the onset latencies of the different visual areas as for example revealed by recordings in macaque by Schmolesky et al. (Schmolesky et al., 1998b).

In terms of its concepts and ideas the model presented in this thesis is definitely the most related to Maass' *Liquid State Machine* (*LSM*). Both perform their computations based on continuous data streams which are produced by a recurrently connected neuronal pool. The two models however emphasize different aspects of computation in recurrently connected ensembles. The *Liquid* (pool) in Maass' model is designed to hold and amplify as many functions as possible in its *Liquid States*, to operate as a source for large numbers of output units which read out and process the information in a memoryless manner. The *enhanced TPC* model presented in this thesis focuses directly on the requirements and the properties of the visual system. As illustrated in the first section of this chapter a model for information processing in the visual pathway, should incorporate the fundamental properties of its biological prototype. We considered the extensive horizontal connectivity, the fast feed-forward connections, the cholinergic modulatory input, as well as the spiking behavior and the feature selective properties of the pyramidal neurons as components which should be reflected in the model. In this view the *enhanced TPC* model could be seen as a specialization of the *LSM* concept, shaped and optimized to process visual scenes, i.e. contextual ensembles of oriented shapes and edges. In the original *TPC* approach Wyss et al. have shown that the horizontal connectivity is able to generate a highly robust and invariant stimulus specific code, which uses the activity of neuronal populations to encode information in the temporal domain. The recurrent excitatory connections between the model pyramidal neurons exhibit distance related transmission delays and transform geometrical stimulus information into a temporal fingerprint. We extend this view by introducing modulatory input which controls contextual interactions in an attentional like manner. The produced code is read out by feed-forward connections which again exhibit distance-related transmission delays. This allows us to augment the purely horizontal interaction based code, by making it robust to distractor noise in close proximity. Additionally we

introduce a simple biologically plausible model for supervised learning of the produced codes. In this learning paradigm the biophysically restricted modulatory input acts as a supervisor signal, which controls synaptic plasticity properties. With this approach we were able to attribute functions to the fundamental network components, which go beyond the capabilities of the previously discussed models. More precisely, we were able to demonstrate that the attentional-like effect of acetylcholine input can be exploited by the horizontal coding network to produce robust temporal code. Further we showed the advantages of a combined coding scheme which relies on the horizontal *and* the feed-forward connectivity. The two represent the substrates for complementary coding systems which produce temporal representations of input stimuli, with the advantage that a combination of the two delivers both, invariance and position and orientation specificity. The code develops fast, and in extreme cases allows stimulus classification with very few and early spikes. This speaks clearly for the importance of information encoded in the temporal domain. We would like to make clear however that our approach is not purely based on temporal information. The separation of information by virtue of feature specific sub-populations, as found for example in the striate cortex allows exploitation of information which is rate-based as well.

However, it has to be stated that although our model is more biologically plausible than most of the previously discussed ones, it cannot yet compete with the performance of the leaders of the other models. Although the produced code in the network proved to be highly robust with the capacity to scale to large number of input classes, we presented here up to now only a proof-of-concept decoder implementation, which performs a binary classification of simple artificial stimuli. The models like the ones proposed by Riesenhuber & Serre et al. (Riesenhuber and Poggio, 1999; Serre et al., 2007a) or Masquelier and colleagues (Masquelier et al., 2007) were optimized and developed over more than a decade, and are currently able to recognize objects in natural scenes. Future investigations have to reveal the limits of our approach. Especially an extension based on an idea of Bohte et al. (Bohte et al., 2002), as it will be discussed and illustrated in the section *Future investigations*, represents a promising way to augment the encoding and decoding power of the system, and to extend it with unsupervised learning.

9.4.2 Localization acuity models

To get further details about the models described below the reader should also refer to the section '*Localization acuity models'* in the introduction of this thesis.

In 1986 H. R. Wilson (Wilson, 1986) presented a model which explained hyperacuity in *Vernier line discrimination tasks* by appropriate weighing of spatial filters. The filters exhibit receptive fields as observed in *V1* simple cells, whereas the excitatory center region flanked by inhibitory domains exceeds the minimal discrimination threshold of trained observers. The authors argued that a small displacement of two bar segments would not change the output of units with aligned receptive fields. However, slightly displaced or tilted units are able to produce differential responses for the two

displacement sides. Thus, in their model not the most strongly activated units are responsible for the ability to perform with hyperpacuity but the slightly displaced and tilted ones with weaker output.

In the 90s of the last century Poggio et al. and Herzog & Fahle (Herzog and Fahle, 1998) presented models which were able to learn the *Vernier* localization task, and which performed with hyperacuity. The models process the information in two steps. First the input is transformed into a set of radial bases functions, or into unit activities by receptive fields analogue to the ones found in simple cells of the primary visual cortex. In the second step a linear combination of the gathered basis functions or activities is computed, which represents the classifier output. The authors show, that in a multilayer network the activity in the hidden layer can be interpreted as the basis function output and the connections to the subsequent layer as the substrate performing the linear summation. Fahle et al. later showed that this type of model is capable to learn the line discrimination task in a supervised and in an unsupervised (by *EDL* –exposure dependent learning) manner.

The Wilson model builds up on purely linear summation of feature banks, and does not include spiking units which would allow exploiting the temporal structure of neuronal activity. The *enhanced TPC* model as presented in this thesis does perform with hyperacuity as well, but goes beyond this concepts of the other models, i.e. it incorporates several biologically relevant components namely horizontal projections which connect orientation selective cells, contains cholinergic modulatory input which dynamically regulates contextual influences in a scene, and comprises fast feed-forward inner-areal connections. The neurons are modeled as conductance based leaky-integrate-and-fire units. The distance related transmission delays of the horizontal connections in combination with the feed-forward connections allow temporal encoding of spatial stimulus information in neuronal populations. The original proposal of the *TPC* model mimicking the primary visual cortex revealed complete rotation symmetry and was not able to introduce individual weighing of the feature banks producing temporal representations of stimulus features. As we show in this thesis the extension to the previous model (Wyss and Verschure, 2003) allow the *enhanced TPC* model to become very specific, i.e. it solves the *Vernier line discrimination task* with hyperacuity, in both, the *Perceptron* based version and the more biologically plausible *NMDAR*-based model.

The proposal of Fahle and colleagues which extended the ideas of Wilson and Poggio et al. by using more realistic orientation tunings and learning functions moves the network closer to biology. However it does not state how these principles are implemented with units that produce temporally structured outputs, i.e. spiking neurons. In addition it is a member of feed-forward (and feedback in the supervised case with a teacher signal) networks. The inner-areal processing exhibited by cortical circuits is neglected. It includes however the concept of unsupervised perceptual learning, which is not yet present in the model we propose in this thesis.

9.5 Future investigations

9.5.1 Improving scaling properties

As mentioned earlier, the temporal encoding of information based on omnipresent connectivity patterns of the cortex has the capacity to scale to large number of stimulus classes. We showed that a simple network comprising plastic bidirectional *NMDA*-synapse properties is able to solve the *Vernier line discrimination task* in a supervised learning paradigm. It is unclear however, how this scheme scales to a larger number of stimulus classes. Given the small number of synapses the model may be quite restricted with respect to scaling. We demonstrated however, that the *NMDA*-synapses reflect the temporal structure of input streams in a non-trivial manner. Frequencies over a large range from very small up to medium frequencies are capable to produce high or low weight values, if they exhibit the appropriate temporal structures. In combination with a recent proposal of clustering based on temporally structured input by *Bohte et al.* (Bohte et al., 2002) the proposed network in this thesis could be extended to acquire both the capacity to scale to larger stimulus classes, and the capacity to learn appropriate stimulus classes in an unsupervised manner. *Bohte et al.* show that temporally encoded stimuli sent over a series of connections which cover a complete range of transmission speeds produce, with training, clustered output in the subsequent layer. The output units act as simple coincidence detectors which change the weight of synapses according to a hebbian learning rule. A similar mechanism could be adopted to improve the scaling properties of the learning part of the network presented in this thesis. A large number of feed-forward connections with various transmission delays, as found between visual areas in the brain, would project the produced temporal stimulus representation to a high dimensional space. Given the increased number and specific responses of the *NMDA*-synapses one would expect that the output neurons would be able to exploit the temporal structure of the input spike trains, and produce stimulus-specific activity patterns. Depending on the temporal structure of the input, distinct neurons would increase their activity while others would decrease their firing rate. Subsequent readout neurons could act as simple coincidence detectors to detect stimulus identity or class. This scheme could either work in an unsupervised manner, or supervised according to the proposal in this thesis, i.e. by modulatory top-down input, to stabilize already learnt relations and to increase the learning speed and magnitude. This scheme could co-exist with the *Liquid State Machine (LSM)* proposal (Knusel et al., 2004) for the decoding of temporal stimulus information.

9.5.2 Closing the behavioral loop

Currently the supervisor signal is represented by a manually set top-down signal which resembles the effects of cholinergic input originating from the basal forebrain. Alternatively the signal could be replaced by an inhibitory top-down signal, carrying error signal information. In either way it would be interesting to close the loop, and let the network generate the top down signal. Hypothetically the model should be able to reproduce the properties of biological systems which only at the beginning need an

external error signal till a category representation has formed. In terms of the network this would correspond to a top-down signal which shapes the response of lower stages, as shown in this thesis. During learning self enforcing loops (*input->processing->feed-forward->…>category identification->top-down signal->input->…*) would establish which more and more take over the top down signal. For categories which are already learnt, no error signal is required, the top-down signal will immediately be generated by the network and will shape and stabilize the category representation. Given this proposal works, in a later step the complete behavioral loop could be closed. This is important since the interaction of an agent with its environment can put severe constraints on the type of coding used. The validity and relevance may only be understood in the context of a fully behaving system, where sensor implementation, motor output, and environment play crucial roles.

9.5.3 Adding more biological relevant components

The presented model covers a number of important anatomical and biophysical properties of the cortical networks found in the visual pathway. This allowed us to pinpoint their putative function. The biological networks include at least two additional components which could be investigated in the framework we propose, i.e. the inter-areal top-down connections, which connect the different visual stages, and the inner-areal inhibition, which may play an important role in selecting the most active neurons during processing, aka winner-take-all. It would be interesting to see how these components interact with our model, and how they reshape the responses produced in the different layers.

Appendix A

Nereda a framework to analyze *Neurolucida*™ data

A.1 Management summary

With the *Nereda* framework we present a *Java*-based open source class library for the analysis and visualization of *Neurolucida* data (open for implementation of other data sources).

The main focus of the software is on expandability, maintainability and robustness. *Nereda* creates a hierarchical object tree out of *Neurolucida* data, and provides flexible access to all contained information. The object-oriented architecture follows an interface-based design and provides clear implementation guidelines for future extensions. A set of analysis functions, mainly implementations of algorithms presented by T. Binzegger et al., are built-in. The interfaces to *Java* and *Matlab* provide flexible routes for future implementations of either existing, or new algorithms. All import and export formats are based on open standards, i.e. *XML*, *STL*, *TXT* and *Matlab MAT*. The documentation and defined design rules provide the basis for robust implementations of future requirements, and guarantee high code reusability.

The visualization part of the framework provides methods to plot 3D-representations of the reconstructed structures and related information, optimized for various use cases.

In summary, *Nereda* with its robust design and good performance, is an alternative to existing script-language based approaches for the analysis and visualization of *Neurolucida* data. With the gathered information about neural anatomy and connectivity the framework contributes to the improvement of computational neural network simulations, which is the main reason why this chapter found its way to into this thesis.

A.2 Introduction – Motivation and requirements of the framework

The motivation for this framework came in the course of the simulations performed for this thesis. As we discuss in chapter 9, the quality of computational modeling of brain functions heavily depends on how close the model reflects the important biological facts. This however turns out to be a very hard to fulfill. It is a difficult and sometimes impossible task to collect enough biological information to be able to restrict the model to the important parts and to model these components as close as possible to anatomy and physiology. Beside of the very time-consuming anatomical data collection available reconstruction tools are still islands. The state-of-the-art reconstruction software *Neurolucida*™ for example which is used at the institute to reconstruct neurons and brain surfaces does not have convenient interfaces to export data into the *Matlab* programming environment. Even though *Neurolucida*™ has some data analysis and illustrations functionality aboard, this makes it hard to exchange data, and to develop and implement custom analysis requirements, which may change rapidly in a scientific environment. Till now the implementation of new requirements was mainly single-user centered, i.e. each researcher developed its own export code or changed routines of others. Since this was done without the use of object-oriented designs and mainly within script languages like *Matlab*, code reusability, robustness, maintainability and performance was quite low. Each new generation of researchers had to work through a bunch of scripts to change them according to their own requirements, which made them unusable for previous tasks. That's why it was decided to design a new compact framework (*Nereda*) that acts as a bridge between reconstruction software solutions like *Neurolucida*™ and data processing environments and presentation packages, i.e. *Matlab* or *Blender*™.

The name *Nereda* is derived from the terms ***Ne****ural* ***re****construction* and ***d****ata* ***a****nalysis*.

The main purpose of the framework is to provide a tool to analyze neuronal 3D reconstruction data to be able to extract building and connectivity rules of neurons which can later be used to improve the quality of computational models. The framework should be capable to incorporate existing analysis code, e.g. the collection of algorithms developed by Tom Binzegger to describe bouton distribution or axonal tree clustering, but should also provide interfaces and guidelines to add new functionality without compromising the robustness of existing code.

To reach the upper goals the software has to reflect the following properties:

- Direct import of anatomical data from neuron reconstruction software packages (currently *Neurolucida* ™ available)
- Representation of the hierarchical nature of neuronal data with access to all important structures of the neuron and their properties, e.g. soma, axon, dendrite…
- Reflecting the space-relationships of several neurons
- Relate neuronal tree structures to the brain surface
- Provide libraries for statistical analysis of the neuronal anatomy
- Provide patterns for expansion of the library with additional analysis functions
- Linking the neuronal anatomy to optical imaging
- Supporting the experimenter in finding reconstruction errors
- Provide plotting functions for ad-hoc illustrations
- Exporting structured data to 3D render software packages for high quality illustrations
- Easy maintainability and expandability

The goals were achieved by the incorporation of the following technical principles:

- Usage of up-to-date standards for software architecture and data formats to achieve flexibility and robustness, e.g. *Java*, *Matlab*, *XML*, *STL*
- Usage of object-oriented coding principles to optimally encapsulate object related data and methods
- Usage of interface based programming to gain optimal maintainability and expandability
- Usage of software coding patterns optimized to traverse hierarchical tree structures, i.e. visitor patterns to achieve easy usability, easy extendibility and robustness against changes in the data format of the 3D reconstruction software or the analysis techniques.
- single-jar file based deployment
- open source solution for complete access to all analysis and data structures
- framework accessibility at runtime in the absence of *Matlab* being installed or licensed on the target machine
- batch operation mode for large analysis jobs
- Framework accessibility from *Java*, *Matlab* or as standalone application for optimal flexibility

A.3 Philosophy of the framework

The framework was designed to work in a very dynamic environment with changing and sometimes conflicting requirements, i.e. quantitative brain research. For not losing the robustness and maintainability of the software package after a short time the framework is designed along specialized guidelines. First the data acquisition in 3D reconstruction modules and the data analysis and visualization in *Nereda* are completely separated. *Nereda* never changes the original data or structures gathered in the reconstruction software. This allows collaboration on stable data sets, and a revalidation of the original data at any point in the analysis process (***Figure A.1***). Second *Nereda* keeps a rigid separation of data on one side and the data processing logic on the other side. All the processing logic is encapsulated in visitor classes which implement a simple interface and exist independent of the hierarchical data structure. The framework can easily be extended in a robust manner by adding additional visitors without compromising existing code or having to take care about the underlying data pool. Third, the consequent interface based programming in the whole framework provides an easy and well-defined mechanism to extend the packages, either on the analysis or more fundamental on the data object representations, which opens the framework for other data pools beside of *Neurolucida*™. Fourth, *Nereda* can be accessed in a very flexible platform independent way from Windows-, Linux- or MacOS environments, from within both *Java*- and *Matlab* programming environments. By using the *Java* programming language the framework is not only platform independent and fully object oriented, but it also outperforms the speed of pure *Matlab* implementations by orders of magnitude.

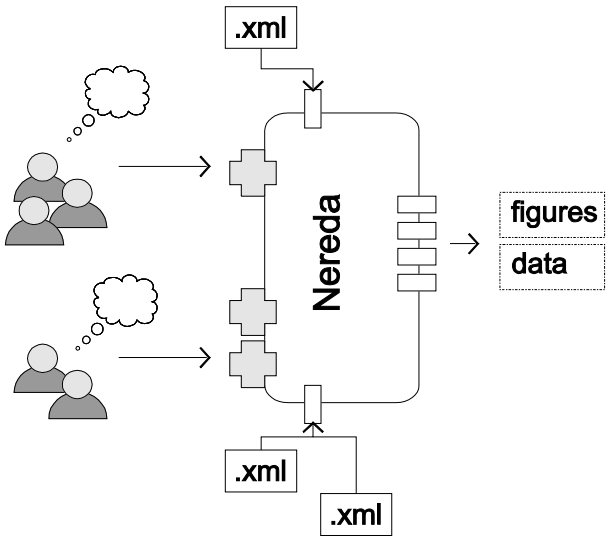

Figure A.1: *Nereda* workflow: Several researchers or groups of researchers develop their own ideas how to analyze chunks of reconstruction data (data provided as *.XML*). Each group implements their analysis as series of new *Nereda* plugins or uses the plugins of other groups or built-in ones. Several of these components can be merged to super-plugins. The framework guarantees the interoperability of the components.

These implementation principles allow keeping the robustness of the framework even if the requirements change rapidly or when several programmers or scientists extend the packages by their own components. The result is a flexible and compact software framework to analyze and visualize neuronal reconstruction data, which keeps its robustness and maintainability over time.

A.4 Architecture

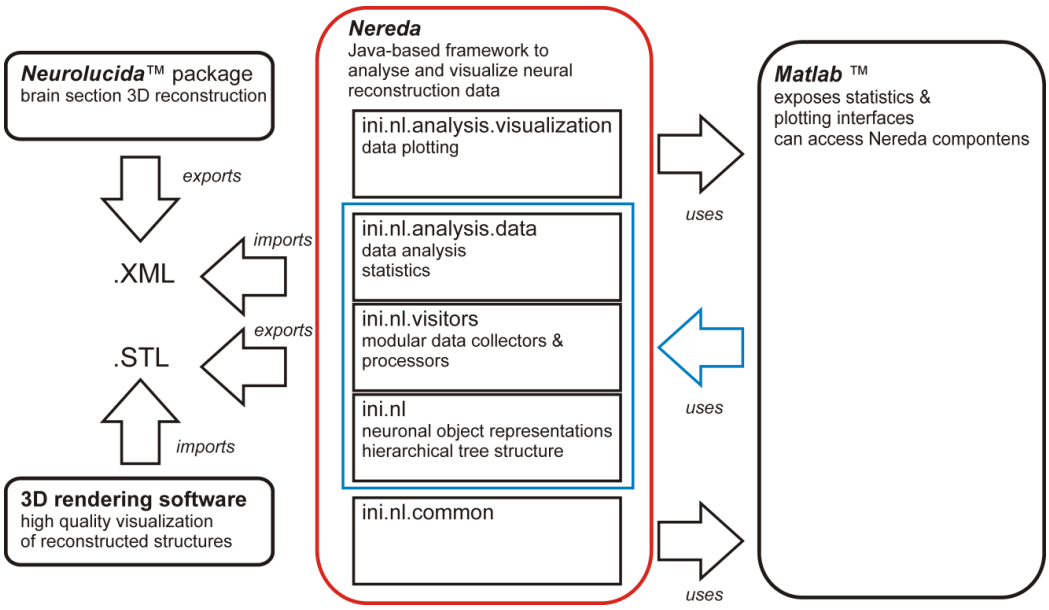

Figure A.2: The *Nereda* architecture: *Nereda* resides in the middle between neural reconstruction packages, i.e. *Neurolucida*™, the data processing language *Matlab* and 3D rendering software packages like *Blender*. *Nereda* is a software framework written in *Java* that encapsulates the complexity of data structures and internal processing logics. The framework provides simple interfaces to plug-in custom analysis code. Several namespaces contain built-in components for data collection, statistics, and visualization. Interfaces to *Matlab* (*Java*-based interfaces) and render software packages (*STL*, Surface Triangulation Language) provide full flexibility for future requirements.

Nereda positions itself in the middle between the data analysis environment *Matlab* and 3D reconstruction software packages, e.g. *Neurolucida* and 3D rendering software solutions (**Figure A.2**). The framework imports neuronal 3D reconstructions via *XML* data structures to build up a *Java* based object hierarchy. Each instance in the hierarchic tree represents a member of an object-oriented class architecture that implements well defined interfaces (*ini.nl*-namespace, *ini.nl.inf*-namespace). Any of the hierarchy elements, e.g. cell soma, axonal/dendritic segment and varicosity, deserves as an entry point for worker classes (*visitors*) that fulfill various tasks, e.g. data collection, statistic analysis and plotting (*ini.nl.visitors*-namespace). The object tree itself guarantees that the worker instance starting from the entry point visits and executes its code for all of

the tree sub-elements. This leads to an optimal separation between code logics and tree internal data organization, i.e. optimal robustness with the most flexibility. Predefined libraries for data analysis and visualization provide easy access to statistics and ad-hoc plots (*ini.nl.analysis.data*- and *ini.nl.analysis.visualization*-namespaces). In addition the interface based approach allows easy extension of the framework parts, while maintaining its robustness. The analysis components of *Nereda* have complete access to *Matlab* data processing procedures. In turn most of the *Nereda* components are accessible from both *Java* and *Matlab* to provide the best freedom of choice for *Nereda* programmers. For high quality visualizations *Nereda* provides functions to export fractions or complete neurons and brain surfaces into the Surface Triangulation Language (*STL*) used in stereo lithographic CAD- and rendering packages like *AutoCAD*™ or *Blender*. In addition *Nereda* allows the saving of complete object trees into the *Matlab* proprietary .mat-format for easy exchange between users or computers.

A.5 Brain domain model (simplified)

The core of the framework is represented by the *ini.nl*-namespace classes. Anatomical real-world entities, e.g. Neuron, Axon, Dendrite etc., are modeled by classes from this namespace. *Nereda* represents the reconstructed data as a hierarchical object tree rooted in the *Brain* entity (***Figure A.3***). A brain contains a series of section outlines which define its spatial borders. In addition the brain object can hold neurons and a number of reference penetrations that deserve as landmarks. To relate the anatomical data to optical imaging a collection of optical maps can be attached to the brain. Each component in the hierarchy that has a specific location or spatial extent is defined as a series of points in x/y/z-space with an optional diameter d.

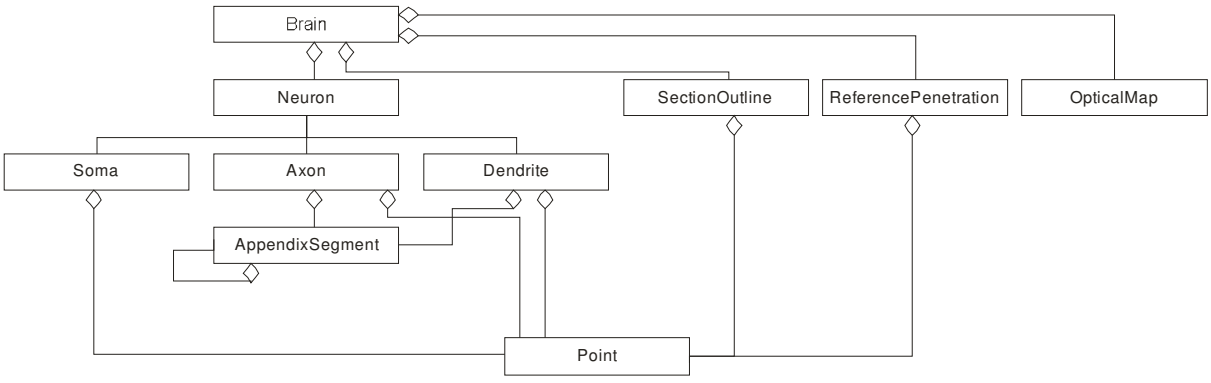

Figure A.3: Simplified *Nereda* brain domain model: The reconstructed brain structures, i.e. brain surface and neuronal compartments, are modeled with a series of related objects. To keep the application of the framework flexible all relations between objects are modeled as aggregations, rather than associations (each component can exist isolated from its parent object). Four main components, i.e. Neuron, OpticalMap and ReferencePenetration all rooted in the Brain object build the backbone of the hierarchy. Together with their subcomponents they form a complete, sequentially accessible object tree, which represents the reconstructed *Neurolucida* data.

A.5.1 Traversing the object tree

Nereda uses data collected in *Neurolucida*™ to construct a hierarchical object structure. The building blocks of the object tree are located in the *ini.nl*-namespace. Once the tree structure is initialized it can be traversed either sequentially or via random-access (***Figure A.4***). Sequential access is provided by typed collections. Since each tree element, beside of the root has exactly one parent object, each tree element and associated data is accessible via a unique path. However, to keep the framework as flexible as possible the relationships between the classes are all modeled as aggregation, rather than compositions, i.e. each element can exist without a parent object. Random access is provided at each tree node via a search-for-element-id mechanism provided via the *getElementById(String id)*-method. More sophisticated filters can easily be added via custom visitor classes.

A third method to traverse the tree, i.e. *visitor-based traversing* is described in the next section. Visitors also sequentially access the tree. The explicit logics how to perform the walk in the complex heterogeneous tree structure is however hidden from the programmer, and replaced by a simple but powerful interface.

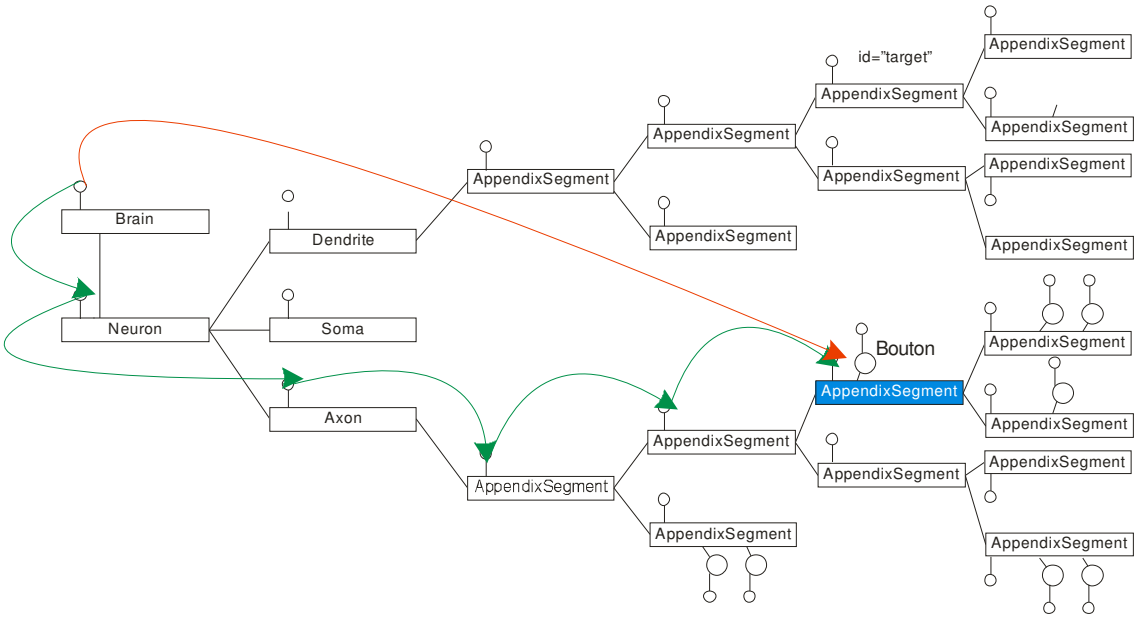

Figure A.4: Schematic, simplified tree structure that represents a brain with one neuron (*see Code examples #1/2*): The figure shows a simplified *Nereda* tree structure to illustrate access modes in *Nereda*. Boxes represent elements/nodes of the tree, large circles boutons on axonal tree segments, and small boutons interfaces exposed by the elements. *Nereda* provides two access modes, i.e. sequential and random. In sequential mode one *walks* element-by-element through the tree to access the target element. In random access internal *Nereda* search functionality allows direct access to the target from any parent element in the tree.

A.5.2 Collecting/processing data

The most easy and flexible way to collect or process data in *Nereda* data structures is to use one of the predefined visitors, or to program additional visitor components (see section 'Extending the framework').

The visitor pattern

Nereda encapsulates internal data structure logics and hides it from the user. The programmer does not have to know the exact structure of the internal object tree, or how to traverse this arbor to collect or process data. In the visitor pattern one distinguishes between the visitor (the component that walks through the tree) and the visited object. In *Nereda*, any tree element can be a *visited object*, i.e. each element in the tree has to implement the *VisitedInf-interface* which allows injecting a visitor. The visitor on the other hand implements the *VisitorInf*-interface, which defines two methods, i.e. *execVisit* and *execAfterVisit*, that are called from the visited element when the visitor arrives at the instance at his way down through the tree and on his way back, when it arrives a second time at the same element. The visitor component automatically *visits* the sub-elements of the entry point to execute its code (***Figure A.5***). This strategy which hides internal tree logics from the programmer is optimized to deal with varying heterogeneous hierarchical structures, e.g. neurons in brains. The visit-procedure comes in two flavors, i.e. a shallow one where only the direct sub-elements of the entry point are considered (*visit*), and a deep visit variant where all the elements of the sub-tree rooted at the entry point are traversed (*visitDeep*). The interface-based separation of internal data structure and data processing code makes the framework robust and flexible at the same time.

For the complete interface definition the reader is referred to the UML diagrams and the framework documentation (see *Resources* section).

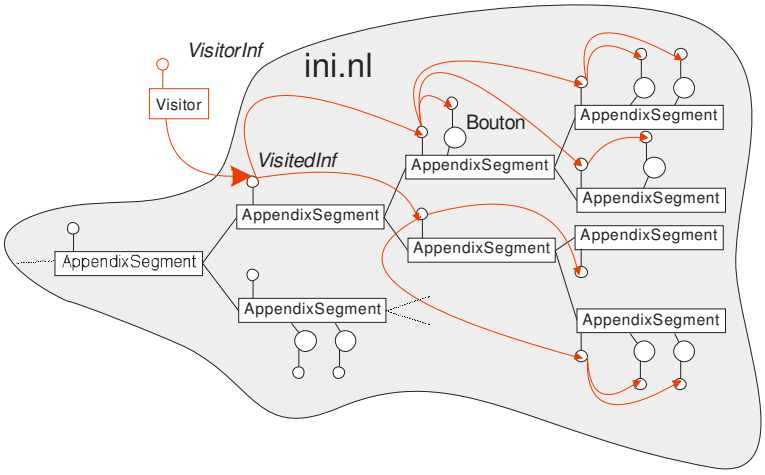

Figure A.5: Visitor pattern in a deep variant (see all *Code examples #1-12*): A customized data processing component (Visitor) is injected into a heterogeneous hierarchical tree. The component automatically travels through the sub-tree and visits each of its elements to execute its customized code. Any element in the tree can deserve as an entry point for the visitor.

A.6 Application field

As mentioned in the previous section *Nereda* focuses on rapid and flexible analysis of neural reconstruction data, as delivered by *Neurolucida*™. Beside of that the framework should also cover presentation demands, i.e. ad-hoc illustrations of reconstructed structures that deserve as a basis for discussion, and it should provide high quality reproductions for journal publications or electronic presentations. In this section a non-complete series of application examples output is given. The data originates from neurons in area 17 of cat. For code examples the reader is referred to the code section of this chapter, and to the *Resources* section.

A.6.1 Visualizations

Nereda provides two visualization types, i.e. a *Matlab*-plot based version (***Figure A.6***, ***Figure A.7*** and ***Figure A.11***) and a rendering version (***Figure A.8*** and ***Figure A.12***) which is accessible via the *STL* export format (Surface Triangulation Language). Depending on the requirements various views of a data set are available **(*Figure A.9*** and ***Figure A.10*).**

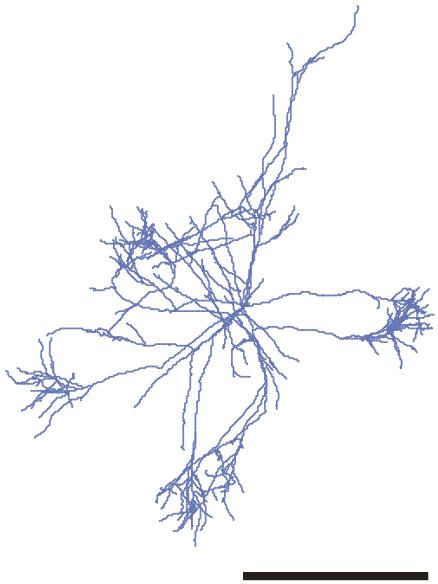

Figure A.6: 2D projection of an axonal tree (see *Code example #6*): A two dimensional projection (top view) of an axonal tree with clear distal patches. Soma and dendrite of the neuron are not shown. For illustration reasons the segment diameters are not in scale. Scale bar corresponds to one millimeter. Since the plotting is performed via the *Nereda* interface within *Matlab*, the complete *Matlab* plotting tools are available to interactively process and export the illustration (see next figure).

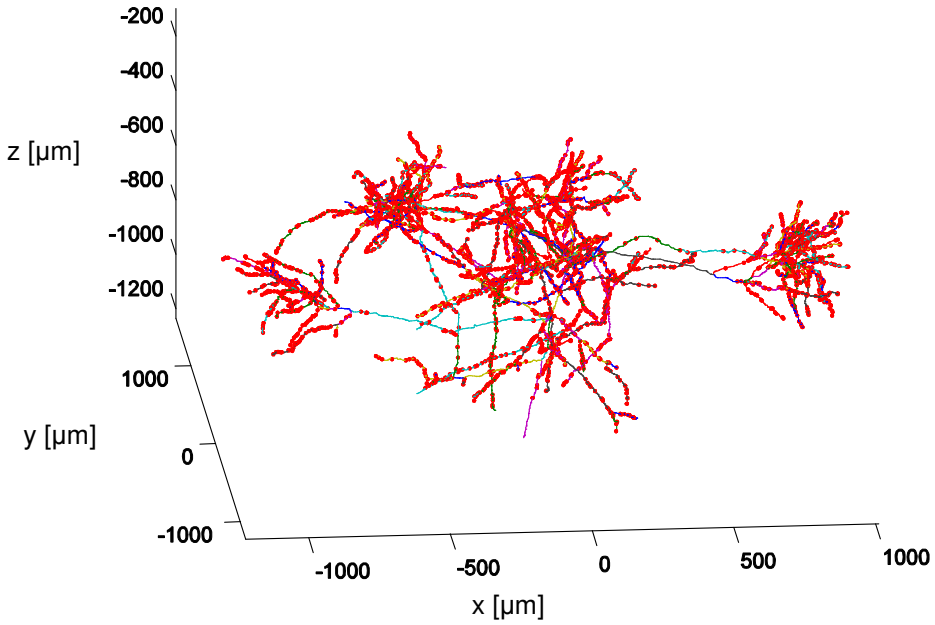

Figure A.7: 3D projection of the same axonal tree as in the previous figure (*see Code example #6*): Boutons are shown in red and neighboring axonal segments are colored differently to facilitate tracking. The tree can be rotated in any direction.

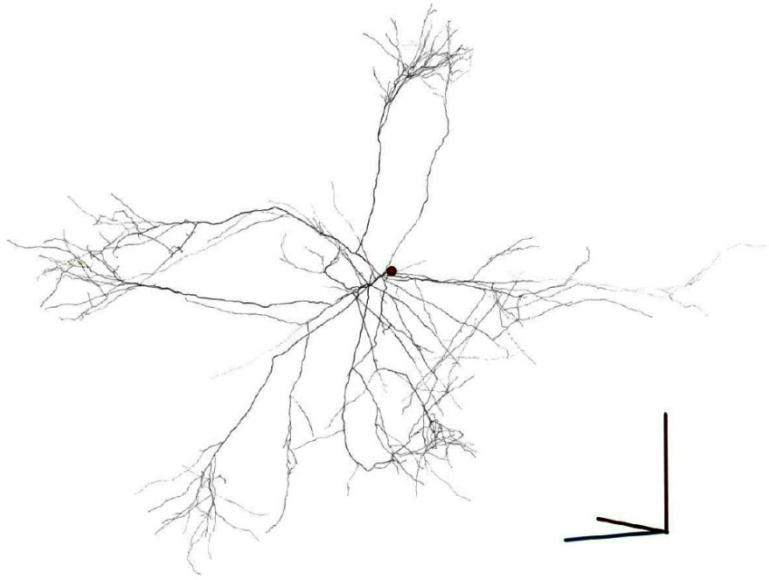

Figure A.8: Rendered 3D representation of the same neuron as in the previous figures (*see Code examples #7/9*): *Nereda* was used to triangulate the axonal tree as tube structures with correct spatial relations. The position of the cell soma is denoted by a red sphere. The face-vertex data structure is exported in the Surface Triangulation Language and subsequently imported into the rendering software *Blender* to produce the upper illustration. With the support of *STL*, the reconstruction data sets are accessible in any render or CAD software package. Reconstruction data can be merged with other data sources, e.g. EM data, to illustrate complex coherences in single snapshots or complete animations.

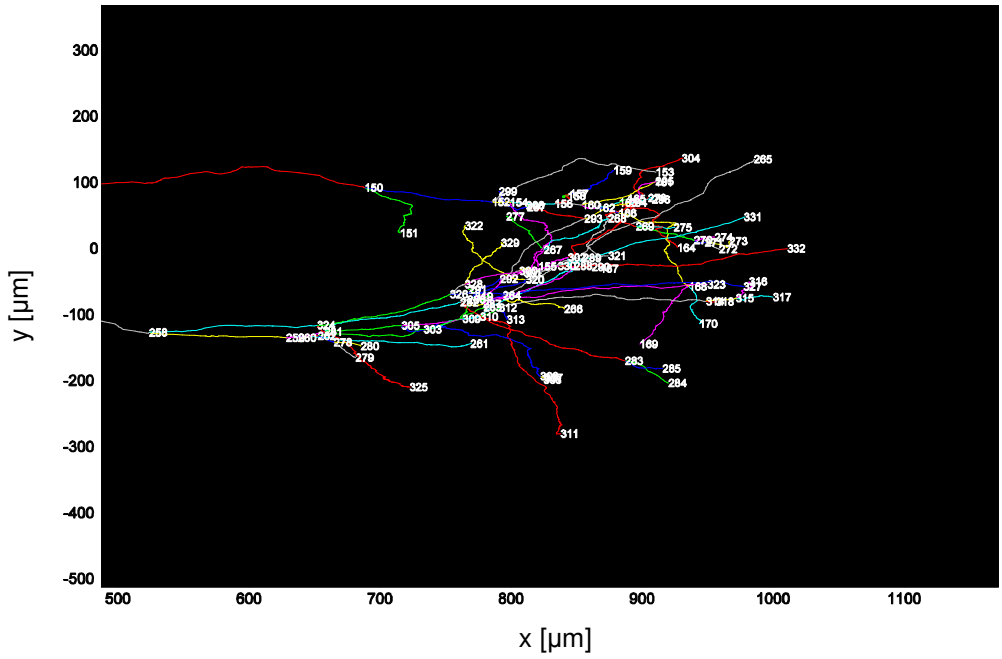

Figure A.9: Close-up of a daisy patch (*see Code example #4/6*): A daisy patch with the unique id (consecutive number) on each segment. Sub-trees, e.g. a single patch, are selectable via their unique ids. Boutons are not shown.

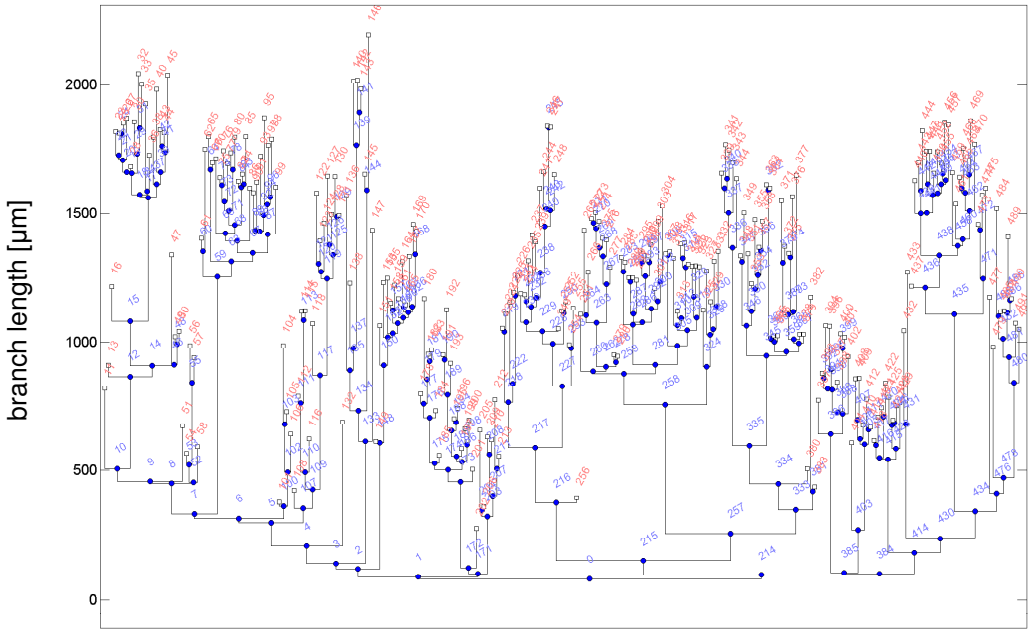

Figure A.10: Dendrogram of the axonal tree (Code example #12): The same data as in the previous figures plotted as dendrogram, to visualize the extent of the tree and to identify ids of interesting sub-tree structures. Blue dots denote tree branches, white squares tree leafs. The numbers indicate the ids of the axon elements. The segment with id=0 corresponds to the point where the axon exits the cell soma.

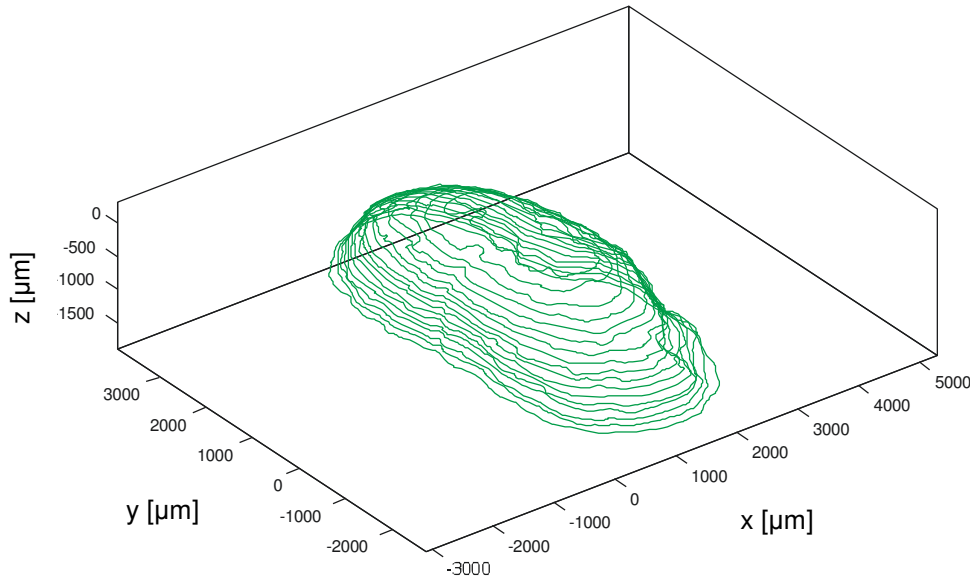

Figure A.11: The brain surface visualized as a series of contour lines (*see Code example #6*): The boundaries of the brain sections used to reconstruct neurons denote a series of contour lines which describe the surface of a piece of brain.

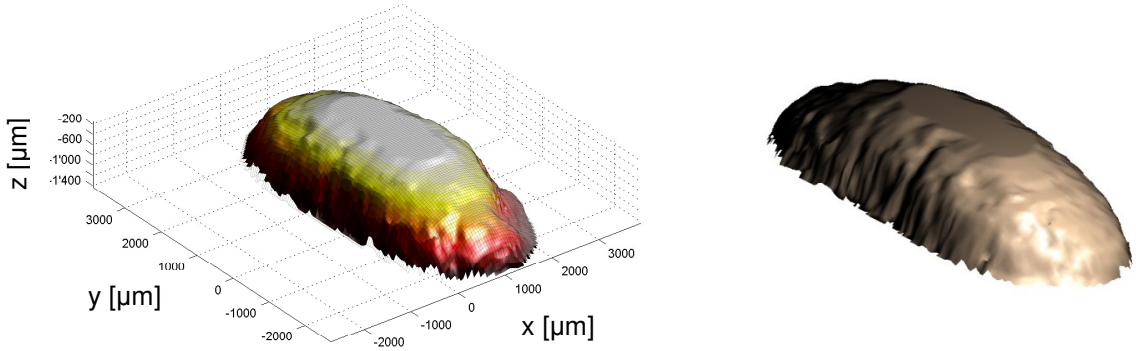

Figure A.12: The triangulated version of the same brain surface as in the previous figure (*see Code example #8*): *Nereda* allows triangulation of the brain surface from a series of contour lines. The two figures show the triangulated and rendered surface in *Matlab* (*A*, via the *Nereda Builder JA* interface to *Matlab*) and in *Blender* (*B, via STL export format*).

A.6.2 Statistical data analysis

Currently *Nereda* mainly implements algorithms introduced by Tom Binzegger (Binzegger et al., 2004, 2005) to describe and analyze the structure of the reconstructions. The architecture is however completely open to add further processing components. Below a few exemplary illustrations about statistical data analysis performed in *Nereda* are shown (***Figure A.13*-16**). Figures similar to the ones below were presented at the FENS meeting 2008 in Geneva on a poster of Elisha Ruesch et al.

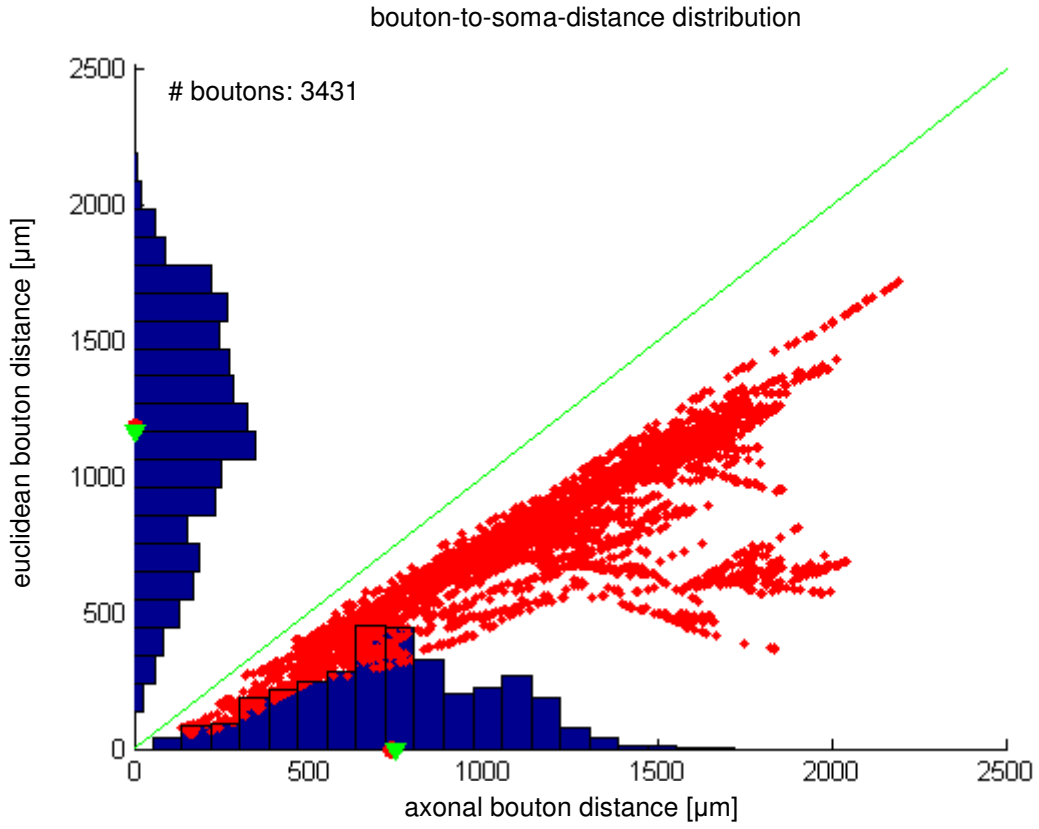

Figure A.13: The distribution of bouton-to-soma distance in one neuron (*see Code example #10*): The axonal tree as seen in the figures of the previous section was used to analyze the distribution of the distances between the boutons and the soma. The histogram on the x-axis denotes the distance as the shortest distance between the bouton and the soma following the axonal segments (red dot denotes the mean of the histogram, the green triangle the median). The y-axis denotes the distribution as Euclidean distance. The red diamonds denote the individual data points (boutons), giving an impression of the curvature of the axonal tree segments. In an extreme case where each path back to the soma would represent a straight line, all data points would fall on to the green diagonal.

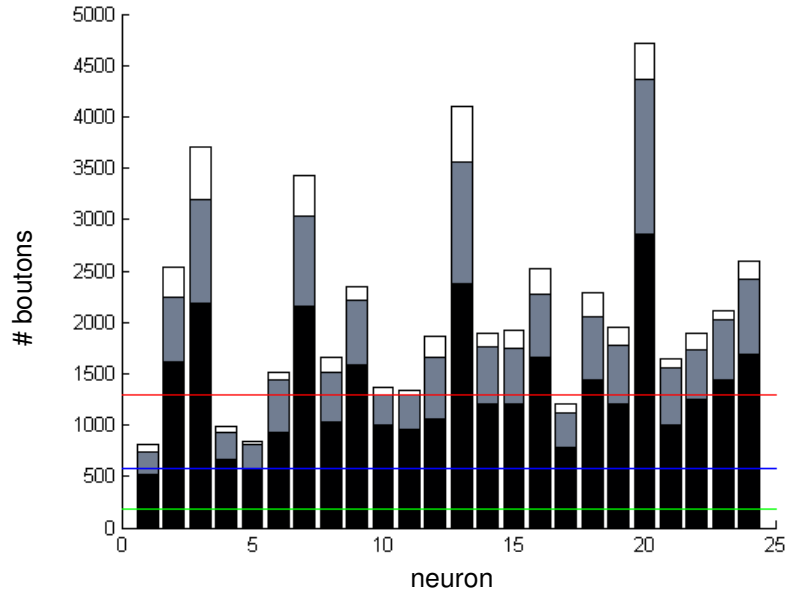

Figure A.14: The distribution of the boutons in various neurons as a function of the Horton-Strahler order of the axonal tree segment they belong to: The figure shows the number of boutons in the 1st (black), 2nd (gray) and 3rd (white) order for each neuron. The algorithm was implemented according to the proposal of Dr. Tom Binzegger (Binzegger et al., 2004, 2005). Raw data was kindly provided by Elisha Ruesch.

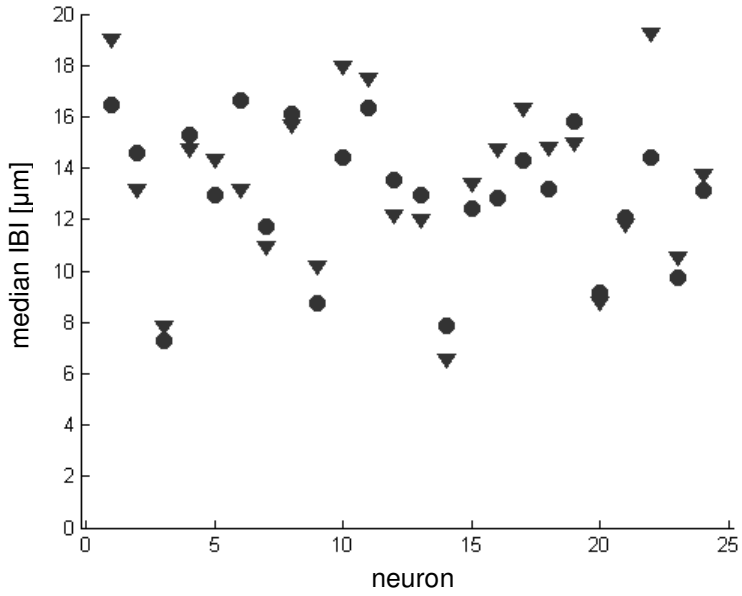

Figure A.15: The inter-bouton-interval (*IBI*) as a function of the Horton-Strahler order: The inter-bouton interval for a series of neurons and for two Horton-Strahler orders of the according axonal segments (dots = 1st order, triangles=2nd order). The algorithm was implemented according to the proposal of Dr. Tom Binzegger (Binzegger et al., 2004, 2005). Raw data was kindly provided by Elisha Ruesch.

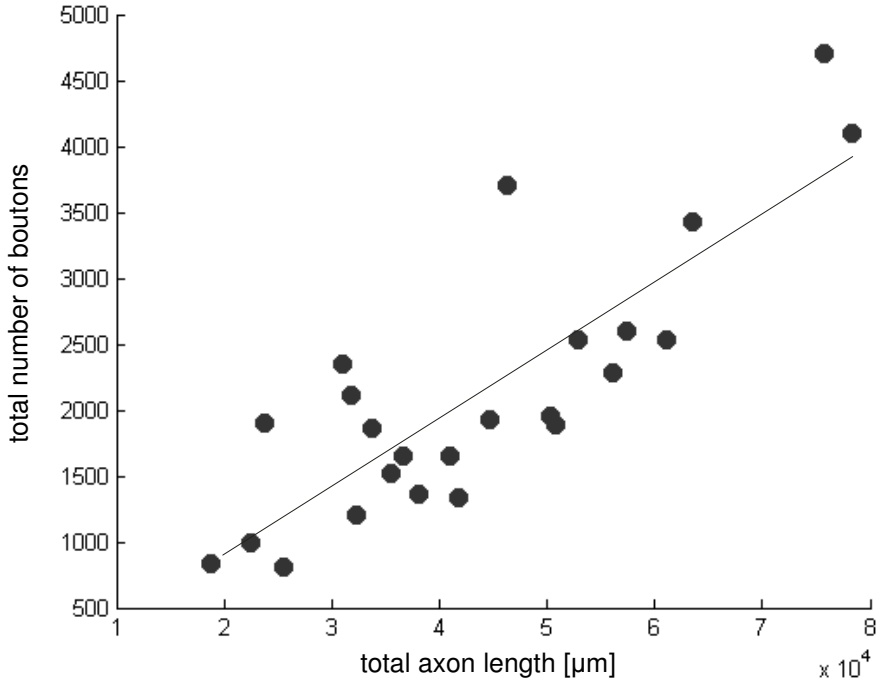

Figure A.16: The number of boutons as a function of the total length of the axonal tree: The total number of boutons depends in an almost linear fashion on the axonal tree length. The algorithm was implemented according to the proposal of Dr. Tom Binzegger (Binzegger et al., 2004, 2005). Raw data was kindly provided by Elisha Ruesch.

A.7 Future steps

Nereda is continuously developed further. The next steps focus on the extension of the statistical data analysis. In the near future all methods proposed by Tom Binzegger for bouton distribution and axonal clusters will be implemented in the framework. In addition methods to relate the neuronal anatomy to optical imaging data will be developed and implemented.

Further, for convenience all major data analysis and plotting routines will be mapped into standalone *Java* executables. They can be run in the absence of any development environment, and will be fully configurable via command switches are alternatively by an *XML*-based configuration structure. By using the *XML* structure, complete analysis batches could be configured without programming knowledge. In a later step a GUI to start individual analysis components, and to load and create *XML*-configuration structures will be made available. The application will run from a local copy or as a web start component.

A.8 Summary and Conclusion

In this chapter we presented a framework (*Nereda*) to flexibly access and process data gathered in neural reconstruction software packages, i.e. *Neurolucida*™. The *Java*/*Matlab*-based solution is designed to remain stable even if the processing requirements change rapidly, as inherent to research environments. Its interface based architecture guarantees collaboration functionality between several researchers and also future extendibility. It should overcome the problems to export data from *Neurolucida* to data processing environments, provides data analysis and visualization functionality, and deserves as a toolbox for collaboration of several researchers.

Given these properties the workflow between anatomical data acquisition and the usage of the analyzed data in computational neural simulations should be speed up, and be more flexible in the future.

A.9 System requirements, installation and usage of the framework

In this section background information about how to use the framework and about the design of the architecture is provided. The information should be seen as a summary. The content should allow to perform the first steps to extend *Nereda* according to the own needs. For a complete documentation the reader is referred to the *Resources* section below.

A.9.1 System requirements

Nereda is based on platform independent technologies. The framework runs on Windows, Linux, and MacOS with *Java* (jre 1.6.0_06 or higher) and Jama (v. 1.0.2). To import large neuronal structures sufficient memory has to be reserved for the Java Virtual Machine (e.g. java -Xmx512m -Xms512m).

At runtime the *Nereda* framework does not require a *Matlab* installation on the target machine (nor is a *Matlab* license required for the machine). During development however, in order to wrap additional m-functions *Builder JA* is needed (requires full *Matlab* installation and valid license!).

A.9.2 Installation

Nereda is distributed as single jar (*Nereda*.jar) file which contains all required packages. For the source code consider the section ‘Resources’.

A.9.3 Resources

Beside of the framework information provided in this thesis, documentation, source code, and latest builds are available on *http://www.ini.uzh.ch/~sro*

A.9.4 Framework documentation

In the following sections a summarized documentation of the framework components in combination with use cases and examples on how to extend the framework is given. The information allows using the framework based on the code examples, and provides an overview on the class relationships and supported attributes and methods. Additionally, information about how to extend the framework with further components to implement custom analysis requirements is provided (for the complete framework documentation consider the *Resources* section).

Interfaces to external architectures

Nereda interfaces to several external architectures on various levels. The most strong interaction is between *Nereda* and *Matlab*. On one hand *Nereda* classes are accessible from within *Matlab* and from *Java* environments. On the other hand *Nereda* plotting and data analysis tools use *Matlab* components via the *Builder JA* wrapper technology. Hence the analysis code can first be written in the flexible and powerful *Matlab* environment, before it is encapsulated into a *Java* wrapper. Currently already a large collection of *Matlab*-based data processing and plotting functionality is available in the *MatlabHelper* class of the *ini.nl.common*-namespace. Beside of explicit implementations, several generic methods that allow parsing of code strings are provided. The list of existing MatlabHelper functions can easily be extended with custom functions. For details the reader is referred to the section '*How to extend the framework*'.

Beside of the seamless interplay of *Nereda*, *Matlab* and *Java*, the more loosely coupled interactions to *Neurolucida* and 3D rendering solutions exist. All these interactions are unidirectional and based on import and export of standard file formats, i.e. *.XML* and *.STL* (***Figure A.1***). As mentioned above, for conceptual reasons *Nereda* does not provide write access to *Neurolucida* output files, i.e. it will never change the content of *.XML*-data files originating from neural reconstructions. On one hand this keeps the processing chain between *Neurolucida* and *Nereda* flexible, on the other hand and probably more important, this also minimizes the risk of bogus analysis because erroneous data insertions which are hard to detect at later stages. The interface to 3D rendering software solutions is provided over the *STL* data export format. The main components of the reconstruction process, i.e. brain surface, axonal- and dendritic tree can be exported as a binary **S**tandard**T**riangulation**L**anguage file, which can easily be imported into rendering tools like *Blender*. *Nereda* performs the triangulation of the surfaces from lines or point cloud structures provided by *Neurolucida*, and allows the user to set the triangulation parameters to control the balance between quality and data size. For detailed information about how to use the functions the reader is referred to the code example sections and the class documentation.

Using the framework (code examples)

Traversing the object tree

Sequential access (Code example #1)

Java version

```
public static void main(String[] args) {
      MatlabHelper.colordef("black");
      MatlabHelper.holdon();

      BrainInf b = new Brain("b0", "b0", "Neurolucida", "1.0", "", "");
      b.addNeuron("neuron1.XML");
      AppendixSegmentInf as = b.getNeurons().get(0).getAxon().
            getSegments().get(0).
            getSegments().get(0).
            getSegments().get(0);
}
```

Matlab version

```
clear java
clear all

close all

javaclasspath({'E:\Data\sro\INI\plotJA\jmatlab\distrib\jmatlab.jar', ...
  'E:\Data\sro\My Documents\workspace\Neurolucida\Neurolucida.jar', ...
  'C:\Program Files\Java\jre1.6.0_03\lib\ext\Jama-1.0.2.jar'})

filename = './neuron1.XML';
b=ini.nl.Brain('b','b');
b.addNeuron(filename);

as = b.getNeurons().get(0).getAxon(). ...
            getSegments().get(0). ...
            getSegments().get(0). ...
            getSegments().get(0);
```

Random access (Code example #2)

Java version

```
public static void main(String[] args) {
      MatlabHelper.colordef("black");
      MatlabHelper.holdon();
      BrainInf b = new Brain("b0", "b0", "Neurolucida", "1.0", "", "");
      b.addNeuron("neuron1.XML");
      AppendixSegmentInf as = b.getElementForId(“target”);
}
```

Matlab version

```
clear java
clear all

close all

javaclasspath({'E:\Data\sro\INI\plotJA\jmatlab\distrib\jmatlab.jar', ...
  'E:\Data\sro\My Documents\workspace\Neurolucida\Neurolucida.jar', ...
  'C:\Program Files\Java\jre1.6.0_03\lib\ext\Jama-1.0.2.jar'})

filename = './neuron1.XML';
b=ini.nl.Brain('b','b');
b.addNeuron(filename);

as = b.getElementForId('target’);
```

Collecting/processing data

The most easy and flexible way to collect or process data in *Nereda* data structures is to use one of the predefined visitors, or to program customized additional visitor components (see section 'Extending the framework').

Using predefined visitors

Nerada contains a predefined collection of visitors that is continuously growing.

Setting unique ids to each element and complete missing color information

(Code example #3)

Java version

```
public static void main(String[] args) {
	MatlabHelper.colordef("black");
	MatlabHelper.holdon();

	BrainInf b0 = new Brain("b0", "b0", "Neurolucida", "1.0", "", "");
	b0.addNeuron("neuron1.XML");

	VisitorInf simpleIdSetVisitor = new SimpleIdVisitor();
	VisitorInf colorVisitor = new SetChildColorByParentVisitor();
	VisitorInf plotVisitor = new OptPlotVisitor();
	VisitorInf plotIdVisitor = new PlotIdVisitor();

	ArrayList<VisitorInf> visitors = new ArrayList<VisitorInf>();
	visitors.add(simpleIdSetVisitor);
	visitors.add(colorVisitor);
	visitors.add(plotVisitor);
	visitors.add(plotIdVisitor);

	VisitorInf visitorContainer = new
VisitorContainerVisitor(visitors);
	b0.visitDeep(visitorContainer);
	visitorContainer.terminate();

	MatlabHelper.axis_vis3d();
	MatlabHelper.axis_equal();
	try {
		MatlabHelper.getJMatlab().jeval(
				"xlabel('x');" + "ylabel('y');" +
"zlabel('z');");
	} catch (Exception e) {
		System.out.println("Exception: " + e.toString());
	} finally {
		/* Free native resources */
	}
}
```

Matlab version

```
clear java
clear all

close all

javaclasspath({'E:\Data\sro\INI\plotJA\jmatlab\distrib\jmatlab.jar', ...
  'E:\Data\sro\My Documents\workspace\Neurolucida\Neurolucida.jar', ...
  'C:\Program Files\Java\jre1.6.0_03\lib\ext\Jama-1.0.2.jar'})

filename = './neuron1.XML';
b=ini.nl.Brain('b','b');
b.addNeuron(filename);

simpleIdVisitor = ini.nl.visitors.SimpleIdVisitor();
colorVisitor =  ini.nl.visitors.SetChildColorByParentVisitor();

visitors = java.util.ArrayList;
visitors.add(simpleIdVisitor);
visitors.add(colorVisitor);
visitorContainer = ini.nl.visitors.VisitorContainerVisitor(visitors);
b.visitDeep(visitorContainer);

getElementByIdVisitor = ini.nl.visitors.GetElementByIdVisitor('15');
b.visitDeep(getElementByIdVisitor);
e = getElementByIdVisitor.terminate();

treeCoordVisitor =  ini.nl.visitors.GetPointCoordinatesVisitor();
e.visitDeep(treeCoordVisitor);
result = treeCoordVisitor.terminate();

colordef('black');
hold on;

x=result.get(ini.nl.common.KeyDef.XTree()); x=jraggedToRect(x,[2 1]);
y=result.get(ini.nl.common.KeyDef.YTree()); y=jraggedToRect(y,[2 1]);
z=result.get(ini.nl.common.KeyDef.ZTree()); z=jraggedToRect(z,[2 1]);
id=result.get(ini.nl.common.KeyDef.Id());

plot3(x, y, z);
for i=1:size(id,1)
  [ix]=find(~isnan(x(:,i)));
  text(x(ix(end),i), y(ix(end),i), z(ix(end),i), id(i), 'FontSize', 8,
'Color', [1 1 1]);
end

xlabel('x'); ylabel('y'); zlabel('z');
```

Searching and referencing elements

(Code example #4)

Java version

```
public static void main(String[] args) {
	BrainInf b0 = new Brain("b0", "b0", "Neurolucida", "1.0", "", "");
	b0.addNeuron("neuron1.XML");

	VisitorInf simpleIdSetVisitor = new SimpleIdVisitor();
	VisitorInf colorVisitor = new SetChildColorByParentVisitor();

	ArrayList<VisitorInf> visitors = new ArrayList<VisitorInf>();
	visitors.add(simpleIdSetVisitor);
	visitors.add(colorVisitor);
	VisitorInf visitorContainer = new
VisitorContainerVisitor(visitors);
	b0.visitDeep(visitorContainer);

	VisitorInf getElementByIdVisitor = new
GetElementByIdVisitor("15");
	b0.visitDeep(getElementByIdVisitor);
	ElementInf as = (ElementInf)getElementByIdVisitor.terminate();

	MatlabHelper.colordef("black");
	MatlabHelper.holdon();

	VisitorInf plotVisitor = new OptPlotVisitor();
	as.visitDeep(plotVisitor);

	try
	{
		MatlabHelper.getJMatlab().jeval(
				"xlabel('x');" + "ylabel('y');" +
"zlabel('z');");
		MatlabHelper.getJMatlab().jeval("campos([10000 10000 0])");
	} catch (Exception e) {
		System.out.println("Exception: " + e.toString());
		MatlabHelper.dispose();
	}
	MatlabHelper.axis_equal();

	MatlabHelper.getJMatlab().waitForFigures();
}
```

Matlab version

```
clear java
clear all

close all

javaclasspath({'E:\Data\sro\INI\plotJA\jmatlab\distrib\jmatlab.jar', ...
  'E:\Data\sro\My Documents\workspace\Neurolucida\Neurolucida.jar', ...
  'C:\Program Files\Java\jre1.6.0_03\lib\ext\Jama-1.0.2.jar'})

filename = './neuron1.XML';
b=ini.nl.Brain('b','b');
b.addNeuron(filename);

simpleIdVisitor = ini.nl.visitors.SimpleIdVisitor();
colorVisitor =  ini.nl.visitors.SetChildColorByParentVisitor();

visitors = java.util.ArrayList;
visitors.add(simpleIdVisitor);
visitors.add(colorVisitor);
visitorContainer = ini.nl.visitors.VisitorContainerVisitor(visitors);
b.visitDeep(visitorContainer);

getElementByIdVisitor = ini.nl.visitors.GetElementByIdVisitor('15');
b.visitDeep(getElementByIdVisitor);
e = getElementByIdVisitor.terminate();

treeCoordVisitor =  ini.nl.visitors.GetPointCoordinatesVisitor();
e.visitDeep(treeCoordVisitor);
result = treeCoordVisitor.terminate();

colordef('black');
hold on;

x=result.get(ini.nl.common.KeyDef.XTree()); x=jraggedToRect(x,[2 1]);
y=result.get(ini.nl.common.KeyDef.YTree()); y=jraggedToRect(y,[2 1]);
z=result.get(ini.nl.common.KeyDef.ZTree()); z=jraggedToRect(z,[2 1]);

plot3(x, y, z);

xlabel('x'); ylabel('y'); zlabel('z');
```

Output element data as text to the console

(Code example #5)

Java version

```
public static void main(String[] args) {
      String filename = "neuron1_parts2.XML";
      BrainInf b = new Brain("b", "b", "Neurolucida", "1.0", "", "");
      b.addNeuron(filename );

      VisitorInf dispVisitor = new DispVisitor();

      b.visitDeep(dispVisitor);
      dispVisitor.terminate();
}
```

Matlab version

```
clear java
clear all

close all

javaclasspath({'E:\Data\sro\INI\plotJA\jmatlab\distrib\jmatlab.jar', ...
  'E:\Data\sro\My Documents\workspace\Neurolucida\Neurolucida.jar', ...
  'C:\Program Files\Java\jre1.6.0_03\lib\ext\Jama-1.0.2.jar'})

filename = './neuron1_parts2.XML';
b=ini.nl.Brain('b','b', 'Neurolucida', '1.0', '', '');
b.addNeuron(filename);

dispVisitor = ini.nl.visitors.DispVisitor();
b.visitDeep(dispVisitor);
dispVisitor.terminate();
```

Output

```
element: id=b name=b
  element: id= name=n
    APPENDIXSEGMENT object id= name=as parent=ini.nl.Neuron@ef5502 color=#00FF00
leaf=Incomplete length=352.50784093754606 segments=2 markers=5 points=186
      POINT object x=-80.69 y=-29.27 z=-950.25 d=0.75 sid=S15
      POINT object x=-81.05 y=-29.07 z=-949.8 d=0.75 sid=S15
            …
     APPENDIXSEGMENT object id= name=as parent=ini.nl.AppendixSegment@910040 color=
leaf=Normal length=43.11917338733334 segments=0 markers=0 points=24
       POINT object x=-337.05 y=119.49 z=-1050.05 d=0.67 sid=S15
            …
       POINT object x=-369.65 y=142.23 z=-1055.75 d=0.67 sid=S15
     MARKER object id=Varicosity name=Varicosity parent=ini.nl.AppendixSegment@910040
type=FilledCircle color=#00FF00 varicosity=false
            …
```

Plotting a 3D representation of the hierarchical object model/ Using visitor collections

(Code example #6)

Neuronal tree

Java version

```
public static void main(String[] args) {
	MatlabHelper.colordef("black");
	MatlabHelper.holdon();

	BrainInf b0 = new Brain("b0", "b0", "Neurolucida", "1.0", "", "");
	b0.addNeuron("neuron1.XML");

	VisitorInf simpleIdSetVisitor = new SimpleIdVisitor();
	VisitorInf colorVisitor = new SetChildColorByParentVisitor();
	VisitorInf plotVisitor = new OptPlotVisitor();

	ArrayList<VisitorInf> visitors = new ArrayList<VisitorInf>();
	visitors.add(simpleIdSetVisitor);
	visitors.add(colorVisitor);
	visitors.add(plotVisitor);

	VisitorInf visitorContainer = new
VisitorContainerVisitor(visitors);
	b0.visitDeep(visitorContainer);
	visitorContainer.terminate();

	MatlabHelper.axis_vis3d();
	MatlabHelper.axis_equal();
	try {
		MatlabHelper.getJMatlab().jeval(
				"xlabel('x');" + "ylabel('y');" +
"zlabel('z');");
	} catch (Exception e) {
		System.out.println("Exception: " + e.toString());
	} finally {
		/* Free native resources */
	}
}
```

Matlab version

```
clear java
clear all

close all

javaclasspath({'E:\Data\sro\INI\plotJA\jmatlab\distrib\jmatlab.jar', ...
  'E:\Data\sro\My Documents\workspace\Neurolucida\Neurolucida.jar', ...
  'C:\Program Files\Java\jre1.6.0_03\lib\ext\Jama-1.0.2.jar'})

filename = './neuron1.XML';
b=ini.nl.Brain('b','b');
b.addNeuron(filename);

simpleIdVisitor = ini.nl.visitors.SimpleIdVisitor();
colorVisitor =  ini.nl.visitors.SetChildColorByParentVisitor();
treeCoodVisitor =  ini.nl.visitors.GetPointCoordinatesVisitor();

visitors = java.util.ArrayList;
visitors.add(simpleIdVisitor);
visitors.add(colorVisitor);
visitors.add(treeCoodVisitor);
visitorContainer = ini.nl.visitors.VisitorContainerVisitor(visitors);

b.visitDeep(visitorContainer);
result = treeCoodVisitor.terminate();

colordef('black');
hold on;

x=result.get(ini.nl.common.KeyDef.XTree()); x=jraggedToRect(x,[2 1]);
y=result.get(ini.nl.common.KeyDef.YTree()); y=jraggedToRect(y,[2 1]);
z=result.get(ini.nl.common.KeyDef.ZTree()); z=jraggedToRect(z,[2 1]);

plot3(x, y, z);

x=double(result.get(ini.nl.common.KeyDef.XMarker()));
y=double(result.get(ini.nl.common.KeyDef.YMarker()));
z=double(result.get(ini.nl.common.KeyDef.ZMarker()));

plot3(x, y, z, 'o', 'MarkerSize', 2, 'MarkerFaceColor', [1 0 0],
'MarkerEdgeColor', [1 0 0]);
xlabel('x'); ylabel('y'); zlabel('z');
```

Brain surface

Java version

```
public static void main(String[] args) {
      MatlabHelper.colordef("black");
      MatlabHelper.holdon();

      BrainInf b0 = new Brain("b0", "b0", "Neurolucida", "1.0", "", "");
      b0.addContours("neuron1_sectionOutlines.XML");

      VisitorInf simpleIdSetVisitor = new SimpleIdVisitor();
      VisitorInf colorVisitor = new SetChildColorByParentVisitor();
      VisitorInf plotVisitor = new OptPlotVisitor();
      ArrayList<VisitorInf> visitors = new ArrayList<VisitorInf>();
      visitors.add(simpleIdSetVisitor);
      visitors.add(colorVisitor);
      visitors.add(plotVisitor);
      VisitorInf visitorContainer = new
VisitorContainerVisitor(visitors);
      b0.visitDeep(visitorContainer);
      visitorContainer.terminate();

      MatlabHelper.axis_vis3d();
      MatlabHelper.axis_equal();
      try {
            MatlabHelper.getJMatlab().jeval(
                        "xlabel('x');" + "ylabel('y');" +
"zlabel('z');");
      } catch (Exception e) {
            System.out.println("Exception: " + e.toString());
      } finally {
      }
}
```

Matlab version

```
clear java
clear all

close all

javaclasspath({'E:\Data\sro\INI\plotJA\jmatlab\distrib\jmatlab.jar', ...
  'E:\Data\sro\My Documents\workspace\Neurolucida\Neurolucida.jar', ...
  'C:\Program Files\Java\jre1.6.0_03\lib\ext\Jama-1.0.2.jar'})

filename = './neuron1_sectionOutlines.XML';
b=ini.nl.Brain('b','b');
b.addContours(filename);

simpleIdVisitor = ini.nl.visitors.SimpleIdVisitor();
colorVisitor =  ini.nl.visitors.SetChildColorByParentVisitor();
treeCoodVisitor =  ini.nl.visitors.GetPointCoordinatesVisitor();

visitors = java.util.ArrayList;
visitors.add(simpleIdVisitor);
visitors.add(colorVisitor);
visitors.add(treeCoodVisitor);
visitorContainer = ini.nl.visitors.VisitorContainerVisitor(visitors);

b.visitDeep(visitorContainer);
result = treeCoodVisitor.terminate();

colordef('black');
hold on;

x=result.get(ini.nl.common.KeyDef.XSectionOutline());
x=jraggedToRect(x,[2 1]);
y=result.get(ini.nl.common.KeyDef.YSectionOutline());
y=jraggedToRect(y,[2 1]);
z=result.get(ini.nl.common.KeyDef.ZSectionOutline());
z=jraggedToRect(z,[2 1]);

plot3(x, y, z, 'g');
axis equal; view(3);

xlabel('x'); ylabel('y'); zlabel('z');
```

Exporting data to 3D render software packages

(Code example #7)

Complete Brain structures (Brain surface/ Neuronal tree/ Vertices)

Java version

```
public static void main(String[] args) {
BrainInf b = new Brain("b", "b", "Neurolucida", "1.0", "", "");
      b.addNeuron("neuron1.XML");

      String filenamePrefix = "neuron1.XML";
      double surfGridSpacing = 50;
      double cylinderFaces = 12;
      double facesReductionFraction = .2;

b.exportToSTL(filenamePrefix, surfGridSpacing, cylinderFaces,
facesReductionFraction);
}
```

Matlab version

```
N/A
```

Brain surface only

(Code example #8)

Java version

```
public static void main(String[] args) {
      BrainInf b = new Brain("b", "b", "Neurolucida", "1.0", "", "");
      b.addContours("neuron1_sectionOutlines.XML");

      VisitorInf pointCoordVisitor = new GetPointCoordinatesVisitor(new
String[] {}, 2);
      b.visitDeep(pointCoordVisitor);
      Hashtable<String, Double[][]> result =
pointCoordVisitor.terminate();

      try
      {
            MatlabHelper.getJMatlab().jexportSurface2STL(
                  "cat2506_surface_only.XML.STL",
                  MatlabHelper.permute(
result.get(KeyDef.XSectionOutline()),new Double[]{Double.valueOf(2),
Double.valueOf(1)}),
                  MatlabHelper.permute(
result.get(KeyDef.YSectionOutline()),new Double[]{Double.valueOf(2),
Double.valueOf(1)}),
```

```
                    MatlabHelper.permute(
result.get(KeyDef.ZSectionOutline()),new Double[]{Double.valueOf(2),
Double.valueOf(1)}),
                    Double.valueOf(50));
      } catch (Exception e) {
            System.out.println("Exception: " + e.toString());
      } finally {
            /* Free native resources */
      }
      MatlabHelper.getJMatlab().waitForFigures();
}
```

Matlab version

```
clear java
clear all

close all

javaclasspath({'E:\Data\sro\INI\plotJA\jmatlab\distrib\jmatlab.jar', ...
  'E:\Data\sro\My Documents\workspace\Neurolucida\Neurolucida.jar', ...
  'C:\Program Files\Java\jre1.6.0_03\lib\ext\Jama-1.0.2.jar'})

filename = './neuron1_sectionOutlines.XML';
gridSpacing=50;

b=ini.nl.Brain('b','b');
b.addContours(filename);

simpleIdVisitor = ini.nl.visitors.SimpleIdVisitor();
pointCoordVisitor =  ini.nl.visitors.GetPointCoordinatesVisitor();
visitors = java.util.ArrayList;
visitors.add(simpleIdVisitor);
visitors.add(pointCoordVisitor);
visitorContainer = ini.nl.visitors.VisitorContainerVisitor(visitors);

b.visitDeep(visitorContainer);
result = pointCoordVisitor.terminate();

sectionOutlinesFilename = [filename '.sectionOutlines.STL'];
x=result.get(ini.nl.common.KeyDef.XSectionOutline());
x=jraggedToRect(x,[2 1]);
y=result.get(ini.nl.common.KeyDef.YSectionOutline());
y=jraggedToRect(y,[2 1]);
z=result.get(ini.nl.common.KeyDef.ZSectionOutline());
z=jraggedToRect(z,[2 1]);

colordef('white'); figure;
plot3(x, y, z);
axis equal; view(3); xlabel('x'); ylabel('y'); zlabel('z');
jexportSurface2STL(sectionOutlinesFilename, x, y, z, gridSpacing);
```

Neuronal Tree

(Code example #9)

Java version

```
public static void main(String[] args) {
      BrainInf b = new Brain("b", "b", "Neurolucida", "1.0", "", "");
      b.addNeuron("cat2506_tree_only.XML");
      NeuronInf n = b.getNeurons().get(0).getAsNeuron();

      String filenamePrefix = "Cat_2506.XML";
      double cylinderFaces = 12;
      double facesReductionFraction = .2;

      n.exportToSTL(filenamePrefix, cylinderFaces,
facesReductionFraction);
}
```

Matlab version

```
clear java
clear all

close all

javaclasspath({'E:\Data\sro\INI\plotJA\jmatlab\distrib\jmatlab.jar', ...
  'E:\Data\sro\My Documents\workspace\Neurolucida\Neurolucida.jar', ...
  'C:\Program Files\Java\jre1.6.0_03\lib\ext\Jama-1.0.2.jar'})

filename = './neuron1.XML';
cylinderSegments=12;
facesFraction=.2;

b=ini.nl.Brain('b','b');
b.addNeuron(filename);

simpleIdVisitor = ini.nl.visitors.SimpleIdVisitor();
pointCoordVisitor =  ini.nl.visitors.GetPointCoordinatesVisitor();
visitors = java.util.ArrayList;
visitors.add(simpleIdVisitor);
visitors.add(pointCoordVisitor);
visitorContainer = ini.nl.visitors.VisitorContainerVisitor(visitors);

b.visitDeep(visitorContainer);
result = pointCoordVisitor.terminate();

neuronSTLFilename = [filename '.neuron.STL'];

x=result.get(ini.nl.common.KeyDef.XTree()); x=jraggedToRect(x,[2 1]);
y=result.get(ini.nl.common.KeyDef.YTree()); y=jraggedToRect(y,[2 1]);
```

```
z=result.get(ini.nl.common.KeyDef.ZTree()); z=jraggedToRect(z,[2 1]);
d=result.get(ini.nl.common.KeyDef.DTree()); d=jraggedToRect(d,[2 1]);

colordef('white'); figure;
plot3(x, y, z);
axis equal; view(3); xlabel('x'); ylabel('y'); zlabel('z');
jexportSegments2STL(neuronSTLFilename, x, y, z, d, cylinderSegments,
facesFraction);
```

Using high level calls

Plotting the bouton-distance-from-the-cell-soma distribution

(Code example #10)

Java version

The function first creates a Matlab figure and axes and plots the distribution into it. For illustration it creates a second figure and plots the neuron into a 3D-axis. The function then pauses its execution till the user closes the figures.

To get different data plots *PlotMarkerFromOriginDistanceDistribution* has to be replaced by one of the other plotting classes of the *ini.nl.analysis.visualization* namespace.

```
public static void main(String[] args) {
      String filename = "neuron1.XML"; //path to the Neurolucida XML
file
      String namePrefix = filename;
String[] excList = new String[]{}; //no elements excluded

      PlotMarkerFromOriginDistanceDistribution markerDists;

      MatlabHelper.figure();
      MatlabHelper.holdon();
      markerDists = new PlotMarkerFromOriginDistanceDistribution(
                  filename, namePrefix, excList);
      markerDists.Execute();
      markerDists = null;

      MatlabHelper.colordef("black");
      MatlabHelper.holdon();
      Plot3D plotter = new Plot3D(filename, namePrefix, excList);
      plotter.Execute();

MatlabHelper.getJMatlab().waitForFigures();
}
```

Matlab version

```
clear java
clear all
close all

javaclasspath({'E:\Data\sro\INI\plotJA\jmatlab\distrib\jmatlab.jar', ...
  'E:\Data\sro\My Documents\workspace\Neurolucida\Neurolucida.jar', ...
  'C:\Program Files\Java\jre1.6.0_03\lib\ext\Jama-1.0.2.jar'})

filename = 'neuron1.XML';
namePrefix = filename;
excList=[];

data_mdod =
ini.nl.analysis.data.DataMarkerFromOriginDistanceDistribution(filename,
namePrefix);
data = data_mdod.getData();

axDists = data.get(ini.nl.common.KeyDef.AxonalDists);
euDists = data.get(ini.nl.common.KeyDef.EuclideanDists);

figure; hold on;

jplot2DDistr(axDists, euDists, 20);

title(['Bouton-to-soma-distance distribution']);
xl=xlim;
yl=ylim;
text(50,yl(2)-50, ['number of boutons: #' num2str(length(axDists))]);
xlabel('axonal bouton distance [um]');
ylabel('euclidean bouton distance [um]');
plot([0 yl(2)], [0 yl(2)], 'g');
xlim([0 xl(2)]);
ylim([0 yl(2)+20]);
```

A.9.5 Extending the framework

Adding visitors

(Code example #11)

To extend the functionality of the framework it is recommended to design and implement additional *visitors*. Visitors are small, specialized classes that implement the *VistorInf* interface. Visitor instances can be injected into the hierarchical object tree, i.e. the neurons, at any desired point, from where they will travel automatically to each sub-element to execute their code. Three examples of how to write visitors are given. In the first example the visitor flattens the hierarchical object tree into a one-dimensional collection of elements. In the second example the principle is used in a slightly more complex context to detect sections in axons or dendrites which may indicate reconstruction errors. In the last example one extracts a Newick-string from the object tree to display a phylogenetic tree that illustrates the extent of the axonal tree.

Flattening-the-hierarchy visitor

This visitor collects references of each AppendixSegment-element in the tree and stores them in a typed collection. Since references are stored the parent- and sub-element(s) of each entry is still accessible.

```
package ini.nl.visitors;

import ini.nl.inf.AppendixSegmentInf;
import ini.nl.inf.ElementInf;
import ini.nl.inf.VisitorInf;

import java.util.ArrayList;

public class FlattenAppendixSegmentsVisitor extends AbstractVisitor
implements VisitorInf
{
      protected ArrayList<AppendixSegmentInf> _as = new
ArrayList<AppendixSegmentInf>();

    public FlattenAppendixSegmentsVisitor(String[] excItems)
    {
      _excItems=excItems;
    }

    public void execVisit(ElementInf visitedObj)
    {
      super.execVisit(visitedObj);
      if(!getIsActive()){
            return;
      }
        if (visitedObj instanceof AppendixSegmentInf){
```

```
            _as.add(visitedObj.getAsAppendixSegment());
        }
    }

    public void execAfterVisit(ElementInf visitedObj)
    {
      super.execAfterVisit(visitedObj);
      if(!getIsActive()){
            return;
      }
    }

    @SuppressWarnings("unchecked")
    public ArrayList<AppendixSegmentInf> terminate()
    {
      return _as;
    }
}
```

How to use the visitor

```
public static void main(String[] args) {
      BrainInf b0 = new Brain("b0", "b0", "Neurolucida", "1.0", "", "");
      b0.addNeuron("neuron1.XML");

      VisitorInf getFlattenedAsVisitor = new
      GetFlattenedAppendixSegmentsVisitor();

      b0.visitDeep(getFlattenedAsVisitor);
      ArrayList<AppendixSegmentInf> as =
getFlattenedAsVisitor.terminate();

      System.out.println("Number of returned segments: " + as.size());
}
```

A slightly more advanced version of this principle is shown below. This visitor traverses the tree and tests whether neighboring points within AppendixSegments exhibit transient z-value changes. This would indicate a mistake during the axon-/dendrite-tracking in *Neurolucida*. The visitor detects these points, returns them in a flat collection and additionally displays the result in a 3D-plot.

```
package ini.nl.visitors;

import ini.nl.common.MatlabHelper;
import ini.nl.inf.AppendixSegmentInf;
import ini.nl.inf.ElementInf;
import ini.nl.inf.PointInf;
import ini.nl.inf.VisitorInf;

import java.util.ArrayList;

public class FindFishySpotsVisitor extends AbstractVisitor implements
VisitorInf
{
      protected ArrayList<PointInf> _fishyPoints = new
ArrayList<PointInf>();
      protected double _maxAllowedZDist;
      protected boolean _plot;
      protected double[][] _col_zTransient = new double[][]{{(double)1,
(double)0, (double)0}};
      protected double[][] _col_branchException = new
double[][]{{(double)0, (double)1, (double)0}};
      protected String _marker_zTransient = "o";
      protected String _marker_branchException = "v";
      protected int _marker_size = 8;

    public FindFishySpotsVisitor(double maxAllowedZDist, boolean plot)
    {
      _maxAllowedZDist=maxAllowedZDist;
      _plot=plot;
    }

    public FindFishySpotsVisitor(String[] excItems, double
maxAllowedZDist, boolean plot)
    {
      _excItems=excItems;
      _maxAllowedZDist=maxAllowedZDist;
      _plot=plot;
    }

    public void execVisit(ElementInf visitedObj)
    {
      super.execVisit(visitedObj);
      if(!getIsActive()){
            return;
      }
        if (visitedObj instanceof AppendixSegmentInf)
```

```
        {
            AppendixSegmentInf appendixSegment =
                  (AppendixSegmentInf) visitedObj;
            for(int i=1; i<appendixSegment.getPoints().size(); i++)
            {
                  PointInf p1=appendixSegment.getPoints().get(i-1);
                  PointInf p2=appendixSegment.getPoints().get(i);
                  if(Math.abs(p1.xyzd()[2]-
p2.xyzd()[2])>_maxAllowedZDist)
                  {
                        _fishyPoints.add(p1);
                        _fishyPoints.add(p2);

                        if(_plot)
                        {
                              try
                              {

      MatlabHelper.getJMatlab().jplot3(p1.xyzd()[0], p1.xyzd()[1],
      p1.xyzd()[2],
      _marker_zTransient,
       "MarkerFaceColor", _col_zTransient,
       "MarkerEdgeColor", _col_zTransient,
       "MarkerSize", _marker_size);

      MatlabHelper.getJMatlab().jplot3(p2.xyzd()[0], p2.xyzd()[1],
      p2.xyzd()[2],
      _marker_zTransient,
      “MarkerFaceColor", _col_zTransient,
      "MarkerEdgeColor", _col_zTransient,
      "MarkerSize", _marker_size);
                              }
                              catch(Exception e)
                              {
                                    System.out.println("Exception: " +
e.toString());
                              }
                        }
                  }
            }
            if(visitedObj.getAsAppendixSegment().getSegments().size() !=
2 &&

      visitedObj.getAsAppendixSegment().getSegments().size() != 0){
                  if(_plot)
                  {
                        try
                        {
                        PointInf
p0=appendixSegment.getPoints().get(appendixSegment.getPoints().size()-
1);

      MatlabHelper.getJMatlab().jplot3(p0.xyzd()[0], p0.xyzd()[1],
```

```
      p0.xyzd()[2],
      _marker_branchException,
      "MarkerFaceColor", _col_branchException,
      "MarkerEdgeColor", _col_branchException,
      "MarkerSize", _marker_size);
                        }
                        catch(Exception e)
                        {
                              System.out.println("Exception: " +
e.toString());
                        }
                      }
            }
            visitedObj.plot3();
        }
    }

    public void execAfterVisit(ElementInf visitedObj)
    {
      super.execAfterVisit(visitedObj);
      if(!getIsActive()){
            return;
      }
    }

    @SuppressWarnings("unchecked")
    public ArrayList<PointInf> terminate()
    {
      return _fishyPoints;
    }
}
```

Newick string visitor

(Code example #12)

The third visitor example represents the AppendixSegment tree structure as a *Newick* string. Newick tree format is a way to represent (*http://en.wikipedia.org/wiki/Graph_theoretical_tree*) tree structures with edge lengths using parentheses and commas (*http://en.wikipedia.org/wiki/Newick_format*). The example demonstrates how to use the Newick string as input to Matlab's bioinformatics toolbox to produce a phylogenetic tree that visualizes the extent of the axonal tree.

```
package ini.nl.visitors;

import ini.nl.inf.AppendixSegmentInf;
import ini.nl.inf.ElementInf;
import ini.nl.inf.VisitorInf;

public class GetNewickStringVisitor extends AbstractVisitor implements
VisitorInf {
      protected String _newickString="";

    public GetNewickStringVisitor()
    {
    }

    public GetNewickStringVisitor(String[] excItems)
    {
      _excItems=excItems;
    }

    public void execVisit(ElementInf visitedObj)
    {
      super.execVisit(visitedObj);
      if(!getIsActive()){
            return;
      }
        if(visitedObj instanceof AppendixSegmentInf){
            AppendixSegmentInf as = (AppendixSegmentInf) visitedObj;
              double sl=as.getSegmentLength();
                if(as.getSegments().size()==0){
                  String endStr =
_newickString.substring(_newickString.length()-1);
                    if("(,".indexOf((String) endStr) != -1)
                    {

_newickString=_newickString+as.getId()+":"+sl+",";
                    }
                    else
                    {

_newickString=_newickString+","+as.getId()+":"+sl;
                    }
```

```
                    }
                  else
                    if(_newickString!=""){
                        String endStr =
_newickString.substring(_newickString.length()-1);
                    String str = "0123456789";
                    if (str.indexOf((String) endStr) != -1){
                          _newickString=_newickString+","+"(";
                    }
                    else{
                          _newickString=_newickString+"(";

                    }
                      }
                    else{
                      _newickString=_newickString+"(";
                    }
          }
    }

     public void execAfterVisit(ElementInf visitedObj)
     {
       super.execAfterVisit(visitedObj);
       if(!getIsActive()){
             return;
       }
         if(visitedObj instanceof AppendixSegmentInf){
             AppendixSegmentInf as = (AppendixSegmentInf) visitedObj;
               double sl=as.getSegmentLength();
                 if(as.getSegments().size()!=0){
                         String endStr =
_newickString.substring(_newickString.length()-1);
                           if(",".indexOf((String) endStr) != -1){
                       _newickString=_newickString.substring(0,
_newickString.length()-2)+")"+ as.getId()+":"+sl;
                           }
                           else{

_newickString=_newickString+")"+as.getId()+":"+sl;
                           }
                  }
          }
     }

     @SuppressWarnings("unchecked")
     public String terminate()
     {
       return _newickString;
     }
}
```

How to use the visitor

In the example the Newick string is used as input for *Matlab*'s phytree function. Default settings for branch name and symbols are used.

Java version

```
protected static void TestNewickStringVisitor(){
	BrainInf b0 = new Brain("b0", "b0", "Neurolucida", "1.0", "", "");
	b0.addNeuron("neuron1.XML");

	VisitorInf getNewickStringVisitor = new GetNewickStringVisitor();
	b0.getNeurons().get(0).getAxon().visitDeep(getNewickStringVisitor)
;
	String newickString = getNewickStringVisitor.terminate();

	System.out.println("Newick string: " + newickString);

	MatlabHelper.phytree(newickString);
}
```

Matlab version

```
clear java
clear all

close all

javaclasspath({'E:\Data\sro\INI\plotJA\jmatlab\distrib\jmatlab.jar', ...
  'E:\Data\sro\My Documents\workspace\Neurolucida\Neurolucida.jar', ...
  'C:\Program Files\Java\jre1.6.0_03\lib\ext\Jama-1.0.2.jar'})

filename = './neuron1.XML';
b=ini.nl.Brain('b','b');
b.addNeuron(filename);

a=b.getNeurons().get(0).getAxon();
simpleIdVisitor = ini.nl.visitors.SimpleIdVisitor();
getNewickStringVisitor = ini.nl.visitors.GetNewickStringVisitor();
a.visitDeep(simpleIdVisitor);
a.visitDeep(getNewickStringVisitor);

newickString = getNewickStringVisitor.terminate()

colordef('white');
pt=phytreeread(char(newickString));
plot(pt,'branchlabels',true, 'leaflabels', true, 'terminallabels',
false, 'Orientation', 'top');
h=get(gcf,'UserData')
set(h.branchNodeLabels,'FontSize',10,'Color',[.5 .5 1])
set(h.leafNodeLabels,'FontSize',10,'Color',[1 .5 .5])
set(gca, 'XTick',[]);
set(gca, 'FontSize',14);
ylabel('um');
```

Adding Matlab components

Matlab developed by Mathworks, is a powerful data processing environment. *Nereda* directly interfaces to *Matlab* to get access to the flexible statistics and visualization libraries. *Nereda* provides a generic way to access all *Matlab* functions via the *MatlabHelper.eval(string)* function. This allows sending command strings which subsequently will be interpreted within *Matlab*. However, a more convenient and robust way to access *Matlab* functions is provided by the *Builder JA* technology. It wraps *Matlab* .m-code into *Java* functions, which are then directly accessible in a type safe way within *Java* development environments.

For more information about how to wrap m-code the reader should consider the *Matlab Builder JA* documentation. Examples how to use the wrapped functions can be found in the upper code examples, and in the MatlabHelper class of the *ini.nl.common*-namespace. Links to a complete list of all *MatlabHelper* built-in functionality and UML diagrams can be found in the *Resources* section.

Adding Import Sources

Currently *Nereda* supports only *Neurolucida* as an import source. The framework can however easily be extended to further sources. The fastest and most robust way is to create a new namespace with classes that inherit from the *ini.nl*-namespace. In each of the new classes, the *createByXML*(*org.w3c.dom.Element* node) function should be overwritten to load the new data source. The interfaced architecture (the new classes again implement the *ini.nl.inf*-interfaces) guarantees compatibility. Alternatively additional data loading methods can be implemented.

A.9.6 Namespace description and class diagrams

This section contains a short summary of the *Nereda* namespaces. For more detailed information the reader should consider the *Resources* section of this chapter.

ini.nl.inf

The *ini.nl.inf*-namespace houses all the interfaces that are implemented by various classes of the ini.nl sub-namespaces. Each *ini.nl*-class implements at least the interface *DispInf*.

ini.nl.common

The *ini.nl.common*–namespace contains helper classes to interface to *Matlab* code, to perform data conversions (*MatlabHelper*), and defines common data structures (*KeyDef, XMLDef*).

- *KeyDef* defines keys for common key/value pairs.
- *XMLDef* defines key/value-pairs to identify tags in the *Neurolucida XML* data structure, and to define enumerators for predefined data attributes.
- *MatlabHelper* contains a series of functions to interface to *Matlab* data processing methods, in conjunction with data conversion methods for easy conversion between *Java* and *Matlab* data types.

ini.nl

ini.nl is the core namespace for objects and classes that directly represent entities of the reconstructed brain structures. Data from the 3D reconstruction software tool is converted into a hierarchical object structure that provides well defined interfaces for data access and data processing.

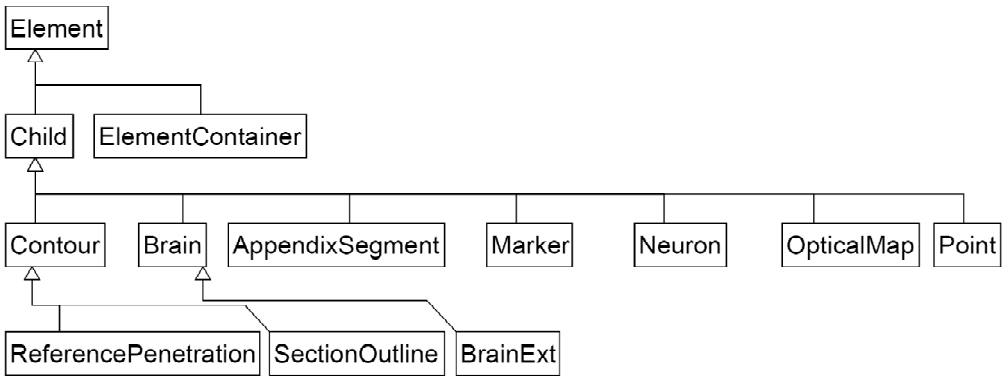

- *AppendixSegment* represents an axonal or dendritic segment. The class is inherited from *Child* and implements the interfaces *AppendixSegmentInf* and *VisitorInf*.
- *Brain* represents the top-level class of the reconstructed neuronal data hierarchy. The class inherits from *Child* and implements the interfaces *BrainInf* and *VisitorInf*.
- *Child* is the base class of all entities that are part of a hierarchical structure. The class inherits from Element and implements the interfaces *ElementInf* and *ChildInf*.

- *Contour* is the base class for structures that are represented by open or closed line structures, i.e. reference penetrations and section outlines (of brain surface contour lines). The class inherits from *Child* and implements *ContourInf*.
- *Element* is the abstract base class of all classes of the *ini.nl* namespace. It implements the interfaces *VisitorInf* and *ElementInf*. Any *ini.nl* class instance can be casted to *ElementInf*.
- *ElementContainer* denotes a specialized element type. It inherits from *Element* and implements *ElementContainerInf*. The class is a collection of *Elements* and is at the same an *Element* itself. It allows definition of ad-hoc *Element* collections whereas the root (the ElementContainer) deserves as a common entry point for visitor class instances.
- *Marker* represents special point-like structures in the neuronal tree. Currently they solely denote *varicosities* on axonal segments. *Marker* inherits from *Child* and implements *ElementInf* and *MarkerInf*.
- *Neuron* is the top-level class for neuronal structures. It contains a soma, an axon and a dendrite. *Neuron* inherits from *Child* and implements *NeuronInf* and *VisitorInf*.
- *OpticalMap* represents neuronal activity data given as images (space dependent gray values). *OpticalMap* inherits from *Child* and implements *OpticalMapInf*.
- *Point* represents a location in space defined by *x-/y-/z*-coordinates and an optional diameter *d*. *Point* is used by all structural components to define their location in space and their shape. The class inherits from *Element* and implements the interface *PointInf*.
- *ReferencePenetration* represents depth lesion of brain tissue defined as a contour structure. *ReferencePenetration* inherits from *Contour* and implements the interface *ReferencePenetrationInf*.
- *SectionOutline* represents a contour line that defines the location and shape of the brain surface at a given tissue depth (brain section). A collection of section outlines define a 3D brain surface. *SectionOutline* inherits from *Contour* and implements *SectionOutlineInf*.

ini.nl.visitors

The ini.nl.visitors namespace represents the core of the data processing and analysis. The highly specialized visitor classes of this package represent the building blocks for more complex statistical or visualization methods. Below the class diagram for the DispVisitor class is shown. It stands as a prototype for all other classes in the ini.nl.visitors. The remaining class diagrams can be found in the ArgoUML project (see *Resources* section).

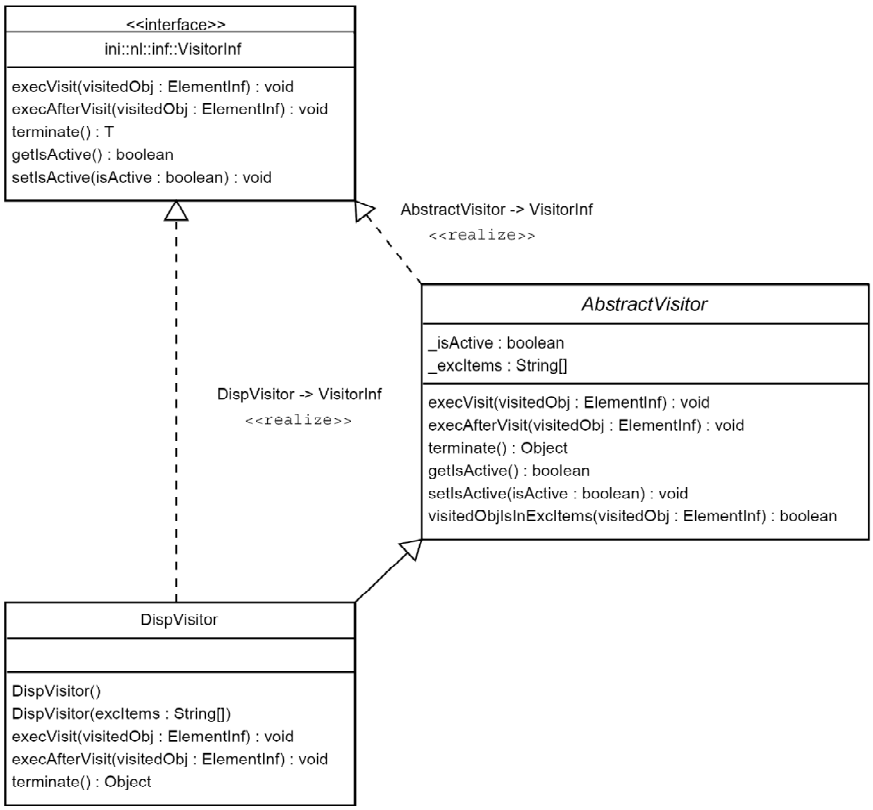

The visitor classes inherit from the abstract class *AbstractVisitor*, implement the *VisitorInf* interface, and denote the processing layer of the *Nereda* framework. Each visitor object performs a well-defined action/worker tasks, e.g. data collection or statistical analysis. The class *VisitorContainerVisitor* deserves as a specialized visitor which houses several visitors. Visitors can be sent into the brain-/neuron-structure at any point from where they will travel automatically through the sub-tree to visit each of its elements to execute their worker code. The *ini.nl.visitors*-namespace denotes the main target for framework extensions.

ini.nl.analysis.data

Ini.nl.analysis.data represents the namespace for classes that perform data collection, data processing and statistics. The components mostly use classes from the *ini.nl.visitors*-namespace to provide convenient statistical methods. Due to *Matlab*'s licensing model, some of these classes may not be accessible from within *Matlab*.

Examples of *ini.nl.analysis.data* component output can be found in the '*Application field*'-section. The current classes mainly implement algorithms proposed by Tom Binzegger to analyze bouton distribution (Binzegger et al., 2004, 2005). Currently the following classes are available:

- *DataIBIWithHortonStrahler*:
  - Provides access to inter-bouton-interval statistics of neurons.
- *DataMarkerFromOriginDistanceDistribution*:
  - Calculates the distance from each bouton to the axonal hillock (where the axon leaves the cell soma). The distance is calculated as the shortest distance from the bouton to the soma along the axonal tree.
- *DataNumberOfMarkersWithHortonStrahler*:
  - Calculates the number of boutons within each Horton-Strahler order of the axonal tree segments.
- *DataNumberOfMarkersWithTotalSegmentLength*:
  - Calculates the number of boutons as a function of the axonal segment length.

ini.nl.analysis.visualization

The visualization part of the *ini.nl.analysis* namespace provides convenient access to external data plotting routines, i.e. by interfacing to *Matlab* plot classes. The visualization components use the *ini.nl.analysis.data* classes to acquire the data. Due to *Matlab*'s licensing model, some of these classes may not be accessible from within *Matlab*.

For links to the complete code documentation and UML models of the namespace, the reader is referred to the *Resources* section of this chapter.

- *PlotNumberOfMarkersWithHortonStrahler*:
  - Plots data acquired by *DataNumberOfMarkersWithHortonStrahler*.
- *PlotNumberOfMarkersWithTotalSegmentLength*:
  - Plots data acquired by *DataNumberOfMarkersWithTotalSegmentLength* .
- *PlotIBIDistributionWithHortonStrahler:*
  - Plots data acquired by *DataIBIWithHortonStrahler*.
- *PlotIBIMedianWithHortonStrahler*:
  - Plots data acquired by *DataIBIWithHortonStrahler*.
- *PlotMarkerFromOriginDistanceDistribution*:
  - Plots data acquired by *DataMarkerFromOriginDistanceDistribution* .
- *Plot3D*:
  - Plots neuronal structures into *Matlab* figures.

A.9.7 Products and Trademarks

- *DocFlex*: DocFlex is a product of Filigris, Inc., to produce code documentations. The company provides free academic licenses.
  - (*http://www.filigris.com*)
- *Matlab*: Matlab is a product of Mathworks, Inc.
  - (*http://www.mathworks.com*)
- *Builder JA*: Builder JA is a technology used in *Matlab* developed by Mathworks.
- *Neurolucida*: *Neurolucida* is a product of MicroBrightField, Inc.
  - (*http://www.mbfbioscience.com/Neurolucida/*)
- *Blender*: Blender is a open-source solution for 3D rendering.
  - (*http://www.blender.org*)
- *ArgoUML*: ArgoUML is an open-source solution for UML modeling and code reverse engeneering.
  - (*http://argouml.tigris.org/*)

Acronyms

The abbreviations that are used in this thesis are listed below in alphabetical order.

***2-afc* task**: Two alternative forced choice task

ACh: Acetylcholine

AUC: Area-under-the-curve

BOLD: Blood oxygen level dependency

BPAP: Back-propagated action potential

Ca^{2+}: Calcium ion

CCh: Carbachol

CT: Continuous transformation/ computer tomography

d': d prime

DOG: Difference-of-Gaussian

EDL: Exposure dependent learning

EEG: Electroencephalogram

ERP: Event related potential

fMRI: function magnet resonance imaging

FP: False positive

GA: Genetic algorithm

GABA: Gamma-aminobutyric acid

GIRKs: G protein-coupled inwardly-rectifying potassium channels

HyperBF: Hyper basis function

IBI: Inter-bouton-interval

IT/ITC: Inferotemporal area/cortex

PSTH: Peri-stimulus-time-histogram

K^{+}: Potassium ion

LFP: Local field potential

LGN: Lateral geniculate nucleus

LIP: Lateral intraparietal area

LTD: Long-term depression

LTP: Long-term potentiation

***M-* and *P*-cells**: Magnocellular-, parvocellular cells

MAT: Matlab data file format

MT: Medial temporal area

NMDA/R: N-Methyl-D-Aspartate-/receptor

PFC: Prefrontal cortex

RBF: Radial basis function

ROC: Receiver operating characteristics

***S-* and *C*-cell**: Simple cell and complex cell

SNR: Signal-to-noise ratio

SOM: Self organizing map

STDP: Spike-timing dependent plasticity

STL: Surface Triangulation Language

SVM: Support vector machine

TN: True negative

TP: True positive

TPC: Temporal population code

TXT: Text (ASCII encoded)

***V1* –Vx**: Visual Areas 1-x

WSCT: Wisconsin sorting card test

XML: Extensible Markup Language

Bibliography

Abbott LF (2003) Balancing homeostasis and learning in neural circuits. Zoology 106:365-371.

Abeles M, Bergman H, Margalit E, Vaadia E (1993) Spatiotemporal firing patterns in the frontal cortex of behaving monkeys. J Neurophysiol 70:1629-1638.

Adrian ED (1926) The impulses produced by sensory nerve endings: Part I. J Physiol 61:49-72.

Adrian ED, Zotterman Y (1926) The impulses produced by sensory nerve-endings: Part II. The response of a Single End-Organ. J Physiol 61:151-171.

Aggelopoulos NC, Rolls ET (2005) Scene perception: inferior temporal cortex neurons encode the positions of different objects in the scene. European Journal of Neuroscience 22:2903-2916.

Aggelopoulos NC, Franco L, Rolls ET (2005) Object Perception in Natural Scenes: Encoding by Inferior Temporal Cortex Simultaneously Recorded Neurons. J Neurophysiol 93:1342-1357.

Aizenstein HJ, MacDonald AW, Stenger VA, Nebes RD, Larson JK, Ursu S, Carter CS (2000) Complementary Category Learning Systems Identified Using Event-Related Functional MRI. J Cogn Neurosci 12:977-987.

Angelucci A, Bullier J (2003) Reaching beyond the classical receptive field of V1 neurons: horizontal or feedback axons? Journal of Physiology-Paris 97:141-154.

Ashby FG, Spiering BJ (2004) The Neurobiology of Category Learning. Behav Cogn Neurosci Rev 3:101-113.

Ashby FG, Maddox WT (2005) HUMAN CATEGORY LEARNING. Annual Review of Psychology 56:149-178.

Ashby FG, O'Brien JB (2005) Category learning and multiple memory systems. Trends in Cognitive Sciences 9:83-89.

Awiszus F (1997) Spike train analysis. Journal of Neuroscience Methods 74:155-166.

Bair W (1999) Spike timing in the mammalian visual system. Curr Opin Neurobiol 9:447-453.

Bair W, Koch C (1996) Temporal precision of spike trains in extrastriate cortex of the behaving macaque monkey. Neural Comput 8:1185-1202.

Bartus RT (2000) On neurodegenerative diseases, models, and treatment strategies: lessons learned and lessons forgotten a generation following the cholinergic hypothesis. Exp Neurol 163:495-529.

Benardete EA, Kaplan E (1999) Dynamics of primate P retinal ganglion cells: responses to chromatic and achromatic stimuli. J Physiol 519:775-790.

Benardete EA, Kaplan E (2000) The dynamics of primate M retinal ganglion cells: Cambridge Journals Online.

Benda J, Longtin A, Maler L (2006) A Synchronization-Desynchronization Code for Natural Communication Signals. Neuron 52:347-358.

Berry MJ, Warland DK, Meister M (1997) The structure and precision of retinal spike trains. Proc Natl Acad Sci U S A 94:5411-5416.

Bi G-q, Poo M-m (1998) Synaptic Modifications in Cultured Hippocampal Neurons: Dependence on Spike Timing, Synaptic Strength, and Postsynaptic Cell Type. J Neurosci 18:10464-10472.

Bi G-q, Poo M-m (2001) SYNAPTIC MODIFICATION BY CORRELATED ACTIVITY: Hebb's Postulate Revisited. Annual Review of Neuroscience 24:139-166.

Bialek W, Rieke F, de Ruyter van Steveninck RR, Warland D (1991) Reading a neural code. Science 252:1854-1857.
Binzegger T, Douglas RJ (2004) A Quantitative Map of the Circuit of Cat Primary Visual Cortex. Journal of Neuroscience 24:8441-8453.
Binzegger T, Douglas RJ, Martin KAC (2004) A Quantitative Map of the Circuit of Cat Primary Visual Cortex. J Neurosci 24:8441-8453.
Binzegger T, Douglas RJ, Martin KAC (2005) Axons in Cat Visual Cortex are Topologically Self-similar. Cereb Cortex 15:152-165.
Bohte SM, La Poutre HA, Kok JN (2002) Unsupervised Clustering with Spiking Neurons by Sparse Temporal Coding and Mutli-Layer RBF Networks. IEEE Transactions on Neural Networks 13:426-435.
Borst A, Haag J (2002) Neural networks in the cockpit of the fly. J Comp Physiol A Neuroethol Sens Neural Behav Physiol 188:419-437.
Bosking WH, Zhang Y, Schofield B, Fitzpatrick D (1997a) Orientation Selectivity and the Arrangement of Horizontal Connections in the Tree Shrew Striate Cortex. The Journal of Neuroscience 17:2112-2127.
Bosking WH, Zhang Y, Schofield B, Fitzpatrick D (1997b) Orientation Selectivity and the Arrangement of Horizontal Connections in Tree Shrew Striate Cortex. J Neurosci 17:2112-2127.
Brincat SL, Connor CE (2004) Underlying principles of visual shape selectivity in posterior inferotemporal cortex. Nat Neurosci 7:880-886.
Buonomano DV (2000) Decoding Temporal Information: A Model Based on Short-Term Synaptic Plasticity. J Neurosci 20:1129-1141.
Buonomano DV (2003) Timing of neural responses in cortical organotypic slices. Proceedings of the National Academy of Sciences 100:4897-4902.
Buonomano DV, Merzenich MM (1995) Temporal information transformed into a spatial code by a neural network with realistic properties. Science 267:1028-1030.
Buonomano DV, Mezernich M (1999) A Neural Network Model of Temporal Code Generation and Position-Invariant Pattern Recognition. Neural Computation 11:103-116.
Buschman TJ, Miller EK (2007) Top-Down Versus Bottom-Up Control of Attention in the Prefrontal and Posterior Parietal Cortices. Science 315:1860-1862.
Buzas P, Volgushev M, Eysel UT, Kisvarday ZF (2003) Independence of visuotopic representation and orientation map in the visual cortex of the cat. Eur J Neurosci 18:957-968.
Carey RG, Rieck RW (1987) Topographic projections to the visual cortex from the basal forebrain in the rat. Brain Research 424:205-215.
Carlson BA, Kawasaki M (2006) Ambiguous Encoding of Stimuli by Primary Sensory Afferents Causes a Lack of Independence in the Perception of Multiple Stimulus Attributes. J Neurosci 26:9173-9183.
Carr CE, Konishi M (1990) A Circuit for Detection of Interaural Time Differnces in the Brain Stem of the Barn Owl. Journal of Neuroscience 10:3227-3246.
Castellani GC, Quinlan EM, Cooper LN, Shouval HZ (2001) A biophysical model of bidirectional synaptic plasticity: Dependence on AMPA and NMDA receptors. Proceedings of the National Academy of Sciences 98:12772-12777.
Castellani GC, Quinlan EM, Bersani F, Cooper LN, Shouval HZ (2005) A model of bidirectional synaptic plasticity: From signaling network to channel conductance. Learn Mem 12:423-432.
Chisum HJ, Fitzpatrick D (2004) The contribution of vertical and horizontal connections to the receptive field center and surround in V1. Neural Networks 17:681-693.

Christine A. Curcio KRSREKAEH (1990) Human photoreceptor topography. The Journal of Comparative Neurology 292:497-523.
Cincotta CM, Seger CA (2007) Dissociation between Striatal Regions while Learning to Categorize via Feedback and via Observation. J Cogn Neurosci 19:249-265.
Cooke SF, Bliss TV (2006) Plasticity in the human central nervous system. Brain 129:1659-1673.
Crish SD, Dengler-Crish CM, Comer CM (2006) Population coding strategies and involvement of the superior colliculus in the tactile orienting behavior of naked mole-rats. Neuroscience 139:1461-1466.
Crist RE, Li W, Gilbert CD (2001) Learning to see: experience and attention in primary visual cortex. Nat Neurosci 4:519-525.
Cummings JA, Mulkey RM, Nicoll RA, Malenka RC (1996) Ca2+ Signaling Requirements for Long-Term Depression in the Hippocampus. Neuron 16:825-833.
Dan Y, Poo M-m (2004) Spike Timing-Dependent Plasticity of Neural Circuits. Neuron 44:23-30.
Dan Y, Poo M-M (2006) Spike Timing-Dependent Plasticity: From Synapse to Perception. Physiol Rev 86:1033-1048.
Dan Y, Alonso J-M, Usrey WM, Reid RC (1998) Coding of visual information by precisely correlated spikes in the lateral geniculate nucleus. Nat Neurosci 1:501-507.
Deco G, Rolls ET (2004) A Neurodynamical cortical model of visual attention and invariant object recognition. Vision Research 44:621-642.
Delorme A, Rousselet GA, Mace MJM, Fabre-Thorpe M (2004) Interaction of top-down and bottom-up processing in the fast visual analysis of natural scenes. Cognitive Brain Research 19:103-113.
Dudek SM, Bear MF (1993) Bidirectional long-term modification of synaptic effectiveness in the adult and immature hippocampus. J Neurosci 13:2910-2918.
Eckhorn R, Bauer R, Jordan W, Brosch M, Kruse W, Munk M, Reitboeck HJ (1988) Coherent oscillations: a mechanism of feature linking in the visual cortex? Multiple electrode and correlation analyses in the cat. Biol Cybern 60:121-130.
Engel A, Konig P, Kreiter A, Singer W (1991) Interhemispheric synchronization of oscillatory neuronal responses in cat visual cortex. Science 252:1177-1179.
Engel AK, Konig P, Schillen TB (1992a) Why does the cortex oscillate? Curr Biol 2:332-334.
Engel AK, Konig P, Kreiter AK, Schillen TB, Singer W (1992b) Temporal coding in the visual cortex: new vistas on integration in the nervous system. Trends Neurosci 15:218-226.
Everitt BJ, Robbins TW (1997) CENTRAL CHOLINERGIC SYSTEMS AND COGNITION. Annual Review of Psychology 48:649-684.
Fabre-Thorpe M, Richard G, Thorpe SJ (1998) Rapid categorization of natural images by rhesus monkeys. Neuroreport 9:303-308.
Fahle M (1994) Human pattern recognition: parallel processing and perceptual learning. Perception 23:411-427.
Fahle M (2004) Perceptual learning: A case for early selection. Journal of Vision 4:879-890.
Fahle M, Poggio T (1981) Visual hyperacuity:spatiotemporal interpolation in human vision. Proc R Soc Lond B Biol Sci 213:451-477.
Fahle M, Morgan M (1996) No transfer of perceptual learning between similar stimuli in the same retinal position. Curr Biol 6:292-297.

Fahle M, Edelman S, Poggio T (1995a) Fast perceptual learning in hyperacuity. Vision Res 35:3003-3013.
Fahle M, Edelman S, Poggio T (1995b) Fast Perceptual Learning in Hyperacuity. Vision Research 35:3003-3013.
Fine I, Jacobs RA (2002) Comparing perceptual learning tasks: A review. Journal of Vision 2:190-203.
Foley-Fisher JA (1973) The effect of target line length on vernier acuity in white and blue light. Vision Research 13:1447-1454.
Fournier GN, Semba K, Rasmusson DD (2004) Modality- and region-specific acetylcholine release in the rat neocortex. Neuroscience 126:257-262.
Freedman DJ, Assad JA (2006) Experience-dependent representation of visual categories in parietal cortex. Nature 443:85-88.
Freedman DJ, Riesenhuber M, Poggio T, Miller EK (2001) Categorical Representation of Visual Stimuli in the Primate Prefrontal Cortex. Science 291:312-316.
Freedman DJ, Riesenhuber M, Poggio T, Miller EK (2002) Visual Categorization and the Primate Prefrontal Cortex: Neurophysiology and Behavior. Journal of Neurophysiology 88:929-941.
Freedman DJ, Riesenhuber M, Poggio T, Miller EK (2003) A Comparison of Primate Prefrontal and Inferior Temporal Cortices during Visual Categorization. J Neurosci 23:5235-5246.
Freedman DJ, Riesenhuber M, Poggio T, Miller EK (2006) Experience-Dependent Sharpening of Visual Shape Selectivity in Inferior Temporal Cortex. Cereb Cortex 16:1631-1644.
Froemke RC, Dan Y (2002) Spike-timing-dependent synaptic modification induced by natural spike trains. Nature 416:433-438.
Froemke RC, Poo MM, Dan Y (2005) Spike-timing-dependent synaptic plasticity depends on dendritic location. Nature 434:221-225.
Fukushima K (1980) Neocognitron: a self organizing neural network model for a mechanism of pattern recognition unaffected by shift in position. Biol Cybern 36:193-202.
Fukushima K (1987) Self-organizing neural network models for visual pattern recognition. Acta Neurochir Suppl (Wien) 41:51-67.
Fukushima K (2003) Neocognitron for handwritten digit recognition. Neurocomputing 51:161-180.
Fukushima K (2004) Neocognitron capable of incremental learning. Neural Netw 17:37-46.
Fukushima K (2007) Interpolating vectors for robust pattern recognition. Neural Netw 20:904-916.
Fusi S, Senn W (2006) Eluding oblivion with smart stochastic selection of synaptic updates. Chaos 16:026112.
Gattass R, Rosa MG, Sousa AP, Pinon MC, Fiorani Junior M, Neuenschwander S (1990) Cortical streams of visual information processing in primates. Braz J Med Biol Res 23:375-393.
Gegenfurtner KR, Kiper DC (2003) COLOR VISION. Annual Review of Neuroscience 26:181-206.
Georgopoulos AP, Schwartz AB, Kettner RE (1986a) Neuronal population coding of movement direction. Science 233:1416-1419.
Georgopoulos AP, Schwartz AB, Kettner RE (1986b) Neuronal population coding of movement direction. Science 233:1416-1419.

Ghose GM (2004) Learning in mammalian sensory cortex. Current Opinion in Neurobiology 14:513-518.
Gilbert CD, Wiesel TN (1989) Columnar Secificity of Intrinsic Horizontal and Corticocortical Connections in Cat Visual Cortex. The Journal of Neuroscience 9:2432-2442.
Gray CM, Engel AK, Konig P, Singer W (1992) Synchronization of oscillatory neuronal responses in cat striate cortex: temporal properties. Vis Neurosci 8:337-347.
Grill-Spector K (2003) The neural basis of object perception. Current Opinion in Neurobiology 13:159-166.
Gross CG, Schonen SD (1992) Representation of Visual Stimuli in Inferior Temporal Cortex [and Discussion]. Philosophical Transactions of the Royal Society B: Biological Sciences 335:3-10.
György B (2005) Theta rhythm of navigation: Link between path integration and landmark navigation, episodic and semantic memory. Hippocampus 15:827-840.
Hampson RE, Pons TP, Stanford TR (2004) Categorization in the monkey hippocampus: A possible mechanism for encoding information into memory. PNAS 101:3184-3189.
Harris JP, Fahle M (1995) The detection and discrimination of spatial offsets. Vision Res 35:51-58.
Harris JP, Fahle M (1996) Differences between fovea and periphery in the detection and discrimination of spatial offsets. Vision Res 36:3469-3477.
Hasegawa I, Miyashita Y (2002) Categorizing the world: expert neurons look into key features. Nat Neurosci 5:90-91.
Haxby JV, Grady CL, Horwitz B, Ungerleider LG, Mishkin M, Carson RE, Herscovitch P, Schapiro MB, Rapoport SI (1991) Dissociation of object and spatial visual processing pathways in human extrastriate cortex. Proc Natl Acad Sci U S A 88:1621-1625.
Hebb DO (1949) The Organization of Behavior: a neuropsychological approach. New York: Wiley.
Herzog MH, Fahle M (1997) The role of feedback in learning a vernier discrimination task. Vision Res 37:2133-2141.
Herzog MH, Fahle M (1998) Modeling perceptual learning: difficulties and how they can be overcome. Biological Cybernetics 78:107-117.
Herzog MH, Fahle M (1999) Effects of biased feedback on learning and deciding in a vernier discrimination task. Vision Res 39:4232-4243.
Hirabayashi T, Miyashita Y (2005) Dynamically Modulated Spike Correlation in Monkey Inferior Temporal Cortex Depending on the Feature Configuration within a Whole Object. J Neurosci 25:10299-10307.
Hirsch JA, Gilbert CD (1991) Synaptic Physiology of Horizontal Connections in the Cat's Visual Cortex. Journal of Neuroscience 11:1800-1809.
Hopfield JJ (1995) Pattern recognition computation using action potential timing for stimulus representation. Nature 376:33-36.
Huang X, Albright TD, Stoner GR (2007) Adaptive Surround Modulation in Cortical Area MT. Neuron 53:761-770.
Hubel DH, Wiesel TN (1959) Receptive fields of single neurones in the cat's striate cortex. J Physiol 148:574-591.
Hung CP, Kreiman G, Poggio T (2005) Fast Readout of Object Identity from Macaque Inferior Temporal Cortex. Science 310:863-866.

Hupe J-M, James AC, Girard P, Bullier J (2001) Response Modulations by Static Texture Surround in Area V1 of the Macaque Monkey Do Not Depend on Feedback Connections From V2. J Neurophysiol 85:146-163.
Ishai A (2007) Let's face it: It's a cortical network. Neuroimage.
Ito M, Westheimer G, Gilbert CD (1998) Attention and Perceptual Learning Modulate Contextual Influences on Visual Perception. Neuron 20:1191-1197.
Itti L, Rees G, Tsotsos J (2005) Neurobiology of attention.
Jensen O, Lisman JE (1996) Novel lists of 7 +/- 2 known items can be reliably stored in an oscillatory short-term memory network: interaction with long-term memory. Learn Mem 3:257-263.
Jiang X, Bradley E, Rini RA, Zeffiro T, VanMeter J, Riesenhuber M (2007) Categorization Training Results in Shape- and Category-Selective Human Neural Plasticity. Neuron 53:891-903.
Johnson JS, Olshausen BA (2005) The earliest EEG signatures of object recognition in a cued-target task are postsensory. Journal of Vision 5:299-312.
Johnston D, Christie BR, Frick A, Gray R, Hoffman DA, Schexnayder LK, Watanabe S, Yuan LL (2003) Active dendrites, potassium channels and synaptic plasticity. Philos Trans R Soc Lond B Biol Sci 358:667-674.
Kalanit G-S, Nancy K (2005) Visual Recognition: As Soon as You Know It Is There, You Know What It Is. Psychological Science 16:152-160.
Kandel ER, Schwartz JH, Jessel TM Principles of Neural Science, 4. Edition: McGraw-Hill.
Kepecs A, van Rossum MCW, Song S, Tegner J (2002) Spike-timing-dependent plasticity: common themes and divergent vistas. Biological Cybernetics 87:446-458.
Kimura F (2000) Cholinergic modulation of cortical function: A hypothetical role in shifting the dynamics in cortical network. Neuroscience Research 38:19-26.
Kimura F, Fukuda M, Tsumoto T (1999) Acetylcholine suppresses the spread of excitation in the visual cortex revealed by optical recording: possible differential effect depending on the source of input. European Journal of Neuroscience 11:3597-3609.
Kiper DC (2003) Colour and form in the early stages of cortical processing. J Physiol 548:335-.
Kirchner H, Thorpe SJ (2006) Ultra-rapid object detection with saccadic eye movements: Visual processing speed revisited. Vision Research 46.
Kirkwood A, Bear MF (1994) Homosynaptic long-term depression in the visual cortex. J Neurosci 14:3404-3412.
Kisvarday ZF, Eysel UT (1992) Cellular organization of reciprocal patchy networks in layer III of cat visual cortex (area 17). Neuroscience 46:275-286.
Kisvarday ZF, Toth E, Rausch M, Eysel UT (1997) Orientation-specific relationship between populations of excitatory and inhibitory lateral connections in the visual cortex of the cat. Cereb Cortex 7:605-618.
Kjaer TW, Hertz JA, Richmond BJ (1994) Decoding cortical neuronal signals: network models, information estimation and spatial tuning. J Comput Neurosci 1:109-139.
Knowlton BJ, Squire LR (1993) The learning of categories: parallel brain systems for item memory and category knowledge. Science 262:1747-1749.
Knusel P, Wyss R, Konig P, Verschure PFMJ (2004) Decoding a Temporal Population Code. Neural Comp 16:2079-2100.

Knusel P, Carlsson MA, Hansson BS, Pearce TC, Verschure PF (2007) Time and space are complementary encoding dimensions in the moth antennal lobe. Network 18:35-62.
Knüsel P, Wyss R, König P, Versure PFMJ (2004) Decoding a temporal population code. Neural Computation 16:2079-2100.
Kobatake E, Wang G, Tanaka K (1998) Effects of Shape-Discrimination Training on the Selectivity of Inferotemporal Cells in Adult Monkeys. J Neurophysiol 80:324-330.
Konig P, Engel AK, Roelfsema PR, Singer W (1995) How precise is neuronal synchronization? Neural Comp 7:469-485.
Kourtzi Z, DiCarlo JJ (2006) Learning and neural plasticity in visual object recognition. Current Opinion in Neurobiology 16:152-158.
Kreiman G, Koch C, Fried I (2000) Category-specific visual responses of single neurons in the human medial temporal lobe. Nat Neurosci 3:946-953.
Kreiman G, Hung CP, Kraskov A, Quiroga RQ, Poggio T, DiCarlo JJ (2006) Object Selectivity of Local Field Potentials and Spikes in the Macaque Inferior Temporal Cortex. Neuron 49:433-445.
Lampl I, Ferster D, Poggio T, Riesenhuber M (2004) Intracellular Measurements of Spatial Integration and the MAX Operation in Complex Cells of the Cat Primary Visual Cortex. J Neurophysiol 92:2704-2713.
Laurent G, Wehr M, Davidowitz H (1996) Temporal Representations of Odors in an Olfactory Network. J Neurosci 16:3837-3847.
Lebedev MA, Nicolelis MAL (2006) Brain-machine interfaces: past, present and future. Trends in Neurosciences 29:536-546.
Lee BB, Kremers JAN, Yeh T (2000) Receptive fields of primate retinal ganglion cells studied with a novel technique: Cambridge Journals Online.
Lee C, Rohrer WH, Sparks DL (1988) Population coding of saccadic eye movements by neurons in the superior colliculus. Nature 332:357-360.
Lehky SR, Sereno AB (2007) Comparison of Shape Encoding in Primate Dorsal and Ventral Visual Pathways. J Neurophysiol 97:307-319.
Lestienne R (1996) Determination of the precision of spike timing in the visual cortex of anaesthetised cats. Biol Cybern 74:55-61.
Li RW, Klein SA, Levi DM (2006) The receptive field and internal noise for position acuity change with feature separation. Journal of Vision 6:311-321.
Li W, Piech V, Gilbert CD (2004) Perceptual learning and top-down influences in primary visual cortex. Nat Neurosci 7:651-657.
Lisman J (1989) A mechanism for the Hebb and the anti-Hebb processes underlying learning and memory. Proc Natl Acad Sci U S A 86:9574-9578.
Little DM, Klein R, Shobat DM, McClure ED, Thulborn KR (2004) Changing patterns of brain activation during category learning revealed by functional MRI. Cognitive Brain Research 22:84-93.
Logothetis NK, Sheinberg DL (1996) Visual Object Recognition. Annual Review of Neuroscience 19:577-621.
Logothetis NK, Pauls J, Poggio T (1995) Shape representation in the inferior temporal cortex of monkeys. Current Biology 5:552-563.
Ma WJ, Beck JM, Latham PE, Pouget A (2006) Bayesian inference with probabilistic population codes. Nat Neurosci 9:1432-1438.
Maass W (1998) A simple model for neural computation with firing rates and firing correlations. Network 9:381-397.

Maass W (2009) Motivation, Theory, and Application of Liquid State Machines. In: Computability in Context: Computation and Logic in the Real World. (Cooper B, Sorbi A, eds): Imperial College Press.
MacKay D, McCulloch W (1952) The limiting information capacity of a neuronal link. Bulletin of Mathematical Biology 14:127-135.
Malenka RC, Nicoll RA (1999) Long-term potentiation--a decade of progress? Science 285:1870-1874.
Marcelja S (1980) Mathematical description of the responses of simple cortical cells. J Opt Soc Am 70:1297-1300.
Markram H, Tsodyks M (1996) Redistribution of synaptic efficacy between neocortical pyramidal neurons. Nature 382:807-810.
Markram H, Lubke J, Frotscher M, Sakmann B (1997) Regulation of Synaptic Efficacy by Coincidence of Postsynaptic APs and EPSPs. Science 275:213-215.
Masquelier T, eacute, Thorpe SJ (2007) Unsupervised Learning of Visual Features through Spike Timing Dependent Plasticity. PLoS Computational Biology 3:e31.
Matsumoto N, Okada M, Sugase-Miyamoto Y, Yamane S, Kawano K (2005) Population Dynamics of Face-responsive Neurons in the Inferior Temporal Cortex. Cereb Cortex 15:1103-1112.
McAlpine D, Grothe B (2003) Sound localization and delay lines - do mammals fit the model? TRENDS in Neurosciences 26:347-350.
McClurkin JW, Optican LM, Richmond BJ (1991) Concurrent Processing and Complexity of Temporally Encoded Neuronal Messages in Visual Perception. Science 253:675-677.
McClurkin JW, Zarbock JA, Optican LM (1996) Primate striate and prestriate cortical neurons during discrimination. II. separable temporal codes for color and pattern. J Neurophysiol 75:496-507.
McGaughy J, Kaiser T, Sarter M (1996) Behavioral Vigilance Following Infusions of 192 IgG-Saporin Into the Basal Forebrain: Selectivity of the Behavioral Impairment and Relation to Cortical AChE-Positive Fiber Density. Behavioral Neuroscience 110:247-265.
McGuire BA, Gilbert CD, Rivlin PK (1991) Targets of Horizontal Connections in Macaque Primary Visual Cortex. The Journal of Comparative Neurobiology 305:370-392.
Mechler F, Victor JD, Purpura KP, Shapley R (1998) Robust Temporal Coding of Contrast by V1 Neurons for Transient But Not for Steady-State Stimuli. J Neurosci 18:6583-6598.
Miller EK, Nieder A, Freedman DJ, Wallis JD (2003) Neural correlates of categories and concepts. Current Opinion in Neurobiology 13:198-203.
Montague PR, Dayan P, Sejnowski TJ (1996) A framework for mesencephalic dopamine systems based on predictive Hebbian learning. J Neurosci 16:1936-1947.
Mulkey RM, Malenka RC (1992) Mechanisms underlying induction of homosynaptic long-term depression in area CA1 of the hippocampus. Neuron 9:967-975.
Norton TT, Corliss DA, Bailey JE (2002) The Psychophysical Measurement of Visual Function: Elsevier, Butterworth Heinemann.
Ohki K, Chung S, Kara P, Hubener M, Bonhoeffer T, Reid RC (2006) Highly ordered arrangement of single neurons in orientation pinwheels. Nature 442:925-928.
Oram MW, Wiener MC, Lestienne R, Richmond BJ (1999) Stochastic nature of precisely timed spike patterns in visual system neuronal responses. J Neurophysiol 81:3021-3033.

Orban GA, Dupont P, Vogels R, De Bruyn B, Bormans G, Mortelmans L (1996) Task dependency of visual processing in the human visual system. Behav Brain Res 76:215-223.
Packard MG, McGaugh JL (1992) Double dissociation of fornix and caudate nucleus lesions on acquisition of two water maze tasks: further evidence for multiple memory systems. Behav Neurosci 106:439-446.
Patricio T. Huerta JEL (1996) Synaptic plasticity during the cholinergic theta-frequency oscillation in vitro. Hippocampus 6:58-61.
Perea G, Araque A (2007) Astrocytes Potentiate Transmitter Release at Single Hippocampal Synapses. Science 317:1083-1086.
Perry E, Walker M, Grace J, Perry R (1999) Acetylcholine in mind: a neurotransmitter correlate of consciousness? Trends Neurosci 22:273-280.
Poggio T, Girosi F (1990) Regularization Algorithms for Learning That Are Equivalent to Multilayer Networks. Science 247:978-982.
Poggio T, Fahle M, Edelman S (1992) Fast perceptual learning in visual hyperacuity. Science 256:1018-1021.
Poggio T, Fahle M, Edelman S (1992b) Fast Perceptual learning in visual hyperacuity. Science 256:1018-1021.
Price JL, Stern R (1983) Individual cells in the nucleus basalis-diagonal band complex have restricted axonal projections to the cerebral cortex in the rat. Brain Research 269:352-356.
Purves D, Riddle DR, LaMantia AS (1992) Iterated patterns of brain circuitry (or how the cortex gets its spots). Trends Neurosci 15:362-368.
Quiroga QR, Reddy L, Kreiman G (2005a) Invariant visual representation by single neurons in the human brain. Nature 435:1102-1007.
Quiroga RQ, Reddy L, Kreiman G, Koch C, Fried I (2005b) Invariant visual representation by single neurons in the human brain. Nature 435:1102-1107.
Rall W (1969) Time constants and electrotonic length of membrane cylinders and neurons. Biophys J 9:1483-1508.
Reber PJ, Stark CEL, Squire BJ (1998a) Cortical areas supporting category learning identified using functional MRI. PNAS 95:747-750.
Reber PJ, Stark CEL, Squire LR (1998b) Cortical areas supporting category learning identified using functional MRI. Proceedings of the National Academy of Sciences 95:747-750.
Reber PJ, Gitelman DR, Parrish TB, Mesulam MM (2003) Dissociating Explicit and Implicit Category Knowledge with fMRI. J Cogn Neurosci 15:574-583.
Richmond BJ, Optican LM, Podell M (1987) Temporal Encoding of Two-Dimensional Patterns by Single Units in Primate Inferior Temporal Cortex. I. Response Characteristics. Journal of Neurophysiology 57:132-146.
Rieke F, Warland D, De Ruyter van Steveninck RR, Bialek W (1999) Spikes, Exploring the Neural Code: MIT Press.
Riesenhuber M, Poggio T Models of object recognition. Nat Neurosci.
Riesenhuber M, Poggio T (1999) Hierarchical models of object recognition in cortex. Nat Neurosci 2:1019-1025.
Ringach DL, Shapley RM, Hawken MJ (2002) Orientation Selectivity in Macaque V1: Diversity and Laminar Dependence. J Neurosci 22:5639-5651.
Robert PV (2005) Hippocampal theta rhythm: A tag for short-term memory. Hippocampus 15:923-935.
Roberts AC, De Salvia MA, Wilkinson LS, Collins P, Muir JL, Everitt BJ, Robbins TW (1994) 6-Hydroxydopamine lesions of the prefrontal cortex in monkeys enhance

performance on an analog of the Wisconsin Card Sort Test: possible interactions with subcortical dopamine. J Neurosci 14:2531-2544.
Roberts MJ, Zinke W, Guo K, Robertson R, McDonald JS, Thiele A (2005) Acetylcholine Dynamically Controls Spatial Integration in Marmoset Primary Visual Cortex. J Neurophysiol 93:2062-2072.
Rolls ET, Milward T (2000) A Model of Invariant Object Recognition in the Visual System: Learning Rules, Activation Functions, Lateral Inhibition, and Information-Based Performance Measures. Neural Comp 12:2547-2572.
Rolls ET, Stringer SM (2006) Invariant visual object recognition: A model, with lighting invariance. Journal of Physiology-Paris 100:43-62.
Rutishauser U, Walther D, Koch C, Perona P (2004) Is Bottom-Up Attention Useful for Object Recognition? Computer Vision and Pattern Recognition, IEEE Computer Society Conference on 2:37-44.
Saalmann YB, Pigarev IN, Vidyasagar TR (2007) Neural Mechanisms of Visual Attention: How Top-Down Feedback Highlights Relevant Locations. Science 316:1612-1615.
Sabatini BL, Oertner TG, Svoboda K (2002) The life cycle of Ca(2+) ions in dendritic spines. Neuron 33:439-452.
Sanchez-Vives MV, Nowak LG, McCormick DA (2000) Membrane mechanisms underlying contrast adaptation in cat area 17 in vivo. J Neurosci 20:4267-4285.
Sarter M, Givens B, Bruno JP (2001) The cognitive neuroscience of sustained attention: where top-down meets bottom-up. Brain Research Reviews 35:146-160.
Schillen TB, Konig P (1994) Binding by temporal structure in multiple feature domains of an oscillatory neuronal network. Biol Cybern 70:397-405.
Schmolesky MT, Wang Y, Hanes DP, Thompson KG, Leutgeb S, Schall JD, Leventhal AG (1998a) Signal timing across the macaque visual system. J Neurophysiol 79:3272-3278.
Schmolesky MT, Wang Y, Hanes DP, Thompson KG, Leutgeb S, Schall JD, Leventhal AG (1998b) Signal Timing Across the Macaque Visual System. J Neurophysiol 79:3272-3278.
Schneidman E, Freedman B, Segev I (1998) Ion channel stochasticity may be critical in determining the reliability and precision of spike timing. Neural Comp 10:1679-1703.
Schrauwen B, D'Haene M, Verstraeten D, Campenhout JV (2008) Compact hardware liquid state machines on FPGA for real-time speech recognition. Neural Netw 21:511-523.
Seeger T, Alzheimer C (2001) Muscarinic activation of inwardly rectifying K+ conductance reduces EPSPs in rat hippocampal CA1 pyramidal cells. J Physiol 535:383-396.
Sejnowski TJ (1995) Pattern recognition. Time for a new neural code? Nature 376:21-22.
Senn W, Fusi S (2005a) Convergence of stochastic learning in perceptrons with binary synapses. Phys Rev E Stat Nonlin Soft Matter Phys 71:061907.
Senn W, Fusi S (2005b) Learning only when necessary: better memories of correlated patterns in networks with bounded synapses. Neural Comput 17:2106-2138.
Serre T, Oliva A, Poggio T (2007a) A feedforward architecture accounts for rapid categorization. PNAS 104:6424-6429.
Serre T, Wolf L, Bileschi S, Riesenhuber M, Poggio T (2007b) Robust Object Recognition with Cortex-Like Mechanisms. IEEE Transactions on Pattern Analysis and Machine Intelligence 29:411-426.

Shadlen MN, Newsome WT (1994) Noise, neural codes and cortical organization. Curr Opin Neurobiol 4:569-579.
Shannon CE (1997) The mathematical theory of communication. 1963. MD Comput 14:306-317.
Shapley R, Hawken M, Xing D, Paul Cisek TDaJFK (2007) The dynamics of visual responses in the primary visual cortex. In: Progress in Brain Research, pp 21-32: Elsevier.
Shi D, Dong C, Yeung DS (1999) Neocognitron's parameter tuning by genetic algorithms. Int J Neural Syst 9:497-509.
Shouval HZ, Bear MF, Cooper LN (2002a) A unified model of NMDA receptor-dependent bidirectional synaptic plasticity. Proceedings of the National Academy of Sciences 99:10831-10836.
Shouval HZ, Castellani GC, Blais BS, Yeung LC, Cooper LN (2002b) Converging evidence for a simplified biophysical model of synaptic plasticity. Biological Cybernetics 87:383-391.
Sigala N (2004) Visual categorization and the inferior temporal cortex. Behavioural Brain Research 149:1-7.
Sigala N, Logothetis NK (2002) Visual categorization shapes feature selectivity in the primate temporal cortex. Nature 415:318-320.
Sillito AM, Kemp JA (1983) Cholinergic modulation of the functional organization of the cat visual cortex. Brain Research 289:143-155.
Sincich LC, Blasdel GG (2001) Oriented Axon Projections in Primary Visual Cortex of the Monkey. J Neurosci 21:4416-4426.
Singer W (1994) Coherence as an organizing principle of cortical functions. Int Rev Neurobiol 37:153-183; discussion 203-157.
Singer W (1999a) Time as coding space? Current Opinion in Neurobiology 9:189-194.
Singer W (1999b) Neuronal Synchrony: A Versatile Code for the Definition of Relations? Neuron 24:49-65.
Sjostrom PJ, Hausser M (2006) A Cooperative Switch Determines the Sign of Synaptic Plasticity in Distal Dendrites of Neocortical Pyramidal Neurons. Neuron 51:227-238.
Sjostrom PJ, Turrigiano GG, Nelson SB (2001) Rate, Timing, and Cooperativity Jointly Determine Cortical Synaptic Plasticity. Neuron 32:1149-1164.
Sjostrom PJ, Turrigiano GG, Nelson SB (2007) Multiple forms of long-term plasticity at unitary neocortical layer 5 synapses. Neuropharmacology 52:176-184.
Skottun BC (1998) Sound localization and neurons. Nature 393:531-531.
Softky WR (1995) Simple codes versus efficient codes. Curr Opin Neurobiol 5:239-247.
Squire LR, Knowlton BJ (1995) Learning about categories in the absence of memory. PNAS:12470-12474.
Stettler DD, Das A, Bennett J (2002) Lateral Connectivity and Contextual Interactions in Macaque Primary Visual Cortex. Neuron 36:739-750.
Stringer S, Perry G, Rolls E, Proske J (2006) Learning invariant object recognition in the visual system with continuous transformations. Biological Cybernetics 94:128-142.
Suzuki W, Matsumoto K, Tanaka K (2006) Neuronal Responses to Object Images in the Macaque Inferotemporal Cortex at Different Stimulus Discrimination Levels. J Neurosci 26:10524-10535.
Tanaka K (2003) Columns for Complex Visual Object Features in the Inferotemporal Cortex: Clustering of Cells with Similar but Slightly Different Stimulus Selectivities. Cereb Cortex 13:90-99.

Tanigawa H, Wang Q, Fujita I (2005a) Organization of Horizontal Axons in the Inferior Temporal Cortex and Primary Visual Cortex of the Macaque Monkey. Cereb Cortex:bhi067.
Tanigawa H, Wang Q, Fujita I (2005b) Organization of Horizontal Axons in the Inferior Temporal and Primary Visual Cortex of the Macaque Monkey. Cerebral Cortex 15:1887-1899.
Theunissen F, Miller JP (1995) Temporal encoding in nervous systems: A rigorous definition. Journal of Computational Neuroscience 2:149-162.
Thomas E, Van Hulle MM, Vogels R (2001) Encoding of Categories by Noncategory-Specific Neurons in the Inferior Temporal Cortex. J Cogn Neurosci 13:190-200.
Thorpe S (1990) Spike arrival times: A highly efficient coding scheme for neural networks. Elsevier:91-94.
Thorpe S (2008) SpikeNet Technology. In.
Tiesinga P, Fellous J-M, Sejnowski TJ (2008) Regulation of spike timing in visual cortical circuits. Nat Rev Neurosci 9:97-107.
Tovee MJ, Rolls ET, Treves A, Bellis RP (1993) Information encoding and the responses of single neurons in the primate temporal visual cortex. J Neurophysiol 70:640-654.
Tucker TR, Katz LC (2003) Spatiotemporal Patterns of Excitation and Inhibition Evoked by the Horizontal Network in Layer 2/3 of Ferret Visual Cortex. J Neurophysiol 89:488-500.
Ungerleider LG, Mishkin M (1982) Analysis of visual behavior
Ungerleider LG, Haxby JV (1994) 'What' and 'where' in the human brain. Curr Opin Neurobiol 4:157-165.
Van Essen DC, Anderson CH, Felleman DJ (1992) Information processing in the primate visual system: an integrated systems perspective. Science 255:419-423.
Van Rullen R, Gautrais J, Delorme A, Thorpe S (1998) Face processing using one spike per neurone. Biosystems 48:229-239.
Verschure PFMJ, Konig P (1999) On the Role of Biophysical Properties of Cortical Neurons in Binding and Segmentation of Visual Scenes. Neural Comp 11:1113-1138.
Verschure PFMJ, König P (1999) On the Role of Biophysical Properties of Cortical Neurons in Binding and Segmentation of Visual Scenes. Neural Computation 11:1113-1138.
Vezoli J, Falchier A, Jouve B, Knoblauch K, Young M, Kennedy H (2004) Quantitative Analysis of Connectivity in the Visual Cortex: Extracting Function from Structure. Neuroscientist 10:476-482.
Victor JD (2000) How the brain uses time to represent and process visual information. Brain Research 886:33-46.
Vogels R, Orban GA (1996) Coding of stimulus invariances by inferior temporal neurons. Prog Brain Res 112:195-211.
Wallis G, Rolls ET (1997) INVARIANT FACE AND OBJECT RECOGNITION IN THE VISUAL SYSTEM. Progress in Neurobiology 51:167-194.
Walther D, Koch C (2006) Modeling attention to salient proto-objects. Neural Netw 19:1395-1407.
Wandell BA (1995) Foundations of Vision. Stanford University.
Wang X-J, Liu Y, Sanchez-Vives MV, McCormick DA (2003) Adaptation and Temporal Decorrelation by Single Neurons in the Primary Visual Cortex. J Neurophysiol 89:3279-3293.

Weiskrantz L, Saunders RC (1984) Impairments of visual object transforms in monkeys. Brain 107 (Pt 4):1033-1072.
Weiss Y, Edelman S, Fahle M (1993) Models of perceptual learning in vernier hyperacuity. Neural Computation 5:695-718.
Westheimer G, McKee SP (1977a) Spatial Configurations for Visual Hyperacuity. Vision Research 17:941-947.
Westheimer G, McKee SP (1977b) Spatial configurations for visual hyperacuity. Vision Research 17:941-947.
Wichmann FA, Hill NJ (2001a) The psychometric function: II. Bootstrap-based confidence intervals and sampling. Perception & Psychophysics 63:1314-1329.
Wichmann FA, Hill NJ (2001b) The psychometric function: I. Fitting, sampling, and goodness of fit. Perception & Psychophysics 63:1293-1313.
Wikipedia (2009) Belief propagation. In.
Wilson HR (1986) Responses of spatial mechanisms can explain hyperacuity. Vision Research 26:453-469.
Wilson HR, Gelb DJ (1984) Modified line-element theory for spatial-frequency and width discrimination. J Opt Soc Am A 1:124-131.
Wolfgang M, Thomas N, ger, Henry M (2002) Real-time computing without stable states: a new framework for neural computation based on perturbations. Neural Comput 14:2531-2560.
Womelsdorf T, Schoffelen J-M, Oostenveld R, Singer W, Desimone R, Engel AK, Fries P (2007) Modulation of Neuronal Interactions Through Neuronal Synchronization. Science 316:1609-1612.
Wyss R, Verschure PFMJ (2003) Properties of a Temporal Population Code. Reviews in the Neurosciences 14:21-33.
Wyss R, Koenig P, Verschure PFMJ (2001) Invariant Encoding of Spatial Stimulus Topology in the Temporal Domain. In.
Wyss R, Konig P, Verschure PFMJ (2003a) Invariant representations of visual patterns in a temporal population code. Proceedings of the National Academy of Sciences 100:324-329.
Wyss R, Koenig P, Verschure PFMJ (2003b) Invariant representations of visual patterns in a temporal population code. PNAS 100:324-329.
Yamane Y, Tsunoda K, Matsumoto M, Phillips AN, Tanifuji M (2006) Representation of the Spatial Relationship Among Object Parts by Neurons in Macaque Inferotemporal Cortex. J Neurophysiol 96:3147-3156.
Yap YL, Levi DM, Klein SA (1987) Peripheral hyperacuity: three-dot bisection scales to a single factor from 0 to 10 degrees. J Opt Soc Am A 4:1554-1561.
Zador AM, Agmon-Snir H, Segev I (1995) The morphoelectrotonic transform: a graphical approach to dendritic function. J Neurosci 15:1669-1682.
Zaki SR, Nosofsky RM (2001a) A single-system interpretation of dissociations between recognition and categorization in a task involving object-like stimuli. Cognitive, Affective, & Behavioral Neuroscience 1:344-359.
Zaki SR, Nosofsky RM (2001b) A single-system interpretation of dissociations between recognition and categorization in a task involving object-like stimuli. Cognitive, Affective, & Behavioral Neuroscience 1:344-359.
Zhou H, Friedman HS, von der Heydt R (2000) Coding of Border Ownership in Monkey Visual Cortex. J Neurosci 20:6594-6611.
Zinke W, Roberts MJ, Guo K, McDonald JS, Robertson R, Thiele A (2006) Cholinergic modulation of response properties and orientation tuning of neurons in primary

visual cortex of anaesthetized Marmoset monkeys. European Journal of Neuroscience 24:314-328.

Zipser K, Lamme VAF, Schiller PH (1996) Contextual Modulation in Primary Visual Cortex. J Neurosci 16:7376-7389.

Curriculum vitae

Dipl. phil. II UZH Stephan Roth

Personal

Date and place of Birth:	May, 8th, 1970, Sursee, Switzerland
Nationality:	Swiss, citizen of Zurich and Altishofen, Switzerland
Marital status:	Single

Education

02/2005-present	PhD-Student at the Institute of Neuroinformatics ETH Zurich (INI)
09/2002-10/2004	Master of Advanced Studies ETH in Medical Physics (MAS ETH MP)
09/1991-01/1997	Studies of biology at the University of Zurich (Dipl. phil. II) - Diploma thesis in genetics.
08/1983-07/1990	High school at KS Sursee (Matura, Typus C)

Employment

07/2003-present	Software Eng. at Ierax AG, Zürich (ZH, Switzerland)
08/2001-06/2003	Software Eng. at Solitas AG, Buchs (SG, Switzerland)
08/1997-07/2001	Software Eng. at Conexus AG, Kloten (ZH, Switzerland)
03/1997-08/1997	Software Eng. and Consultant at Promatis AG, Zürich; place of work Karlsbad (Germany)

Conferences

Roth, S., Kiper, D. C., *A model of perceptual learning in a Vernier acuity task*, NCCR Meeting 2008, Zurich (Switzerland)

Roth, S., Kiper, D. C. Verschure, P. F. M. J., *The classification and segmentation of visual stimuli in a biophysical constrained model of the primary visual cortex*, Cajal Centenary Conference 2006, Barcelona (Spain)

Roth, S., Kiper, D. C. Verschure, P. F. M. J., *The classification and segmentation of visual stimuli in a biophysically constrained neuronal model of the primary visual cortex*, ECVP 2006,
St. Petersburg (Russia)

Roth, S., Kiper, D. C. Verschure, P. F. M. J., *The encoding and segmentation of complex patterns in cortical networks: A temporal population code (*TPC*)*, SSN 2006, Basel (Switzerland)

Roth, S., Kiper, D. C. Verschure, P. F. M. J., *The classification and segmentation of visual stimuli in a biophysical constrained model of the primary visual cortex*, VSS 2006, Sarasota (USA)